

Generation of genome-edited hiPSC-derived cell models for malignant brain tumors

Inaugural-Dissertation

zur Erlangung des Doktorgrades
der Mathematisch-Naturwissenschaftlichen Fakultät
der Heinrich-Heine-Universität Düsseldorf

vorgelegt von

Constanze Krambrich

aus Wuppertal

Düsseldorf, April 2023

aus dem Forschungslabor der Klinik für Neurochirurgie des Universitätsklinikums Düsseldorf
in Kooperation mit dem IUF – Leibniz Institut für umweltmedizinische Forschung,
Arbeitsgruppe Entwicklung von Alternativmethoden zur umwelttoxikologischen Testung.

Gedruckt mit der Genehmigung der
Mathematisch-Naturwissenschaftlichen Fakultät der
Heinrich-Heine-Universität Düsseldorf

Berichtersteller:

1. Prof. Dr. Ellen Fritsche
2. Prof. Dr. Thomas Klein

Tag der mündlichen Prüfung: 23.10.2023

Eidesstaatliche Erklärung

Hiermit versichere ich an Eides statt, dass ich die vorliegende Arbeit „Generation of genome-edited hiPSC-derived cell models for malignant brain tumors“ selbstständig verfasst und ausschließlich die von mir angegebenen Hilfsmittel verwendet habe. Die Dissertation wurde in der vorgelegten oder einer ähnlichen Form noch bei keiner anderen Institution eingereicht, ich habe bisher keine erfolglosen Promotionsversuche unternommen.

Constanze Krambrich

Abstract

Medulloblastoma (MB) and Glioblastoma (GBM) are the most aggressive brain tumors in children and adults, respectively. Treatment of both tumors includes resection, chemotherapy, and radiation. Although most MB patients have a good prognosis they often develop secondary tumors or have mental disabilities due to the aggressive treatment. In contrast, GBM patients in general have a prognosis of 14 – 16 months after diagnosis and treatment. Further, recurrence of GBM tumors is common. One explanation for the fast recurrence of GBMs, is the cancer stem cell (CSC) hypothesis. This hypothesis describes that a small quantity of tumor cells have stem cell-like characteristics and are resistant against treatment and initiate the recurrence of the tumor. Within the last decades, molecular subgroups of the MB and GBM tumors could be identified due to genetic changes e.g., mutations or gene amplifications and it was discovered that the prognosis for each subtype is different. These findings offer a new opportunity for a more effective treatment.

This PhD thesis aims to investigate the utility of human induced pluripotent stem cells (hiPSCs) to generate subtype-specific MB and GBM tumor cell models and evaluate their applicability for testing chemical compounds. First, subtype-specific mutations of MB and GBM tumors are introduced into the hiPSCs. These generated hiPSC-oncogene models are characterized and utilized for a small-scale chemical compound screening. One advantage of the hiPSC-oncogene models is the possibility to differentiate the cells into the cell type of interest. In this work, the hiPSC-oncogene models were neurally differentiated and the resulting three dimensional neurospheres were also screened for the endpoints cytotoxicity and proliferation, after chemical compound screening. The characterization of the hiPSC and iNPC models revealed that these models are suitable to study MB and GBM. The utilization of the chemical compound screening showed that new treatment approaches can be identified. Using this approach, copanlisib was identified as a promising drug for the MB Group 3 model as it significantly reduced the migration of the tumor models and increased the cytotoxicity, compared to control cells.

In conclusion, this work showed that hiPSCs can be utilized to generate tumor models and are applicable for chemical compound screenings to identify new treatment approaches.

Zusammenfassung

Medulloblastom (MB) und Glioblastom (GBM) sind die aggressivsten Hirntumore bei Kindern bzw. Erwachsenen. Die Behandlung beider Tumoren umfasst Resektion, Chemotherapie und Bestrahlung. Obwohl die meisten MB-Patienten eine gute Prognose haben, entwickeln sie aufgrund der aggressiven Behandlung häufig Zweittumore oder haben geistige Einschränkungen. Die GBM-Patienten hingegen haben im Allgemeinen eine voraussichtliche Lebenserwartung von 14 bis 16 Monaten nach der Diagnose und Behandlung. Zudem entsteht oft innerhalb von wenigen Monaten nach der Tumorentfernung ein neuer Tumor. Eine Erklärung für das schnelle Wiederauftreten von GBMs ist die Krebsstammzellhypothese (CSC). Diese Hypothese besagt, dass eine kleine Anzahl von Tumorzellen stammzellähnliche Eigenschaften haben und resistent gegen die Behandlung sind und somit das Wiederauftreten des Tumors fördern.

In den letzten Jahrzehnten konnten molekulare Untergruppen der MB- und GBM-Tumore aufgrund genetischer Veränderungen, z. B. Mutationen oder Genamplifikationen identifiziert werden und es wurde festgestellt, dass die Prognose für jeden Subtyp unterschiedlich ist. Diese Erkenntnisse bieten eine neue Chance für eine wirksamere Behandlung.

In dieser Arbeit wurden Modelle für einen Teil der molekularen Subgruppen von MB- und GBM-Tumoren mithilfe von human induzierten pluripotenten Stammzellen (hiPSZ) generiert. Die hergestellten hiPSZ Modelle wurden charakterisiert und anschließend in einem Medikamentenscreening eingesetzt. Es wurden neun Medikamente getestet, die abhängig vom hiPSZ Modell die Lebensfähigkeit der Zellen unterschiedlich stark reduziert haben. Im Vergleich zu den Kontrollen wurden bereits für einzelne hiPSZ Modelle wirksame Medikamente identifiziert. Zudem wurden die hiPSZ Modelle neural differenziert und anschließend als dreidimensionale Neurosphären kultiviert. Mit den Neurosphären wurden zwei Medikamentenscreenings durchgeführt und die Migration, Zytotoxizität und Proliferation untersucht. Die Charakterisierung der hiPSZ und der induzierten neuralen Vorläuferzellen-Modelle zeigte, dass diese Modelle für die Untersuchung von MB und GBM geeignet sind. Mit Hilfe dieses Ansatzes wurde Copanlisib als vielversprechendes Medikament für das MB Gruppe 3 Modell identifiziert, da es die Migration der Tumormodelle deutlich reduzierte und die Zytotoxizität im Vergleich zu den Kontrollzellen und sogar zur Standardbehandlung mit Cisplatin erhöhte.

Zusammenfassend hat diese Arbeit gezeigt, dass hiPSZ zur Erzeugung von Tumormodellen verwendet werden können und für das Screening chemischer Substanzen zur Identifizierung neuer Behandlungsansätze geeignet sind.

Table of contents

Eidesstaatliche Erklärung	i
Abstract	ii
Zusammenfassung	iii
1 Introduction.....	6
1.1 Brain cancer.....	6
1.2 Medulloblastoma	7
1.2.1 MB subgroups	9
1.3 GBM.....	12
1.3.1 GBM Subgroups	14
1.4 Cancer stem cells.....	16
1.5 Human induced pluripotent stem cells (hiPSCs).....	18
1.5.1 Neural Differentiation of hiPSCs	20
1.6 Aim of this thesis	22
2 Material and Methods	23
2.1 Materials	23
2.1.1 List of laboratory equipment.....	23
2.1.2 Consumables.....	25
2.1.3 Cell lines	26
2.1.4 Cell culture media components.....	27
2.1.5 Media composition.....	28
2.1.6 Cell culture components	29
2.1.7 Chemicals.....	31
2.1.8 Buffers and solutions	34
2.1.9 Vector.....	35
2.1.10 Kits	36
2.2 Methods	37
2.2.1 Generation of the plasmid including the gene of interest.....	37
2.2.2 Polymerase chain reaction.....	37
2.2.3 Restriction digest of insert and vector	40
2.2.4 Sequences of all inserted genes	42
2.2.5 Ligation.....	49
2.2.6 Cold Fusion™ Cloning.....	49
2.2.7 Bacteria transformation and plasmid extraction	50
2.2.8 Cell Culture.....	51
2.2.9 Characterization of hiPSC-oncogene models.....	56

2.2.10	Cell culture of hiNPC-oncogene models	67
2.2.11	Characterization of hiNPC-oncogene models	71
2.3	Statistic and Software	80
3	Results	81
3.1	Generation of the hiPSC-oncogene models	81
3.2	Characterization of the hiPSC-oncogene models	83
3.3	Metabolic transcription of hiPSC-oncogene models	87
3.4	Transcriptomic characterization of hiPSC-oncogene models.....	92
3.5	Pharmacological screening of hiPSC-oncogene models	96
3.6	Longer cultivation of neural progenitor cells decreases proliferation and viability of spheres.....	100
3.7	Characterization of generated 2D hiNPC-oncogene models	101
3.8	Characterization of 3D hiNPC-oncogene models	107
3.9	Compound screening of the 3D hiNPC-oncogene models.....	110
3.9.1	Compound screening of the MB hiNPC-oncogene model	111
3.9.2	Compound screening of the GMB hiNPC-oncogene model	115
4	Discussion	121
4.1	Application of <i>in vitro</i> test systems	121
4.2	Subtype-specific hiPSC-oncogene model generation	122
4.3	Characterization of the hiPSC-oncogene models	123
4.4	Pharmacological screening of the hiPSC-oncogene models and 3D hiNPC-oncogene models in a small-scale approach	127
4.5	Neural Differentiation of hiPSC-oncogene models was only successful in 3D	129
4.6	Compound screening of 3D hiNPC-oncogene detects promising candidates	131
4.7	Conclusion and outlook	135
5	Literature	136
6	Abbreviations.....	176
7	List of Figures.....	180
8	List of Tables	182
9	Publications	184
10	Danksagung	232

1 Introduction

1.1 Brain cancer

Cancer is the leading cause of death worldwide and is responsible for around ten million deaths alone in the year 2020 (Sung et al., 2021). The most common cancers are lung, breast, and prostate cancer. However, tumors of the central nervous system (CNS) are also common (about 1.6 % of the new cases) and located to over 90 % in the brain (G. B. D. Brain & Other, 2019; Sung et al., 2021). Diagnosis of brain tumors is done using magnetic resonance imaging (MRI) or positron emission tomography (PET) to determine the location and size of the tumor (Price & Gillard, 2011; Shukla et al., 2017; Verger & Langen, 2017). Contrast-enhancing substances are thereby applied which can detect a disruption of the blood-brain barrier (BBB) which might be an indicator for malignant tumors due to angiogenesis and metastasis (Nduom et al., 2013; Tiwary et al., 2018). However, most of the time brain tumors are diagnosed when the patients experience the first side effects, such as constant headaches or motor and speech deficits (Dhall, 2009; Wirsching et al., 2016). Due to the rapid growth of malignant brain tumors, the patient can develop severe limitations within a few months (Alther et al., 2020; Chang et al., 2005; Wilne et al., 2006). The treatment and outcome of brain tumors are very diverse, as low-grade glioma e.g. astrocytoma or oligodendroglioma, are highly responsive to treatment, while high-grade glioma e.g. glioblastoma (GBM) are not (Goodenberger & Jenkins, 2012; Oberheim Bush & Chang, 2016; Schiff et al., 2007). In addition, treatment of brain tumors is more challenging compared to other tumor types as pharmaceuticals must first pass through the BBB, a semipermeable barrier consisting of endothelial cells that regulates the exchange of molecules between the blood and CNS (Daneman, 2012; Risau & Wolburg, 1990; Zlokovic, 2008). Thus, compounds have to pass the BBB to be effective for treatment and still need to reach an effective plasma concentration.

In 1979, the World Health Organization (WHO) implemented a CNS tumor grading and classification system which is regularly updated, last in 2021 (Louis et al., 2016; Louis et al., 2021; WHO Classification of Tumours Editorial Board, 2021; Zulch, 1979). Based on histopathological characteristics such as necrosis, proliferation, and mitotic activity, tumors are classified in one of four grades (Figure 1). In 2021 the WHO added molecular markers to the classification system of the tumors as they gain more importance during diagnosis (Louis et al., 2021). Grade I tumors have a low proliferation rate and are treated by surgical resection while grade II tumors have a higher recurrence rate and can gain more malignancy.

Introduction

Grade III tumors have atypical cell structures and aggressive treatments using chemotherapeutics are necessary. Grade IV tumors are highly differentiated, are most aggressive, and show the poorest survival rate (Kernohan et al., 1949). Common grade IV brain tumors are e.g. medulloblastoma (MB) in children and GBM in adults.

Grade I	Grade II	Grade III	Grade IV
Low proliferative potential	Low proliferative potential	High proliferative potential	High proliferative potential
Possibility of cure after surgical resection	Infiltrative	Infiltrative	Highly infiltrative
Differentiated cells	Moderately differentiated cells	Poorly differentiated cells	Undifferentiated cells
Not common to recur	Might recur as a higher grade	High chance to recur as higher grade	Rapid recurrence
Pilocytic astrocytoma, Gangliocytoma	Pineocytoma, Diffuse astrocytoma	Anaplastic astrocytoma, Anaplastic oligodendroglioma	Medulloblastoma, Glioblastoma



Figure 1 WHO classification of brain tumor.

Tumor brains are distinguished into four different tumor grades based on their malignancy. Grade I tumors are the least malignant tumors and can be treated by surgical resection alone. Brain tumors with a higher grade have the potential to infiltrate the surrounding tissue and might recur as a higher grade tumors. The figure was adapted from Rao and Karunakara (2021).

1.2 Medulloblastoma

In children, most solid tumors are brain tumors, of which 10-20% are classified as MB, the most common malignant brain tumor in children (Rossi et al., 2008; Ward et al., 2014). Bailey and Cushing first described MB in 1925 (Bailey & Cushing, 1925). The tumor originates in the cerebellum or *posterior fossa* and can metastasize to other parts of the CNS. In adults the development of MB is less likely as the origin of MB is assumed to be from embryonic cells (Giordana et al., 1999). In addition, treatment of adult MB is more challenging as the transcriptome of MB in adults is different from that of children and different treatment regimens have to be applied as adults do not tolerate cytotoxic chemotherapies as well as

Introduction

children (Beier et al., 2018; Brandes & Franceschi, 2014; Korshunov et al., 2010; Parsons et al., 2011). The overall survival of MB patients after 5 years is about 70 %, but highly dependent on age and subtype (Grill et al., 2005; Rutkowski et al., 2005). Children with a recurrence of MB have a lower survival rate and after 5 years about 12 % are still alive (Johnston et al., 2018). Further, an improvement in treatment is highly necessary due to the side effects of the current aggressive treatment. Especially, children develop secondary tumors years after the initial treatment or have psychological and neurological deficits due to the aggressive treatment (Glauser & Packer, 1991; Goldstein et al., 1997; Packer et al., 1989). Treatment of MB includes at first surgical resection, whereby maximal resection of the tumor already provides better survival chances for the patients. Since the 1950s craniospinal irradiation and since the 1990s chemotherapy is additionally applied for treatment of MB (Martin et al., 2014; Thompson et al., 2020). Add-on therapy is decided on various factors e.g., if the tumor has metastasized, indications of anaplasia and amount of remaining tumor tissue. For patients older than 3 years, the radiation dose depends on the aggressiveness of the tumor and the tumor site gets a high-dose treatment to prevent recurrence (Quinlan & Rizzolo, 2017). Further, the WHO identified four molecular subtypes: wingless-related integration site (WNT), SHH, Group 3, and Group 4 with different survival chances and different affected age groups. For all age groups, the identification of molecular subgroups offers the chance to identify pathway-specific inhibitors which can be used for treatment. New approaches using small molecules and viruses are tested to further improve the treatment (Romer & Curran, 2005; Studebaker et al., 2010; Xiao et al., 2015). Additionally, new technology and the close cooperation between research and clinic allow new precision medicine approaches. For example, tumor material from patients is used for *in vitro* screenings where hundreds of drugs can be tested within a short time frame (Nickel et al., 2021). This offers a fast transfer from workbench-to-bedside if common treatment approaches e.g., standard of care using cisplatin, radiation, and chemotherapy are not sufficient enough. As a result of improvement in treatment, children now have an overall survival rate of 60 % (high-risk) or up to 80 % (average-risk; (Gajjar et al., 2006; Ramaswamy & Taylor, 2017; Rutkowski et al., 2010; Taylor et al., 2003)). High-risk patients have a residual tumor after surgery from ≥ 1.5 cm, and are sorted into the Chang staging system using the four groups (M1 to M4) to describe the status from the extent of metastases, where group one describes microscopic metastases while group M4 describes metastases outside the cerebrospinal axis (Chang et al., 1969; Zeltzer et al., 1999). Depending on the subtype, recurrence of the tumor is observed in about one third of these cases at the same or a different site. Interestingly, it was observed that the subgroup does not change at recurrence (Ramaswamy et al., 2013). Therefore, an improvement of new

treatment options is necessary to offer children a better prognosis and reduce these adverse effects.

1.2.1 MB subgroups

In 2010, an international panel of experts classified MB tumors into four distinguished groups, which can be further divided into different subtypes (Cavalli et al., 2017; Cho et al., 2011; Kool et al., 2012; Kool et al., 2008; Northcott, Jones, et al., 2012; Taylor et al., 2012). Classification of MBs is based on molecular expression profiles of the tumor and defined diagnostic criteria, e.g. clinical symptoms and imaging (Kool et al., 2012; Northcott, Korshunov, et al., 2011; Thompson et al., 2006). Unlike other tumors, where histopathologic markers play a major role in the diagnosis, they are not considered in the classification of MBs, as similar markers might be found in each subgroup. However, each subgroup is considered to have a different cell of origin (Figure 2). In most cases, recurrent tumors belong to the same subgroup as the primary tumor, regardless of the tumor site (Ramaswamy et al., 2013). Altogether, the applied classification system allows for the prediction of survival, and it is the aim to develop subgroup-specific treatments to provide the best outcome for patients (Gottardo et al., 2014; Ray et al., 2021; Taylor et al., 2012). The MB tumors are divided into four subtypes: WNT, SHH, Group 3, and Group 4 (Figure 2). In 2021 the classification system was adapted by the WHO according to the new data. For example more subtypes were identified for the molecular subgroups, e.g. Group 3 and Group 4 consist of eight subtypes in total based on the DNA methylation profile (WHO Classification of Tumours Editorial Board, 2021). Further, molecular markers gain even more importance and the SHH subgroup is separated into *TP53*-wildtype and *TP53*-mutant (WHO Classification of Tumours Editorial Board, 2021). In this thesis, the classification system of the WHO was used before it was revised in 2021 (Figure 2).

Introduction

	WNT			SHH			Group 3			Group 4		
Frequency	9 %			29 %			19 %			43 %		
Subtypes	WNT α	WNT β	SHH α	SHH β	SHH γ	SHH δ	Group 3 α	Group 3 β	Group 3 γ	Group 4 α	Group 4 β	Group 4 γ
Age	Children, teens	Teens, adults	Infants, children	Infants	Infants	Adults	Infants, children	Children, teens	Infants, children	Infants, children	Infants, children	Infants, children
5-year survival rate	97 %	100 %	70 %	67 %	88 %	89 %	66 %	56 %	42 %	67 %	75 %	83 %
Origin	Cells in the lower rhombic lip			Cerebellar granule neuron progenitors			Uncertain			Uncertain		
Anatomical location	Midline, dorsal brainstem			Cerebellar hemisphere			Midline			Midline		

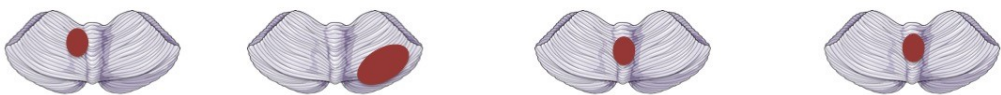


Figure 2 Overview of medulloblastoma subtypes.

Overview of the four medulloblastoma (MB) subgroups. Each subgroup can be further distinguished into different subtypes. Depending on the age of the patients the subtypes and survival chance after 5 years can be different. The age is defined as follows: Infant 0-3 years, children >3 – 10 years, teens >10 – 17 years, and adults >17 years. The origin of each subgroup could be identified, yet the origin of Group 3 and Group 4 is still uncertain. The figure was adapted from Cavalli et al. (2017) and Juraschka and Taylor (2019). The figure was partly created using Servier Medical Art, provided by Servier, licensed under a Creative Commons Attribution 3.0 unported license (<https://smart.servier.com>).

In the WNT subgroup, the signature mutation is in the β -catenin 1 (*CTNNB1*) gene which is responsible for the activation of the WNT pathway, and the cell of origin in this subgroup appears to be from the lower rhombic lip (Gibson et al., 2010; MacDonald et al., 2009). Under normal circumstances, the WNT pathway is important during embryonic development and in maintaining stem cell pluripotency, as well as in regulating cell growth and proliferation (Komiya & Habas, 2008). However, up to 90 % of WNT subtype tumors have a mutation in the *CTNNB1* gene that results in constant activation of the WNT pathway by the accumulation of *CTNNB1* in the nucleus (Jiang et al., 2014; Morin et al., 1997). The remaining 10 % have variants of the adenomatous polyposis coli (*APC*) gene, which is an interaction partner of *CTNNB1* and responsible for its degradation (Rubinfeld et al., 1993; Su et al., 1993; Waszak et al., 2018). The WNT subtype is also characterized by loss of one copy of chromosome 6, which is detected in 85 % of cases and is associated with a favorable prognosis when combined with mutations in *CTNNB1* (Northcott, Shih, et al., 2012). In general, this subgroup has the best prognosis with survival rates of 95 – 100 % (Kool et al., 2012; Massimino et al., 2016; Taylor et al., 2012). Patients have a good prognosis, including treatment by surgery and radiation (Kool et al., 2012).

Activation of the sonic hedgehog (SHH) pathway describes the second MB subgroup and includes about 30 % of all MBs (Kool et al., 2012). The SHH pathway regulates cellular differentiation, organ formation, and later tissue regeneration during embryogenesis

Introduction

(Choudhry et al., 2014; Simpson et al., 2009). Common markers of the SHH subtype are gene mutations in Patched1 (*PTCH1*), smoothed (*SMO*) and suppressor of fused homolog (*SUFU*), or amplification of glioma-associated oncogene 1 (*GLI1*) and *GLI2* (Kool et al., 2008; Northcott et al., 2017). A predisposition to the development of MB was found in patients who are carrying germline mutations in *PTCH1* or *SUFU*, as well as patients with e.g. Li-Fraumeni syndrome (Northcott, Korshunov, et al., 2011; Rieber et al., 2009; Taylor et al., 2002; Taylor et al., 2012). In patients with the Li-Fraumeni syndrome, a mutation of *TP53* is commonly observed to increase the risk of highly malignant cancers (Correa, 2016; Mai et al., 2016). SHH MB mostly occurs in infants (until the age of 3) and adults, representing 65 % and 71% of all infant and adult MBs, respectively, and is believed to originate in granule cell precursors (Leary & Olson, 2012; Northcott, Hielscher, et al., 2011; Schüller et al., 2008; Yang et al., 2008). In general, the prognosis is intermediate but survival chances are higher if the patients are younger (Kool et al., 2012). The SHH subgroup can be further divided into four subtypes, SHH α , SHH β , SHH γ , and SHH δ (Figure 2). Each subtype has an additional common mutation and affects different age groups and their prognosis (Cavalli et al., 2017). For example, the subtype SHH α has an additional tumor protein 53 (*TP53*) mutation that increases the aggressiveness of the tumor and is predominant in patients between the age of 3 – 16 years of age (Zhukova et al., 2013).

The third MB subgroup is characterized by the gain or loss of longer DNA fragments instead of specific genes and pathways and is classified/characterized by myelocytomatosis oncogene (*MYC*) amplification and occurrence of isochromosome 17q (Hatten & Roussel, 2011; Kool et al., 2008; Northcott, Jones, et al., 2012; Pan et al., 2005). Further, genes involved in the signaling pathways of notch and *TGF- β 1* (*TGF- β 1*) were found to be overexpressed in this subgroup (Lin et al., 2016; Northcott et al., 2017; Northcott, Shih, et al., 2012). Analysis at the epigenetic level revealed enhancer-hijacking, in which regulatory elements are translocated near coding regions (Menyhárt et al., 2019). Similar to the SHH MB subgroup this group can be subdivided into three additional subtypes, Group 3 α , Group 3 β , and Group 3 γ (Cavalli et al., 2017). Group 3 γ has a survival rate of 42 %, probably due to the amplification of *MYC*, while Group 3 α and Group 3 β have a moderate survival prognosis of 66 % and 56 %, respectively (Aggarwal et al., 2018). *MYC* is commonly mutated in cancer diseases and increases their aggressiveness by e.g., promoting metastases. Consequently, Group 3 patients show a higher rate of metastases in comparison to the other subgroups (Northcott, Korshunov, et al., 2011). The cell of origin is still controversial, but it is assumed to be a postnatal neuroepithelial stem cell protein (NESTIN) positive cerebellar progenitor cell (Louis et al., 2016; Schüller et al., 2008; Vladoiu et al., 2019; Yang et al., 2008). Overall, Group 3 tumors have the worst outcome in patients compared to all other subtypes. Depending on the treatment and age the 5 years of overall survival is around 50 %.

Introduction

The majority of MB tumors, about 35 – 40 %, are classified as Group 4 tumors. Similar to the Group 3 classification, it is based on transcriptional profiles instead of specific genes or pathways. Amplification of myelocytomatosis oncogene N (*MYCN*), isochromosome 17q, and nucleotide variants in lysine demethylase A (*KDM6A*) are commonly detected as well as enhancer-hijacking to overexpress putative histone-lysine N-methyltransferase (Kool et al., 2012; Menyhárt et al., 2019). The Group 4 tumors can be subdivided into three subtypes, Group 4 α , Group 4 β , and Group 4 γ and have a survival rate of 67 %, 75 %, and 83 %, respectively (Cavalli et al., 2017). The cell of origin of this subgroup is yet unknown.

1.3 GBM

Glioblastomas (GBM) belong to the glioma group of brain cancers and are classified as grade IV tumors (Ostrom et al., 2014). In 90 % of the cases, GBM arises *de novo* and only 10 % of the cases develop from a previously diagnosed low-grade glioma II or III (Louis et al., 2016; Ohgaki & Kleihues, 2013). GBM is characterized by high heterogeneity and infiltration of the surrounding healthy brain tissue (Shergalis et al., 2018; Wilson et al., 2014). Therefore, the possibilities for the removal of tumor tissue are limited and a high recurrence rate is observed. Within five years after the initial treatment and tumor removal, GBM recurrence occurs in 90 % of the patients (Weller et al., 2013). Most of the recurrent GBMs occur at the original tumor site, however they have a worse prognosis than the primary tumor (Choucair et al., 1986; Gaspar et al., 1992; Sonoda et al., 2014). The heterogeneity and genetic stability of the recurrent tumor depend on the subtype itself, but generally, about 50 % of the recurrence tumors belong to the same subgroup as the primary tumor (Behnan et al., 2019). The origin of this highly aggressive tumor is still unclear and a matter of debate within the scientific community. Several suggestions are made e.g. neural stem cells, glial precursors, or oligodendrocyte precursor cells (Yao et al., 2018).

Within the last decade, the molecular classification system gained importance for the prognosis, treatment approach, and prediction of patient survival. In addition, the O-6-methylguanine-DNA methyltransferase (*MGMT*) promoter methylation and isocitrat dehydrogenase 1 (*IDH1*) and isocitrat dehydrogenase 2 (*IDH2*) mutation status have been identified as clinically relevant markers (Hegi et al., 2005; Louis et al., 2016; Louis et al., 2021). Both markers can predict better or less aggressive disease progression. For example, patients carrying an *IDH1* mutation have a survival rate of 31 months in comparison to the *IDH1* wildtype with 15 months because the disease progresses more slowly (Dekker et al., 2022; S. Han et al., 2020; Yan et al., 2009). In 2021 the new WHO classification system was published and *IDH1*-mutant tumors are from now on classified as grade 4 astrocytomas instead of GBMs (WHO Classification of Tumours Editorial Board, 2021). As the new

Introduction

classification was published after the practical work of this thesis was completed, the *IDH1*-mutant tumors were still classified as GBM tumors. Therefore, all GBM tumors have according to the new classification system the *IDH1* wildtype gene (WHO Classification of Tumours Editorial Board, 2021).

All tumors classified based on tumor subgroup and age, GBM patients have a predicted mean survival of around 15 months after diagnosis under standard therapy (Ostrom et al., 2014; Weller et al., 2013). The standard of care for GBM includes maximal safe surgical resection, radiation therapy, and chemotherapy with temozolomide (TMZ, (Stupp et al., 2005)). In general, GBM diagnosis is made after the appearance of the first side effect symptoms, caused by increased cranial pressure leading to e.g. seizures or headaches. Computer tomography (CT) or MRI is then used to visualize the irregular cell mass and the center of necrosis, commonly found in GBM tumors (Raza et al., 2002). In addition, methylation analysis is performed as it has gained importance to determine the status of marker genes and in identifying molecular subgroups of GBM offering patients a better prediction. For example, a methylated *MGMT* promoter is an indication of a better prognosis, as this inactivates *MGMT* and prevents the repair of the DNA damage caused by TMZ treatment (Hegi et al., 2005; Stupp et al., 2009). Nevertheless, more radical resection has a significant impact on the overall survival of the patients (Q. Han et al., 2020). The chemotherapeutic TMZ crosses the BBB and initiates apoptosis in the cells by delivering a methyl group to purine bases of the DNA (O-6-guanine; N-7-guanine and N-3-adenine), which in the case of *MGMT* causes a mismatched base pair during DNA replication causing apoptosis of the cells (D'Atri et al., 1998; Roos et al., 2007; Shah et al., 2011). Recurrence of GBM tumors is high as the tumor is highly invasive into the surrounding tissue and resection of the primary tumor is limited due to the location of the tumor e.g. near to the area of speech or motor function (Molina et al., 2010). Therefore, new treatment approaches are tested to offer the patients a better prognosis and prolong their survival. In 2015 the FDA approved the application of tumor-treating fields (TTFields) after the standard of care. In this approach, alternating electrical fields interrupt the cell division leading to apoptosis, as the mitotic spindle cannot form properly (Kirson et al., 2007; Kirson et al., 2004). The first results indicate an increase in survival by 5 months (Stupp et al., 2015). Furthermore, new drugs have been approved for a single treatment or in addition to the standard of care. Clinical trials approach new treatment options where immune checkpoints or receptors are the target e.g. targeting chimeric antigen receptor (CAR) T cells (Han et al., 2019; Sanders & Debinski, 2020). The idea is to modify the CAR T cells to tumor-specific antigens and use the patient's immune system to treat the tumor (Fesnak et al., 2016; Zhang et al., 2017). However, many trials have failed due to the characteristics of GBM e.g., abnormal blood vessels, necrosis, and heterogeneous drug distribution. Another option would be the enhancement of drug

Introduction

delivery by manipulation of the BBB as the endothelial cells shrink due to the osmotic exposure (Rapoport, 2001; Siegal et al., 2000). Currently, several approaches to GBM treatment are tested and clinical trials are conducted (Aldoghachi et al., 2022; Cruz Da Silva et al., 2021; Yuan et al., 2022).

1.3.1 GBM Subgroups

Several approaches have been made to classify GBM tumors to better understand their development and progression. One approach is the molecular classification based on gene expression profiles performed by Verhaak et al. (2010). Around 260 publicly available expression profiles of GBMs were analyzed and clusters were identified, that were used to classify four GBM subgroups (Network, 2008; Verhaak et al., 2010). These subgroups were subdivided based on the gene expression or previous designations into classical, mesenchymal, neural, and proneural (Verhaak et al., 2010). However, xenograft studies could not recreate the neural subtype and therefore it was later removed from the classification system due to the similarity to neural tissue in general (Behnan et al., 2017; Gill et al., 2014; Sidaway, 2017; Verhaak et al., 2010). Therefore, the classification of GBMs is done into three subgroups (Table 1). Furthermore, patients' *IDH1* status was included as a clinically relevant marker in the classification system of GBMs by the WHO (Louis et al., 2016). Since 2021 *IDH1*-mutant tumors are not classified as GBM anymore, but as astrocytomas (WHO Classification of Tumours Editorial Board, 2021). As the new classification was published after the practical work of this thesis was completed, the *IDH1*-mutant tumors were still classified as GBM tumors. About 90 % of the GBM patients have *IDH1* wild-type status and only 10 % have a mutation, that is commonly found in younger patients and secondary GBMs (Ichimura et al., 2009; Louis et al., 2016). For example, the point mutation R132H of *IDH1* was observed in 73 % of the secondary GBMs (Nobusawa et al., 2009). Through enzymatic function, this mutation causes an accumulation of oncometabolites which support the migration of tumor cells (Dang et al., 2009; Lu et al., 2019). In general, patients having a secondary GBM have a better overall survival (Nobusawa et al., 2009; SongTao et al., 2012). In 2021, the WHO adapted the tumor grading and classification of CNS tumors.

Table 1 Overview of the glioblastoma subgroups.

Overview of the three glioblastoma (GBM) subgroups. For each subgroup's characteristic mutations or deletions were identified. Further, the age group, as well as the survival after diagnosis, depends on the GBM subgroup. The figure was adapted from Scheer et al. (2022). del, deletion; ampl., amplification; mut., mutation.

	Classical	Mesenchymal	Proneural
Frequency [%]	36	39	25
Mutation	<i>CDKN2A</i> del.	17q11.2 del.	<i>CDKN2A</i> del.
	<i>EGFR</i> ampl./mut.	<i>NF1</i> mut.	<i>PDGFRA</i> ampl.
	<i>PTEN</i> mut.	<i>RB1</i> mut.	<i>IDH1</i> mut.*
Age group	> 60 years	All ages	< 40 years
Survival [months]	14.7	11.5	17

*according to WHO classification before 2021

The classical GBM subgroup is defined by amplification of chromosome 7 and at the same time loss of chromosome 10 (Verhaak et al., 2010). Epidermal growth factor receptor (*EGFR*) is located on chromosome 7 and EGFR protein accumulates in nearly 40 % of all GBM tumors (Libermann et al., 1985; Wong et al., 1987). In half of these tumors a deletion between exons 2 and 7, so-called epidermal growth factor receptor variant 3 (*EGFRvIII*), can be found (Ekstrand et al., 1992; Sugawa et al., 1990). The deletion results in the absence of the ligand-binding site from the extracellular domain and thus a constitutively active *EGFR* that stimulates the growth in GBM through EGFR-regulated processes. A deletion of cyclin-dependent kinase inhibitor 2A (*CDKN2A*) is also frequently found in the classical GBM-type (Verhaak et al., 2010). Expression of the Notch and SHH signaling pathways, and the neural precursor and stem cell marker NESTIN are upregulated in the classical subgroup (Verhaak et al., 2010).

The mesenchymal subgroup is characterized by lower neurofibromin 1 (*NF1*) expression due to deletion or mutation of the gene, high expression of microglial markers, and signs of inflammatory signaling pathways (Phillips et al., 2006; Verhaak et al., 2010). Most of the time the tumor samples also had a co-mutation of phosphatase and tensin homolog (*PTEN*) and expression of mesenchymal markers. Verhaak et al. (2010) also identified a higher activity of mesenchymal and astrocytic markers, e.g. CD44 molecule (*CD44*) and MER proto-oncogene tyrosine kinase (*MERTK*). The mesenchymal subgroups seem to be more aggressive in comparison to the other subgroups based on transcriptomic analysis (Kim et al., 2021). This might be due to the transmembrane protein CD44 as it supports tumor growth and migration

Introduction

(Si et al., 2020). Migration of the tumor is associated with the epithelial-to-mesenchymal transition (EMT) as the tumor cells lose their polarity and can migrate to other tissues or sites and metastasize (Micalizzi & Ford, 2009; Thiery, 2002). Further, recurrent tumors often belong to the mesenchymal subgroup. It is assumed that molecular events support a transition similar to EMT, which is known from several cancer diseases e.g. breast, bladder or colon cancer (Adam et al., 2009; Brabletz et al., 2005; Fedele et al., 2019; Kahlert et al., 2013; Kalluri & Weinberg, 2009; Trimboli et al., 2008). The mesenchymal state is thought to promote metastasis and chemo-resistance (Fedele et al., 2019; Jia et al., 2018; Sui et al., 2014; Thiery, 2002).

The proneural subgroup of GBM was already characterized in 2016 and is commonly found in younger patients (Phillips et al., 2006). In expression analysis, this GBM subgroup reveals a high similarity to normal brain tissue as oligodendrocytic genes like the platelet-derived growth factor receptor alpha (*PDGFRA*), are found. The *IDH1* mutation improves the prognosis of the GBM patients as the proneural subgroup was found to be more aggressive after excluding *IDH1*-mutant patients (Sturm et al., 2012; Yan et al., 2009). However, the WHO revised the GBM classification system in 2021. Tumors with *IDH1* mutations are now classified as astrocytomas and no longer belong to the group of GBMs. All GBM tumors must have a *IDH1* wild-type status.

Additional mutations to the subgroup-specific mutations, so-called background mutations, are also commonly found in GBM. *TP53* is a tumor suppressor and crucial during the G1 phase of the cell cycle to maintain homeostasis (Zhang et al., 2018). In half of all cancer diseases, *TP53* is mutated and supports tumor development and growth (Liu et al., 2010). In all GBM subgroups, except for the classical subgroups, a *TP53* mutation can be found (Verhaak et al., 2010). Comprehensive genomic characterization defines human GBM genes and core pathways. A common point mutation in GBM is *TP53R175H*, where arginine is exchanged through histidine causing a structural change that leads to the immortalization of the cells (Sigal & Rotter, 2000).

1.4 Cancer stem cells

Stem cells describe an entity of cells that are undifferentiated, have the ability to self-renew, and can develop into any kind of cell of the body. Parts of these characteristics were also found in a group of tumor cells, which are called cancer stem cells (CSCs). In 1997, CSCs were described for the first time in acute myeloid leukemia (Bonnet & Dick, 1997). Over the years several observations have been made about CSCs. A small number of isolated cells, assumed CSCs, from a tumor can initiate tumor development in immunodeficient mice (Furth

Introduction

et al., 1937). CSCs can be separated from the tumor mass due to the expression of surface markers such as CD44 and CD133 (Al-Hajj et al., 2003; Glumac & LeBeau, 2018; Uchida et al., 2000). Serial xenotransplantation of CSCs confirms their self-renewal capacity as they initiate tumor development including tumorigenic and non-tumorigenic cells (Clarke et al., 2006; Prince & Ailles, 2008; Reya et al., 2001). In non-adherent cell cultures CSCs can form spheres and in the case of brain CSCs generation of brain cells like astrocytes, neurons, and oligodendrocytes was achieved (Chen et al., 2012; Reynolds et al., 1992; Reynolds & Weiss, 1992; Singh et al., 2003). Furthermore, it was shown that CSCs can be more resistant to chemotherapy (Ahmed et al., 2017; Dean et al., 2005; Visvader & Lindeman, 2008; Zhao, 2016).

Over the years, several studies have been conducted to identify CSCs in brain tumors and confirmed their existence in MB and GBM (Galli et al., 2004; Hemmati et al., 2003; Singh et al., 2003; Yuan et al., 2004). For example, cells expressing the surface marker CD133 initiated glioma growth in immunodeficient mice and were called brain tumor-initiating cells (Singh et al., 2004). This is in agreement with the observation that after radiation a higher number of CD133 positive cells were seen in glioma and recurrent GBM in comparison to healthy brain tissue (Bao et al., 2006; Liu et al., 2006). CD133 is a cell surface marker and is used to isolate CSCs from the tumor tissue (Kim & Ryu, 2017). In MB on the other site, the surface marker CD15 was identified as an indicator of CSCs (Lowry & Temple, 2009; Read et al., 2009). CD15 is a marker for myeloid differentiation (Gooi et al., 1983). Due to the resistance towards apoptosis-inducing treatments, CSCs might initiate the recurrence or metastasis of tumors. It is assumed that CSCs have a niche and that e.g. endothelial cells keep the CSCs in GBMs in a self-renewal state through signaling including e.g., WNT, Notch, and SHH (Calabrese et al., 2007; Takebe et al., 2011). In addition, it could be shown that CSCs derived from a patients' tumor initiate the same tumor with chemotherapy resistance in xenotransplants (Valent et al., 2012). However, the development of CSCs is still controversial and several hypotheses exist. One theory is, that stem cells gain mutations over time and differentiate into cancer cells, while another one suggests that progenitor cells gain mutations, which give them again the ability to self-renew (Cozzio et al., 2003; Jamieson et al., 2004).

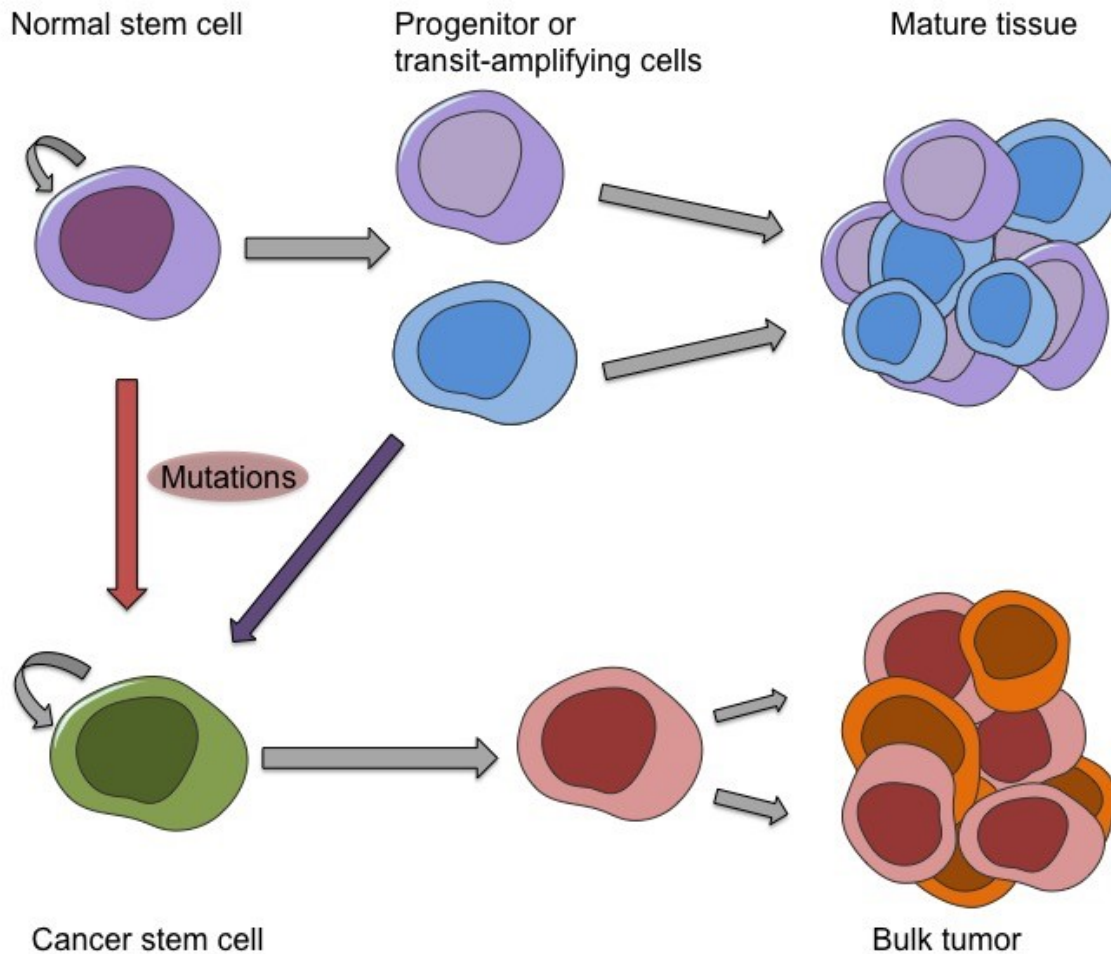


Figure 3 Simplified model about the origin of cancer stem cells.

Several hypothesis about the origin of CSCs exists. One hypothesis is that progenitor cells accumulate mutations and gain the ability for self-renewal while another one suggests that stem cells gain the mutation (Cozzio et al., 2003; Jamieson et al., 2004). The figure was adapted from Jordan et al. (2006). The figure was created using Servier Medical Art, provided by Servier, licensed under a Creative Commons Attribution 3.0 unported license (<https://smart.servier.com>).

1.5 Human induced pluripotent stem cells (hiPSCs)

In 2006 Yamanaka published a new method to reprogram somatic mouse cells into so-called induced pluripotent stem cells (iPSCs) and in 2012 received the Nobel Prize in Physiology or Medicine for this discovery (Takahashi & Yamanaka, 2006). He and his colleagues showed that the generation of iPSC was achieved through the retroviral transduction of mouse fibroblasts using four transcription factors: octamer-binding transcription factor 4 (*OCT4*), Krüppel-like factor 4 (*KLF4*), SRY-box transcription factor 2 (*SOX2*) and *c-MYC* (Takahashi & Yamanaka, 2006). The generated cells revealed high similarities to embryonic stem cells (ESCs) as they were pluripotent and had self-renewal capacity. In the following year, human somatic cells were reprogrammed to human iPSCs (hiPSCs) for the first time (Takahashi et

Introduction

al., 2007; Yu et al., 2007). Additionally, the four factors *OCT4*, *SOX2*, Nanog homeobox (*NANOG*), and lin-28 homolog A (*LIN28*) were proven to be sufficient to generate hiPSC as well (Yu et al., 2007). The first introduced reprogramming approaches were based on retroviral delivery, which caused a high expression of the target genes but also a random integration into the genome (Zhou & Zeng, 2013). Utilization of the transcription factors *OCT4*, *c-MYC*, and *SOX2* during reprogramming, increased tumor development through reactivation (Okita et al., 2007). Over the years, several other reprogramming methods were published to prevent the occurrence of side effects. Therefore, new reprogramming techniques were applied using lentiviral, adenoviral, or non-viral systems using for example episomal plasmids (Hotta et al., 2009; Malik & Rao, 2013; Okita et al., 2008; Somers et al., 2010; Stadtfeld et al., 2008). It is also possible to directly reprogram cells without the pluripotent state, which reduces the time needed for model generation (Liu et al., 2020). Each method has its advantages and disadvantages e.g., efficiency and integration (Karagiannis et al., 2019; Malik & Rao, 2013). Pluripotency of hiPSCs is verified by the ability of these cells to differentiate into cells of the three germ layers: endoderm, mesoderm, and ectoderm. Further, formation of teratomas and expression of pluripotency markers e.g., tumor rejection antigen 1-60 (TRA-1-60), tumor rejection antigen 1-81 (TRA-1-81), and octamer-binding transcription factor 3/4 (*OCT3/4*) can be used for the validation of pluripotency (Pamies et al., 2017; Schopperle & DeWolf, 2007). Human iPSCs have the advantage that a donation of any tissue, such as skin or blood, and even urine, is enough to generate a viable cell culture with unlimited proliferative potential and has the potential to replace the previous sources of pluripotent stem cells, human embryonic tissues, or mouse embryos, which are ethically more problematic and in the latter case bare the problem of species differences (Liu et al., 2020; Wert & Mummery, 2003; Yee, 2010; Zhou et al., 2011). Further, the application of hiPSC in personalized medicine can overcome immunorejection responses as the cells are obtained from the patient and the cells have the genetic background of the patient which can be used for treatment recommendations and disease analysis (Hackett & Fortier, 2011). In summary, since their discovery in 2007, hiPSCs gained highly in significance due to their high potential in helping to understand disease development, progression, and treatment.

Introduction

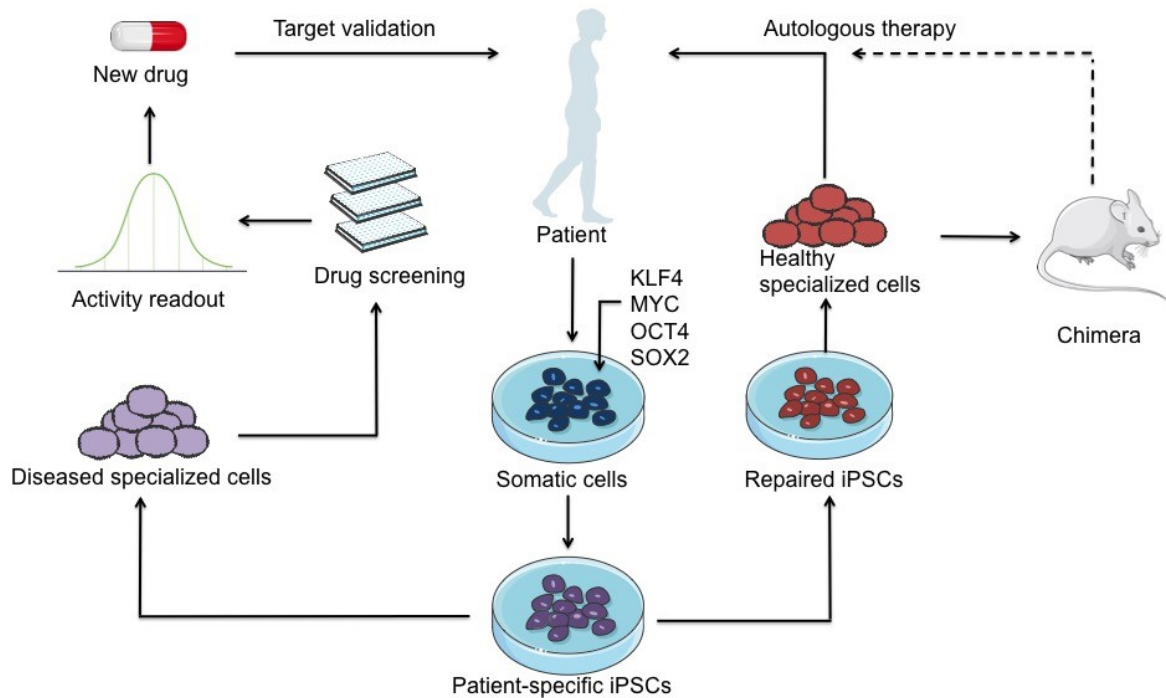


Figure 4 Overview over the usage of hiPSC.

Human iPSCs are generated from somatic cells through reprogramming using transcription factors. Afterward, hiPSCs can be used for different approaches. Generated hiPSCs are used to optimize the treatment of diseases through utilization of the hiPSCs in drug screening and getting a better understanding of the disease. Further, hiPSCs are utilized for personalized disease treatment. Mutations in patient specific hiPSCs are repaired through genetic modification. Afterward, hiPSCs are differentiated into the desired cells and reimplanted into the patient. The figure was adapted from Rowe and Daley (2019). The figure was created using Servier Medical Art, provided by Servier, licensed under a Creative Commons Attribution 3.0 unported license (<https://smart.servier.com>).

1.5.1 Neural Differentiation of hiPSCs

Human iPSCs keep their stem cell characteristics *in vitro* through several factors e.g., constant exposure to specific growth factors, cell-cell communication, and cytokines (van der Sanden et al., 2010; Yan et al., 2014). If these conditions are changed, hiPSCs can be forced to differentiate into any desired cell type (Eglen & Reisine, 2018). Several differentiation protocols were established using ESCs instead of hiPSCs and later on commercial kits were available, offering optimized protocols for successful differentiation of hiPSCs to e.g., neural structures with high efficiency (Chambers et al., 2009; Denham & Dottori, 2011; Hu et al., 2010; Zahumenska et al., 2020). Brain tissue is derived from the ectoderm, one of the three germ layers. Thus, to generate models of the CNS the hiPSCs need to be differentiated into the ectodermal lineage. One ectodermal differentiation approach is to prevent the differentiation into mesodermal and endodermal directions by inhibiting the *TGF- β 1* and the bone morphogenetic protein (BMP) pathway. For instance, hiPSCs can be differentiated into neural progenitor cells (NPCs) by blocking *TGF- β 1*/BMP-dependent cell differentiation also known as dual SMAD inhibition (SMADi), and can be

Introduction

further differentiated into neurons or glia cells (Chambers et al., 2009; Denham & Dottori, 2011; Hofrichter et al., 2017). These differentiation protocols are applied to develop *in vitro* models for testing (Porterfield, 2020).

This offers the opportunity to introduce tumor-specific mutations into the iPSCs *in vitro* before they are differentiated to better understand the disease, the development, the progression, or even to test new treatment approaches, and then differentiate them into the cell type of interest for further experiments. Within the last years, *in vitro* testing gained more importance due to the feasibility, time, and throughput in compound screening. For example, the iPSC-derived induced neural progenitor cells (iNPCs), can be further differentiated into e.g., neurospheres (Nimtz et al., 2020; Uemura et al., 2012). These generated neurospheres can help to reduce the costs of new drug developments as they can be applied for *in vitro* screening (Fritsche et al., 2011; Fukusumi et al., 2018; Hofrichter et al., 2017; Koch et al., 2022). These screenings can give an idea about the mode of action and efficacy of the investigated drug.

Since the development of hiPSCs, the aim is to utilize these cells in tumor research to better understand the development of tumors and improve the treatment (Karagiannis et al., 2019; Papapetrou, 2016). One approach is the reprogramming of somatic cells which contain the desired mutation into hiPSCs and differentiate them into neural tissue before they are transplanted into animals (Susanto et al., 2020). Another approach combines the ideas to generate hiPSC-oncogene models and the tumor-growth in *in vivo* models. Koga et al. (2020) introduced one GBM-specific mutation into iPSCs using clustered regularly interspaced palindromic repeats (CRISPR)/ CRISPR associated protein 9 (Cas9) before the cells were injected into the flank of mice. One new emerging approach is the generation of three-dimensional organoids (Lancaster et al., 2013). These organoids can mimic brain tissue and can be discriminated into specific regions e.g., cortex and choroid plexus and a specific extracellular matrix even allows to stimulate the stem cell niche (Heo et al., 2022; Lancaster et al., 2013). It is also possible to perform co-cultivation of different cell types e.g., neurons and glial cells to better understand the interaction of the cells and the development of organs or tissues and therefore the development and progression of diseases (Kim et al., 2020). One example is the use of organoids during the Zika virus outbreak, which helped to understand the relationship between the Zika virus and microcephaly (Dang et al., 2016; Garcez et al., 2016).

1.6 Aim of this thesis

MB and GBM tumors have been known for a long time as highly aggressive brain tumors in children and adults, respectively. However, the treatment is still not sufficient enough as patients are suffering from side effects of the treatment or still have a poor survival prognosis. Within the last decades, the diagnosis of MB and GBM tumors has been constantly improving and it was possible to distinguish molecular subgroups for both tumors. It is now possible to give patients a better prognosis and it was also possible to adapt the treatment already for the first MB subgroups e.g., using less aggressive treatment with the same outcome. However, the aim is to offer each patient a treatment based on the unique expression profile of the tumor. As the establishment of proliferating cell culture from patient-derived tumor cells is challenging, established cell lines are used. Unfortunately, due to the *in vitro* cultivation of these cells, selection processes take place so that the cells do not represent the original tumor anymore. Therefore, this thesis aimed to develop hiPSC models with MB and GBM subgroup-specific mutations in a genetically stable background and utilize them for drug screenings. Specifically, the aims of this thesis were:

1. Generation of hiPSC-oncogene models which express subgroup-specific genes for MB and GBM.
2. Generation of a proliferating three-dimensional neurosphere culture using a neural differentiation protocol.
3. Molecular and functional characterization of the hiPSC-oncogene models as well as of the derived three-dimensional neurospheres.
4. Utilization of the generated models in pharmacological screenings to test their applicability to identify subgroup-specific treatments.

2 Material and Methods

2.1 Materials

2.1.1 List of laboratory equipment

Laboratory equipment	Company
2D shaker	IKA®-Werke GmbH &CO. KG (Staufen, Germany) LAUDA-GFL (Lauda-Königshofen, Germany)
Accurate weighing scale	KERN & Sohn GmbH (Balingen, Germany)
Bacteria incubator	B.BRAUN Biotech International GmbH (Melsungen, Germany) Eppendorf (Hamburg, Germany)
Binocular Leica DMS1000	Leica Microsystems (Wetzlar, Germany)
CEA CAWOMAT 2000 IR (film developer)	CEA GmbH (Hamburg, Germany)
Cell culture incubator	Binder GmbH (Tuttlingen, Germany)
Cell culture sterile bench	Clean Air Techniek bv (Woerden, The Netherlands)
Cellomics ArrayScan VTI	Thermo Fisher Scientific™ (Waltham, Massachusetts, USA)
Flow cytometer	Becton, Dickinson, and Company (Franklin Lakes, NJ, USA) Cantor Beckman Coulter Diagnostics (Brea, California, USA)

Material & Methods

Gel imager	INTAS Science Imaging Instruments GmbH (Göttingen, Germany)
Heating block	Eppendorf (Hamburg, Germany)
LI-COR Odysseys CLX Imager	LI-COR Biosciences (Lincoln, Nebraska, USA)
McIlwain Tissue Chopper	Mickle Laboratory Engineering Co. Ltd (Guildford, United Kingdom)
Microscope	Nikon Inc. (Tokyo, Japan)
Nikon Eclipse Ti-S	Nikon Inc. (Tokyo, Japan)
Paradigm™ multiplate reader	Beckman Coulter (Pasadena, CA, USA)
Paradigm® microplate reader	Molecular Devices LLC (San Jose, CA, USA)
Phottometrics™ X1 camera	Thermo Fisher Scientific™ (Waltham, Massachusetts, USA)
Polymerase chain reaction (PCR) cyclers	Analytik Jena GmbH (Jena, Germany)
Power supply	Bio-Rad Laboratories (Hercules, California, USA)
Protean chamber WB	Bio-Rad Laboratories (Hercules, California, USA)
Safire multiplate reader	Tecan Group Männedorf, Switzerland
Table-top centrifuge	Hettich (Kirchlengern, Germany) Eppendorf (Hamburg, Germany)
Water deionizer	Merck Millipore (Darmstadt, Germany)

Material & Methods

2.1.2 Consumables

Consumable supplies	Company
10 cm dishes	Greiner Bio-One GmbH (Essen, Germany)
10 ml Syringe	B. Braun (Melsungen, Germany)
12-well plate	Greiner Bio-One GmbH (Essen, Germany)
15 ml conical tubes	Greiner Bio-One GmbH (Essen, Germany)
50 ml conical tubes	Greiner Bio-One GmbH (Essen, Germany)
6-well plate	Greiner Bio-One GmbH (Essen, Germany)
96-well plate	Greiner Bio-One GmbH (Essen, Germany)
Disposable serological pipettes	Thermo Fisher VWR International (Radnor, Pennsylvania, USA)
Falcon® Dishes	Corning Inc. (Corning, New York, USA)
Parafilm®	Pechiney (Paris, France)
PCR tubes	VWR International (Radnor, Pennsylvania, USA)
Pipette tips 1000 µl, 200 µl, 10 µl	STARLAB GmbH (Hamburg, Germany)
Safeseal reaction tube 1.5 ml	Sarstedt AG & Co. KG (Nümbrecht, Germany)
Serological pipette 5 ml, 10 ml, 25 ml, and 50 ml	Eppendorf (Hamburg, Germany) VWR International (Radnor, Pennsylvania, USA)

Material & Methods

Syringe filter 0.45 µm	VWR International (Radnor, Pennsylvania, USA)
Thermo CL-X Posure™ Film	Thermo Fisher Scientific™ (Waltham, Massachusetts, USA)
TipOne® Pipette filter tips 1000 µl, 200 µl, 20 µl, 20/10 µl	STARLAB GmbH (Hamburg, Germany)

2.1.3 Cell lines

Cell line	Organism	Cell type	Provider
HEK293T	<i>Homo sapiens</i>	Embryonic kidney	Provided by Astrid Weyerbrock (University Hospital Freiburg, Germany)
iPS11	<i>Homo sapiens</i>	Human induced pluripotent stem cell	Alstem, Inc. (Richmond, California, USA)

Material & Methods

2.1.4 Cell culture media components

Cell culture media components	Company
DMEM/F12 with 15 mM 4-(2-hydroxyethyl)-1-piperazineethanesulfonic acid (HEPES)	STEMCELL Technologies (Vancouver, Canada)
Fetal bovine serum (FBS)	Sigma-Aldrich (St. Louis, Missouri, USA)
Gibco™ DMEM high glucose, GlutaMAX™ Supplement, pyruvate	Thermo Fisher Scientific™ (Waltham, Massachusetts, USA)
Gibco™ Dulbecco's Modified Eagle Medium (DMEM), high glucose, no pyruvate	Thermo Fisher Scientific™ (Waltham, Massachusetts, USA)
Gibco™ Ham's F12 GlutaMax	Thermo Fisher Scientific™ (Waltham, Massachusetts, USA)
Gibco™ Knockout Serum Replacement (KSR)	Thermo Fisher Scientific™ (Waltham, Massachusetts, USA)
Gibco™ N-2 supplement	Thermo Fisher Scientific™ (Waltham, Massachusetts, USA)
Gibco™ B-27™ supplement	Thermo Fisher Scientific™ (Waltham, Massachusetts, USA)
human epidermal growth factor (hEGF)	PeptoTech Inc. (Rocky Hill, New Jersey, USA)
Humane fibroblast growth factor (hFGF)	PeptoTech Inc. (Rocky Hill, New Jersey, USA)
LDN-193189	Sigma-Aldrich (St. Louis, Missouri, USA)
mTeSR™ 1	STEMCELL Technologies (Vancouver, Canada)
NutriFreeze D10 Cryopreservation Medium	Biological Industries (Beit HaEmek, Israel)
Penicillin/Streptomycin (P/S)	Sigma-Aldrich (St. Louis, Missouri, USA)
Recombinant human basic FGF (bFGF)	R&D Systems Inc. (Minneapolis, Minnesota, USA)

Material & Methods

SB-431542	Sigma-Aldrich (St. Louis, Missouri, USA)
STEMdiff™ Neural Induction Kit	STEMCELL Technologies (Vancouver, Canada)

2.1.5 Media composition

Medium name	Composition	Cell line
mTeSR1™	89 % mTesR1 basal medium 10 % mTeSR1 Supplement 1 % P/S	hiPSC
DMEM/FBS	89 % DMEM GlutaMax 10 % FBS 1 % P/S	HEK293T
B27-Proliferation medium for iPS-neurospheres (NS)	64.4 % DMEM GlutaMax 32.2 % F12 GlutaMax 2 % B27 supplement 1 % P/S 20 ng/ml hEGF 20 ng/ml FGF	Differentiated human iNPCs
Differentiation medium (2D)	STEMdiff™ Neural Induction Medium SMADi	2D neural induction
Neural induction medium (NIM)	82.5 % B27 medium 0.83 % N2 supplement 16.5 % KSR 10 µM SB-431542 0.5 µM LDN-192189	3D neural induction

Material & Methods

2.1.6 Cell culture components

Cell culture component	Company
0.5 mM Ethylenediaminetetraacetic acid (EDTA) in DPBS -/-	Carl Roth GmbH + Co. KG (Karlsruhe, Germany)
Almotriptan malate	MedChemExpress LLC (Monmouth Junction, NJ, USA)
Apatinib mesylate	MedChemExpress LLC (Monmouth Junction, NJ, USA)
Calcium folinate	MedChemExpress LLC (Monmouth Junction, NJ, USA)
Cariprazine	APEX BIO Technology LLC (Houston, Texas, USA)
Corning® Matrigel® Matrix, growth factor reduced (MG)	Corning Inc. (Corning, New York, USA)
Dimethylsulfoxid (DMSO)	Sigma-Aldrich (St. Louis, MO, USA)
Duvelisib	MedChemExpress LLC (Monmouth Junction, NJ, USA)
Gentle Dissociation Reagent	STEMCELL Technologies (Vancouver, Canada)
Gibco™ Dulbecco Phosphate buffer saline without Magnesium and chloride (DPBS -/-)	Thermo Fisher Scientific™ (Waltham, Massachusetts, USA)
Gibco™ KnockOut™ (KO) DMEM	Thermo Fisher Scientific™ (Waltham, Massachusetts, USA)
Gibco™ Puromycin Dihydrochloride	Thermo Fisher Scientific™ (Waltham, Massachusetts, USA)
Gibco™ StemPro™ Accutase™ Cell Dissociation Reagent	Thermo Fisher Scientific™ (Waltham, Massachusetts, USA)
Gibco™ TrypLE™ Express	Thermo Fisher Scientific™ (Waltham, Massachusetts, USA)
Gibco™ TrypLE™ Select	Thermo Fisher Scientific™ (Waltham, Massachusetts, USA)

Material & Methods

Laminin	Sigma-Aldrich (St. Louis, MO, USA)
Lomustine	MedChemExpress LLC (Monmouth Junction, NJ, USA)
Panobinostat	MedChemExpress LLC (Monmouth Junction, NJ, USA)
Acetaminophen	Sigma-Aldrich (St. Louis, MO, USA)
Phosphate buffer saline without Magnesium and chloride (PBS-/-)	Biochrom GmbH (Berlin, Germany)
Poly-L-ornithine (PLO)	Sigma-Aldrich (St. Louis, MO, USA)
Rivastigmine	MedChemExpress LLC (Monmouth Junction, NJ, USA)
Staurosporine	Sigma-Aldrich (St. Louis, MO, USA)
Trypan blue solution 0.4 %	Thermo Fisher Scientific™ (Waltham, Massachusetts, USA)
UltraPure™ 0.5 M EDTA, pH 8.0	Thermo Thermo Fisher Scientific™ (Waltham, Massachusetts, USA)
Vinblastine sulfate	MedChemExpress LLC (Monmouth Junction, NJ, USA)
Rho-associated protein kinase Y-27632 2HCl (Rock-Inhibitor)	Selleck Chemical Llc (Houston, Texas, USA)

Material & Methods

2.1.7 Chemicals

Chemical / Reagent	Company
2x SYBR Green qPCR Master Mix	Bimake (Houston, TX, USA)
Agarose	AppliChem GmbH (Darmstadt, Germany)
Ampicillin sodium salt	Carl Roth GmbH + Co. KG (Karlsruhe, Germany)
Bovine serum albumin (BSA)	Sigma-Aldrich (St. Louis, MO, USA)
Bromphenol blue	Carl Roth GmbH + Co. KG (Karlsruhe, Germany)
Cold Fusion Cloning Kit	System Biosciences (Palo Alto, CA, USA)
Deoxycholic acid	Sigma-Aldrich (St. Louis, Missouri, USA)
DNA Gel Loading Dye (6x)	Thermo Fisher Scientific™ (Waltham, Massachusetts, USA)
FuGENE®	Promega Corporation (Madison, Wisconsin, USA)
GeneRuler 1kb DNA ladder	Thermo Fisher Scientific™ (Waltham, Massachusetts, USA)
Glycerol	Carl Roth GmbH + Co. KG (Karlsruhe, Germany)
Glycine	Carl Roth GmbH + Co. KG (Karlsruhe, Germany)
Hydrochloric acid (HCl) 25 %	Carl Roth GmbH + Co. KG (Karlsruhe, Germany)
Isopropanol	VWR International (Radnor, Pennsylvania, USA)
KnockOut™ Serum Replacement (KSR)	Thermo Fisher Scientific™ (Waltham, Massachusetts,

Material & Methods

	USA)
Lysogeny broth (LB)-Agar	Carl Roth GmbH + Co. KG (Karlsruhe, Germany)
LB-Medium	Carl Roth GmbH + Co. KG (Karlsruhe, Germany)
Moloney murine leukemia virus (M-MLV) reverse transcriptase	Promega Corporation (Madison, Wisconsin, USA)
β -Mercaptoethanol	Carl Roth GmbH + Co. KG (Karlsruhe, Germany)
Methanol	Carl Roth GmbH + Co. KG (Karlsruhe, Germany)
Milk powder	Carl Roth GmbH + Co. KG (Karlsruhe, Germany)
<i>Nde</i> I	New England Biolabs (Ipswich, MA, USA)
NucleoBond Midi Prep	Macherey-Nagel GmbH & Co. KG (Düren, Germany)
NucleoBond Xtra Midi Kit	Macherey-Nagel GmbH & Co. KG (Düren, Germany)
NucleoSpin RNA Kit	Macherey-Nagel GmbH & Co. KG (Düren, Germany)
<i>Pac</i> I	New England Biolabs (Ipswich, MA, USA)
Paraformaldehyde (PFA)	Sigma-Aldrich (St. Louis, Missouri, USA)
Page Ruler Plus Prestained Protein Ladder	Thermo Fisher Scientific™ (Waltham, Massachusetts, USA)
Phusion® High-Fidelity DNA polymerase	New England Biolabs (Ipswich, MA, USA)
Polyethylene glycol (PEG)	Sigma-Aldrich (St. Louis, Missouri, USA)

Material & Methods

Precast western blot gels	Bio-Rad Laboratories (Hercules, California, USA)
Proteinase inhibitor	Roche Applied Science (Basel, Switzerland)
Rapid Fixierer	Agfa-Gevaert Group (Mortsel, Belgium)
RD-90 Developer-Replenisher	Fujifilm (Tokyo, Japan)
RiboLock RNase Inhibitor	Thermo Fisher Scientific™ (Waltham, Massachusetts, USA)
Sodium chloride (NaCl)	Carl Roth GmbH + Co. KG (Karlsruhe, Germany)
Sodium dodecyl sulfate (SDS)	Carl Roth GmbH + Co. KG (Karlsruhe, Germany)
SYBR™ Safe DNA Gel Stain	Thermo Fisher Scientific™ (Waltham, Massachusetts, USA)
T4 DNA Ligase	New England Biolabs (Ipswich, MA, USA)
Thiazolyl Blue Trazolium Bromide (MTT)	Sigma-Aldrich (St. Louis, Missouri, USA)
Tris(hydroxymethyl)aminomethane (Tris)	Carl Roth GmbH + Co. KG (Karlsruhe, Germany)
Tris-HCl	Carl Roth GmbH + Co. KG (Karlsruhe, Germany)
Triton™ X-100	Sigma-Aldrich (St. Louis, Missouri, USA)
Tween® 20	Carl Roth GmbH + Co. KG (Karlsruhe, Germany)

Material & Methods

2.1.8 Buffers and solutions

Name	Composition
0.5 mM EDTA (working solution)	0.5 M EDTA DPBS -/-
1.5 M NaCl	1.5 M NaCl in dH ₂ O
10x Tris-acetate-EDTA (TAE)	400 mM Tris 200 mM Glacial acetic acid 10 mM EDTA
10x TBS-T	500 mM Tris 1.5 M NaCl 1 % Tween® 20 adjust pH to 8.5
10x Western blot running Buffer	250 mM Tris 1.92 M Glycine 1 % SDS
10x Western blot transfer buffer (Towbin)	250 mM Tris 1.92 M Glycine 20 % (v/v) Methanol
3x SDS loading dye	80 mM Tris-HCl pH 6.8 6 % SDS 15 % β-Mercaptoethanol 45 % Glycerol 0.03 % Bromphenol blue
50 % PEG	50 % PEG in dH ₂ O
Cell lysis buffer	50 mM Tris-HCl 150 mM NaCl 0.5 % Triton™ X-100 0.5 % Deoxycholic acid
LB-medium (Lennox)	20 g/l LB medium 100 µg/ml Ampicillin
LB-agar	35 g/l LB-agar 100 µg/ml Ampicillin
MTT lysis buffer	90 % Isopropanol 10 % Triton™ X-100 0.66 % HCl acid 25%

Material & Methods

2.1.9 Vector

Vector	Company
Beta-catenin S33Y	Cloned as published in Kahlert et al. (2012)
pCDH-Flag-c-Myc #102626	Addgene (Watertown, Massachusetts, USA)
pMDLg/pRRE #12251	Addgene (Watertown, Massachusetts, USA)
hGli1 6x his #84923	Addgene (Watertown, Massachusetts, USA)
PB-CMV-TO-EGFRvIII-IRES-nlsChe #116039	Addgene (Watertown, Massachusetts, USA)
pLenti-GIII-CMV-GFP-2A-Puro-CD44 #LV590 Custom made	Applied Biological Materials (Richmond, Canada)
pDONR223-PDGFR #23892	Addgene (Watertown, Massachusetts, USA)
pLenti6/V5-p53_R175H #22936	Addgene (Watertown, Massachusetts, USA)
pMD2.G #12259	Addgene (Watertown, Massachusetts, USA)
pRSV-REV #12253	Addgene (Watertown, Massachusetts, USA)
pSin-EF2-Nanog-Pur #16578	Addgene (Watertown, Massachusetts, USA)

Material & Methods

2.1.10 Kits

Kit	Company
Amersham ECL	GE Healthcare (Chicago, Illinois, USA)
CellTiter-Glo® Luminescent Viability Assay	Promega (Madison, Wisconsin, USA)
Cold Fusion™ Cloning Kit	System Biosciences Inc. (Mountain View, California, USA)
DC Protein Assay Kit	Bio-Rad Laboratories (Hercules, California, USA)
DNeasy Blood & Tissue Kit	Qiagen (Hilden, Germany)
GeneJET™ Plasmid-Miniprep-Kit	Thermo Fisher Scientific™ (Waltham, Massachusetts, USA)
Human Pluripotent Stem Cell Transcription Factor Analysis Kit	Becton, Dickinson and Company (Franklin Lakes, NJ, USA)
NucleoBond™ Midi Kit	Macherey-Nagel GmbH & Co. KG (Düren, Germany)
NucleoSpin RNA Kit	Macherey-Nagel GmbH & Co. KG (Düren, Germany)
PCR Mycoplasma Test Kit I/C	PromoCell GmbH (Heidelberg, Germany)
Peqlab PCR Clean Up	VWR International (Radnor, Pennsylvania, USA)
Peqlab Plasmid Miniprep Kit I, peqGOLD	VWR International (Radnor, Pennsylvania, USA)
QuickTiter Lentivirus Titer Kit (Lentivirus-Associated HIV p24)	Cell Biolabs, Inc (San Diego, California, USA)
SuperSignal™ West Pico PLUS Chemiluminescent Substrate	Thermo Fisher Scientific™ (Waltham, Massachusetts, USA)

Material & Methods

2.2 Methods

2.2.1 Generation of the plasmid including the gene of interest

Subgroup-specific genes of interest (GOI; Table 2) were cloned into the modified third-generation lentiviral vector pSin, which was kindly provided by Prof. Dr. Jay Gopalakrishnan (Institute of Human Genetics, UKD). Jay Gopalakrishnan (UKD) and Dr. Andrea Rossi (IUF) kindly provided the cloning materials. The cloning procedure was published in detail in Uhlmann et al. (2020).

Table 2 Medulloblastoma (MB) and glioblastoma (GBM) subgroup-specific genes of interest.

MB and GBM can be divided into three subgroups. For each subgroup, one representative gene was introduced into the lentiviral vector. As a tumor protein 53 (*TP53*) point mutation is commonly found in GBM, *TP53R175H* was introduced into the GBM models as well (Verhaak et al., 2010).

	Subgroup	Gene
MB	WNT	Beta catenin S33Y
	SHH	<i>GLI1</i>
	Group 3	<i>c-MYC</i>
GBM	classic	<i>EGFRvIII</i>
	mesenchymal	<i>PDGFRA</i>
	proneural	<i>CD44</i>
	Background mutation	<i>TP53R175H</i>

2.2.2 Polymerase chain reaction

Amplification of the gene via polymerase chain reaction (PCR) is necessary to integrate the sequence of the respective GOI into the target vector. The lab of Gopalakrishnan modified the receiver vector pSin-EF2-Nanog-Puro (Addgene, MA, USA) by removing the gene sequence of NANOG and introducing an N-terminal enhanced green fluorescent protein (EGFP) sequence and a multiple cloning site (MCS). The GOIs were cloned into this MCS using the restriction enzymes *PacI* and *NdeI* (New England Biolabs, MA, USA). At first, the GOI sequence was amplified via PCR from commercially available vectors (Table 8). Primers were designed using the software SnapGene (from Insightful Science; available at snapgene.com) and included specific restriction enzymes (RE) bases for *PacI* and *NdeI*. The

Material & Methods

PCR protocol using the Phusion® High-Fidelity DNA polymerase (New England Biolabs, MA, USA) was as follows:

Table 3 Phusion polymerase PCR reaction mix.

Reagent	Volume
5x Phusion buffer	10 µl
10 mM desoxynucleosidtriphosphate (dNTPs)	1 µl
10 µM forward (FWD) primer	2.5 µl
10 µM reverse (RV) primer	2.5 µl
Template DNA	50 – 250 ng
Phusion Polymerase	0.5 µl
dH ₂ O	Up to 50 µl final volume

PCR reaction mix was run in a thermo cycler with the PCR program as follows:

Table 4 Phusion polymerase PCR conditions.

Step	Temperature	Time
1. Initial denaturation	98°C	5 min
2. 35 cycles:		
Denaturation	98°C	10 s
Annealing	60°C	30 s
Elongation	72°C	30 s per kb
3. Final extension	72°C	10 min
4. Hold	4°C	

Table 5 Primers for gene amplification.

Oligonucleotide primer	Sequence 5'-3'
c-MYC	FWD* CCTTAATTTAAAATGCCCTCAACGTTAGCT RV** GGAATTCCATATGTTACGCACAAGAGTTCCGTA
CD44	FWD CCTTAATTTAAAATGGACAAGTTTTGGTGGCACG RV GGAATTCCATATGTTACACCCCAATCTTCATGTCC
CTNNB1	FWD CCTTAATTTAAAATGGCTACTCAAGCTGATTTGATGGA RV TGCATGCATTTACAGGTCAGTATCAAACCAGGCCAGCT
EGFRvIII	FWD CTGTACAAGATCGATATGCGACCCTCCGGGACG RV TTCGCTAGCACGGCGTTCATGCTCCAATAAATTC
GLI1	FWD CCTTAATTTAAAATGTTCAACTCGATGACCCACCA RV TGCATGCATTTAGGCACTAGAGTTGAGGAATTCTGT
PDGFRA	FWD CCTTAATTTAAaATGGGGACTTCCCATCCGG RV GGAATTCCATATGTTACAGGAAGCTGTCTTCC
TP53	FWD CCTTAATTTAAAATGGAGGAGCCGCAGTCA RV GGAATTCCATATGTCAGTCTGAGTCAGGCCCTT

*Forward (FWD); **Reverse (RV)

For the evaluation of the PCR reaction, gel electrophoresis was performed using a 2 % agarose gel prepared with 1x TAE buffer and stained with SYBR safe (Invitrogen, MA, USA). From the PCR product 5 µl were mixed with 1 µl of 6x DNA loading dye (Thermo Fisher Scientific™, MA, USA). As a reference the Gene ruler 1kb Plus marker (Thermo Fisher Scientific™, MA, USA) was loaded. Gel electrophoreses were carried out at 120 V for approximately 20 min. Visualization was done using a gel imager. If the band size of the PCR product was in accordance with the expected amplicon size, the remaining product was purified using a PCR purification kit (VWR International, PA, USA).

2.2.3 Restriction digest of insert and vector

Inserts, as well as the target vector, were digested with the restriction enzymes *NdeI* and *PacI* in a double digest approach. The samples were incubated in a thermo cycler at 37°C overnight.

Table 6 Digestion of insert with the gene of interest.

Reagent	Volume
Insert	24 µl
10x Restriction enzyme buffer	3 µl
<i>NdeI</i>	1 µl
<i>PacI</i>	1 µl
Deionized H ₂ O (dH ₂ O)	1 µl

Table 7 Digestion of the modified pSin receiver vector.

Reagent	Amount
Undigested modified pSin vector	2 µg
10x Restriction enzyme buffer	2 µl
<i>NdeI</i>	1 µl
<i>PacI</i>	1 µl
dH ₂ O	Up to 20 µl final volume

Digested inserts and vectors were loaded on a 1 % agarose gel as described before in 2.2.2. Therefore, the whole sample was mixed with 6x DNA loading dye and loaded on the gel. Gel electrophoresis was carried out at 120 V for 30 min. DNA bands were visualized using a gel imager. Desired bands were cut out using a scalpel and transferred to a 1.5 ml reaction tube. The product was purified using a commercially available gel extraction Kit (VWR International, PA, USA) following the manufacturer's instructions. Digested and purified products were directly used for the ligation.

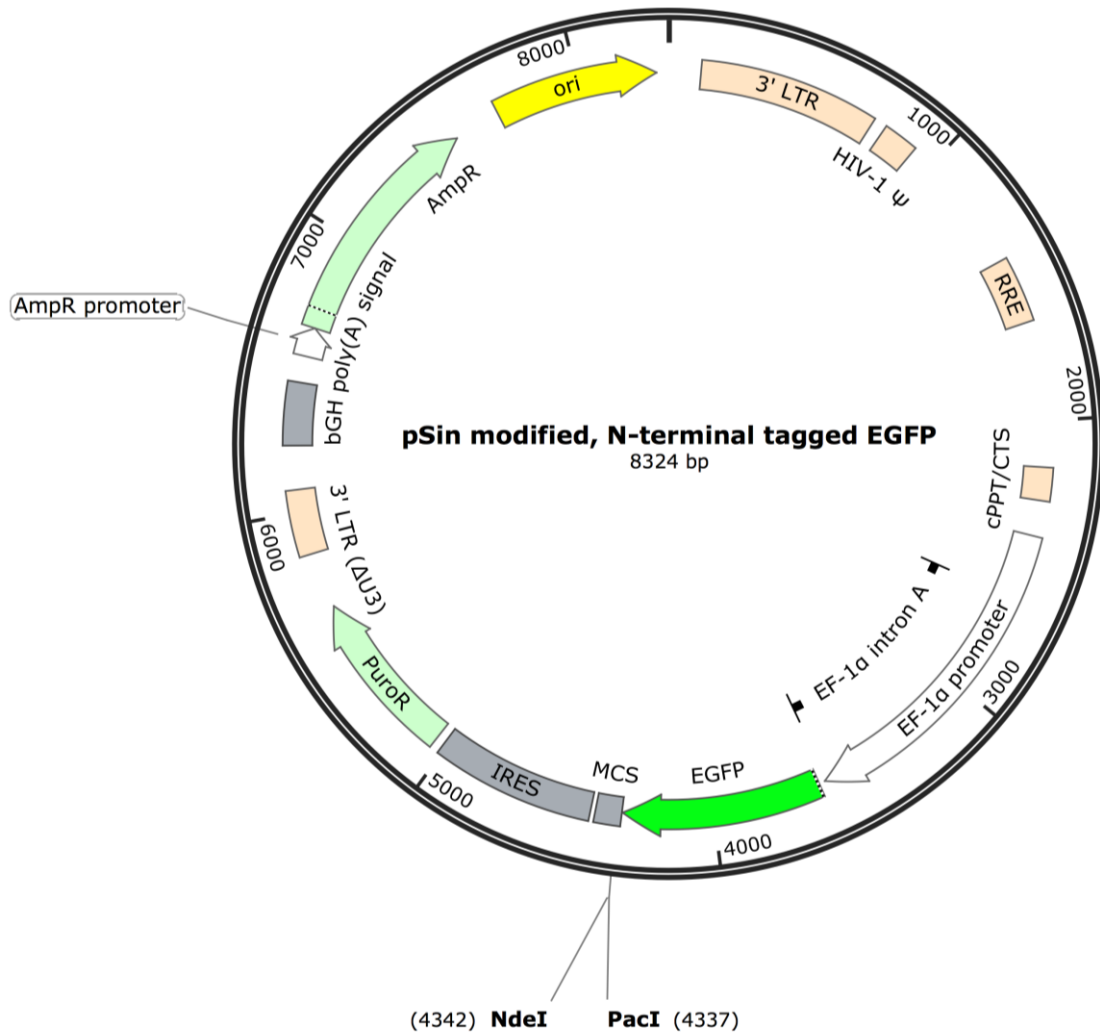


Figure 5 Vector map of the modified pSin vector.

The vector was modified to include an enhanced green fluorescent protein (EGFP) at the N-terminus and a multiple cloning site (MCS) was inserted. Respective sequences of genes of interest were inserted at the MCS site. The restriction site of *PacI* and *NdeI* was used to cut the vector. The figure was created using SnapGene software (www.snapgene.com).

2.2.4 Sequences of all inserted genes

Table 8 Overview of all sequences of the respective genes of interest (5' – 3').

Sequences were cloned into the vector following the cloning protocol as described above.

<i>TP53R175H</i>	<p>ATGGAGGAGCCGCAGTCAGATCCTAGCGTCGAGCCCCCTCTGAGTCAG GAAACATTTTCAGACCTATGGAACTACTTCCTGAAAACAACGTTCTGTC CCCCTTGCCGTCCCAAGCAATGGATGATTTGATGCTGTCCCCGGACGAT ATTGAACAATGGTTCACTGAAGACCCAGGTCCAGATGAAGCTCCCAGAA TGCCAGAGGCTGCTCCCCCGTGGCCCCTGCACCAGCAGCTCCTACAC CGGCGGCCCTGCACCAGCCCCCTCCTGGCCCCTGTCATCTTCTGTCC CTTCCCAGAAAACCTACCAGGGCAGCTACGGTTTCCGTCTGGGCTTCTT GCATTCTGGGACAGCCAAGTCTGTGACTTGCACGTA CTCCCCTGCCCTC AACAAAGATGTTTTGCCAACTGGCCAAGACCTGCCCTGTGCAGCTGTGG GTTGATTCCACACCCCCGCCCGGCACCCGCGTCCGCGCCATGGCCATC TACAAGCAGTCACAGCACATGACGGAGGTTGTGAGGCACTGCCCCCAC CATGAGCGCTGCTCAGATAGCGATGGTCTGGCCCCTCCTCAGCATCTTA TCCGAGTGAAGGAAATTTGCGTGTGGAGATTTGGATGACAGAAACAC TTTTCGACATAGTGTGGTGGTGCCCTATGAGCCGCCTGAGGTTGGCTCT GACTGTACCACCATCCACTACA ACTACATGTGTAACAGTTCTGCATGG GCGGCATGAACCGGAGGCCATCCTCACCATCATCACACTGGAAGACT CCAGTGGTAATCTACTGGGACGGAACAGCTTTGAGGTGCGTGTGGTG CTGTCTGGGAGAGACCGGCGCACAGAGGAAGAGAATCTCCGCAAGAA AGGGGAGCCTCACCACGAGCTGCCCCAGGGAGCACTAAGCGAGCAC TGCCCAACAACACCAGCTCCTCTCCCCAGCCAAAGAAGAAACCACTGGA TGAGAAATATTTACCCTTCAGATCCGTGGGCGTGAGCGCTTCGAGATG TTCCGAGAGCTGAATGAGGCCTTGGAACTCAAGGATGCCCAGGCTGGG AAGGAGCCAGGGGGGAGCAGGGCTCACTCCAGCCACCTGAAGTCCAA AAAGGGTCAGTCTACCTCCCGCCATAAAAACTCATGTTCAAGACAGAA GGCCTGACTCAGACTGA</p>
<i>EGFRvIII</i>	<p>ATGCGACCCTCCGGGACGGCCGGGGCAGCGCTCCTGGCGCTGCTGGC TGCGCTCTGCCCCGGCGAGTCGGGCTCTGGAGGAAAAGAAAGGTAATTA TGTGGTGACAGATCACGGCTCGTGCCTCCGAGCCTGTGGGGCCGACA GCTATGAGATGGAGGAAGACGGCGTCCGCAAGTGTAAAGAAGTGCGAAG GGCCTTGCCGCAAAGTGTGTAACGGAATAGGTATTGGTGAATTTAAAGA CTCACTCTCCATAAATGCTACGAATATTAACA CTCAAAACTGCACCT CCATCAGTGGCGATCTCCACATCCTGCCGGTGGCATTAGGGGTGACT CCTTCACACATACTCCTCCTCTGGATCCACAGGAACTGGATATTCTGAAA ACCGTAAAGGAAATCACAGGGTTTTTGTGATT CAGGCTTGGCCTGAAA ACAGGACGGACCTCCATGCCTTTGAGAACCTAGAAATCATAACGCGGCA GGACCAAGCAACATGGTCAGTTTTCTCTTGCAGTCGT CAGCCTGAACAT AACATCCTTGGGATTACGCTCCCTCAAGGAGATAAGTGATGGAGATGTG ATAATTT CAGGAAACAAAATTTGTGCTATGCAAATACAATAA ACTGGAA AAA ACTGTTTGGGACCTCCGGTCAGAAAACCAA AATTATAAGCAACAGA GGTGAAAACAGCTGCAAGGCCACAGGCCAGGTCTGCCATGCCTTGTGC TCCCCCGAGGGCTGCTGGGGCCCGAGCCCAGGGACTGCGTCTCTTG CCGGAATGTCAGCCGAGGCAGGGAATGCGTGGACAAGTGCAACCTTCT GGAGGGTGAGCCAAGGGAGTTTGTGGAGA ACTCTGAGTGCATACAGTG CCACCCAGAGTGCCTGCCTCAGGCCATGAACATCACCTGCACAGGACG GGGACCAGACA ACTGTATCCAGTGTGCCCACTACATTGACGGCCCCCA</p>

CTGCGTCAAGACCTGCCCGGCAGGAGTCATGGGAGAAAACAACACCCT
 GGTCTGGAAGTACGCAGACGCCGGCCATGTGTGCCACCTGTGCCATCC
 AACTGCACCTACGGATGCACTGGGCCAGGTCTTGAAGGCTGTCCAAC
 GAATGGGCCTAAGATCCCGTCCATCGCCACTGGGATGGTGGGGGCCCT
 CCTCTTGCTGCTGGTGGTGGCCCTGGGGATCGGCCTCTTCATGCGAAG
 GCGCCACATCGTTCCGGAAGCGCACGCTGCGGAGGCTGCTGCAGGAGA
 GGGAGCTTGTGGGGCCTCTTACACCCAGTGGAGAAGCTCCCAACCAAG
 CTCTCTTGAGGATCTTGAAGGAACTGAATTCAAAAAGATCAAAGTGCTG
 GGCTCCGGTGC GTTCCGGCACGGTGTATAAGGGACTCTGGATCCCAGAA
 GGTGAGAAAGTTAAAATCCCGTCGCTATCAAGGAATTAAGAGAAGCAA
 CATCTCCGAAAGCCAACAAGGAAATCCTCGATGAAGCCTACGTGATGGC
 CAGCGTGGACAACCCCCACGTGTGCCGCCTGCTGGGCATCTGCCTCAC
 CTCCACCGTGCAGCTCATCACGCAGCTCATGCCCTTCGGCTGCCTCCT
 GACTATGTCCGGGAACACAAGACAATATTGGCTCCAGTACCTGCTC
 AACTGGTGTGTGCAGATCGCAAAGGGCATGAACTACTTGGAGGACCGT
 CGTTGGTGCACCGTGACCTGGCAGCCAGGAACGTACTGGTGAAAACA
 CCGCAGCATGTCAAGATCACAGATTTTGGGCTGGCCAAACTGCTGGGT
 GCGGAAGAGAAAGAATACCATGCAGAAGGAGGCAAAGTGCCTATCAAG
 TGGATGGCATTGGAATCAATTTTACACAGAATCTATACCCACCAGAGTGA
 TGTCTGGAGCTACGGGGTGACCGTTTGGGAGTTGATGACCTTTGGATC
 CAAGCCATATGACGGAATCCCTGCCAGCGAGATCTCCTCCATCCTGGA
 GAAAGGAGAACGCCTCCCTCAGCCACCCATATGTACCATCGATGTCTAC
 ATGATCATGGTCAAGTGCTGGATGATAGACGCAGATAGTCGCCCAAAGT
 TCCGTGAGTTGATCATCGAATTCTCCAAAATGGCCCGAGACCCCCAGCG
 CTACCTTGTCAATCAGGGGGATGAAAGAATGCATTTGCCAAGTCTTACA
 GACTCCAACCTTCTACCGTGCCCTGATGGATGAAGAAGACATGGACGAC
 GTGGTGGATGCCGACGAGTACCTCATCCCACAGCAGGGCTTCTTCAGC
 AGCCCCCTCCACGTACGGACTCCCCTCCTGAGCTCTCTGAGTGCAACC
 AGCAACAATTCCACCGTGGCTTGCATTGATAGAAATGGGCTGCAAAGCT
 GTCCCATCAAGGAAGACAGCTTCTTGCAGCGATACAGCTCAGACCCCCA
 AGGCGCCTTGACTGAGGACAGCATAGACGACACCTTCTCCAGTGCC
 TGAATACATAAACCAGTCCGTTCCCAAAGGCCCGCTGGCTCTGTGCAG
 AATCCTGTCTATCACAATCAGCCTCTGAACCCCGCGCCCAGCAGAGACC
 CACTACTACCAGGACCCCCACAGCACTGCAGTGGGCAACCCCGAGTATC
 TCAACACTGTCCAGCCCACCTGTGTCAACAGCACATTCGACAGCCCTGC
 CCACTGGGCCAGAAAGGCAGCCACCAAATTAGCCTGGACAACCCTGA
 CTACCAGCAGGACTTCTTTCCAAAGGAAGCCAAGCCAATGGCATCTTT
 AAGGGCTCCACAGCTGAAAATGCAGAATACCTAAGGGTCGCGCCACAA
 AGCAGTGAATTTATTGGAGCATAG

CD44

ATGGACAAGTTTTGGTGGCACGCAGCCTGGGGACTCTGCCTCGTGCCG
 CTGAGCCTGGCGCAGATCGATTTGAATATAACCTGCCGCTTTGCAGGTG
 TATCCACGTGGAGAAAAATGGTCGCTACAGCATCTCTCGGACGGAGG
 CCGCTGACCTCTGCAAGGCTTTCAATAGCACCTTGCCACAATGGCCCA
 GATGGAGAAAGCTCTGAGCATCGGATTTGAGACCTGCAGGTATGGGTT
 CATAGAAGGGCACGTGGTGTATCCCGGATCCACCCCAACTCCATCTGT
 GCAGCAAACAACACAGGGGTGTACATCCTCACATCCAACACCTCCCAGT
 ATGACACATATTGCTTCAATGCTTCAGCTCCACCTGAAGAAGATTGTACA
 TCAGTCACAGACCTGCCCAATGCCTTTGATGGACCAATTACCATAACTAT
 TGTTAACCGTGATGGCACCCGCTATGTCCAGAAAGGAGAATACAGAACG
 AATCCTGAAGACATCTACCCAGCAACCCTACTGATGATGACGTGAGCA
 GCGGCTCCTCCAGTGAAAGGAGCAGCACTTCAGGAGGTTACATCTTTTA

CACCTTTTCTACTGTACACCCCATCCCAGACGAAGACAGTCCCTGGATC
 ACCGACAGCACAGACAGAATCCCTGCTACCACTTTGATGAGCACTAGTG
 CTACAGCAACTGAGACAGCAACCAAGAGGCAAGAAACCTGGGATTGGT
 TTTTCATGGTTGTTTCTACCATCAGAGTCAAAGAATCATCTTCACACAACA
 ACACAAATGGCTGGTACGTCTTCAAATACCATCTCAGCAGGCTGGGAGC
 CAAATGAAGAAAATGAAGATGAAAGAGACAGACACCTCAGTTTTTCTGG
 ATCAGGCATTGATGATGATGAAGATTTTATCTCCAGCACCATTTC AACCA
 CACCACGGGCTTTTGACCACACAAAACAGAACCAGGACTGGACCCAGT
 GGAACCCAAGCCATTCAAATCCGGAAGTGCTACTTCAGACAACCACAAG
 GATGACTGATGTAGACAGAAATGGCACCCTGCTTATGAAGGAAACTGG
 AACCCAGAAGCACACCCTCCCCTCATTACCATGAGCATCATGAGGAAG
 AAGAGACCCACATTCTACAAGCACAATCCAGGCAACTCCTAGTAGTAC
 AACGGAAGAAACAGCTACCCAGAAGGAACAGTGGTTTGGCAACAGATG
 GCATGAGGGATATCGCCAAACACCCAAAGAAGACTCCCATTTCGACAACA
 GGGACAGCTGCAGCCTCAGCTCATAACAGCCATCCAATGCAAGGAAGG
 ACAACACCAAGCCCAGAGGACAGTTCTGGACTGATTTCTTCAACCCAA
 TCTCACACCCCATGGGACGAGGTCATCAAGCAGGAAGAAGGATGGATA
 TGGACTCCAGTCATAGTATAACGCTTCAGCCTACTGCAAATCCAAACAC
 AGGTTTGGTGGAAAGATTTGGACAGGACAGGACCTCTTTCAATGACAACG
 CAGCAGAGTAATTCTCAGAGCTTCTCTACATCACATGAAGGCTTGGAAAG
 AAGATAAAGACCATCCAACAATTCTACTCTGACATCAAGCAATAGGAAT
 GATGTCACAGGTGGAAGAAGAGACCCAAATCATTCTGAAGGCTCAACTA
 CTTTACTGGAAGGTTATACCTCTCATTACCCACACACGAAGGAAAGCAG
 GACCTTCATCCCAGTGACCTCAGCTAAGACTGGGTCCTTTGGAGTTACT
 GCAGTTACTGTTGGAGATTCCAACTCTAATGTCAATCGTTCCTTATCAGG
 AGACCAAGACACATTCCACCCCAGTGGGGGGTCCCATAACCACTCATGG
 ATCTGAATCAGATGGACACTCACATGGGAGTCAAGAAGGTGGAGCAAAC
 ACAACCTCTGGTCTATAAAGGACACCCCAAATTCCAGAATGGCTGATCA
 TCTTGGCATCCCTCTTGGCCTTGGCTTTGATTCTTGCAGTTTGCATTGCA
 GTCAACAGTCGAAGAAGGTGTGGGCAGAAGAAAAGCTAGTGATCAAC
 AGTGGCAATGGAGCTGTGGAGGACAGAAAGCCAAGTGGACTCAACGGA
 GAGGCCAGCAAGTCTCAGGAAATGGTGCATTTGGTGAACAAGGAGTCG
 TCAGAAACTCCAGACCAGTTTATGACAGCTGATGAGACAAGGAACCTGC
 AGAATGTGGACATGAAGATTGGGGTGTA

PDGFRA ATGGGGACTTCCCATCCGGCGTTCCTGGTCTTAGGCTGTCTTCTCACAG
 GGCTGAGCCTAATCCTCTGCCAGCTTTCATTACCCTCTATCCTTCCAAAT
 GAAAATGAAAAGGTTGTGCAGCTGAATTCATCCTTTTCTCTGAGATGCTT
 TGGGGAGAGTGAAGTGAGCTGGCAGTACCCCATGTCTGAAGAAGAGAG
 CTCCGATGTGGAAATCAGAAATGAAGAAAACAACAGCGGCCTTTTTGTG
 ACGGTCTTGGAAAGTGAGCAGTGCCTCGGCGGCCACACAGGGTTGTAC
 ACTTGCTATTACAACCACACTCAGACAGAAGAGAATGAGCTTGAAGGCA
 GGCACATTTACATCTATGTGCCAGACCCAGATGTAGCCTTTGTACCTCTA
 GGAATGACGGATTATTTAGTCATCGTGGAGGATGATGATTCTGCCATTAT
 ACCTTGTCGCACAACCTGATCCCAGACTCCTGTAACCTTACACAACAGT
 GAGGGGGTGGTACCTGCCTCCTACGACAGCAGACAGGGCTTTAATGGG
 ACCTTCACTGTAGGGCCCTATATCTGTGAGGCCACCGTCAAAGGAAAGA
 AGTTCAGACCATCCCATTTAATGTTTATGCTTTAAAAGCAACATCAGAG
 CTGGATCTAGAAATGGAAGCTCTTAAAACCGTGTATAAGTCAGGGGAAA
 CGATTGTGGTCACCTGTGCTGTTTTTAACAATGAGGTGGTTGACCTTCAA
 TGGACTTACCCTGGAGAAGTGAAGGGCAAAGGCATCACAATACTGGAAG
 AAATCAAAGTCCCATCCATCAAATTGGTGTACACTTTGACGGTCCCCGA

GGCCACGGTGAAAGACAGTGGAGATTACGAATGTGCTGCCCGCCAGGC
 TACCAGGGAGGTCAAAGAAATGAAGAAAGTCACTATTTCTGTCCATGAG
 AAAGTTTTATTGAAATCAAACCCACCTTCAGCCAGTTGGAAGCTGTCA
 ACCTGCATGAAGTCAAACATTTTGTGTTAGAGGTGCGGGCCTACCCACC
 TCCAGGATATCCTGGCTGAAAAACAATCTGACTCTGATTGAAAATCTCA
 CTGAGATCACCCTGATGTGGAAAAGATTTCAGGAAATAAGGTATCGAAG
 CAAATTAAGCTGATCCGTGCTAAGGAAGAAGACAGTGGCCATTATACT
 ATTGTAGCTCAAATGAAGATGCTGTGAAGAGCTATACTTTTGAAGTGT
 AACTCAAGTTCCTTCATCCATTCTGGACTTGGTCGATGATCACCATGGCT
 CAACTGGGGGACAGACGGTGGAGTGCACAGCTGAAGGCACGCCGCTT
 CCTGATATTGAGTGGATGATATGCAAAGATATTAAGAAATGTAATAATGA
 AACTTCCTGGACTATTTTGGCCAACAATGTCTCAAACATCATCACGGAGA
 TCCACTCCCGAGACAGGAGTACCGTGGAGGGCCGTGTGACTTTCCGCA
 AAGTGGAGGAGACCATCGCCGTGCGATGCCTGGCTAAGAATCTCCTTG
 GAGCTGAGAACCAGAGCTGAAGCTGGTGGCTCCCACCCTGCGTTCTG
 AACTCACGGTGGCTGCTGCAGTCTGGTGGCTGTTGGTGATTGTGATCAT
 CTCACTTATTGTCCTGGTTGTCAATTTGGAAACAGAAACCGAGGTATGAAA
 TTCGCTGGAGGGTCATTGAATCAATCAGCCCGGATGGACATGAATATAT
 TTATGTGGACCCGATGCAGCTGCCTTATGACTCAAGATGGGAGTTTCCA
 AGAGATGGACTAGTGCTTGGTCGGGTCTTGGGGTCTGGAGCGTTTGGG
 AAGGTGGTTGAAGGAACAGCCTATGGATTAAGCCGGTCCCAACCTGTCA
 TGAAAGTTGCAGTGAAGATGCTAAAACCCACGGCCAGATCCAGTGAAAA
 ACAAGCTCTCATGTCTGAACTGAAGATAATGACTCACCTGGGGCCACAT
 TTGAACATTGTAACTTGTGGGAGCCTGCACCAAGTCAGGCCCCATTT
 ACATCATCACAGAGTATTGCTTCTATGGAGATTTGGTCAACTATTTGCAT
 AAGAATAGGGATAGCTTCTGAGCCACCACCCAGAGAAGCCAAAGAAA
 GAGCTGGATATCTTTGGATTGAACCCTGCTGATGAAAGCACACGGAGCT
 ATGTTATTTTATCTTTTGAACAATGGTGAATACATGGACATGAAGCAG
 GCTGATACTACACAGTATGTCCCATGCTAGAAAGGAAAGAGGTTTCTA
 AATATTCCGACATCCAGAGATCACTCTATGATCGTCCAGCCTCATATAAG
 AAGAAATCTATGTTAGACTCAGAAGTCAAAAACCTCCTTTTTCAGATGATAA
 CTCAGAAGGCCTTACTTTATTGGATTTGTTGAGCTTCACCTATCAAGTTG
 CCCGAGGAATGGAGTTTTTGGCTTCAAAAATTGTGTCCACCCTGATCT
 GGCTGCTCGCAACGTCCTCCTGGCACAAGGAAAAATTGTGAAGATCTGT
 GACTTTGGCCTGGCCAGAGACATCATGCATGATTCGAACTATGTGTCTGA
 AAGGCAGTACCTTTCTGCCCGTGAAGTGGATGGCTCCTGAGAGCATCTT
 TGACAACCTCTACACCACACTGAGTGTGCTGGTCTTATGGCATTCTG
 CTCTGGGAGATCTTTTCCCTTGGTGGCACCCCTTACCCCGGCATGATGG
 TGGATTCTACTTTCTACAATAAGATCAAGAGTGGGTACCGGATGGCCAA
 GCCTGACCACGCTACCAGTGAAGTCTACGAGATCATGGTGAAATGCTG
 GAACAGTGAGCCGGAGAAGAGACCCTCCTTTTACCACCTGAGTGAGATT
 GTGGAGAATCTGCTGCCTGGACAATATAAAAAGAGTTATGAAAAAATTCA
 CCTGGACTTCTGAAGAGTGACCATCCTGCTGTGGCACGCATGCGTGT
 GACTCAGACAATGCATACATTGGTGTACCTACAAAACGAGGAAGAC
 AAGCTGAAGGACTGGGAGGGTGGTCTGGATGAGCAGAGACTGAGCGCT
 GACAGTGGCTACATCATTCTCTGCCTGACATTGACCCTGTCCCTGAGG
 AGGAGGACCTGGGCAAGAGGAACAGACACAGCTCGCAGACCTCTGAAG
 AGAGTGCCATTGAGACGGGTTCCAGCAGTTCCACCTTCATCAAGAGAGA
 GGACGAGACCATTGAAGACATCGACATGATGGACGACATCGGCATAGA
 CTCTTCAGACCTGGTGAAGACAGCTTCTCTGTAA

β-catenin ATGGCTACTCAAGCTGATTTGATGGAGTTGGACATGGCCATGGAACCG

S33Y ACAGAAAAGCGGCTGTTAGTCACTGGCAGCAACAGTCTTACCTGGACTA
 TGGAATCCATTCTGGTGCCACTACCACAGCTCCTTCTCTGAGTGGTAAA
 GGCAATCCTGAGGAAGAGGATGTGGATACCTCCCAAGTCCTGTATGAGT
 GGGAACAGGGATTTTCTCAGTCCTTCACTCAAGAACAAGTAGCTGATAT
 TGATGGACAGTATGCAATGACTCGAGCTCAGAGGGTACGAGCTGCTAT
 GTTCCCTGAGACATTAGATGAGGGCATGCAGATCCCATCTACACAGTTT
 GATGCTGCTCATCCCCTAATGTCCAGCGTTTGGCTGAACCATCACAGA
 TGCTGAAACATGCAGTTGTAACTTGATTA ACTATCAAGATGATGCAGAA
 CTTGCCACACGTGCAATCCCTGAACTGACAAA ACTGCTAAATGACGAGG
 ACCAGGTGGTGGTTAATAAGGCTGCAGTTATGGTCCATCAGCTTTCTAA
 AAAGGAAGCTTCCAGACACGCTATCATGCGTTCTCCTCAGATGGTGTCT
 GCTATTGTACGTACCATGCAGAATACAAATGATGTAGAAACAGCTCGTT
 GTACCGCTGGGACCTTGCATAACCTTTCCCATCATCGTGAGGGCTTACT
 GGCCATCTTTAAGTCTGGAGGCATTCTGCCCTGGTGAAAATGCTTGGT
 TCACCAGTGGATTCTGTGTTGTTTTATGCCATTACA ACTCTCCACAACCT
 TTTATTACATCAAGAAGGAGCTAAAATGGCAGTGCGTTTAGCTGGTGGG
 CTGCAGAAAATGGTTGCCTTGCTCAACAAAACAAATGTTAAATTCTTGGC
 TATTACGACAGACTGCCTTCAAATTTTAGCTTATGGCAACCAAGAAAGCA
 AGCTCATCATACTGGCTAGTGGTGGACCCCAAGCTTTAGTAAATATAAT
 GAGGACCTATACTTACGAAA ACTACTGTGGACCACAAGCAGAGTGTCTG
 AAGGTGCTATCTGTCTGCTCTAGTAATAAGCCGGCTATTGTAGAAGCTG
 GTGGAATGCAAGCTTTAGGACTTCACCTGACAGATCCAAGTCAACGTCT
 TGTTCAGA ACTGTCTTTGGACTCTCAGGAATCTTTCAGATGCTGCAACTA
 AACAGGAAGGGATGGAAGGTCTCCTTGGGACTCTTGTT CAGCTTCTGG
 GTTCAGATGATATAAATGTGGTCACCTGTGCAGCTGGAATTCTTTCTAAC
 CTCACTTGCAATAATTATAAGAACAAGATGATGGTCTGCCAAGTGGGTG
 GTATAGAGGCTCTTGTGCGTACTGTCCTTCGGGCTGGTGACAGGGGAAG
 ACATCACTGAGCCTGCCATCTGTGCTCTTCGTCATCTGACCAGCCGACA
 CCAAGAAGCAGAGATGGCCCAGAATGCAGTTCGCCTTCACTATGGACTA
 CCAGTTGTGGTTAAGCTCTTACACCCACCATCCC ACTGGCCTCTGATAA
 AGGCTACTGTTGGATTGATTCGAAATCTTGCCCTTTGTCCC GCAAATCAT
 GCACCTTTGCGTGAGCAGGGTGCCATTCCACGACTAGTTCAGTTGCTTG
 TTCGTGCACATCAGGATACCCAGCGCCGTACGTCCATGGGTGGGACAC
 AGCAGCAATTTGTGGAGGGGGTCCGCATGGAAGAAATAGTTGAAGGTT
 GTACCGGAGCCCTTACATCCTAGCTCGGGATGTT CACAACCGAATTGT
 TATCAGAGGACTAAATACCATTCCATTGTTTGTGCAGCTGCTTTATTCTC
 CCATTGAAAACATCCAAGAGTAGCTGCAGGGGGTCTCTGTGAACTTGC
 TCAGGACAAGGAAGCTGCAGAAGCTATTGAAGCTGAGGGAGCCACAGC
 TCCTCTGACAGAGTTACTTCACTCTAGGAATGAAGGTGTGGCGACATAT
 GCAGCTGCTGTTTTGTTCCGAATGTCTGAGGACAAGCCACAAGATTACA
 AGAAACGGCTTT CAGTTGAGCTGACCAGCTCTCTCTTCAGAACAGAGCC
 AATGGCTTGGAAATGAGACTGCTGATCTTGGACTTGATATTGGTGCCCAG
 GGAGAACCCTTGGATATCGCCAGGATGATCCTAGCTATCGTTCTTTTC
 ACTCTGGTGGATATGGCCAGGATGCCTTGGGTATGGACCCCATGATGG
 AACATGAGATGGGTGGCCACCACCCTGGTGTGCTGACTATCCAGTTGATG
 GGCTGCCAGATCTGGGGCATGCCCAGGACCTCATGGATGGGCTGCCTC
 CAGGTGACAGCAATCAGCTGGCCTGGTTTGATACTGACCTGTAA

GLI1 ATGTTCAACTCGATGACCCACCACCAATCAGTAGCTATGGCGAGCCCT
 GCTGTCTCCGGCCCTCCCAAGTCAGGGGGCCCCCAGTGTGGGGACA
 GAAGGACTGTCTGGCCCGCCCTTCTGCCACCAAGCTAACCTCATGTCC
 GGCCCCACAGTTATGGGCCAGCCAGAGAGACCAACAGCTGCACCGAG

GGCCACTCTTTTCTTCTCCCCGGAGTGCAGTCAAGTTGACCAAGAAGC
GGGCACTGTCCATCTCACCTCTGTCGGATGCCAGCCTGGACCTGCAGA
CGTTATCCGCACCTCACCCAGCTCCCTCGTAGCTTTCATCAACTCGCG
ATGCACATCTCCAGGAGGCTCCTACGGTCATCTCTCCATTGGCACCATG
AGCCCATCTCTGGGATTCCCAGCCCAGATGAATCACCAAAAAGGGCCCT
CGCCTTCCTTTGGGGTCCAGCCTTGTGGTCCCCATGACTCTGCCCGGG
GTGGGATGATCCACATCCTCAGTCCCGGGGACCCTCCCAACTTGCCA
GCTGAAGTCTGAGCTGGACATGCTGGTTGGCAAGTGCCGGGAGGAACC
CTTGGAAGGTGATATGTCCAGCCCCAACTCCACAGGCATACAGGATCCC
CTGTTGGGGATGCTGGATGGGCGGGAGGACCTCGAGAGAGAGGAGAA
GCGTGAGCCTGAATCTGTGTATGAAACTGACTGCCGTTGGGATGGCTG
CAGCCAGGAATTTGACTCCCAAGAGCAGCTGGTGCACCACATCAACAG
CGAGCACATCCACGGGGAGCGGAAGGAGTTCGTGTGCCACTGGGGGG
GCTGCTCCAGGGAGCTGAGGCCCTTCAAAGCCCAGTACATGCTGGTGG
TTCACATGCGCAGACACACTGGCGAGAAGCCACACAAGTGACGTTTG
AAGGGTGCCGGAAGTCATACTCACGCCTCGAAAACCTGAAGACGCACC
TGCGGTACACCCGGGTGAGAAGCCATACATGTGTGAGCACGAGGGCTG
CAGTAAAGCCTTCAGCAATGCCAGTGACCGAGCCAAGCACCAAGATCG
GACCCATTCCAATGAGAAGCCGTATGTATGTAAGCTCCCTGGCTGCACC
AAACGCTATACAGATCCTAGCTCGCTGCGAAAACATGTCAAGACAGTGC
ATGGTCTGACGCCCATGTGACCAAACGGCACCGTGGGGATGGCCCCC
TGCCTCGGGCACCATCCATTTCTACAGTGGAGCCCAAGAGGGAGCGGG
AAGGAGGTCCCATCAGGGAGGAAAGCAGACTGACTGTGCCAGAGGGTG
CCATGAAGCCACAGCCAAGCCCTGGGGCCCAGTCATCCTGCAGCAGTG
ACCACTCCCCGGCAGGGAGTGACGCAATACAGACAGTGGTGTGGAAA
TGA CTGGCAATGCAGGGGGCAGCACTGAAGACCTCTCCAGCTTGGACG
AGGGACCTTGCAATTGCTGGCACTGGTCTGTCCACTCTTCGCCGCCTTGA
GAACCTCAGGCTGGACCAGCTACATCAACTCCGGCCAATAGGGACCCG
GGGTCTCAAACCTGCCAGCTTGTCCCACACCCGGTACCACTGTGTCCCG
CCGCGTGGGCCCCCCAGTCTCTCTTGAACGCCGCAGCAGCAGCTCCAG
CAGCATCAGCTCTGCCTATACTGTCAGCCGCCGCTCCTCCCTGGCCTCT
CCTTTCCCCCCTGGCTCCCCACCAGAGAATGGAGCATCCTCCCTGCCT
GGCCTTATGCCTGCCAGCACTACCTGCTTCGGGCAAGATATGCTTCAG
CCAGAGGGGGTGGTACTTCGCCCACTGCAGCATCCAGCCTGGATCGGA
TAGGTGGTCTTCCCATGCCTCCTTGGAGAAGCCGAGCCGAGTATCCAG
GATAACAACCCAATGCAGGGGTCACCCGGAGGGCCAGTGACCCAGCC
CAGGCTGCTGACCGTCTGCTCCAGCTAGAGTCCAGAGGTTCAAGAGC
CTGGGCTGTGTCCATACCCCACCCACTGTGGCAGGGGGAGGACAGAAC
TTTGATCCTTACCTCCCAACCTCTGTCTACTACCACAGCCCCCAGCA
TCACTGAGAATGCTGCCATGGATGCTAGAGGGCTACAGGAAGAGCCAG
AAGTTGGGACCTCCATGGTGGGCAGTGGTCTGAACCCCTATATGGACTT
CCCACCTACTGATACTCTGGGATATGGGGGACCTGAAGGGGCAGCAGC
TGAGCCTTATGGAGCGAGGGGTCCAGGCTCTCTGCCTCTTGGGCCTGG
TCCACCCACCAACTATGGCCCCAACCCCTGTCCCAGCAGGCCTCATAT
CCTGACCCACCCAAGAAACATGGGGTGAGTTCCCTTCCCCTCTGGG
CTGTACCCAGGCCCCAAGGCTCTAGGTGGAACCTACAGCCAGTGTCTCT
CGACTTGAACATTATGGACAAGTGCAAGTCAAGCCAGAACAGGGGTGC
CCAGTGGGGTCTGACTCCACAGGACTGGCACCCCTGCCTCAATGCCAC
CCCAGTGAGGGGGCCCCACATCCACAGCCTCTCTTTTCCCATTACCCCC
AGCCCTCTCCTCCCCAATATCTCCAGTCAGGCCCTATACCCAGCCACC
CCCTGATTATCTTCTTCAGAACCAGGCCTTGCCTGGACTTTGATTCC
CCCACCCATTCCACAGGGCAGCTCAAGGCTCAGCTTGTGTGTAATTATG

TTCAATCTCAACAGGAGCTACTGTGGGAGGGTGGGGGCAGGGAAGATG
CCCCGCCCAGGAACCTTCCTACCAGAGTCCCAAGTTTCTGGGGGGTT
CCCAGGTTAGCCCAAGCCGTGCTAAAGCTCCAGTGAACACATATGGAC
CTGGCTTTGGACCCAATTGCCCAATCACAAGTCAGGTTCTATCCCAC
CCCTTCACCATGCCATGAAAATTTTGTAGTGGGGGCAAATAGGGCTTCA
CATAGGGCAGCAGCACACCCTCGACTTCTGCCCCATTGCCCACTTGCT
ATGGGCCTCTCAAAGTGGGAGGCACAAACCCCAGCTGTGGTCATCCTG
AGGTGGGCAGGCTAGGAGGGGGTCTGCCTTGTACCCTCCTCCCGAAG
GACAGGTATGTAACCCCCTGGACTCTCTTGATCTTGACAACACTCAGCT
GGACTTTGTGGCTATTCTGGATGAGCCCCAGGGGCTGAGTCTCCTCC
TTCCCATGATCAGCGGGGCAGCTCTGGACATACCCCACCTCCCTCTGG
GCCCCCAACATGGCTGTGGGCAACATGAGTGTCTTACTGAGATCCCTA
CCTGGGGAAACAGAATTCTCAACTCTAGTGCCTAA

c-MYC

ATGCCCTCAACGTTAGCTTCACCAACAGGAACTATGACCTCGACTACG
ACTCGGTGCAGCCGTATTTCTACTGCGACGAGGAGGAGAACTTCTACCA
GCAGCAGCAGCAGAGCGAGCTGCAGCCCCCGCGCCCAGCGAGGATA
TCTGGAAGAAATTCGAGCTGCTGCCACCCCCGCCCTGTCCCCTAGCC
GCCGCTCCGGGCTCTGCTCGCCCTCCTACGTTGCGGTCACACCCTTCT
CCCTTCGGGGAGACAACGACGGCGGTGGCGGGAGCTTCTCCACGGCC
GACCAGCTGGAGATGGTGACCGAGCTGCTGGGAGGAGACATGGTGAA
CCAGAGTTTCATCTGCGACCCGACGACGAGACCTTCATCAAAAACATC
ATCATCCAGGACTGTATGTGGAGCGGCTTCTCGGCCGCCGCAAGCTC
GTCTCAGAGAAGCTGGCCTCCTACCAGGCTGCGCGCAAAGACAGCGGC
AGCCCGAACCCCGCCCCGCGGCCACAGCGTCTGCTCCACCTCCAGCTTG
TACCTGCAGGATCTGAGCGCCGCGCCTCAGAGTGCATCGACCCCTCG
GTGGTCTTCCCCTACCCTCTCAACGACAGCAGCTCGCCCAAGTCCTGC
GCCTCGCAAGACTCCAGCGCCTTCTCTCCGTCTCGGATTCTCTGCTCT
CCTCGACGGAGTCCTCCCCGCAGGGCAGCCCCGAGCCCCTGGTGCTC
CATGAGGAGACACCGCCCACCACCAGCAGCGACTCTGAGGAGGAACAA
GAAGATGAGGAAGAAATCGATGTTGTTTCTGTGGAAAAGAGGCAGGCTC
CTGGCAAAGGTCAGAGTCTGGATCACCTTCTGCTGGAGGCCACAGCA
AACCTCCTCACAGCCCCTGGTCTCAAGAGGTGCCACGTCTCCACACA
TCAGCACAACTACGCAGCGCCTCCCTCCACTCGGAAGGACTATCCTGCT
GCCAAGAGGGTCAAGTTGGACAGTGTGAGAGTCTGAGACAGATCAGC
AACAAACGAAAATGCACCAGCCCCAGGTCTCGGACACCGAGGAGAAT
GTCAAGAGGCGAACACACAACGTCTTGGAGCGCCAGAGGAGGAACGAG
CTAAAACGGAGCTTTTTTGCCTGCGTGACCAGATCCCGGAGTTGGAAA
ACAATGAAAAGGCCCCCAAGGTAGTTATCCTTAAAAAAGCCACAGCATA
CATCCTGTCCGTCCAAGCAGAGGAGCAAAGCTCATTTTCTGAAGAGGAC
TTGTTGCGGAAACGACGAGAACAGTTGAAACACAACTTGAACAGCTAC
GAACTCTTGTGCGTAA

Material & Methods

2.2.5 Ligation

Insert and vector were ligated using the T4 DNA ligase (New England Biolabs, MA, USA) following the manufacturer's instructions. This cloning procedure was applied for *CD44* and *c-MYC*. The amount needed for the insert was calculated using the ligation calculator of the Heinrich-Heine-University Düsseldorf (www.insilico.uni-duesseldorf.de). The molar ratio of vector to insert was 1:3. Each ligation was set up in a reaction tube as follows:

Table 9 Ligation reaction mix with *CD44* and *c-MYC* and vector using T4 DNA ligase.

Reagent	Amount
Vector	50 ng
Insert	Calculated amount of insert
<i>CD44</i>	40.17 ng (1.10 µl)
<i>c-MYC</i>	24.52 ng (2.13 µl)
10x ligase buffer	1 µl
T4 DNA ligase	1 µl
dH2O	Up to 10 µl final volume

A control ligation without the insert was performed to determine the amount of false positive clones in the next step. Ligations were incubated at 16°C overnight.

2.2.6 Cold Fusion™ Cloning

A second cloning protocol was applied for *CTNNB1*, *GLI1*, *TP53R175H*, *EGFRvIII*, and *PDGFRA* as it was either not possible to get bacterial colonies or the Sanger sequencing was negative using the first cloning protocol. For the Cold Fusion™ Cloning Kit (System Biosciences, CA, USA) PCR was conducted as described before (Table 4) but the annealing temperature was reduced to 58°C and PCR products were purified using the GeneJET PCR Purification Kit (Thermo Fisher Scientific™, MA, USA). If the concentration of the purified DNA was between 20 to 200 ng, 1 µl was used for the reaction set up. Following the manufacturer's instructions the Cold Fusion™ reaction was set up as follows:

Table 10 Reaction set up for the Cold Fusion™.

Reagent	Volume/Concentration/Amount
Linearized vector	2 µl
PCR insert (20 – 200 ng)	1 µl
Cold Fusion™ 5x master mix	2 µl
dH ₂ O	Up to 10 µl

The reaction was incubated for 5 min at RT and then placed on ice for 10 min. The ligation product was used for the bacterial transformation.

2.2.7 Bacteria transformation and plasmid extraction

Bacteria transformation was performed to generate a high amount of the vector. Ligated products from both cloning strategies were used for the bacteria transformation. Chemically competent *Escherichia coli* (*E. coli*) TOP10 or alpha bacteria were used for transformation. Bacteria were thawed on ice for 10 min before the ligated vector was added. After incubation on ice for 20 - 30 min, *E. coli* were incubated at 42°C for 1 min (heat-shock) and directly put on ice for 2 min (cold-shock). Afterward, LB-medium without antibiotics or super optimal broth with catabolite repression (S.O.C) medium was added to the bacteria and incubated at 37°C at 300 rotations per minute (rpm) for 1 h. After the incubation, 100 µl of transformed *E. coli* were plated on ampicillin (100 µg/ml) LB-agar plates at 37°C overnight as the used vector contains an ampicillin resistance, which was used for selection. The next day, the control plate of the ligation was checked for false positive colonies to evaluate the efficiency of the digest. Five colonies were picked from each LB-plate with the respective GOI and transferred to a 15 ml conical tube with 5 ml LB-medium with ampicillin (100 µg/ml). Cultures were incubated at 37°C at 250 rpm overnight. To verify if the vector contained the insert, the plasmid was extracted using the GeneJET Plasmid Miniprep Kit (Thermo Fisher Scientific™, MA, USA) and sent to Eurofins Scientific SE (Luxembourg, Luxembourg) or biological-medical research center (BMFZ) Genomics and Transcriptomics Laboratories (Düsseldorf, Germany) for Sanger sequencing. Positive colonies were then grown in 150 ml LB-medium with ampicillin (100 µg/ml) at 37°C at 250 rpm overnight. Bacteria cultures were centrifuged at 2770 g for 30 min at 4°C. The respective plasmid was extracted using the NucleoBond™ Midi Kit (Macherey-Nagel, Germany) to reach a higher concentration of the desired vector.

Material & Methods

2.2.8 Cell Culture

2.2.8.1 Cell culture of HEK293T cells

HEK293T cells have a mutant version of the SV40 large T antigen, which increases transfection and transduction efficiency (DuBridge et al., 1987; Lin et al., 2014; Merten et al., 2011; Merten et al., 2016). The cells were cultured in a humidified incubator at 37°C and 5 % CO₂. Depending on the use, HEK293T cells were cultured in a T25 (after thawing), T75 (expanding) flasks, or 10 cm dishes (virus production) in DMEM/FBS medium. Spent cell culture medium was exchanged every 2 – 3 days.

2.2.8.2 Passaging of HEK293T cells

HEK293T cells were passaged when the cells reached a confluency of 80 %. The spent medium was removed and cells were washed twice using Dulbecco's phosphate-buffered saline without calcium or magnesium (DPBS -/-). Afterwards, cells were incubated with 4 ml of TrypLE™ Express (Thermo Scientific, MA, USA) at 37°C for up to 3 min. Still, adherent cells were detached by gentle shaking. The enzymatic reaction was stopped through dilution using 6 ml medium. The suspension was transferred to a conical 15 ml tube and centrifuged at 200 g for 5 min. After removal of the supernatant, cells were resuspended in 1 ml of medium and plated in a new flask or plates for lentivirus production. Plating ratio depended on the time of use and was 1:10 for expanding or 1:4 for lentivirus production.

2.2.8.3 Cryopreservation and thawing of HEK293T

HEK293T cells were prepared for cryopreservation when they reached a confluency of 80 – 90 %. For mycoplasma analysis 100 µl of the spent medium was transferred to a 1.5 ml reaction tube (please refer to 2.2.8.15). Cells were detached according to the protocol described before. After centrifugation, cells from a T75 flask were resuspended in 4 ml of freezing medium for suspension cells, consisting of DMEM and 10 % DMSO. One ml of cell suspension was transferred to a properly labeled cryovial and put in an isopropanol freezing container at -80°C. After excluding mycoplasma contamination the cells were stored in the liquid nitrogen tank.

For thawing, cells were warmed up in a water bath until only a small piece of ice was still visible. Cells were carefully resuspended in 1 ml of DMEM/FBS medium and transferred to a conical 15 ml tube. The vial was washed once with 1 ml medium, which was also added to the conical tube. Additionally, 4 ml of DMEM/FBS medium were added. Cells were

Material & Methods

centrifuged at 130 g for 5 min. The supernatant was removed and the cell pellet was resuspended in DMEM/FBS medium and transferred to a T25 cell-culturing flask for adherent cells. After two days the supernatant of the growing cell culture was tested for mycoplasma contamination (please refer to 2.2.8.15). After three passages, cells were used for experiments or virus production.

2.2.8.4 Matrigel® coating of plates

One flask of Matrigel® (MG; Corning, NY, USA) was thawed on ice overnight at 4°C. The next morning, thawed MG was gently swirled to verify an even distribution and kept on ice during the procedure. KO DMEM (Thermo Fisher Scientific™, MA, USA) was added to reach a 1:1 dilution and mixed gently by pipetting it up and down without the introduction of air bubbles. Precooled pipette tips were used to prepare 500 µl aliquots in conical 15 ml tubes and stored at -20°C until further use. For coating of hiPSC cell culture plates, one MG aliquot was used. At first, 1 ml of cold KO DMEM was added to the frozen MG and mixed by inverting the tube. When it was thawed and no residual pellet was visible, MG was further diluted with 13.5 ml KO DMEM and pipetted up and down. Wells were coated using MG: 1 ml for one 6-well, 500 µl for one 12-well, and 50 µl for one 96-well. Plates were sealed using Parafilm® (Pechiney, France) and incubated for 1 h at RT before being stored at 4°C for up to two weeks. If plates were needed, they were equilibrated to RT for at least 30 min before use. KO DMEM was removed and replaced by 2 ml of fresh mTeSR™1 medium (STEMCELL Technologies, Canada) prior to seeding of hiPSCs. Please refer also to Tigges et al. (2021).

2.2.8.5 Cultivation of hiPSCs

The hiPSCs cell line, iPS11, was purchased from Alstem (Alstem, Inc., CA, USA). Cells were cultivated in colonies on MG-coated 6-well plates in mTeSR™1 medium containing 1 % Penicillin/Streptomycin (P/S; Sigma-Aldrich, MO, USA). The medium was changed on 6 out of 7 days and supplied with the double amount for the 7th day to survive the prolonged culture time without medium exchange. Human iPSCs were cultured in a humidified incubator at 37°C and 5 % CO₂. Regularly hiPSCs were tested for mycoplasma contamination using a PCR-based method (please refer to 2.2.8.15). To guarantee a similar quality of the hiPSCs, they were kept in culture for a maximum of 10 passages.

2.2.8.6 *Passaging of hiPSCs in clusters*

Four methods were applied to detach or split hiPSCs: EDTA splitting to split small clusters of hiPSCs and single-cell splitting using Accutase™, TrypLE™ Select, or Gentle Cell Dissociation Reagent.

Under normal cell culture conditions, hiPSCs colonies were split as clusters when they reached a confluency of 70 – 80 % using the dissolving reagent 0.5 mM EDTA in DPBS -/-. Spent medium was removed from the hiPSCs, cells were washed twice by adding 1 ml of EDTA, swirling the plate, and removing it. For dissociation 1 ml of EDTA was incubated at 37°C for 5 min. After the incubation, EDTA was removed and cells were washed off using 1 ml of mTeSR™1 medium. Cell clusters were transferred in a dilution of 1:6, 1:10, or 1:12, depending on the cell growth and need, into a new MG-coated 6-well supplied with 2 ml mTeSR™1 medium. If needed, the remaining cells were collected as a pellet or frozen.

2.2.8.7 *Single-cell splitting of hiPSCs*

For experiments, where a specific number of cells were needed, hiPSCs colonies were split as single-cells. Three different approaches were used to generate a single-cell suspension. The first approach is the removal of the media and addition of 1 ml of StemPro™ Accutase™ Cell Dissociation Reagent (Thermo Fisher Scientific™, MA, USA) containing 10 µM Rock inhibitor (Selleck Chemical Llc., TX, Houston). Human iPSCs were incubated until cells dissociated for up to 10 min at 37°C and 5 % CO₂. One ml of medium was added to the well and cells were resuspended as single-cells. The addition of 3 ml of DMEM/F-12 stopped the enzymatic dissociation and single-cell suspension was collected in a conical tube. This approach was used to singularize the cells for cell viability assay.

For the second approach to singularize the cells for flow cytometry and drug screening, TrypLE™ Select (Thermo Fisher Scientific™, MA, USA) was used. Cells were washed twice using 1 ml DPBS -/- before 1 ml/well of TrypLE™ Select was added. Cells were incubated at 37°C for 5 min. After the incubation, cells were resuspended as single-cells and transferred to a 50 ml conical tube with 4 ml DPBS -/- (flow cytometry analysis) or medium (drug screening). To increase the cell yield, wells were washed once using 1 ml DPBS -/- and added to the conical tube. Single-cell suspensions were centrifuged at 300 g for 5 min. The supernatant was removed and cells were resuspended in 1 ml of mTeSR™1 medium containing 10 µM Rock inhibitor. Cells were counted by trypan blue staining and dead cells were excluded. Therefore, ten µl of the cell suspension were mixed with 40 µl trypan blue (Thermo Fisher Scientific™, MA, USA) before they were transferred to a Neubauer counting

Material & Methods

chamber. The desired number of cells was plated in mTeSR™1 containing 10 µM Rock inhibitor to inhibit apoptosis of single cells.

The third approach was used for the neural induction of hiPSC. Hence, cells were cultured under standard conditions in mTeSR™1 medium. Cells were washed once using sterile DPBS -/- and incubated with Gentle Cell Dissociation Reagent (Stemcell Technologies, Canada) for 8 – 10 min at 37°C and 5 % CO₂. Through gentle pipetting cells were dissociated and single-cells were confirmed under the microscope. All hiPSCs were collected in a conical tube. Each well was washed using 1.5 ml of DMEM/F-12 substituted with 15 mM HEPES and wash was added to the conical tube. Cells were further processed for neural induction (2.2.10.2).

2.2.8.8 Cryopreservation of hiPSCs

For cryopreservation hiPSCs were cultured until they reached a confluency of around 70 – 80 %. A sample of the spent medium was taken for mycoplasma testing (please refer to 2.2.9.1). Cells were split according to the protocol of passaging cells using 0.5 mM EDTA. After the incubation cells were washed off using 1 ml of D10 NutriFreeze medium and an additional 1 ml of freezing medium was added to the cell suspension. For each well, two cryo vials were properly labeled and 1 ml of cell suspension was transferred using a serological pipette to prevent the disruption of the colonies. Vials were transferred to an isopropanol freezing container and stored at -80°C overnight. After confirmation of the absence of mycoplasma, cells were transferred to the liquid nitrogen tank for long term storage.

For thawing, one vial was removed from the liquid nitrogen tank and warmed up in a water bath at 37°C until it was nearly thawed and only a small piece of ice was still visible. Cells were transferred to a 15 ml conical tube using a serological pipette and 1 ml of cold medium was added dropwise. The tube was shaken during the addition of medium to ensure even distribution. Afterwards, 2 more ml cold medium was added. The cryovial was washed once using 1 ml cold medium, which was added dropwise to the conical tube. Then cells were centrifuged at 200 g for 5 min. Supernatant was removed and cells were carefully resuspended using mTeSR™1 medium at room temperature and plated in one or two wells in a total volume of 2 ml medium. Cells were passaged three times before they were used for experiments. Thawed cells were tested again for mycoplasma contamination after two passages.

2.2.8.9 Lentivirus generation

HEK293T cells were used for lentivirus production. Cells were plated in a 1:4 ratio in a 10 cm dish and cultured in DMEM/FBS. The next day, HEK293T had a confluency of ~70 % and were transfected using the lentiviral packaging plasmids and the vector containing the GOI as previously described in Kahlert et al. (2012). In a 1.5 ml reaction tube, the transfection mixture was prepared. At first, 800 μ l of DMEM were mixed with 8 μ g of the vector containing the GOI and the lentiviral packaging plasmids (4 μ g of VSVG, 2 μ g REV, and 2 μ g g'p). 60 μ l of the transfection reagent FuGENE® HD (Promega, WI, USA) were added and the reaction was incubated for at least 10 min at RT. During the incubation time, spent medium was removed from the HEK293T cells and washed once using DPBS -/- and 10 ml of fresh medium DMEM/FBS without P/S was added. When the incubation time was over, the transfection mixture was added dropwise to the medium, and plates were moved in an eight-shaped manner to ensure even distribution. Cells were incubated at 37°C and 5 % CO₂ until the next day. After 24 h, spent medium was replaced by fresh medium containing 1 % P/S and after 48 h, 72 h, and 96 h supernatant was collected and filtered in a 15 ml conical tube. The filtrate was mixed with 50 % PEG and 1.5 M NaCl and stored at 4°C. On the day after the last collecting day, supernatants were centrifuged at 7000 g for 30 min at 4°C. Supernatant was removed and the pellets were resuspended and pooled in 400 μ l DPBS -/-. Aliquots with a volume of 40 μ l were prepared and stored at -80°C until further use.

2.2.8.10 Lentiviral transduction of hiPSC

On the day before the lentiviral transduction, hiPSCs were split onto a MG coated 12-well (*GLI1* and *c-MYC*) or six-well plate (*TP53R175H* and *EGFRvIII*). Spent medium was removed and replaced by fresh medium. One aliquot of the lentivirus was added to the media. For the transduction of cells using the vectors containing the GOIs *CD44*, *PDGFRA*, and *CTNNB1* S33Y, both plate formats and higher virus concentration e.g. two vials per well were tested. The following two days, half of the medium was replaced by fresh cell culture medium. Antibiotic selection was started 72 h after transduction by supplementing the medium with 1 μ g/ml puromycin. The selection was continued for one week before the hiPSCs were kept in selection medium with 0.2 μ g/ml puromycin.

2.2.8.11 P24 ELISA to determine the viral load in the hiPSC models

Determination of the viral load was done using the commercially available QuickTiter Lentivirus Kit (Cell Biolabs, Inc, CA, USA). One ml of the supernatant of hiPSC-oncogene models was collected in a reaction tube. As a control 1 ml of fresh mTeSR1 medium was used. The supernatant, HIV control standard, and the ELISA plate were prepared as described in the manual instructions. In short, 1 ml of medium was mixed with 10 µl of ViralBind™ Lentivirus Reagent A, mixed by inverting and 10 µl of ViralBind™ Lentivirus Reagent B. The mixture was incubated for 30 min at 37°C in a water bath. The samples were centrifuged at 12,000 rpm and the supernatant was discarded. Pellets were resuspended in 250 µl of Sample Diluent, vortexed, and incubated at 37°C to inactivate the viruses. The standard curve was prepared according to the manual instructions. From the standard curve, samples, and controls, 100 µl were plated in the wells in duplicate and inoculated on the plate overnight at 4°C. On the next day, wells were washed using the provided washing buffer and incubated using the primary and secondary antibodies. To each well 100 µl Substrate Solution was added and incubated on an orbital shaker. The reaction was stopped when the solution reached saturation. Read-out was done by measuring the absorbance at 450 nm. Virus concentration was calculated in comparison to the control. If the value of the sample was lower than the control, it was declared virus free. The transduced cells could be moved to a biosafety level 1 laboratory e.g. for neurosphere induction (2.2.10.2).

2.2.9 Characterization of hiPSC-oncogene models

2.2.9.1 Detection of a mycoplasma contamination

Mycoplasma are small self-replicating bacteria, that depend on eukaryotic cells and have an impact on the behavior of cells. Mycoplasma contamination is often not visible due to the absence of visible markers e.g. turbidity of medium or phenotypic changes (Nikfarjam & Farzaneh, 2012). To detect mycoplasma, a lab-derived PCR or a commercially available PCR mycoplasma Test Kit (PromoCell GmbH, Germany) were used according to the manufacturer's instructions. For the in-house established method (used for HEK293T cells) 100 µl of spent medium was collected in a 1.5 ml reaction tube and boiled to 95°C for 5 min. Afterwards, the supernatant sample was stored on ice until needed. A mycoplasma primer mix was prepared using 0.25 µl of Mycoplasma- FWD1 primer and 0.15 µl of Mycoplasma-RV1 primer (Table 11 and Table 12).

Material & Methods

Table 11 Primer sequence for lab-derived mycoplasma PCR.

Primer	Sequence 5' to 3'
Mycoplasma-FWD1	ACACCATGGGAGCTGGTAAT
Mycoplasma-RV1	CTTCWTCGACTTYCAGACCCAAGGCAT

Table 12 Reaction set-up for mycoplasma PCR master mix.

Reagent	Volume
2x GoTaq G2 Master Mix	12.5 µl
Mycoplasma-FWD1 and Mycoplasma RV1 primer mix	0.25 µl
Nuclease free water	7 µl
Boiled supernatant	5 µl

The PCR was started using the PCR protocol as follows.

Table 13 PCR conditions for lab-derived mycoplasma PCR.

Process	Temperature	Time
Activation of Taq DNA polymerase	95°C	3 min
<u>35 cycles:</u>	95°C	30 s
Denaturation		
Annealing	55°C	2 min
Elongation	72°C	1 min
Final Elongation	72°C	5 min
Hold	4-8°C	hold

As negative control water was used and as positive control a spiked sample. Eight µl of the PCR products were loaded on a 1.5 % agarose gel and run for 25 min at 100 V. Gel was evaluated using a gel imager.

Material & Methods

For all hiPSC models, a commercially available method with a higher sensitivity was applied. One ml of spent medium was collected in a reaction tube and centrifuged at 500 g for 5 min. Supernatant was transferred to a new tube and centrifuged at 14,000 g for 15 min. Pellet was resuspended in 100 µl of fresh cell culture medium or DNA-free water. The lyophilized master mix was rehydrated using 23 µl of the provided rehydration buffer and 2 µl of the prepared cell culture sample was added. The master mix includes an internal control and the test kit provides a positive control. As negative control water was used. PCR was performed according to the manual instructions. Eight µl of the PCR products were loaded on a 1.5 % agarose gel and run for 25 min at 100 V. The gel was evaluated using a gel imager.

Table 14 PCR conditions for commercially mycoplasma PCR.

Process	Temperature	Time
Activation of Taq DNA polymerase	95°C	2 min
<u>40 cycles:</u>	94°C	30 s
Denaturation		
Annealing	55°C	30 s
Elongation	72°C	40 s
Hold	4-8°C	hold

2.2.9.2 Cell viability assay

Cellular viability of each hiPSC-oncogene model and the controls was measured using the thiazolyl blue tetrazolium bromide (MTT) assay (Mosmann, 1983). Cells were split as single cells using StemPro™ Accutase™. In each well 3,000 cells were plated in 100 µl mTeSR™1 medium containing 10 µM Rock inhibitor in a 96-well plate. Cells were incubated at 37°C and 5 % CO₂. Spent medium was replaced with 100 µl of fresh medium every day. The cell viability was measured after 1 h, 2 days, and 4 days. Therefore, ten µl MTT reagent were added to each well and incubated between 1 to 3 h at 37°C and 5 % CO₂ until formazan crystals were visible under the microscope. To each well, 100 µl of MTT lysis buffer were added and the 96 well plate was placed on a plate shaker for 10 min at RT and 200 rpm to dissolve the formed crystals. In case the crystals were not completely dissolved, either the crystals were dissolved by extending the incubation on the plate shaker or a pipette was

Material & Methods

used to carefully resuspend the remaining crystals. Absorbance was measured at 570 nm and the background absorbance was measured at 650 nm using a Paradigm™ multiplate reader (Beckman Coulter, CA, USA) for the compound screening and Safire multiplate reader (Tecan, Switzerland) for viability. Human iPSC culture medium was measured as reference. For analysis, the absorbance from the background was subtracted from the measured values to determine the cell viability. For each model, the experiment was performed three independent times in triplicates.

2.2.9.3 Western Blot

Verification of protein expression was done with lysed cell samples as previously described (Koch et al., 2016). Briefly: Proteins were extracted from hiPSC pellets using an appropriate amount (approx. 20 – 30 µl) of cold protein lysis buffer and a proteinase inhibitor mixture (approx.. 1 µl; Roche Applied Science, Switzerland). Samples were incubated on ice for 30 – 45 min and vortexed every 10 – 15 min. Afterwards, they were centrifuged for 10 min at 15,870 g and 4°C. The supernatant was transferred to a new reaction tube and protein concentration was determined by preparing a 1:10 dilution of the samples for the DC Protein Assay Kit (Bio-Rad Laboratories Inc., CA, USA). On the SDS Page gradient gels, 30 – 40 µg of protein mixed with 3x SDS loading dye were loaded. The gel was run at 60 V for 15 min and then switched to 120 V for approximately 1 h. Transfer of the proteins was done in a semi-dry application on a nitrocellulose membrane at 250 mA for 2.5 h. Afterwards, the membrane was blocked using 5 % milk powder (TP53, GAPDH and secondary antibodies) or bovine serum albumin (BSA; GLI1, c-MYC, EGFR, GAPDH; VWR International, PA, USA) in TBS-T for 1 h at RT. Primary antibodies were incubated in the blocking buffer on a vertical shaker at 4°C overnight (Table 15). The next day, the membrane was washed three times for 10 min with TBS-T and incubated with respective secondary antibodies in blocking buffer on a vertical shaker for 1h at RT (Table 16). After incubation, the membrane was washed again three times using TBS-T. Signal detection was performed using the LI-COR Odyssey CLX Imager (LI-COR Biosciences, NE, USA) or a film-based system for peroxidase-coupled antibodies to detect the chemiluminescent signal with SuperSignal™ West Pico Chemiluminescent Substrate (Thermo Fisher Scientific, MA, USA). The film-based system was used to detect the protein expression of c-MYC and CD44, all other proteins were detected via the fluorescence signal. Densitometry of the proteins was measured using Image Studio (LI-COR Biosciences, NE, USA) or ImageJ (Schneider et al., 2012) for fluorescence or film, respectively.

Material & Methods

Table 15 Primary antibodies used for Western blot and detection of the proteins.

Antibody	Dilution	Company
TP53 (1C12) #2524S	1:1000	Cell Signaling Technology (Danvers, Massachusetts, USA)
EGFR #4267S	1:1000	Cell Signaling Technology (Danvers, Massachusetts, USA)
GAPDH #60004-1-Ig	1:5,000	ProteinTech Group (Rosemont, Illinois, USA)
c-MYC #13-2500	1:1000	Invitrogen (Carlsbad, California, USA)
GLI1 #2643	1:1000	Cell Signaling Technology (Danvers, Massachusetts, USA)
PDGFRA #ab65258	1:50	Abcam (Cambridge, UK)
CD44 #AF3660	1:500	R&D Systems (Minneapolis, Minneapolis, USA)

Table 16 Secondary antibodies used for Western blot and protein detection.

Secondary antibody	Primary antibody	Dilution	Company
IRDye® 680RD Donkey anti-Goat IgG Antibody	CD44	1:5,000	LI-COR Biosciences (Lincoln, Nebraska, USA)
IRDye® 680RD Donkey anti-Mouse IgG Antibody	c-MYC, TP53, GAPDH, GLI1	1:10,000	LI-COR Biosciences (Lincoln, Nebraska, USA)
IRDye® 800CW Goat-anti-Rabbit Antibody	PDGFRA	1:10,000	LI-COR Biosciences (Lincoln, Nebraska, USA)
Peroxidase-conjugated AffiniPure Goat Anti-Mouse IgG (H + L)	CD44, GAPDH	1:10,000	Jackson ImmunoResearch Laboratories Inc. (West Grove, Pennsylvania, USA)
Peroxidase-conjugated AffiniPure Goat Anti-Rabbit IgG (H + L)	EGFR	1:10,000	Jackson ImmunoResearch Laboratories Inc. (West Grove, Pennsylvania, USA)

2.2.9.4 Cytogenetic analysis of generated hiPSC-oncogene models – Karyogram

All hiPSC-oncogene models were cytogenetically analyzed using GTG-banding of chromosomes adapted from Howe et al. (2014) to see if chromosomal changes occurred due to the transduction. Cells were expanded and transferred as a proliferating culture in a T25 MG coated flask to the Institute of Human Genetics (University Clinic Düsseldorf). The next day, hiPSC medium was replaced. When cells reached a confluency of 80 %, 10 µl/ml colcemid were added to arrest hiPSCs in the metaphase. After 2 – 5 h of incubation time cultures were microscopically assessed for rounded cells. Supernatant was removed and kept for later use, while the cells were washed with 2 mL Hanks' solution. One ml of pre-warmed trypsin was added to the cells and incubated for 2 to 5 min. Dislodging of the cells was increased by tapping against the flask and verified using microscopic assessment. Cells

Material & Methods

were transferred to the conical tube with the supernatant from the previous step and centrifuged at 1,000 g for 10 min. Supernatant was discarded and cells were resuspended in 10 ml 0.075 M KCl using a vortexer at medium speed. Afterwards, hiPSCs were incubated for 20 min in the KCl solution at RT and centrifuged at 1000 g for 10 min. The cell pellet was resuspended using 8 ml of fresh Carony's Fixative (methanol/glacial acetic acid, ratio 3:1) on a vortexer and again centrifuged at 1,000 g for 10 min. Carony's Fixative was used to resuspend the cell pellet. Cytogenic analysis was performed on slides. At first, cells were centrifuged at 1,000 g for 10 min, and the supernatant was discarded. In the remaining supernatant, approx. 0.5 ml, cells were resuspended. Three drops of this cell suspension were transferred on a tilted slide and ran over the slide to separate the chromosomes. Carony's Fixative was added to the slide and left to dry for at least 10 min at RT. Afterward, each slide was dipped in a solution containing di-sodium hydrogen phosphate/potassium dihydrogen phosphate + 0.5 % trypsin for 3 min and rinsed in a 0.9 % NaCl solution. To discriminate between gene-poor heterochromatic and active euchromatic regions, slides were dried and stained with fresh Giemsa Staining Solution (Gurr Buffer and Giemsa Stain, ratio 3:1) for 5 min and washed with distilled water before they were dried at RT. Slides were covered with Entellan® (Merck, Germany). Between 2 to 16 slides were scanned using the scanning system Metafer (MetaSystems Hard & Software GmbH, Germany). Up to 24 metaphases were analyzed and karyotyped using the karyotyping system Ikaros from MetaSystems and described according to McGowan-Jordan et al. (2016). Quality ranged from 200 – 350 band levels.

2.2.9.5 Flow cytometric assessment of stem cell marker in hiPSC-oncogene models

The expression of stem cell markers on protein level in hiPSCs was done using the BD™ Human Pluripotent Stem Cell Transcription Factor Analysis fluorescence-activated cell sorting (FACS) Kit (Becton, Dickinson and Company, NJ, USA). Cells were cultured until they reached a confluency of maximal 80 % after 3 to 5 days after the last splitting. Single-cell suspension was achieved using the TrypLE™ Select splitting protocol as described above (please refer to 2.2.8.7). For each split well, 3 ml of DPBS -/- were added in a 50 ml conical tube. Single-cells were pooled and wells washed once using 1 ml of DPBS -/- and added to the tube as well. One million cells were transferred to a flow cytometry tube. In total seven staining conditions were analyzed (Table 17). Cells were stained according to the manufacturer's instruction but centrifugation steps were extended to 10 min to increase the cell yield.

Material & Methods

Table 17 Overview of the flow cytometry staining.

Samples were stained using viability dye, OCT3/4-PerCP, Sox2-Alexa647, Nanog-PerCP, and the isoform controls. Viability dye was used to determine the viable number of cells.

Staining sample	Viability dye	Antibody
1	-	-
2	+	-
3	-	Isotype-PerCP Isotype-Alexa647 Isotype-PE V450 Mouse anti-Ki 67
4	+	OCT3/4-PerCP Sox2-Alexa647 Nanog-PE
5	+	Nanog-PE
6	-	OCT3/4-PerCP
7	-	Sox2-Alexa647

As controls, unstained samples and a viability control were used as well as the respective isotypes controls for the antibodies. Cells were stained at first with the fixable viability dye Fvs510 (Becton, Dickinson and Company, CA, USA) for 15 min at RT and washed using prepared staining buffer (DPBS -/- with 2% heat-inactivated KSR; Thermo Fisher Scientific, MA, USA). After washing, hiPSCs were fixed using the provided BC fixation buffer for 20 min at RT. Human iPSCs were washed and permeabilized using the provided Perm/Wash buffer for 20 min at RT. In the last step, hiPSCs were stained using the PerCP-Cy™ 5.5 Mouse anti-OCT3/4, PE Mouse anti-human Nanog, Alexa Fluor® 647 Mouse anti-Sox2, and the respective isotype controls for 30 min at RT. After washing the cells were measured on the CyAn Beckman Coulter (CA, USA) and analyzed using the provided software Summit V4.3.03 (Beckman Coulter, CA, USA).

2.2.9.6 Methylome analysis

DNA was extracted using the Qiagen DNA Blood and Tissue Kit (Qiagen, Germany). As described before (please refer to 2.2.8.7) cell pellets were collected using the protocol for EDTA splitting and washed once using DPBS $-/-$. DNA concentration was measured using the NanoDrop device and diluted to reach a concentration of 25 ng/ μ l and sent to the German Cancer Research Center (Heidelberg, Germany) for further analysis. For each hiPSC-oncogene model, one biological replicate was analyzed. Each DNA sample was bisulfite converted and applied to the Infinium MethylationEPIC Array (Illumina Inc., CA, USA). Molecular subgrouping, copy number profiling, and beta-methylation were performed as described in Capper et al. (2018). Covariance Principle Component analysis (PCA) was performed where genes with a higher variance have more influence on the clustering using the Partek® Genomics Suite® software (Partek Incorporated, MO, USA). Additionally, Ingenuity Pathway Analysis (IPA; Qiagen, Germany) was conducted by filtering the samples for uniquely regulated genes (<0.3582 unmethylated and >0.3582 methylated) with an exception of *TP53R175H*, *EGFRvIII*, and *EGFRvIII/TP53R175H*. For these three models, the same genes were expected to be present in all of them. IPA was performed to identify upstream regulators and canonical pathways of the respective oncogenes that were introduced to the cells. Both were run with default settings except for the knowledge where high-confidence predictions were added. The significance cut-off for IPA was set to a p-value of <0.05 . For the upstream regulators, biological drugs, all chemical and miRNA entries were filtered out and had to include at least three target genes to be considered for analysis.

2.2.9.7 Transcriptome analysis

The cell pellet was collected from either one well of a 6-well plate following the EDTA splitting protocol or 20 human neurally induced hiPSC (hiNPC) spheres. RNA was isolated from the pellet using the RNA Nucleospin Kit (Macherey-Nagel, Germany) according to the manufacturer's instructions. Concentration was measured using a NanoDrop device and RNA was stored at -80°C . Total RNA was extracted as described (please refer to 2.2.11.1) and transferred to the Biological-Medical Research Center (BMFZ) of the Heinrich-Heine-University Düsseldorf, Germany. A transcriptome library was generated from 300 ng RNA using the VAHTS™ Stranded mRNA-Seq Library Prep Kit for Illumina® V2 (Vazyme, China) and sequenced using the HiSeq 3000 platform (Illumina Inc., CA, USA). Each sample was sequenced with 2x 151 base pairs (bp) paired-end reads and with at least 50 million reads. Analysis of the results was performed using R (R Development Core Team, 2010). All generated hiPSC-oncogene models were compared to the EV control using the unpaired

Material & Methods

student's *t*-test. Fold change was calculated with the ratio of the average gene expression. The results of the differentially expressed genes were displayed in volcano plots. Significantly expressed genes had a *p*-value of <0.05 and fold change >2. Decreased genes had a *p*-value of <0.05 and a fold change of <-2. Significantly increased or decreased genes identified from the volcano plot were further analyzed using DAVID Bioinformatics Resources 6.8 (Huang da et al., 2009a, 2009b). As background *homo sapiens* was selected. Obtained gene ontology (GO) terms from the analysis were sorted in ascending order.

2.2.9.8 Immunocytochemistry

Immunocytochemistry (ICC) was done with a co-staining of antibodies to verify the stem cell character (OCT3/4 and TRA-1-60) for hiPSCs. Induced neurospheres were incubated with the neural markers beta-III-Tubulin and NESTIN. Based on the staining the pluripotency and neural differentiation can be evaluated.

In a 96-well plate, the hiPSCs were cultured until they reached the desired density (approx. 40 – 50 %) where single colonies were still visible. Induced neurospheres were chopped two days before plating to reach a size of approx. 300 µm. One sphere was plated in one well of a coated 96-well plate in 100 µl medium. For each condition, six technical replicates were done. Human iPSCs and neurospheres were fixed by the application of 100 µl 4 % paraformaldehyde (PFA) in DPBS -/- and incubated at 37°C for 30 min. Cells were washed after the incubation 2 – 3 times using DPBS -/- and stored in 100 µl DPBS -/- at 4°C. Immunocytochemical staining was performed within two weeks after fixation. At first, cells were permeabilized using 0.1 % Triton X-100 diluted in PBS for 20 min at RT. Cells were washed and blocked in 10 % goat serum (Merck, Germany). Human iPSCs were incubated in 0.2 % goat serum with the conjugated primary antibodies against TRA-1-60 and OCT3/4 overnight at 4°C. Neurospheres were incubated overnight with the primary antibody β-III Tubulin (Table 18). The next day, spheres were washed three times using PBS and incubated with the secondary antibody (Table 18). At the same time, nuclei were stained using 1 % Hoechst. Secondary antibodies and Hoechst were incubated for 1h at 37°C. Cells were washed three times using 100 µl PBS. Signal was detected using the Cellomics Arraycan CTI (Thermo Fisher Scientific, MA, USA), and pictures were taken using the Photometrics™ X1 camera (Thermo Fisher Scientific, MA, USA). Pictures were merged and adapted for their brightness in ImageJ (Schneider et al., 2012).

Material & Methods

Table 18 Antibodies used for immunocytochemical staining.

Antibodies were used for immunocytochemical (ICC) staining of the human induced pluripotent cells (hiPSC) oncogene models to verify pluripotency. Further, neurally induced hiPSC (hiNPC) spheres were analyzed for the expression of neural marker.

Antibody	Dilution	Company
BD™ Oct3/4 Alexa Fluor® 555 #560306	1:50	Becton, Dickinson, and Company (Franklin Lakes, NJ, USA)
BD™ TRA-1-60 Alexa Fluor® 647 #560122	1:50	Becton, Dickinson, and Company (Franklin Lakes, NJ, USA)
BD™ Anti-Nestin Alexa Fluor® 647 #560341	1:200	Becton, Dickinson, and Company (Franklin Lakes, NJ, USA)
Anti-β-Tubulin III antibody produced in rabbit; #T2200	1:250	Merck (Darmstadt, Germany)
Goat anti-Rabbit IgG(H+L) Cross- Absorbed Secondary Antibody, Alexa Fluor™ 546; A11010	1:500	ThermoFisher Scientific (Waltham, Massachusetts, USA)

2.2.9.9 Pharmacological screening of hiPSC-oncogene models

Generated hiPSC-oncogene models were tested in a pharmacological screening to identify sensibility or resistance towards nine U.S. Food and Drug Administration (FDA)-approved drugs and two controls (Table 19). As negative control acetaminophen was used and as positive control staurosporine. At first, 96-wells were coated using Matrigel® resuspended in KO DMEM. Clusters of each hiPSC model were treated using TrypLE™ Select to get single-cells and plated out in a density of 10,000 cells/well in a volume of 50 µl with 10 µM Rock inhibitor. The next day, medium was removed and cells were exposed to the selected substances. For each drug, a serial dilution was prepared to reach concentrations of 20 µM, 2 µM, 200 nM, 20 nM, 2 nM, 200 pM, and 20 pM. After 48 h incubation at 37°C and 5 % CO₂, viability was analyzed according to the MTT protocol as described above (please refer to 2.2.9.2). Absorbance was measured and normalized to the DMSO-treated control and the two lowest concentrations (Krebs et al., 2018). For each model, the experiment was performed three independent times in triplicates. The efficacy of the drugs was analyzed based on their effective concentration 50 (EC₅₀) using the GraphPad Prism software (GraphPad Software, CA, USA). The upper threshold was set to 100 for curve fitting.

Material & Methods

Table 19 Drugs used for the pharmacological screening in hiPSCs.

The pharmacological screening was conducted with nine drugs. For each drug the chemical abstract service registry number (CAS) and disease was identified. *Italic written drugs were used as controls.* The information for each drug was taken from the website www.drugbank.com (Wishart et al., 2006).

Drugs	CAS number	Disease/Treatment
Almotriptan malate	181183-52-8	Migraine
Apatinib mesylate	1218779-75-9	Gastric cancer
Calcium folinate	1492-18-8	Anemia
Cariprazine	1083076-69-0	Schizophrenia
Duvelisib	1201438-56-3	Chronic lymphocytic leukemia or small lymphocytic lymphoma
Lomustine	13010-47-4	Primary and metastatic brain tumors, Hodgkin's disease
Panobinostat	404950-80-7	Multiple myeloma
<i>Acetaminophen</i>	103-90-2	Pain treatment and reduction of fever
Rivastigmine	123441-03-2	Dementia and Parkinson's
<i>Staurosporine</i>	62996-74-1	Not approved, induces apoptosis
Vinblastine sulfate	143-67-9	Several cancer diseases e.g. breast cancer, neuroblastoma non-Hodgkins lymphoma

2.2.10 Cell culture of hiNPC-oncogene models

2.2.10.1 Matrix coating of plates for neural induction and cultivation of neurospheres

Neural induction following the protocol for the 2D induction was done on poly-L-ornithine (PLO; Sigma-Aldrich, MO, USA) and laminin (Sigma-Aldrich, MO, USA) coated 6-well plates. At first, PLO was diluted using DPBS -/- to reach a final concentration of 0.015 mg/ml. Each

Material & Methods

well of a 6-well plate was coated using 1 ml of PLO solution and incubated for either 2 h at RT or overnight at 4°C. PLO solution was removed after incubation and washed twice using 1 ml of DPBS -/- and once using DMEM/F12 with 15 mM HEPES (STEMCELL Technologies, Canada). Laminin was diluted using DMEM/F12 with 15 mM HEPES to reach a final concentration of 0.01 mg/ml. One ml of laminin was added to each 6-well and again incubated for 2 h at RT or overnight at 4°C. Plates were wrapped using Parafilm® and stored for up to 2 weeks at 4°C. Before use, plates were warmed up to RT for at least 30 min.

Neurospheres were cultured on poly-HEMA coated dishes to prevent attachment. At first, 39.5 ml of 96 % (vol/vol) ethanol were mixed with 500 µl of deionized water and 1.2 g of poly-HEMA. To dissolve poly-HEMA it was stirred for 5 – 16 h on a magnetic stirrer and stored afterward at 4°C for up to 2 months. A 10 cm dish was plated using 3 ml of poly-HEMA solution and distributed to cover the whole surface. To allow the poly-HEMA solution to evaporate the lid was removed and the plate left under the sterile hood for 2 – 16 h. Coated dishes were stored at RT for up to 3 months in the dark.

2.2.10.2 Neural induction of hiPSC-oncogene models in 2D and in 3D

The 2D neural induction of hiPSCs was established using the STEMdiff™ SMADi Neural Induction Kit (Stemcell Technologies, Canada). Human iPSCs were split as single-cells using Gentle Cell Dissociation Reagent (please refer to 2.2.8.7). Dissociated cells were centrifuged and resuspended in 1 ml of neural induction medium (NIM). Cells were counted using trypan blue staining to exclude dead cells in a Neubauer counting chamber. In each PLO-laminin coated well, 5.0×10^5 cells were plated in 2 ml of STEMdiff™ SMADi medium with 10 µM Rock inhibitor. Spent medium was replaced every day by fresh medium. When hiNPCs reached a confluency of 80 %, they were split using Accutase™. One mL of Accutase™ was added to each well and incubated for 5 - 10 min at 37°C and 5 % CO₂. Single cells were generated by pipetting up and down and single cells were confirmed under the microscope. Afterwards, cells were resuspended in 1.5 mL of DMEM/F12, and the cell suspension was transferred in a 15 ml conical tube and centrifuged at 300 g for 5 min. The cell pellet was resuspended in 1 ml of STEMdiff™ SMADi medium. Cells were counted and stained with trypan blue to exclude dead cells. Between 3.25×10^5 – 4.25×10^5 cells were plated in 2 ml of STEMdiff™ SMADi medium with 10 µM Rock inhibitor. Induced NPCs were evenly distributed in the 6-well plate by moving the plate in an eight-shaped manner. Medium was changed daily until hiNPCs reached a confluency of 80 – 90 % and split again using Accutase™ as described above. After two passages, single-cells were collected as described above in a conical tube, counted, and 1.2×10^6 cells were plated in one well of a 6-well AggreWell™ plate (Figure 6). Before use, AggreWell™ wells were pre-treated using the

Material & Methods

provided anti-adherence rinsing solution and centrifuged at 1,300 g for 5 min. Microscopic assessment was done to verify the absence of air bubbles in the wells. Anti-adherence solution was removed by pipetting and the well was washed once using 2.5 ml of DPBS -/- before 5 ml of STEMdiff™ SMADi medium was added to one 6-well of the AggreWell™ plate. In each well, 1.2×10^6 cells were plated and gently pipetted up and down to reach an even distribution of the hiNPCs. To guarantee a sphere formation with a similar number of hiNPCs, the plate was centrifuged at 100 g for 3 min. Microscopic assessment verified the collection of cells and the absence of air bubbles within the wells. Plates were incubated at 37°C and 5 % CO₂. The next day, spheres within the individual AggreWells™ had similar sizes in the plate. Two ml of medium were removed and cells were resuspended in the remaining medium and transferred to a poly-HEMA coated 10 cm dish supplied with B27 proliferation medium (Figure 6).

The neural induction of hiPSCs can also be performed in 3D by using the NIM medium and transferring the cells to poly-HEMA coated dishes (Denham & Dottori, 2011; Hofrichter et al., 2017; Nimitz et al., 2020). One day prior to the neural induction, 3 - 4 wells of a 6-well plate of hiPSCs are assessed for differentiated cells. If differentiated hiPSCs were observed, they were removed carefully using the tip of a 100 µl pipette. On the next day, 1 ml of spent medium was removed and 1 µl of Rock inhibitor was added to the remaining medium. After 1 h incubation at 37°C and 5 % CO₂ the remaining medium was discarded and the cells were washed once with pre-warmed PBS -/- containing 1 % P/S. To each well, 1 ml of NIM was added before the passage tool was rolled once from top to bottom and once from left to right through the well (Figure 6). The cut colony-fragments were carefully lifted using a cell scraper and transferred to a poly-HEMA coated 6 cm dish with 5 ml of fresh NIM and Rock inhibitor. The spent medium was replaced every second day. After 7 days post neural induction, a new poly-HEMA coated 6 cm dish was prepared and 5 ml of NIM containing 10 ng/ml basic fibroblast growth factor (bFGF; Figure 6). The spheres were transferred to the prepared 6 cm dish and cultivated for another 14 days. Spent medium was replaced every second day by fresh NIM containing 10 ng/ml bFGF. After 21 days post neural induction, the neurospheres were transferred to a new poly-HEMA coated 6 cm dish and cultivated in B27 proliferation medium (Figure 6). Spent medium is changed every second day and cells are passaged by chopping the cells as described above.

Material & Methods

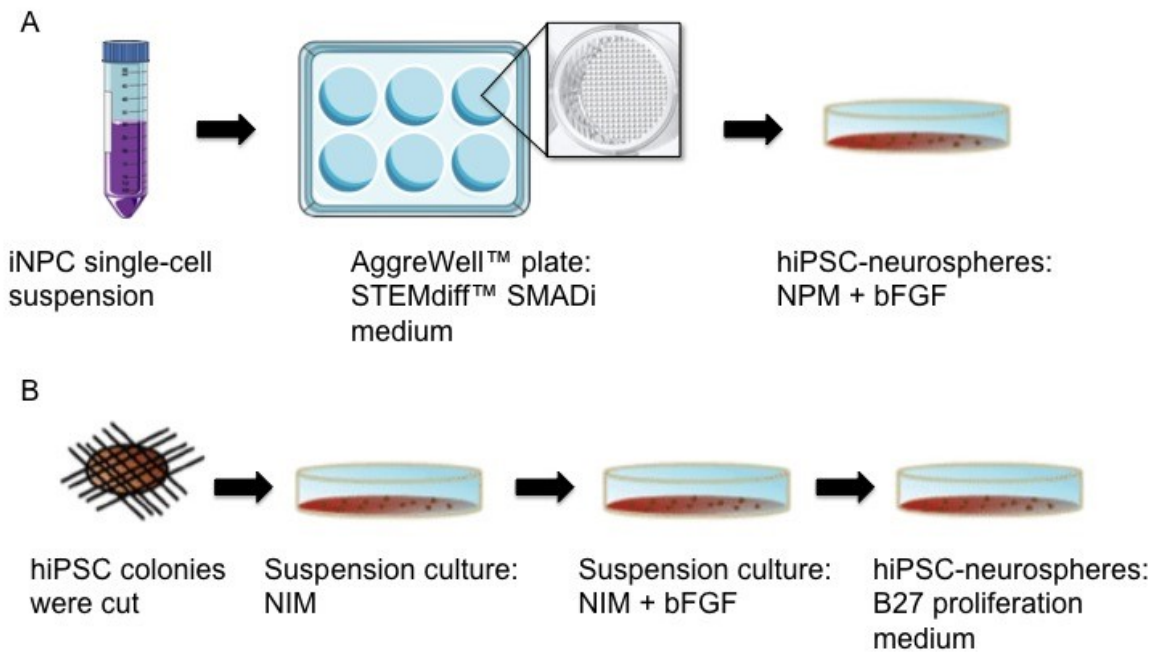


Figure 6 Neural induction of hiPSC in 2D and 3D.

Neural induction of hiPSC-oncogene models in 2D is done by plating single-cell suspension of human induced neural progenitor cells (hiNPC) into the AggreWell™ plate in STEMdiff™ medium (A). The next day, spheres are transferred to poly-HEMA coated dishes. For the neural induction in 3D, hiPSC-oncogene colonies are cut and transferred to poly-HEMA coated dishes (B; (Denham & Dottori, 2011)). The suspension culture is cultivated for 7 days in NIM before 10 ng/ml bFGF are added. After 21 days post neural induction, the hiPSC-neurospheres are cultivated in B27 proliferation medium. The figure was adapted from (Hofrichter et al., 2017). The figure was created using Servier Medical Art, provided by Servier, licensed under a Creative Commons Attribution 3.0 unported license (<https://smart.servier.com>).

2.2.10.3 Culturing of hiNPC-oncogene models

Neurally induced spheres were cultivated on poly-HEMA coated 10 cm dishes in a humidified incubator (37°C, 5 % CO₂) in B27 proliferation medium. The growth factor FGF was added directly to the medium before the medium was changed to prevent degradation. Half of the spent medium was replaced by fresh cell culture medium twice a week. Briefly, the plate was moved circularly to collect all spheres in the middle of the plate. Half of the medium was carefully removed from the side and fresh medium was added. Depending on the growth, spheres were passaged once per week (please refer to 2.2.8.14). After passaging, spheres are transferred to a new poly-HEMA coated dish supplied with 15 – 20 ml of fresh medium.

2.2.10.4 Passaging of neurospheres

Neurospheres were passaged using a McIlwain tissue chopper (Mickle Laboratory, UK) in a cell culture hood. A razor blade was sterilized using 70 % EtOH and attached to the tissue chopper. Proliferating neurospheres were collected in the middle of the 10 cm dish by

Material & Methods

moving it in a circular motion. Spheres were taken up using a Pasteur pipette or a 1000 μ l pipette tip and transferred to the inside of a 5 cm lid as a drop. As much medium as possible was removed from the cells. Afterward, the dish was placed under the razor blade and the neurospheres were cut into smaller pieces with a diameter of approx. 200 μ m. The dish was turned by 90° and the neurospheres were cut again. Cells were resuspended in medium and transferred to one (for culturing) or two (for expanding) 10 cm poly-HEMA coated dishes with fresh medium.

2.2.11 Characterization of hiNPC-oncogene models

2.2.11.1 RNA extraction

RNA of the 2D hiNPC-oncogene models was isolated using the RNA Nucleospin Kit (Macherey-Nagel, Germany) according to the manufacturer's instructions. The RNA concentration was measured using the NanoDrop2000 spectrometer (Thermo Scientific, USA) and stored at -80°C until further use. Following the manufacturer's instructions, RNA was transcribed into cDNA using the M-MLV reverse transcriptase (Promega, USA) and random hexameric primers (Thermo Scientific, USA). At first, 2,000 ng of RNA were diluted in 14 μ l of nuclease free water. One μ l of random hexamer primers was added to the reaction and incubated at 70°C for 5 min in the CFX connect thermocycler (Bio-Rad Laboratories Inc, CA, USA). After the incubation, the remaining components were added as follows:

Table 20 Reverse transcription of RNA into cDNA reaction mix.

Reagent	Volume
5x buffer	5 μ l
dNTP mix	2.5 μ l
RNase inhibitor	1 μ l
Reverse transcriptase	1 μ l

Material & Methods

The cDNA synthesis was performed in a thermo cycler using the following program:

Table 21 Thermocycler conditions for cDNA synthesis.

Temperature	Time
25°C	10 min
42°C	60 min
70°C	10 min
72°C	30 s per kb
10°C	hold

The reaction mix was diluted using 175 µl nuclease free water to reach a final cDNA concentration of 10 ng/ µl.

To perform quantitative real-time PCR (qPCR), a reaction mix containing 10 ng cDNA, 10 pmol/primer, and 2x SYBR Green qPCR Master Mix (Absource Diagnostics GmbH, Germany) was prepared. The reaction mix was run in a CFX Connect Thermocycler (Bio-Rad Laboratories Inc, CA, USA) using the following program:

Table 22 Thermo cycler protocol for qPCR.

Step	Temperature	Time
1. Initial denaturation	95°C	5 min
2. 39 cycles:		
Denaturation	95°C	15 s
Annealing	60°C	30 s
Elongation	72°C	30 s per kb
3. Final extension	72°C	10 min
4. Hold	4°C	

Relative expression of the target genes was compared to the housekeeping gene *β-Actin*. Evaluation of the messenger RNA (mRNA)-expression was done using the Bio-Rad CFX Manager software (Bio-Rad Laboratories Inc, CA, USA) and GraphPad Prism 8 software (GraphPad Software, CA, USA). Three technical replicates in three biological replicates were analyzed.

Table 23 Primer used for qPCR.

Primer	Forward primer (5' – 3')	Reverse primer (3' – 5')
<i>β-actin</i>	CCCAGCACAATGAAGATCAA	CGATCCACACGGAGTACTTG
<i>TP53</i>	CCTCAGCATCTTATCCGAGTGG	GCTCTGACTGTACCACCATCCA
<i>EGFR</i>	TAGCAGTCTTATCTAACTATGAT	CGCCCTGTATCAGTCGTAC
<i>EGFRvIII</i>	GGCTCTGGAGGAAAAGAAAGGTAATT ATGT	TCACACATTGCCTTATCCATAAC CA

2.2.11.2 Analysis of neural progenitor cell markers in hiNPC-oncogene models by flow cytometry

Human iNPCs were stained using antibodies against OCT3/4, PAX6, NESTIN, and the proliferation marker Ki-67 (Table 24).

Table 24 Antibodies used for detection of neural progenitor markers by flow cytometry.

Antibody	Company
Oct3/4-PerCP-Cy5.5	Becton, Dickinson, and Company
Pax6-PE	Becton, Dickinson, and Company
Nestin-Alexa 647	Becton, Dickinson, and Company
V450 Mouse anti-Ki67	Becton, Dickinson, and Company
Isotype control PerCP-Cy5.5	Becton, Dickinson, and Company
Isotype PE	Becton, Dickinson, and Company
Isotype AF 647	Becton, Dickinson, and Company
Isotype V450	Becton, Dickinson, and Company

Human iPSC-NPC spheres of two plates were collected in a reaction tube and centrifuged at 300 g for 5 min and then washed once using pre-warmed PBS *-/-*. The cell pellet was resuspended using 600 μ l Accutase™ and three times incubated for 5 min at 37°C and centrifuged at 800 rpm. Every 5 min the pellets were resuspended by pipetting 10 – 15 times up and down. After the last incubation step, cells were centrifuged for 5 min at 300 g and washed once using PBS *-/-*. Cells were resuspended in 1 ml PBS *-/-* and counted using a

Material & Methods

Neubauer counting chamber. For each staining condition at least 5×10^5 cells were needed. On the first day, samples 1, 5, 6, 7, and 8 and samples 2, 3, and 4 (Table 24) were processed in one reaction tube. Cells were centrifuged and washed once in PBS -/- before they were resuspended in 500 μ l PBS -/-. Fixable viability stain 510 was added to the tube containing samples 2,3 and 4 and directly vortexed. The samples were incubated for 15 min at RT in the dark and afterward centrifuged at 300 g for 5 min, and washed twice using the BD staining buffer. For fixation cells were incubated in BD Cytfix Fixiation Buffer for 20 min at RT in the dark and washed twice using 300 μ l and centrifuged at 500 g for 5 min. After the last washing step cells were vortexed to dissociate the cells and 100 μ l of ice-cold BD Phosflow Perm Buffer III per sample were added, vortexed, and incubated on ice for 30 min. After this step cells were frozen at -80°C and either processed the next day or stored at -20°C for up to 6 months. Thawed samples were then distributed evenly to get the 8 samples. Cells were washed twice using 200 μ l BD Stain Buffer and centrifuged at 500 g for 5 min and resuspended in 100 μ l BD Stain Buffer. Samples were stained using the antibodies against OCT3/4, PAX6, NESTIN, and Ki-67 as well as the respective isotype controls for 30 min at RT in the dark and washed twice using 1 ml of BD Stain Buffer, centrifuged for 5 min at 500 g, and resuspended in 300 μ l BD Stain Buffer. Resuspended cells were measured using the BD Canto™ flow cytometer.

Table 25 Overview of the staining and used antibodies for each sample.

Staining sample	Viability dye	Antibody
1	-	-
2	+	-
3	+	Oct3/4-PerCP-Cy5.5 Pax6-PE Nestin-Alexa 647 V450 Mouse anti-Ki 67
4	+	Isotype control PerCP-Cy5.5 Isotype control PE Isotype control AF 647 Isotype control V450
5	-	Oct3/4-PerCP-Cy5.5
6	-	Pax6-PE
7	-	Nestin-Alexa 647
8	-	V450 Mouse anti-Ki 67

2.2.11.3 Pharmacological screening of the hiNPC-oncogene models

Pharmacological screening was conducted of proliferating cultures derived from the 3D hiNPC-oncogene models. The substances panobinostat, vinblastine sulfate, lomustine, and duvelisib, were tested as they showed cell viability reducing effects in hiPSC-oncogene models (please refer to 2.2.9.9). Acetaminophen and staurosporine were examined as negative and positive control, respectively. The compounds were serial diluted to reach a final concentration of 20 μ M, 2 μ M, 200 nM, 20 nM, 2 nM, 200 pM, and 20 pM using B27 proliferation medium. The hiNPC-oncogene models were washed once with DPBS -/- before they were treated with TrypLE™ for 3 min to dissociated the neurospheres. The enzymatic dissociation of the cells was stopped by adding 5 ml of B27 proliferation medium. Single-cell suspension was centrifuged at 300 g for 5 min. The supernatant was removed and cells were resuspended in 1 ml of B27 proliferation medium. Cells were counted by trypan blue staining and dead cells were excluded. In each well of a 384-well plate, 5,000 cells were seeded in 30

Material & Methods

μ l B27 proliferation medium. Cell viability was assessed after 72 h using luminescence-based CellTiterGlo® (Promega, USA) according to manufacturer's protocol. Briefly, CellTiterGlo® reagent was diluted 1:1 using DPBS -/- and 30 μ l of CTG solution was added to each well. The plate was incubated for 10 min in the dark before the luminescence was evaluated using the Paradigm® microplate reader (Molecular Devices LLC, CA, USA). Three technical replicates in three biological replicates were analyzed. The EC of each compound was determined as described above in 2.2.8.24.

In addition, a second pharmacological screening was conducted. Gene expression profiles of clinical MB and GBM subtypes were accessed through TCGA (<https://www.cancer.gov/tcga>) or Chinese Glioma Gene Atlas (CGGA; <http://www.cgga.org.cn/index.jsp>) and used for a drug prediction based on the effectiveness (D-score) and the affected gene (G-score; Table 26). From these predicted substances, the top three candidates were chosen for each MB and GBM subgroup based on the ability to pass the BBB, modes of action as well as their applicability in the laboratory. To ensure that concentrations are used that can be also achieved *in vivo*, the C_{Max} , and protein binding to the respective substances was researched in the literature (Samir S. Ayoub, 2021; Dutreix et al., 2013; Liston & Davis, 2017). Further, the calculated free drug concentration (cfdc) was determined and defined that the observed effect within the *in vitro* models must be in the range of $cfdc_{high}$ ($cfdc \times 3$) to be considered a specific effect (Table 26).

Material & Methods

Table 26 Identified compounds for the compound-screening in hiNPCs.

Based on the gene expression profiles of MB and GBM a drug prediction was done and nine compounds were identified. Some compounds were predicted for treatment of MB and GBM. Further, the standard of care (SoC) cisplatin (MB) and temozolomide (GBM) were used as positive controls while acetaminophen was used as a negative control (NC). For each compound the maximal concentration, protein binding and calculated free drug concentration (cfdc) was calculated.

Substance	CAS #	C _{max} [μM]	Protein binding [%]	cfdc [μM]	Cfdc _{high} [μM]	Model
Acetaminophen	103-90-2	120.00	20.00	96.00	288.00	MB/GBM*
Arsenic trioxide	1327-53-3	0.91	75.00	0.69	2.08	MB
Bosutinib	380843-75-4	0.38	96.00	0.02	0.05	GBM
Cabozantinib	849217-68-1	4.61	99.70	0.01	0.04	GBM
Cisplatin	15663-27-1	14.40	0.00	14.40	43.20	MB**
Copanlisib	1032568-63-0	0.96	84.20	0.15	0.46	MB/GBM
Dabrafenib	1195765-45-7	4.86	99.70	0.01	0.04	GBM
Dasatinib	302962-49-8	0.26	96.00	0.01	0.03	MB
Midostaurin	120685-11-2	2.78	99.80	0.01	0.02	MB/GBM
Olaparib	763113-22-0	13.10	82.00	2.36	7.07	GBM
Regorafenib	755037-03-7	8.08	99.50	0.04	0.12	MB/GBM
Temozolomide	85622-93-1	37.60	15.00	31.96	95.88	GBM**
Trametinib	871700-17-3	0.02	97.00	0.00	0.00	GBM
Tretinoin	302-79-4	1.15	95.00	0.06	0.17	MB
Vandetanib	443913-73-3	2.16	90.00	0.22	0.65	MB/GBM

* NC; **SoC

Effectiveness of the compound was determined by measuring the proliferation, migration, and cytotoxicity of the hiNPC-oncogene models (Koch et al., 2022). To bioinformatically evaluate and subsequently classify the data as shown in Figure 7, a custom-generated and R-based evaluation pipeline was applied (Keßel et al., 2022). The compound-treated samples were normalized to the respective solvent controls and the curves were subsequently re-normalized (Krebs et al., 2018). The R package drc served as the basis for

Material & Methods

the curve fits (Ritz et al., 2015). To find the fit model that best describes the given data, a linear, sigmoidal, monotonic, and non-monotonic curve fit model and the Akaike information criterion of each model as an indicator of the best fit were used (Buatois et al., 2018; Portet, 2020). The data was analyzed according to the decision diagram shown in Figure 7. Briefly, first it was determined if the BMC for a given endpoint was reached. If yes, the upper limit (BMCU) was available and lower than the calculated $cf_{dc_{high}}$ was defined as a specific hit (Figure 7). If the BMCU was reached but the BMC was higher than the $cf_{dc_{high}}$, the hit was defined as unspecific. If the BMCU was not reached, and the effect was not significant, it was defined as an unspecific hit. Finally, if the respective BMC_{15} for migration or BMC_{10} for cytotoxicity was not reached, the compound was classified as no hit in the MB compound screening (Figure 7). If the respective BMC_{30} for migration, BMC_{10} for cytotoxicity, and BMC_{50} for proliferation was not reached the compound was classified as no hit in the GBM compound screening. The data was evaluated using the benchmark method. This is used in toxicology as a statistical-mathematical analysis of concentration-response data. A benchmark concentration (BMC) for each endpoint was estimated, which leads to an effect with a certain probability. The BMC was thus linked to a BM-response (BMR) fixed in advance (based on the dispersion of the solvent controls), e.g. a 15% reduction in migration distance.

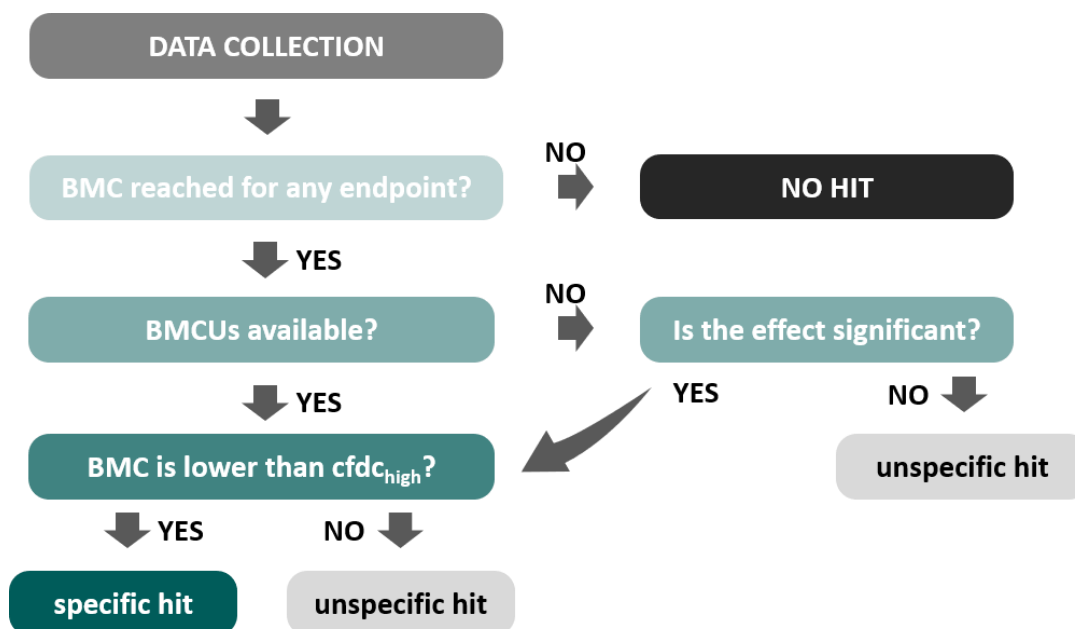


Figure 7 Decision tree of data evaluation for hiNPC compound screening.

An unspecific hit was reached if the BMC was higher than the $cf_{dc_{high}}$. If the BMCU was not reached, and the effect was not significant, it was defined as an unspecific hit. Finally, if the respective BMC_{15} for migration or BMC_{10} for cytotoxicity was not reached, the compound was classified as no hit in the MB compound screening. If the respective BMC_{30} for migration, BMC_{10} for cytotoxicity, and BMC_{50} for proliferation was not reached compound was classified as no hit in the GBM compound screening.

Material & Methods

For all experiments, at least three independent biological replicates with at least three technical replicates each were performed. Experiments were defined as independent if they were generated with hiNPCs from a different passage number. Results are presented as mean \pm SEM. For calculating concentration-response curves, a sigmoidal curve fit was applied using GraphPadPrism software. Statistical significance was calculated using the step-down multiple test procedure of Dunnett and Tamhane $p \leq 0.05$ was considered significant (Dunnett & Tamhane, 1991).

2.2.11.4 Proliferation Assay for hiNPC-oncogene models

The proliferation assay was performed as described in Hofrichter et al. (2017). Proliferation of the 3D hiNPC-oncogene models was assessed using the bromodeoxyuridine (BrdU, Roche, Switzerland) assay. Proliferating 3D hiNPC-oncogene models were chopped as described in 2.2.10.4 about one to three days before assay start. The proliferation assay is started when the neurospheres have a diameter of 300 μm . Poly-HEMA coated 96-well plates were used for the proliferation assay. As serial dilution of the compounds (Table 26) was prepared in B27 proliferation medium. In each well of the 96-well plate 100 μl medium containing the compound was added. Afterward, one neurosphere was plated in each well. The neurospheres were incubated for 3 days at 37°C and 5 % CO₂ and pictures were taken daily. After 56 h of incubation time, 10 μl of BrdU labeling solution were added to each well and incubated for 18 h at 37°C and 5 % CO₂. To evaluate the proliferation, the neurospheres had to be dissociated. In each well, 25 μl of Accutase® were added to the side of each well and pre-heated to 37°C for 30 min. After the incubation time, the neurospheres were transferred to the Accutase® drop and incubated for 10 min at 37°C. The cells were singularized by pipetting the cells up and down using a pipette and distributed over the well. Accutase® was removed by heating the plate using a hairdryer and singularized-cells were fixed following manufacture's instruction. Briefly, singularized-cells were fixed by addition of 200 μl to each well of the provided FixDenant. Fixation solution was discarded after 45 min incubation time at RT and 100 μl of Anti-BrdU-POD working solution was added to each well and incubated for 1.5 h at RT. Cells were washed three times for 1 min using 200 μl washing solution to each well. For evaluation, 100 μl substrate solution was added to each well and incubated for 10 min at RT. Fluorescence was measured in a plate reader (Tecan, Switzerland).

2.2.11.5 Migration Assay for hiNPC-oncogene models

Inhibitory effects of the substances were determined on the migration of the hiNPC-oncogene models. In one well of a PDL coated 96-well plate, one neurospheres with a size of 300 µm diameter was plated. Pictures of the spheres were taken to determine the radial migration of each neurosphere by measuring the migration distance at four locations after 24 h and 72 h. Migration distance was determined from the edge of the sphere core to the furthest migrated cells using ImageJ (Schneider et al., 2012). For each condition, the mean value of five technical replicates was calculated. Five technical replicates in three biological replicates were measured.

2.3 Statistic and Software

Statistical analysis was performed using GraphPad Prism 8 software and Microsoft Excel. As a statistical test Student's t-test (viability assay and volcano plot) and one way Anova (qPCR and pharmacological screening) were performed. Methylome and transcriptome results were analyzed using Partek software (Partek Incorporated, MO, USA). Additionally, Qiagen IPA analysis was conducted for the methylome results (Qiagen, Germany). The transcriptome was further analyzed using R and GO terms analysis from DAVID Functional Annotation Bioinformatics Microarray Analysis (Huang da et al., 2009a, 2009b; R Development Core Team, 2010). Evaluation of protein expression was performed using the provided software Image Studio (LI-COR) as well as ImageJ (Schneider et al., 2012). Pictures of the ICC staining were adjusted for brightness using ImageJ (Schneider et al., 2012).

3 Results

3.1 Generation of the hiPSC-oncogene models

For the model generation, the gene sequence of the GOI was amplified by PCR and loaded onto a 2 % agarose gel and identified based on their product size (Figure 8). Samples showing the correct product size were further processed for cloning, bacterial transformation, and plasmid extraction. The plasmids were extracted and sequenced to verify the correct integration before the third generation lentiviral production.

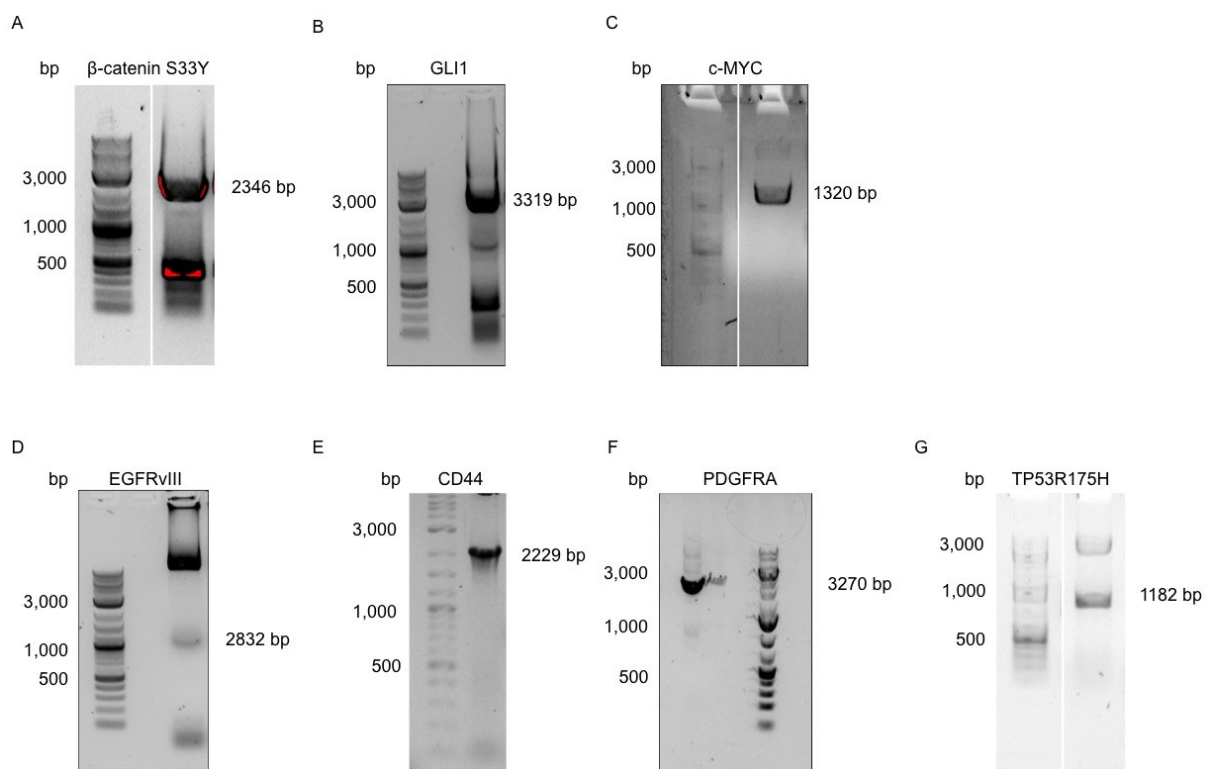


Figure 8 Gel electrophoresis of the amplification of the GOI.

For each model, one GOI was amplified using PCR. Products were loaded on an agarose gel to control the amplification and size of the product. PCR products were cut out and used for the cloning.

In the next step, the hiPSC line iPS11 was transduced using a target transgene model specific third-generation lentivirus with the respective GOI. After one week of antibiotic selection, the surviving cells were expanded for analysis and cultivated in less concentrated antibiotic selection medium. Two MB models could be created, one for the SHH model with overexpression of *GLI1* and the Group 3 model with a *c-MYC* protein overexpression (Figure 9). To create a WNT model, *CTNNB1 S33Y* was introduced, but the protein expression of the active beta-catenin was similar to the empty vector (EV) control (Figure 9).

Results

The creation of artificial GBM models was only successful for the classical subtype containing the altered EGFRvIII protein. This model was further modified after protein validation and was transduced using the TP53R175H vector to generate the double mutation *TP53R175H/EGFRvIII*. Western blot analysis verified the integration and expression of *TP53R175H* and *EGFRvIII* in the hiPSCs (Figure 9). Overexpression of *CD44* and *PDGFRA* in comparison to the EV control could not be validated in hiPSCs to mimic the mesenchymal and proneural subtype, respectively.

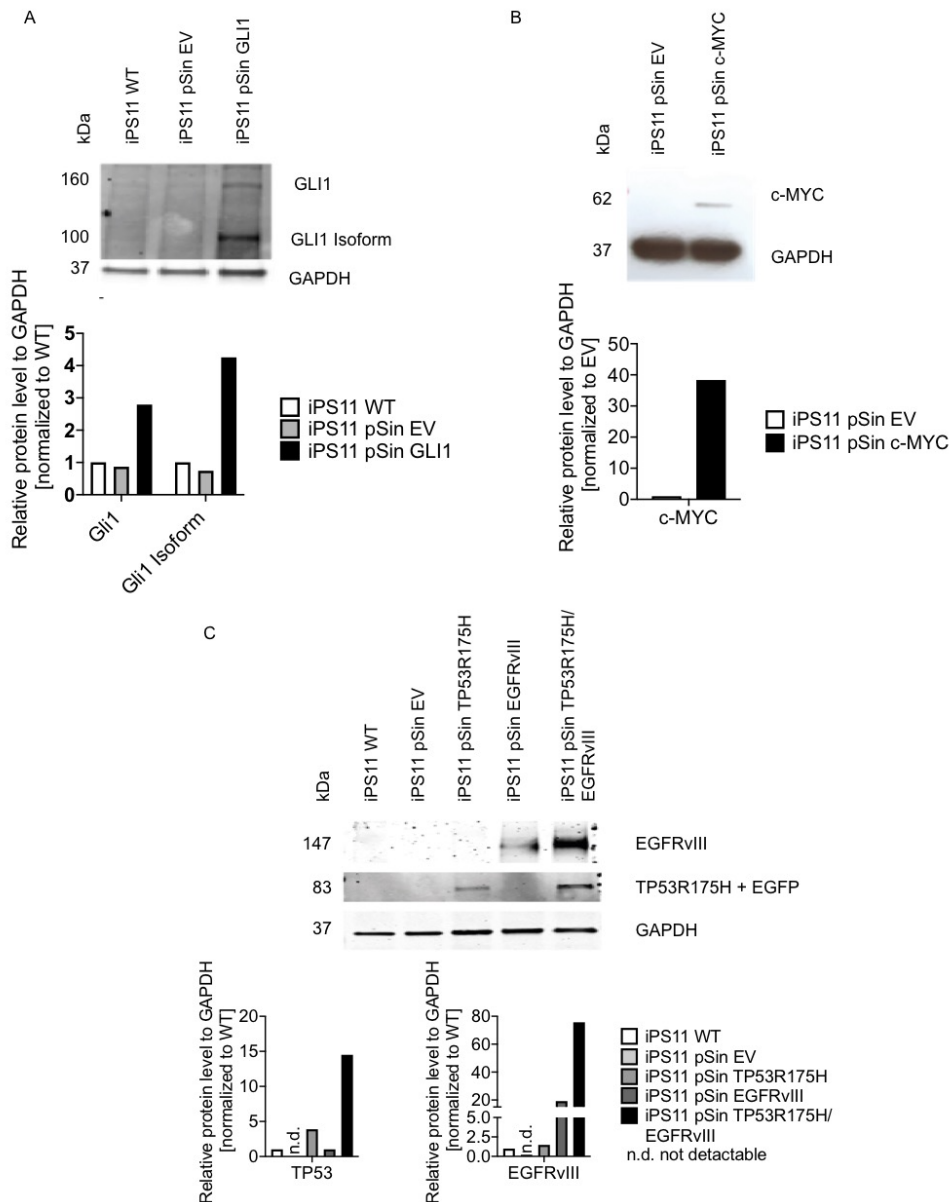


Figure 9 Protein expression of introduced target genes in the successfully generated hiPSC-oncogene models.

Human iPSCs were transduced with the lentiviral plasmids including the gene of interest. Successful integration was verified by protein expression.

All protein-validated hiPSC-oncogene models were tested for mycoplasma contamination before they were used for further experiments (Figure 10). Contamination with mycoplasma

Results

must be excluded, as these influence the behavior of cells and are detectable in epigenome and transcriptome analyses. Positive samples run at a size of 270 bp while negative samples run higher at 479 bp. Positive and negative controls were run in addition to the tested samples. All analyzed models tested negative for mycoplasma and could be used for the following experiments and analyses (Figure 10).

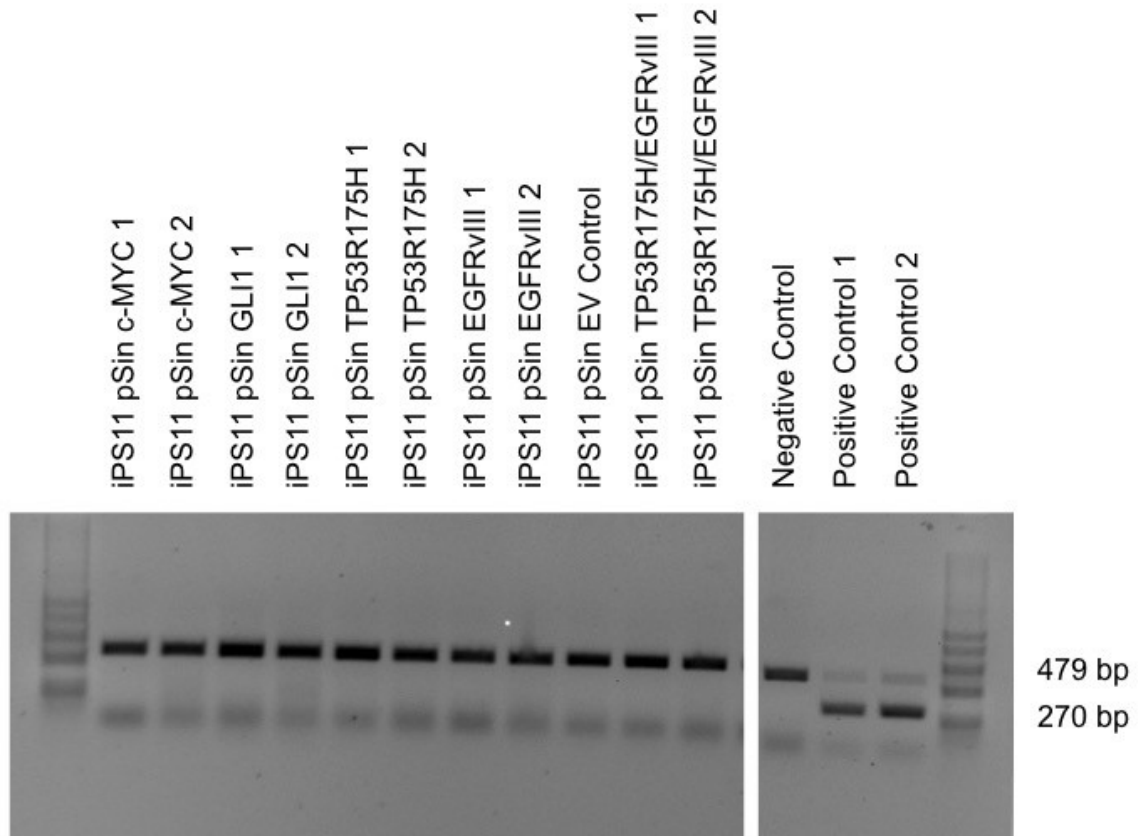


Figure 10 Mycoplasma gel picture of the successfully generated hiPSC-oncogene models.

PCR products were loaded on a 1.5 % agarose gel to check for mycoplasma contamination. The used PCR Mycoplasma Test Kit I/C (PromoCell GmbH, Germany) contains an internal control that runs at 479 bp and positive samples have a second band at 270 bp.

3.2 Characterization of the hiPSC-oncogene models

Several experiments were conducted to characterize the generated models regarding their viability and stemness. At first, the viability between the hiPSC-oncogene models and WT was compared using the MTT viability assay. No significant difference regarding viability was observed over four days of sample taking (Figure 11).

Results

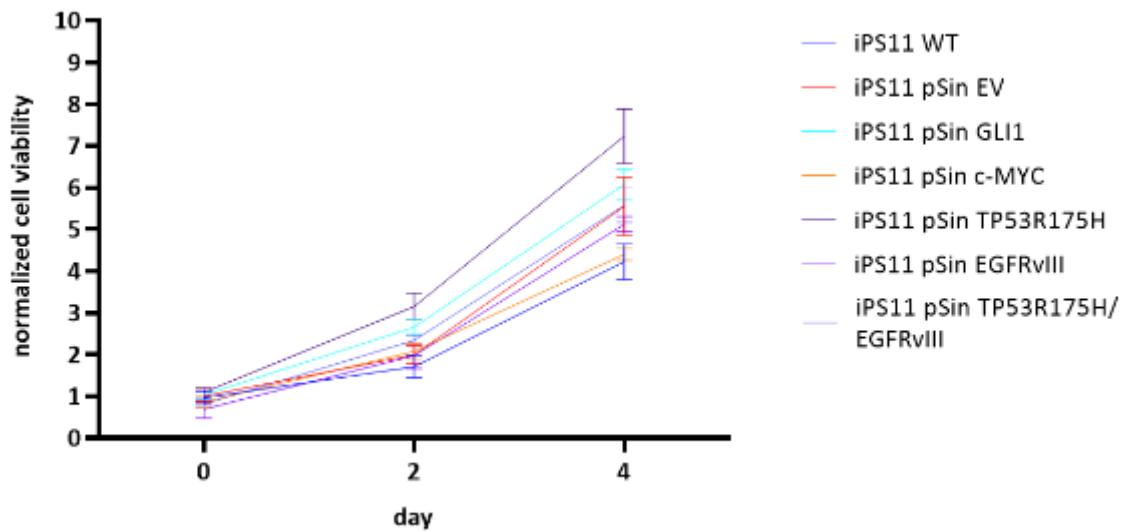


Figure 11 Viability of hiPSC-oncogene models.

The viability of hiPSC-oncogenic models was measured with the MTT assay on days 0, 2, and 4. Results were normalized to iPS11 EV control on day 0. Three technical replicates in three biological replicates were analyzed. Significance was tested with unpaired student's t-test, no significance was detected.

To verify that the lentivirally transduced hiPSCs retained their stem cell characteristics and did not start to differentiate, two separate analyses were performed: Flow cytometry and ICC staining. The stemness marker NANOG, OCT3/4, and SOX2 were detected by flow cytometry while OCT3/4 and TRA-1-60 were visualized using ICC staining. The different stem cell markers belong either to the group of transcription factors (OCT3/4, NANOG, and SOX2) or are transmembrane proteins (TRA-1-60).

Double positive cells for NANOG/SOX2 and SOX2/OCT3/4 were gated by flow cytometry and all models reached the threshold of 70 % marker expression (Sullivan et al., 2018). Only in three models, *GLI1*, *EGFRvIII*, and *TP53R175H/EGFRvIII*, expression level of the marker NANOG/SOX2 was below 90 % (Table 27). Almost all cell models have a positivity above 90 % for the marker SOX2/OCT3/4 except for the double mutated hiPSC-oncogene model *TP53R175H/EGFRvIII*, of with only around 84 % of the cells were positive for both markers.

Results

Table 27 FACS expression of the stem cell marker in the generated hiPSC-oncogene models.

Cell line	NANOG/SOX2 [%]	SOX2/OCT3/4 [%]
EV	94.45	93.84
<i>GLI1</i>	78.16	92.06
<i>c-MYC</i>	90.98	94.38
<i>TP53R175H</i>	91.37	94.97
<i>EGFRvIII</i>	86.39	92.36
<i>TP53R175H/EGFRvIII</i>	75.78	84.22

ICC staining was performed to validate the expression of TRA-1-60 and OCT3/4 in all of the generated hiPSC-oncogene models (Figure 12). Expression of OCT3/4 is in all models weaker than TRA-1-60 expression, especially in the models EV control and *EGFRvIII*. OCT3/4 expression is low. In general, expression of the stem cell marker is weaker in *EGFRvIII*. Nuclei were stained using Hoechst and even distribution over the hiPSC colony was detected.

Results

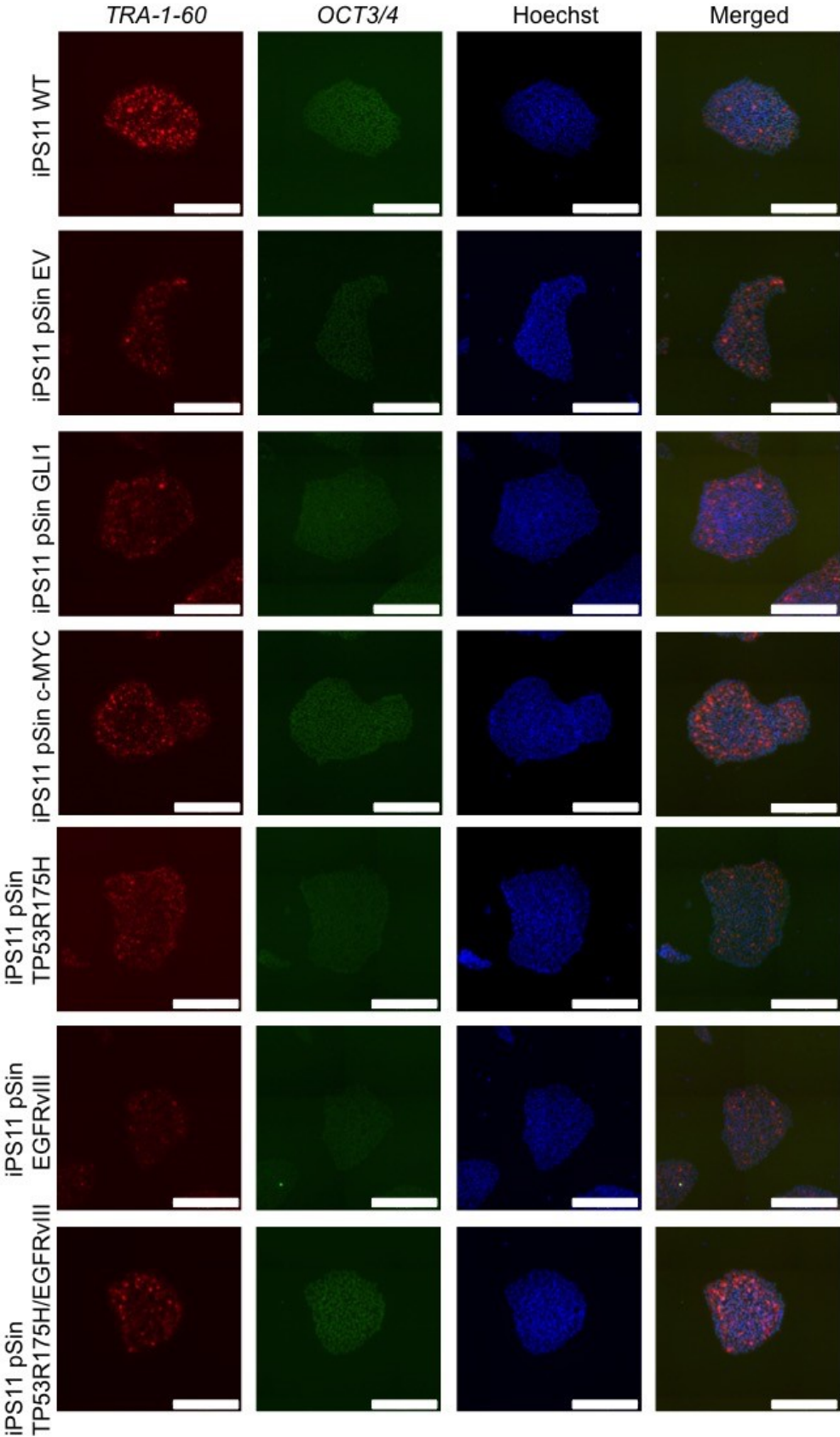


Figure 12 Immunocytochemical staining of the hiPSC-oncogene models.

Generated hiPSC models were stained with stem cell markers to verify their stemness properties using antibodies against TRA-1-60 (red) and OCT3/4 (green), nuclei were counterstained with Hoechst 33258 (blue). Six technical replicates were stained for each model. One representative hiPSC colony is displayed for each marker. The scale bar is 250 μm. Pictures were evaluated with ImageJ.

Results

Further, the karyogram of the EV control and the hiPSC-oncogene models were analyzed after the genetic modification (Figure 13). In the EV control and all hiPSC-oncogene models no chromosomal abnormalities were detected and in all models a normal male karyotype was verified (Figure 13).

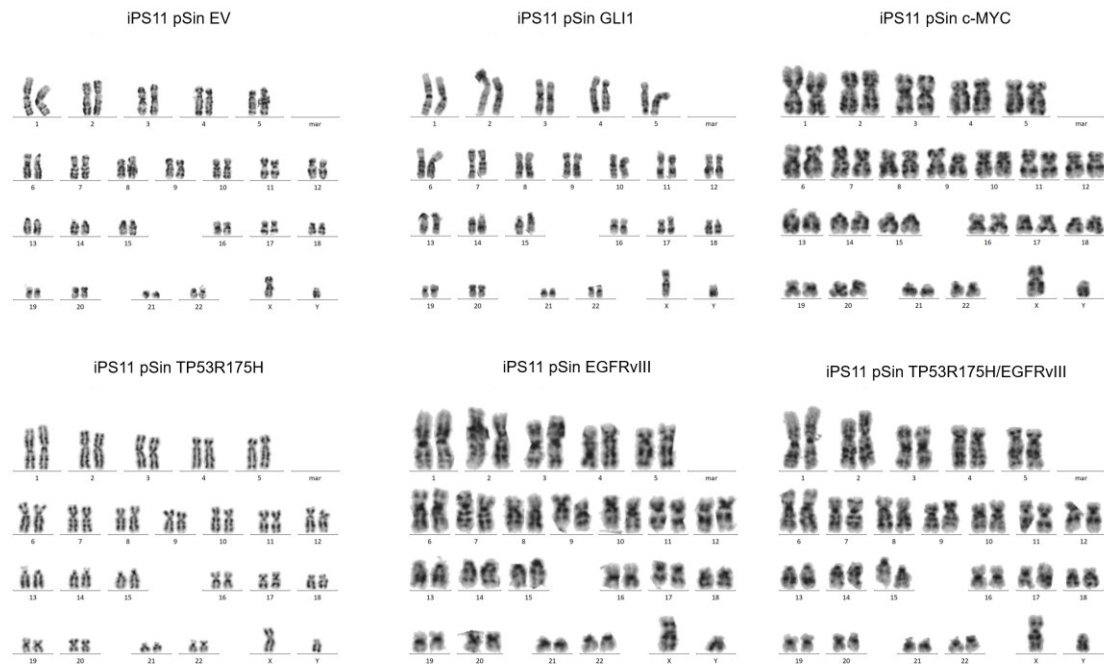


Figure 13 Karyograms of all hiPSC-oncogene models.

Mitosis of the EV control and all hiPSC-oncogene models were analyzed to see if chromosomal abnormalities can be detected. For all models a normal male karyotype was verified.

3.3 Metabolic transcription of hiPSC-oncogene models

RNA and DNA expression analyses were performed to identify differences in the regulation of pathways and genes. For epigenome analysis, DNA was extracted from all generated hiPSC-oncogene models. First, hierarchical clustering was conducted with uniquely regulated genes to analyze the relationship between the hiPSC-oncogene models (Figure 14). Here, the control cell line iPS11 WT had the highest similarity to the EV control (Figure 14). Further, the MB models *GLI1* and *c-MYC* as well as the GBM models *TP53R175H*, *EGFRvIII*, and *TP53R175H/EGFRvIII* had a high similarity (Figure 14). Comparing the individual models, unique methylation profiles could be detected, which were further analyzed.

Results

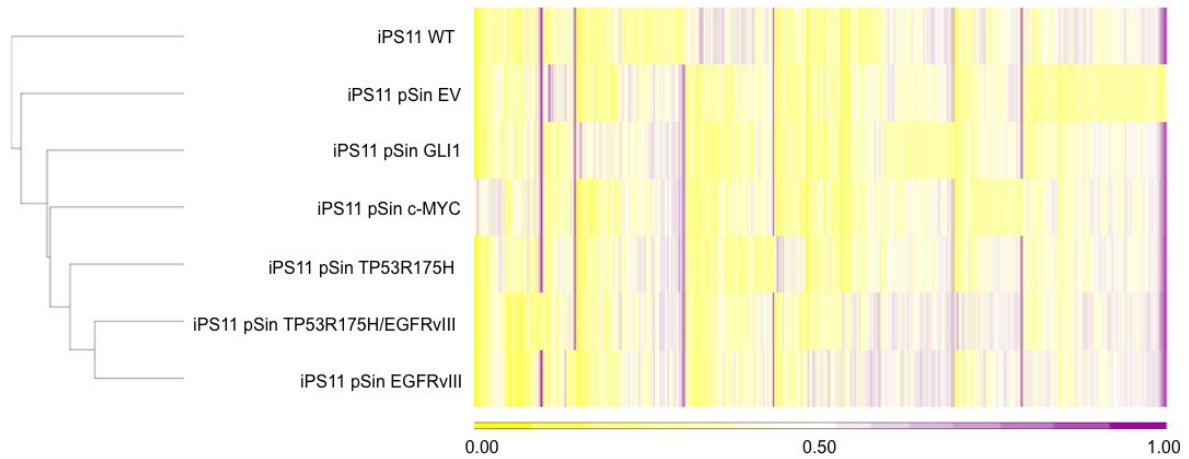


Figure 14 Hierarchical clustering of hiPSC-oncogene models.

Methylation profiles of the hiPSC-oncogene models were compared to each other to identify uniquely regulated genes and visualized in a hierarchical cluster using Partek Genomics Suite (Partek Incorporated, MO, USA). Uniquely regulated genes were identified by comparison to the pSin EV model.

Following the hierarchical clustering, a PCA clustering to identify epigenetic variations for each model was performed (Figure 15). Unique regulation was not considered for the *TP53R175H*, *EGFRvIII*, and *TP53R175H/EGFRvIII* hiPSC-oncogene models due to the introduction of the same genes. PCA clustering revealed that the EV control was the most different from all samples (Figure 15). In accordance with the hierarchical clustering, the highest similarity was detected between the *EGFRvIII* and *TP53R175H/EGFRvIII* models (Figure 15). Both also showed a similarity toward the single mutant *TP53R175H* (Figure 15). The remaining models *GLI1*, *c-MYC*, and the WT could not be clustered to any other model (Figure 15). In summary, the PCA clustering confirmed that all hiPSC-oncogene models could be distinguished from each other, while the GBM models revealed higher similarity to each other than the MB models.

Results

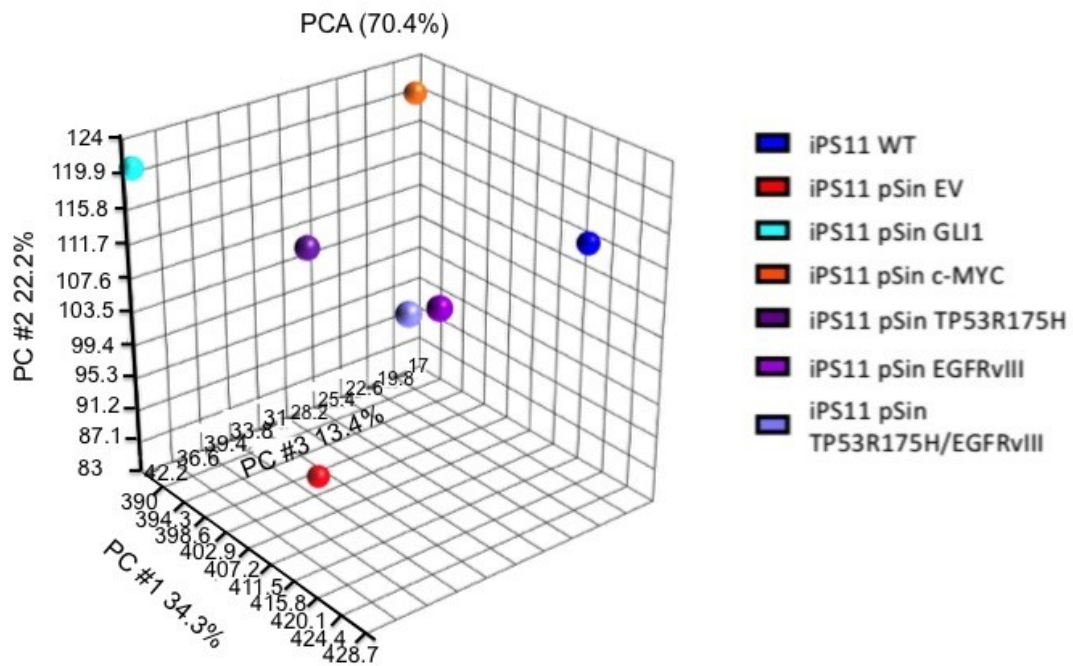


Figure 15 PCA of hiPSC-oncogene models.

Principal component analysis (PCA) was performed using Partek Genomics Suite (Partek Incorporated, MO, USA). Methylation profiles were compared to each other to identify the highest similarity to each other. The three GBM models, *TP53R175H*, *EGFRvIII*, and *TP53R175H/EGFRvIII* were analyzed together.

In addition, QIAGEN IPA was conducted to identify significantly regulated canonical pathways of the generated hiPSC-oncogene models (Figure 16). The canonical pathway analysis revealed no significance in the WT and MB models. Four signaling pathways were identified in the EV model that regulate between four to seven target genes (Figure 16). Two of these pathways, 'CREB signaling in neurons' and 'protein kinase A signaling', are regulating transcription factors through cAMP while the other two pathways are 'breast cancer regulation by stathimin 1' and 'estrogen receptor signaling' pathways (Figure 16). For the models, *TP53R175H*, *EGFRvIII*, and *TP53R175H/EGFRvIII* a higher amount of significantly differentially regulated pathways was identified, and the top ten pathways are displayed in Figure 16. All three models have similar or the same pathways significantly regulated (Figure 16). For the models *EGFRvIII* and *TP53R175H*, the signaling pathway with the highest number of target genes is the 'glucocorticoid receptor signaling'. This pathway can be part of the stress response and epidermal morphogenesis and has 10 and 19 target genes in *TP53R175H* and the *EGFRvIII* model, respectively (Figure 16). In both models, the 'sirtuin signaling pathway' is also significantly regulated, which is important in a variety of cellular processes including apoptosis, metabolism, and cellular stress response. The second highest number of target genes was detected in the *TP53R175H* model, the

Results

'molecular mechanisms of cancer' pathway. In the *EGFRvIII* model, signaling pathways that are part of the immune response and intracellular communication are differently regulated (Figure 16). The 'hepatic cholestasis' pathway was identified in the models *EGFRvIII* and *TP53R175H/EGFRvIII* (Figure 16). In all three models pathways are involved in the 'systemic lupus erythematosus' signaling with a difference in the number of target genes. (Figure 16) Especially in the *EGFRvIII* model and the *TP53R175H/EGFRvIII* models, these pathways have a higher number of target genes than in the *TP53R175H* model.

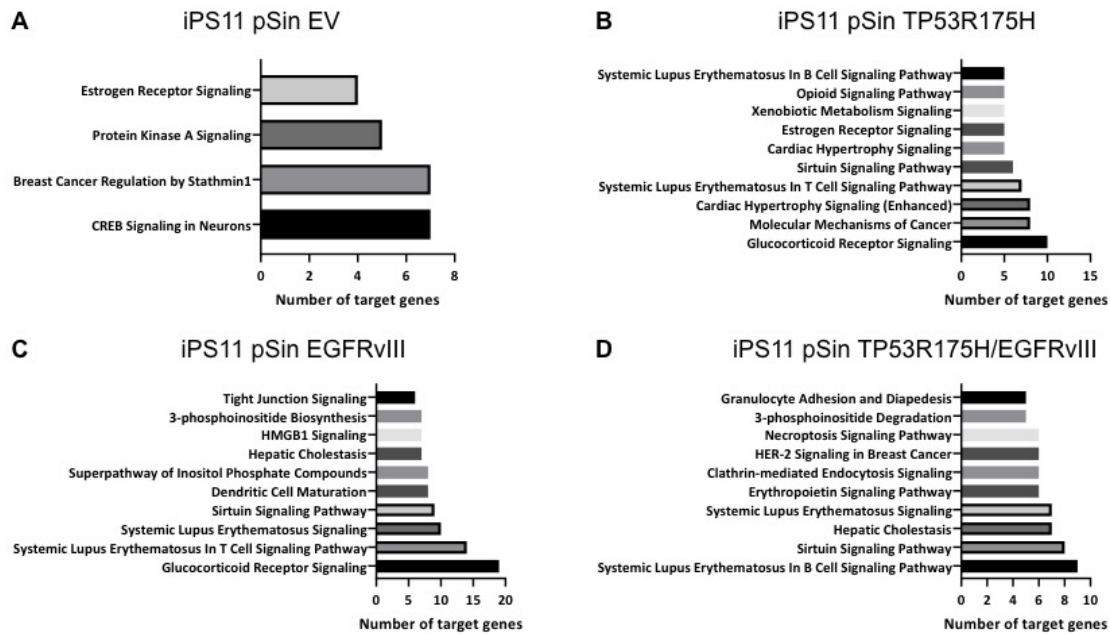


Figure 16 Significantly regulated canonical signaling pathways of hiPSC-oncogene models.

Signaling pathways were filtered for the number of target genes and the top 10 results are displayed. The analysis showed only four signaling pathways for pSin EV control and more than 10 for TP53R175H, EGFRvIII, and TP53R175H/EGFRvIII. Three models (wild type, GLI1, c-MYC) did not show any significantly regulated pathways. Analysis was performed using QIAGEN Ingenuity Pathway Analysis (IPA, Netherlands). The significant cut-off was set to p-value <0.05. One biological replicate was analyzed for each hiPSC-oncogene model.

Furthermore, QIAGEN IPA upstream target analysis was conducted of the generated hiPSC-oncogene models using the unique expression profiles except for the *TP53R175H*, *EGFRvIII*, and *TP53R175H/EGFRvIII* models as described above. Results were analyzed and filtered after their significance and number of target genes (Figure 17). The number of identified target genes varies tremendously between the models from three (*GLI1*) to 126 (*EGFRvIII*; Figure 17). Upstream targets of the WT and EV model are transcription factors that regulate cell proliferation, development, and apoptosis. The tumor protein 73 (*TP73*) gene was found in both models as an upstream target and has around 20 and 6 target genes in the WT and EV model, respectively. In general, fewer upstream targets were found for the WT model than for the upstream targets of the EV model (Figure 17). Only three upstream targets were found in the *GLI1* model, *PRKCD*, *GLI1*, and *RARA*, and each gene had three target genes.

Results

For all other models at least ten upstream targets were identified. The *c-MYC* model has several target genes which are known interaction partners and regulators of *MYC*. For example, the upstream target nuclear factor k-light-chain-enhancer of activated B cells (*NFκB*) is a well-known regulator of *c-MYC* and is responsible for cellular immune responses and proliferation. *NFκB* has six target genes while the other upstream targets have three or four target genes. In the *TP53R175H* model, the upstream target *TGFB1* had over 50 target genes (Figure 17). *TGFB1* and *TP53* regulate each other and are important for cell proliferation, growth, and differentiation. Further identified upstream targets were e.g. enhancement of zeste homolog 2 (*EZH2*), hypoxia-inducible factor 1-alpha (*HIF1A*), and homeobox protein Hox-A9 (*HOXA9*) with 10 to 20 target genes each (Figure 17). In comparison to all other models, the highest amount of target genes, over 100, was identified in the models *EGFRvIII* and *TP53R175H/EGFRvIII*. Listed upstream targets of both of them are *TGFB1*, *TP53*, *TNF*, and *MYC*. In conclusion, all of the identified upstream targets of the hiPSC-oncogene models are involved in various cellular processes e.g. proliferation, development, and stress response. All processes play a role in cancer development and progression.

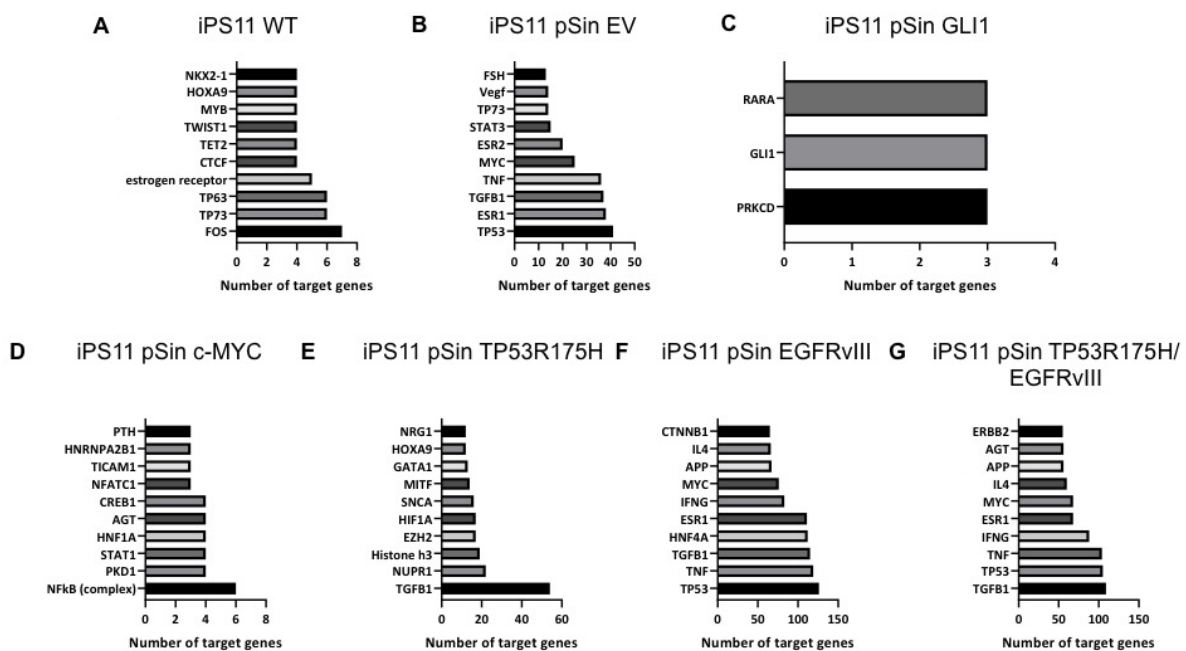


Figure 17 Significantly regulated upstream targets of all hiPSC-oncogene models. Uniquely regulated genes were identified by comparing all hiPSC-oncogene models with each other.

TP53R175H, *EGFRvIII*, and *TP53R175H/EGFRvIII* were analyzed together. Upstream targets were filtered after the number of target genes and the top 10 results are displayed. The analysis showed only three upstream targets for the *GLI1* model, all others had more than 10. Analysis was performed using the QIAGEN Ingenuity Pathway Analysis software (IPA; Netherlands). The significance cut-off was set to p-value <0.05. One biological replicate was analyzed for each hiPSC-oncogene model.

3.4 Transcriptomic characterization of hiPSC-oncogene models

The hiPSC-oncogene models were further characterized by transcriptome analysis. RNA expression profiles were compared to the EV control to identify differentially expressed genes. Significantly up- and downregulated genes were determined by calculating the fold change of the genes and visualized in a volcano plot. In all models around 30 to 60 genes are either significantly up- or downregulated while the majority are not significantly regulated. In all models, one or two genes were identified that either had a higher significance or a higher fold change in comparison to the other genes. Each of the generated hiPSC-oncogene models *GLI1*, *c-MYC*, and *EGFRvIII* had one gene highly significantly upregulated with a fold change >4 (Figure 18). These genes were identified to be *GLI1*, *MYC*, and *EGFR*, respectively (Figure 18). The highly significantly regulated genes in the models *TP53R175H* and *TP53R175H/EGFRvIII* did not reach a fold change >4 (Figure 18). However, the *TP53R175H/EGFRvIII* model is the only model where one gene, *CAVEOLIN-3* (CAV-3), is remarkably downregulated with a fold change of $-1.39 \log_2$.

Results

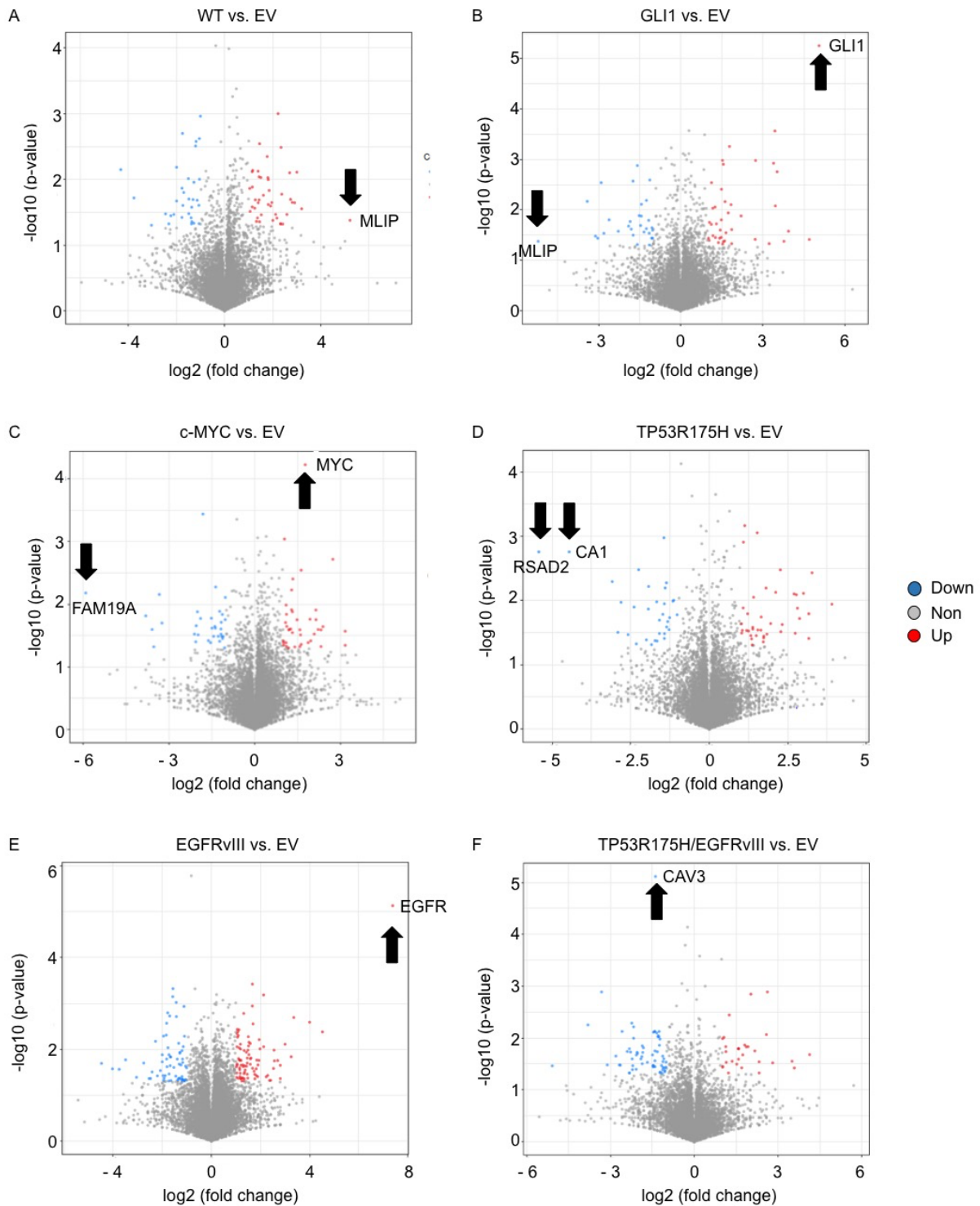


Figure 18 Volcano plot for all hiPSC-oncogene models.

Based on the RNA transcriptome sequencing, the significance (unpaired student's *t*-test, p -value < 0.05) and fold change were analyzed for each hiPSC-oncogene model (A – F). Genes are either significantly increased (fold change > 2 , red), decreased (fold change < 0.5 , blue) or not significantly regulated (< 2 and > 0.5 , gray). The y-axis indicates the significance of the gene regulation. Arrows are used to mark the respective highest specific up- and down-regulated genes. The volcano plots were created with *R*.

To continue the characterization of the hiPSC-oncogene models, GO term analyses were conducted. Significantly overexpressed genes identified using the volcano plot analysis were further analyzed in comparison to the EV control. It was not possible to identify any

Results

significantly enriched GO terms in the WT model. However, all MB and GBM models had at least ten significant GO terms. All models had a gene count between two and ten with one exception in the *EGFRvIII* model with over 25 gene counts. The GO terms identified for the *GLI1* model are involved in development or differentiation (Figure 19). The most significant GO term is responsible for dorsal/ventral pattern while others regulate the neural and osteoblast formation. In the *c-MYC* model, the most significant GO terms negatively regulate the apoptotic processes of the cell, 'GO:0043066 negative regulation of apoptotic processes', 'GO:0043069 negative regulation of programmed cell death', and 'GO:0060548 negative regulation of cell death' (Figure 19). In contrast to the *c-MYC* model, the *TP53R175H* model has several GO terms which regulate the programmed cell death either positively or negatively (Figure 19). Only three of the ten GO terms do not regulate apoptotic processes. The respective genes are involved in e.g. transmembrane signaling. The *EGFRvIII* model had several GO terms involved in cell-cell interaction, protein secretion, and signal transduction. However, the most gene counts were counted for the GO term 'nervous system development', which was the second most significant one. The GO terms of the *EGFRvIII* models had a p-value > 10 while all other models had a p-value < 10 (Figure 19). In comparison to the single mutation models, the double mutation *TP53R175H/EGFRvIII* model has other GO terms regulated. The two most significant GO terms are involved in the urea cycle and metabolic processes. Most of the other GO terms have a higher gene count and regulate the viral entry, symbiotic processes, and inflammatory responses.

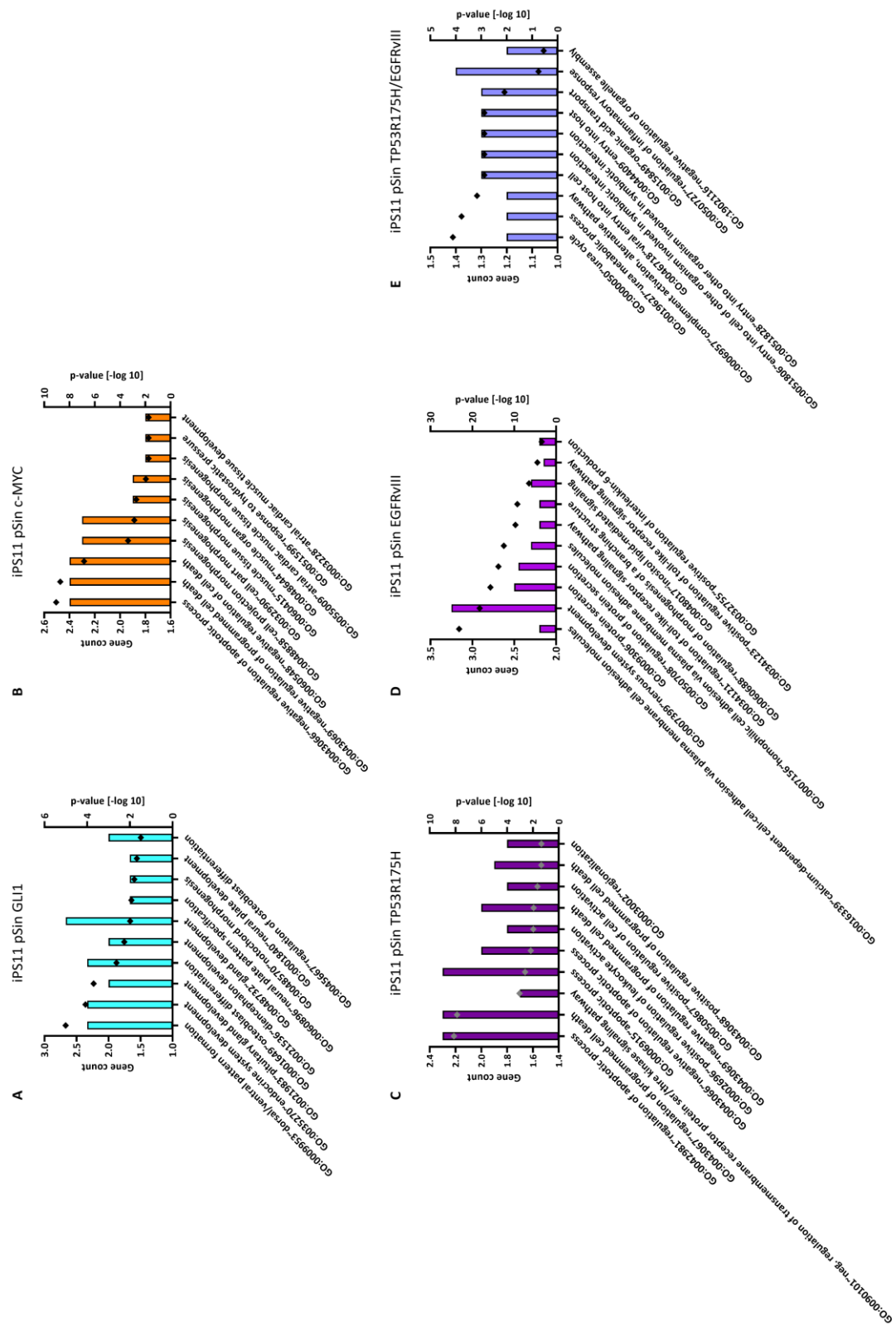


Figure 19 GO terms of all hiPSC-oncogene models.

Overrepresented gene ontologies (GO) of all hiPSC-oncogene models. GO enrichment of significantly up- and downregulated genes were analyzed using the online tool DAVID Bioinformatics. Results were sorted based on the significance in ascending order. Additionally, gene counts were analyzed. Gene regulations were identified by comparison to the EV control. The WT model did not show any significantly enriched GO terms. Columns represent the gene count and dots the p-value. hiPSC, human induced pluripotent stem cells; WT, wild type; EV, empty vector; GLI1, glioma associated oncogene 1; TP53, tumor protein 53; EGFRvIII, epidermal growth factor receptor variant III.

3.5 Pharmacological screening of hiPSC-oncogene models

Application of the hiPSC-oncogene models was conducted in pharmacological screening. Nine FDA-approved drugs were tested in comparison to the positive control staurosporine and the negative control acetaminophen. For each cell line, the drugs were clustered into three groups called good, medium, and non-working based on their reduction of cell viability. The first group includes the drugs with high efficacy defined by a reduced cell viability to under 50 %. For most cell models, five drugs could be identified as good working compounds (Figure 20). In the second group two to four drugs reduced the cell viability by 10 – 30 % (Figure 20). Non-working drugs did not have any influence on cell viability. As an exception, acetaminophen had a reducing effect on the cell viability of the iPS11 pSin *GLI1* model in low concentrations, but at high concentrations, cell viability reached 100 % (Figure 20). *TP53R175H* was the only model to have one non-working drug which was acetaminophen. All other models had at least one drug next to acetaminophen which did not reduce the cell viability (Figure 20). It should be mentioned that high variances between the three repetitions were observed for the good working compounds.

Results

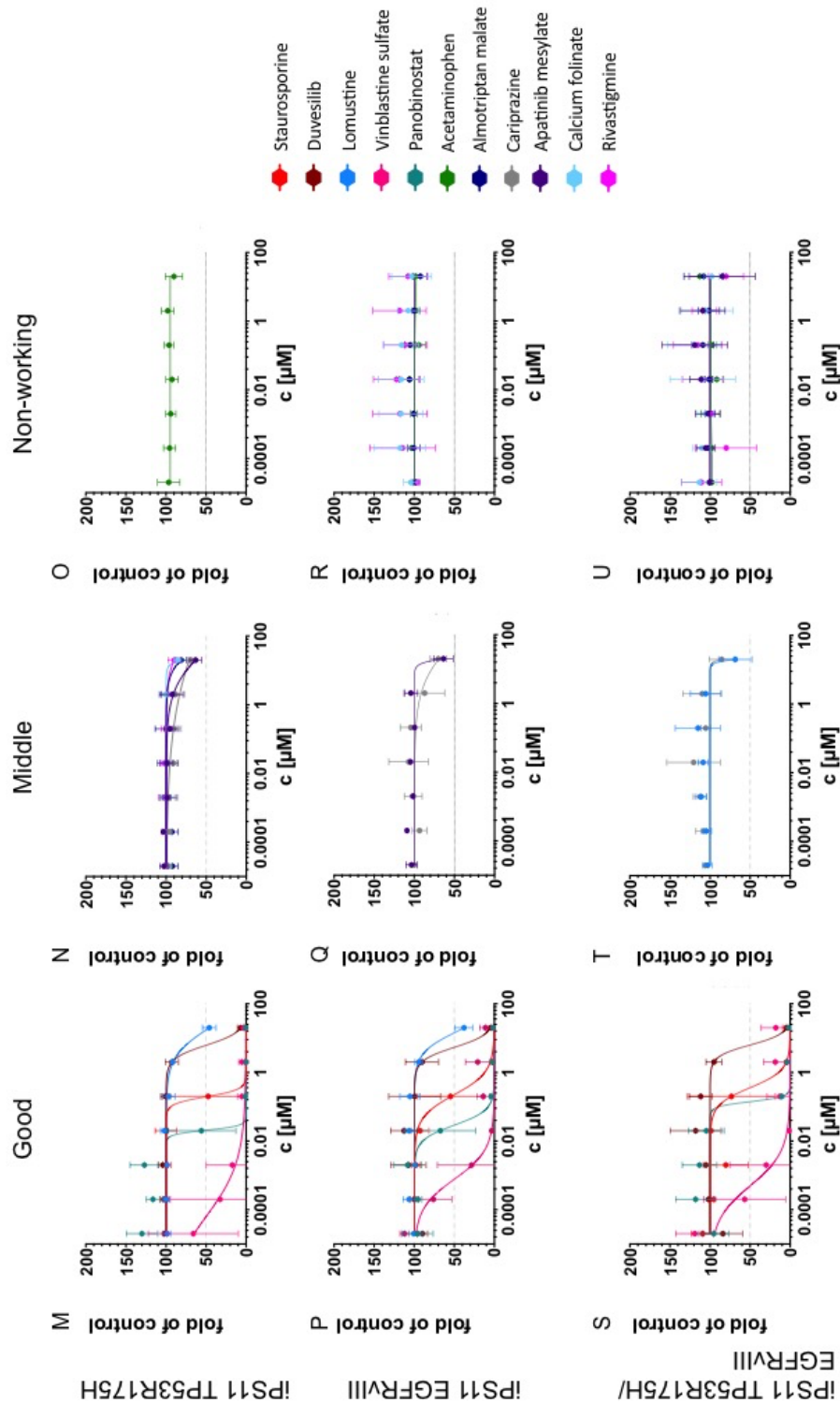


Figure 20 Concentration-response curves to determine the EC_{50} for all hiPSC-oncogene models.

Effective concentration (EC_{50}) was calculated using the cell viability after the manually performed *in vitro* pharmacology screening for the control models (A – F), hiPSC-oncogene MB models (G – L), and hiPSC-oncogene GBM models (M – U). Nine drugs, staurosporine (positive control) and acetaminophen (negative control) were applied in a serial dilution (20 μ M, 2 μ M, 200 nM, 20 nM, 2 nM, 200 pM and 20 pM). Viability was measured after 48 h using thiazolyl blue tetrazolium bromide (MTT). Results were normalized to the DMSO treated hiPSCs and the two lowest concentrations (Krebs et al., 2018). The mean cell viability of three biological replicates was calculated. EC_{50} was calculated using the sigmoidal curve fitting using GraphPad Prim 8 (GraphPad Software, CA, USA). hiPSCs, human induced pluripotent stem cells; TP53, tumor protein 53; EGFRvIII, epidermal growth factor receptor variant III; DMSO, dimethyl sulfoxide.

Results

Further, the EC_{50} was calculated for each drug which reduced the cell viability by 50 %. All hiPSC-oncogene models had a sensitivity toward three to four drugs. The controls WT and EV showed similar responses towards the chemical compounds. Vinblastine sulfate had the highest efficacy as the EC_{50} was reached at concentrations between 0.0001 – 0.0072 μ M and decreased the cell viability in all models (Table 28). Panobinostat also reduced the cell viability but the EC_{50} ranged between 0.0531 μ M to 0.207 μ M. Interestingly, in the double mutation, the EC_{50} of panobinostat was as high as 14.01 μ M. In comparison, the third best reacting drug, duvelisib, had EC_{50} values which ranged between 5.37 – 16.21 μ M (Table 28). Lomustine was the only other drug for which an EC_{50} could be calculated with concentrations between 10.16 – 19.54 μ M. However, for the hiPSC-oncogene models *GLI1* and *TP53R175H/EGFRVIII* the EC_{50} could not be calculated since the cell viability was not reduced below 50 %. Both of the MB models, *GLI1* and *c-MYC*, had a higher resistance to the treatment with duvelisib and panobinostat in comparison to the GBM models (Table 28). The positive control staurosporine had EC_{50} values ranging from 0.1621 to 1.4940 μ M, which indicates a lower reducing capability than vinblastine sulfate and panobinostat. In general, it was observed that the control models iPS11 WT and iPS11 pSin EV reveal a higher sensitivity towards the drugs which indicates resistance in the generated hiPSC-oncogene models towards the applied drugs.

Results

Table 28 Effective concentration (EC)₅₀ of the drugs were determined for all hiPSC-oncogene models.

If no EC₅₀ could be determined the field was marked with an 'X'. All EC₅₀ values are in μM and were calculated using GraphPad Prism 8 (GraphPad Software, CA, USA). Results of cell viability were normalized to DMSO treated hiPSC and the two lowest concentrations (Krebs et al., 2018).

	iPS11 WT	iPS11 pSin EV	iPS11 pSin GLI1	iPS11 pSin c-MYC	iPS11 pSin TP53R175H	iPS11 pSin EGFRv III	iPS11 pSin TP53R175H/ EGFRvIII
Acetaminophen	X	X	X	X	X	X	X
Almotriptan malate	X	X	X	X	X	X	X
Apatinib mesylate	X	X	X	X	X	X	X
Calcium folinate	X	X	X	X	X	X	X
Cariprazine	X	X	X	X	X	X	X
Duvesilib	7.91	5.81	16.21	13.03	6.17	5.37	6.28
Lomustine	10.16	16.76	X	19.54	17.33	14.25	X
Panobinostat	0.0228	0.0222	0.1085	0.0531	0.207	0.0290	14.01
Rivastigmine	X	X	X	X	X	X	X
Staurosporine	0.3972	0.1621	0.3872	1.4940	0.1951	0.2240	0.3585
Vinblastine sulfate	0.0003	0.0001	0.0072	0.0006	0.0001	0.0008	0.0005

3.6 Longer cultivation of neural progenitor cells decreases proliferation and viability of spheres

To determine the variable parameters of the 2D neural induction protocol, iPS11 pSin EV and iPS11 pSin *TP53R175H/EGFRvIII* were used. Two variants of the protocol were tested. Sphere formation was induced either after two weeks or three weeks of culturing the cells as adherent neural progenitor cells. The quality of neural induction was validated using flow cytometry and ICC staining of the spheres, using antibodies against OCT3/4 and NESTIN. Based on the expression of stem cell and neural stem cell markers, the quality of the neural induction could be evaluated. The stem cell marker *OCT3/4* had a higher decrease after three weeks compared to two weeks in both models (Table 29). However, in comparison to the WT control, the expression of *OCT3/4* was higher in both hiPSC-oncogene models. The neural marker NESTIN was used as an indicator for the efficiency of neural induction. In the EV control, the time of cultivation of neural progenitor cells had a bigger influence on the expression of neural marker expression. After two weeks of cultivation, about 98.50 % of the cells expressed the marker NESTIN, (Table 29). One additional week of culturing the cells decreased the expression of NESTIN by 40 % (Table 29). In comparison, the double mutant did not show such a difference between the cultivation times, as the marker expression was only 10 % apart after one week. In summary, sphere formation after two weeks resulted in both models in a higher expression of the neural markers.

Table 29 Quality of the 2D neural induction.

Stem cell and neural marker expression was measured using flow cytometry.

	iPS11 pSin EV [%]		iPS11 pSin TP53R175H/EGFRvIII [%]		iPS11 WT [%]
	2 weeks	3 weeks	2 weeks	3 weeks	2 weeks
OCT3/4	72.85	53.45	83.9	69.2	2,0
NESTIN	98.5	62.7	98.75	90.1	81,8

Based on the results of the flow cytometry the neural induction of all generated hiPSC-oncogene models was performed using the protocol with the sphere formation after two weeks. It was possible to successfully generate a proliferating culture for the WT, EV, and *TP53R175H/EGFRvIII* models which were used for further characterization studies. However, during neural induction, the *TP53R175H* model stopped proliferating while the

Results

spheres of the *GLI1* and *c-MYC* models stopped proliferating soon after the differentiation was finished. Even though several inductions of these hiPSC-oncogene models were performed, it was not possible to end the induction or generate a proliferating sphere culture. These models could be used only for some characterization studies as not enough cell material could be generated. Therefore in parallel a 3D neural induction protocol was established, nevertheless, 2D generated models were characterized

3.7 Characterization of generated 2D hiNPC-oncogene models

At first, the *c-MYC*, *TP53R175H*, and *TP53R175H/EGFRvIII* hiNPC-oncogene models were analyzed by ICC staining. As it was not possible to generate a proliferating cell culture for all hiNPC-oncogene models, the *GLI1* and *EGFRvIII* models could not be analyzed. The development of neurons and NPCs were analyzed for each model (Figure 21). Therefore, hiNPC-oncogene models were stained against NESTIN and β -III-TUBULIN and nuclei were counterstained with Hoechst (Figure 21). As control the hiNPCs of pSin EV control were used. In all models the expression of TUBULIN is similar to each other (Figure 21). The weakest expression of NESTIN and β -III-TUBULIN was detected in the *c-MYC* model, while higher expressions were detected within the *TP53R175H/EGFRvIII*, EV control and *TP53R175H* model (Figure 21). Staining of the 2D hiNPC-oncogene models using Hoechst showed the migration of hiNPCs out of the sphere core (Figure 21). The highest migration distance was observed in the *c-MYC* and *TP53R175H/EGFRvIII* models. In summary, ICC staining against NESTIN and β -III-TUBULIN confirmed in all generated models the formation of NPCs and neurons (Figure 21).

Results

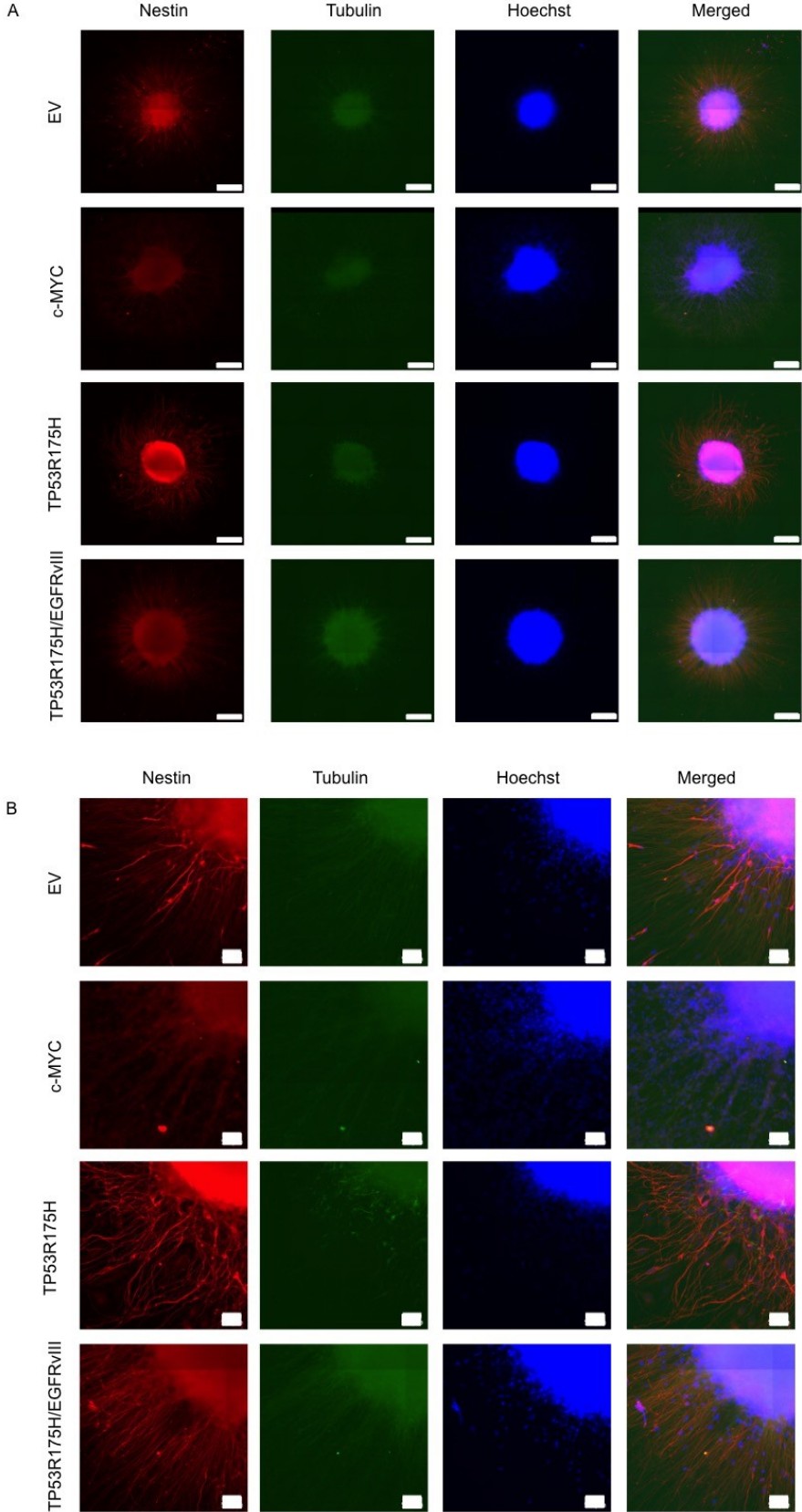


Figure 21 ICC staining of 2D hiNPC-oncogene models.

All 2D hiNPC-oncogene models were stained against NESTIN, β -III-TUBULIN, and Hoechst. The bar indicates a size of 250 μ m (A) or 50 μ m (B).

Results

Additionally, protein validation of the hiNPCs was done to validate if the spheres still expressed the GOI. The overexpression of *TP53* and *EGFRvIII*, which was detected in the hiPSC models could not be confirmed in the 2D neurospheres. However, the expression of *EGFR* was detected in all three models *TP53R175H*, *EGFRvIII*, and *TP53R175H/EGFRvIII* (Figure 22). The *EGFR* protein can be distinguished from the *EGFRvIII* protein due to its molecular size. As the neurospheres of *GLI1* stopped to proliferate shortly after the neural induction and the *c-MYC* model stopped to proliferate during the induction, it was not enough material generated to evaluate the samples for their protein expression.

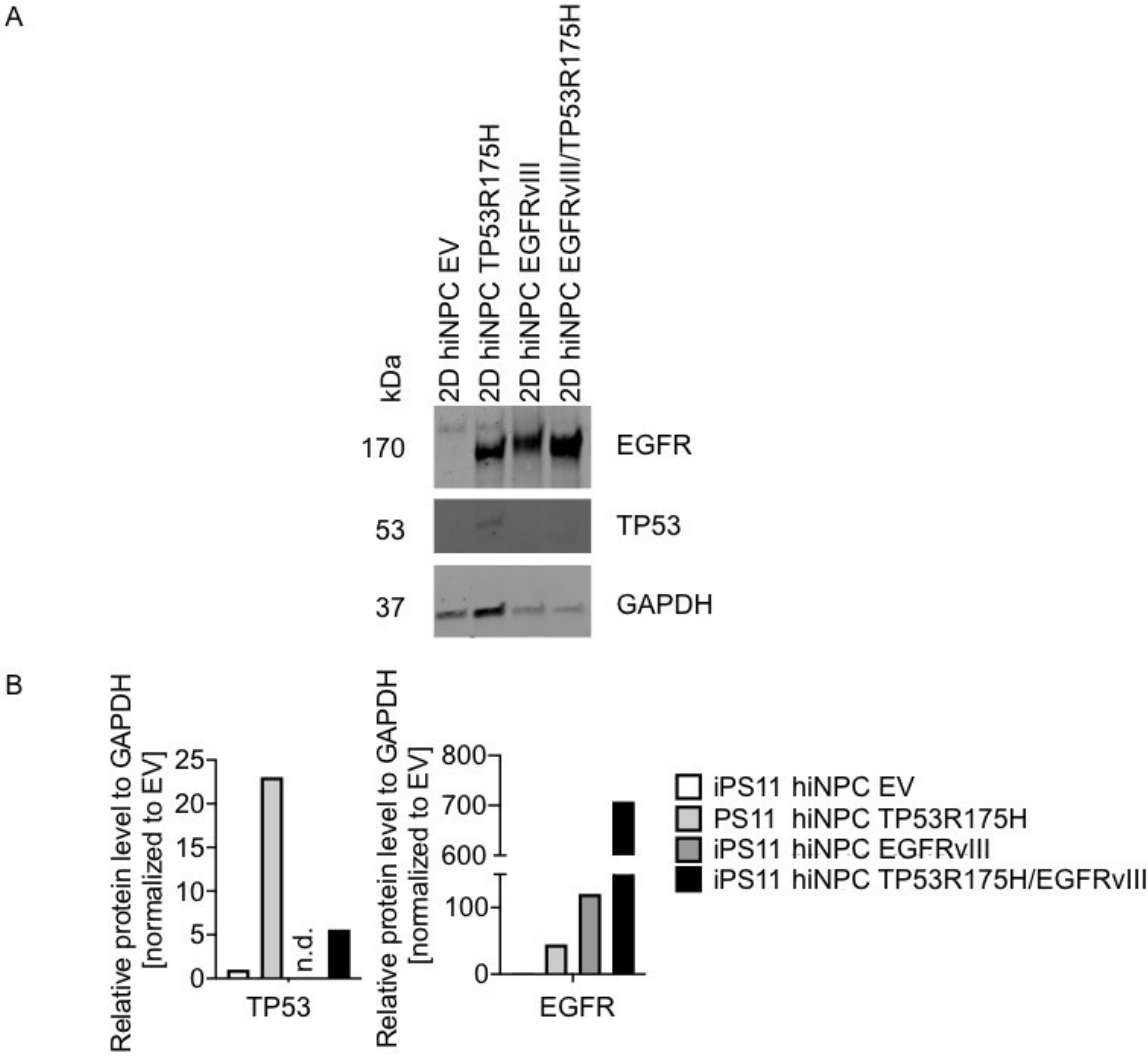


Figure 22 Protein expression of EGFR in 2D hiNPC-oncogene models.

Protein expression of EGFR in the 2D hiNPC-oncogene models was detected using Western blot (A). Relative protein expression was normalized to the housekeeping gene GAPDH (B).

Results

Methylome analyses were conducted to see if the 2D hiNPC-oncogene models can be distinguished from the hiPSC-oncogene models. The hierarchical clustering of the hiPSC-oncogene models was used as described above and the results from the differentiated neurosphere models were introduced (Figure 14). In comparison to the hierarchical clustering shown above (Figure 14), this hierarchical clustering can be separated into four instead of two branches (Figure 23). The first branch consists of the differentiated 2D hiNPC-oncogene models *EV* and *TP53R175H/EGFRvIII* while the second one has only the MB model *c-MYC*. Additionally, the methylation profiles have between them the highest consistency. The next branch holds the differentiated *TP53R175H* hiNPCs. This model has a higher similarity to the hiPSC-oncogene models than to the 2D hiNPC-oncogene models *c-MYC*, *EV*, and *TP53R175H/EGFRvIII*. All of the hiPSC-oncogene models are clustered on the same branch and reveal a high similarity. In addition, the hierarchical clustering visualizes the methylation profile of the uniquely regulated genes. In contrast, between the hiPSC-oncogene models and the differentiated neurospheres, differences are detectable (Figure 23). The neurosphere models for *EV* and *TP53R175H/EGFRvIII* have mainly the opposite methylation profile than the hiPSC-oncogene models. An intermediate expression profile could be observed for the *c-MYC* hiNPCs (Figure 23).

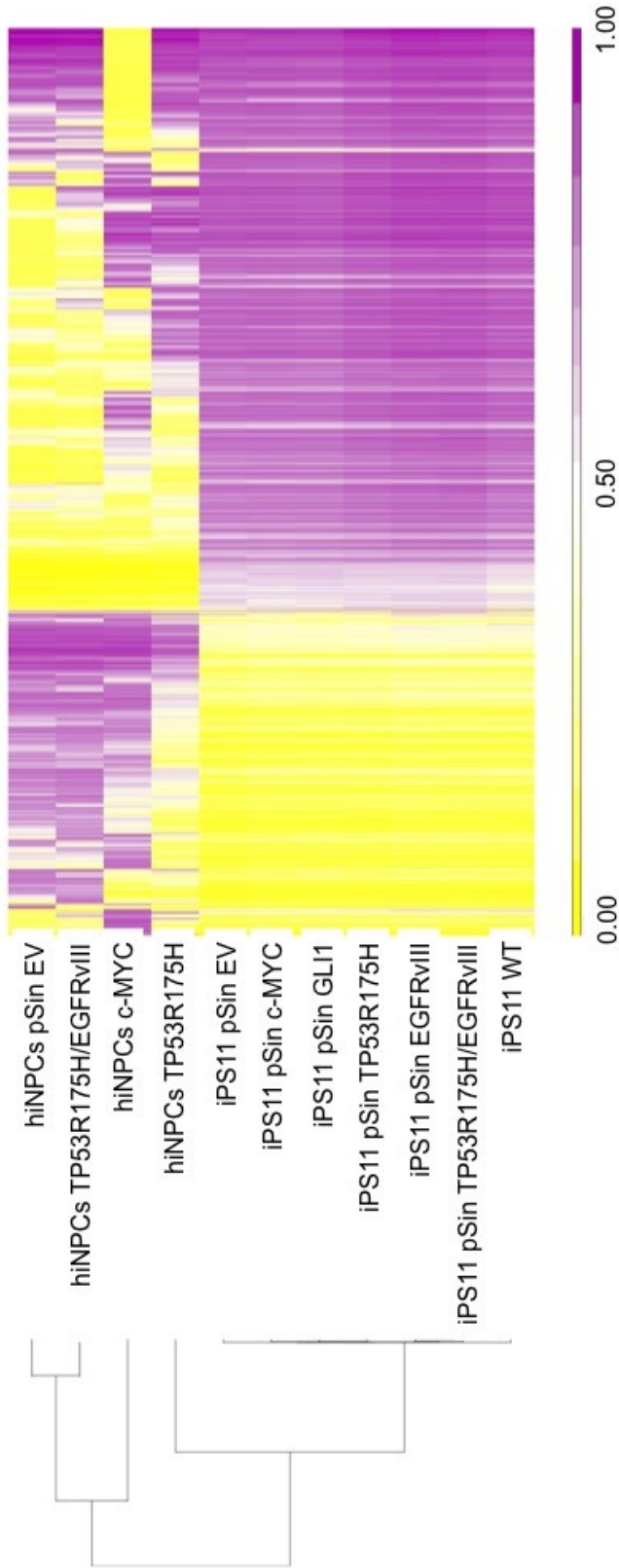


Figure 23 Hierarchical clustering of the hiPSC-oncogene and 2D iNPC-oncogene models.

Methylome analyses of the iNPC-oncogene models, neural induced in 2D, were compared to the methylome analyses of the hiPSC-oncogene models. The samples were clustered on four branches. All hiPSC-oncogene models clustered together on one branch, while the iNPC-oncogene models clustered on three different branches.

Results

In addition, 2D induced hiNPC-oncogene models were analyzed using PCA clustering. Both of the control models reveal a difference in their expression and do not cluster together. The highest similarity to each other have the EV control and the double mutation *TP53R175H/EGFRvIII* (Figure 24). The furthest away from all hiNPC-oncogene models is the only analyzed MB model, *c-MYC*.

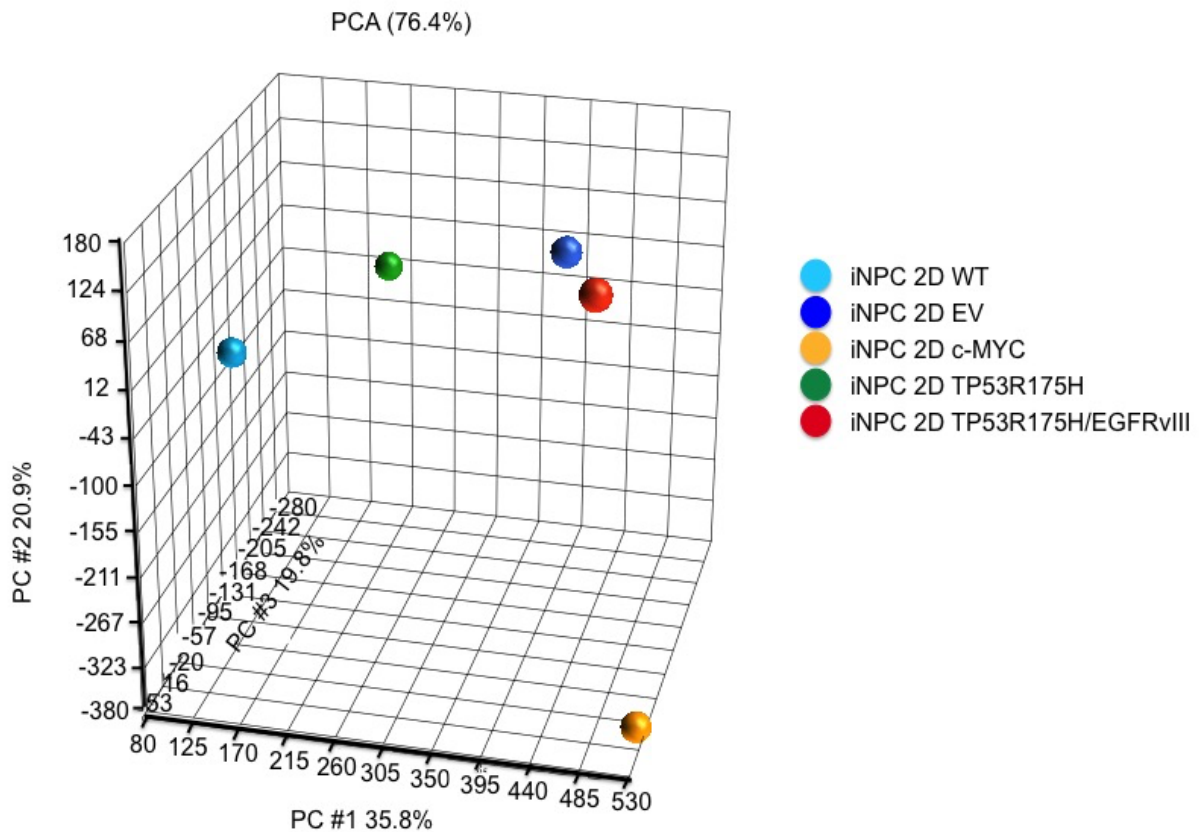


Figure 24 PCA clustering of 2D iNPC-oncogene models.

Methylome analysis was conducted for the 2D neural-induced hiPSC-oncogene models.

No further experiments could be conducted using the 2D neurally induced neurospheres. As loss of target gene expression was confirmed by the validation of the expression on protein level and because of the reduced proliferation, it was decided not to proceed using this approach. However, another neural induction protocol, this time in 3D, was tested to evaluate if this was more suitable for the generated hiPSC oncogene models. As this approach generated proliferating hiNPC-oncogene models, they were characterized and also used for compound screening.

3.8 Characterization of 3D hiNPC-oncogene models

As the 2D neural induction of all hiPSC-oncogene models did not generate a proliferating culture containing the GOI for each aspired model, neural induction following the 3D neural induction protocol was performed. For each hiPSC-oncogene model generated in 3D, an hiNPC culture could be established. Further, the expression of the stem cell marker OCT3/4 and the NPC marker NESTIN were measured using FACS (Table 30). The control as well as both MB models, *GLI1* and *c-MYC*, had an expression of OCT3/4 of under 8 % while the GBM models, *EGFRvIII*, *TP53R175H*, and *EGFRvIII/TP53R175H*, had an expression between 15.3 % and 34.1 % (Table 30). For the NPC marker, the highest expression was measured in the GBM models in comparison to the MB models as well as the EV control (Table 30). Based on the reduction of the stem cell marker and the high expression of the NPC marker, the neural induction using the 3D protocol seemed to be more successful even though it was expected that the 2D neural induction would be more successful as the cells are evenly exposed to the 2D induction medium.

Table 30 Expression of the stem cell marker and NPC marker in 3D neural induced hiNPC-oncogene models.

The expression of the stem cell marker OCT3/4 and NPC marker NESTIN was measured for all hiNPC-oncogene models using FACS analysis.

hiNPC line	OCT3/4 [%]	NESTIN [%]
pSin EV	7.9	78.4
<i>GLI1</i>	7.9	93.7
<i>c-MYC</i>	7.6	89.2
<i>TP53R175H</i>	29.9	97.3
<i>EGFRvIII</i>	15.3	91.8
<i>TP53R175H/EGFRvIII</i>	34.1	98.0

Expression of the GOI after neural induction was confirmed using RT-qPCR (Figure 25). In each 3D hiNPC-oncogene model the GOI was significantly higher expressed compared to the EV control (Figure 25). These results indicate, that the 3D hiNPC-oncogene models did not lose the expression of the GOI on RNA-level during the neural induction, making this protocol more suitable for the generated hiPSC oncogene models (Figure 25).

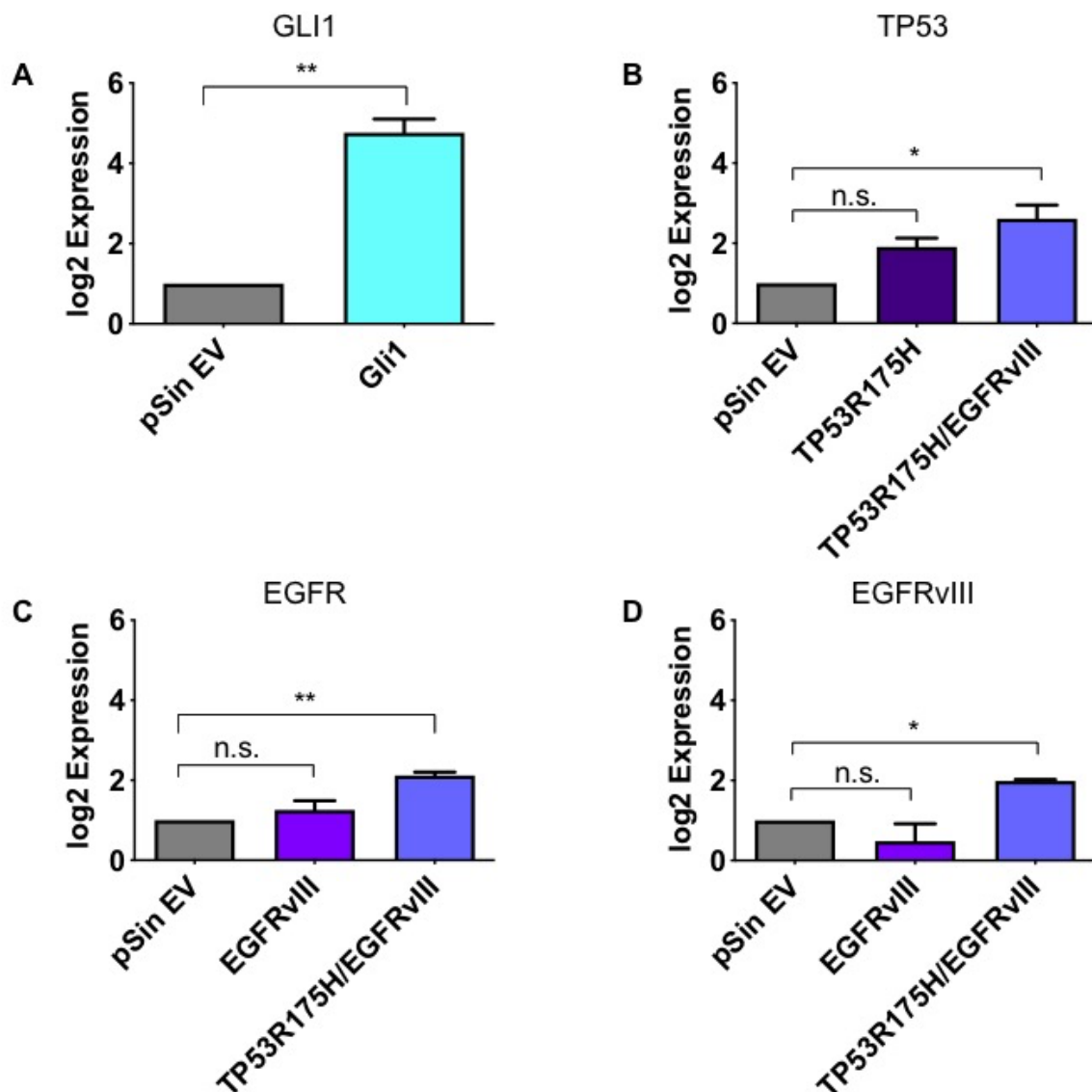


Figure 25 mRNA Expression of the GOI in 3D hiNPC-oncogene models.

The mRNA expression of the GOI was detected in the 3D hiNPC-oncogene models. Primers were used against *GLI1* (A), *TP53* (B), *EGFR* (C), and *EGFRvIII* (D). Significance was determined using one way Anova (*, p-value < 0.05; **, p-value < 0.03; n.s., not significant).

The methylome of the 3D hiNPC-oncogene models were compared to the methylome of the hiPSC-oncogene models (Figure 26). The neural models can be distinguished from the stem cell models as they cluster on different branches. A high similarity can be detected for all 3D hiNPC-oncogene models as they cluster on one branch (Figure 26). In comparison, the hiPSC-oncogene models are separated on more branches and the methylome profiles shows a higher variability to each other (Figure 26). A high similarity was detected for the *TP53R175H* and *TP53R175H/EGFRvIII* hiPSCs models, while the *EGFRvIII* models had a higher similarity to the EV control (Figure 26). The *c-MYC* hiPSC model was clustered on a

Results

separate branch between the *GLI1* and EV control model. The 3D neural induced *GLI1* hiNPC- oncogene model stopped proliferating shortly after the neural induction and it was not possible to perform any other assays expect for the FACS quality control. These results were confirmed with a second neural induction.

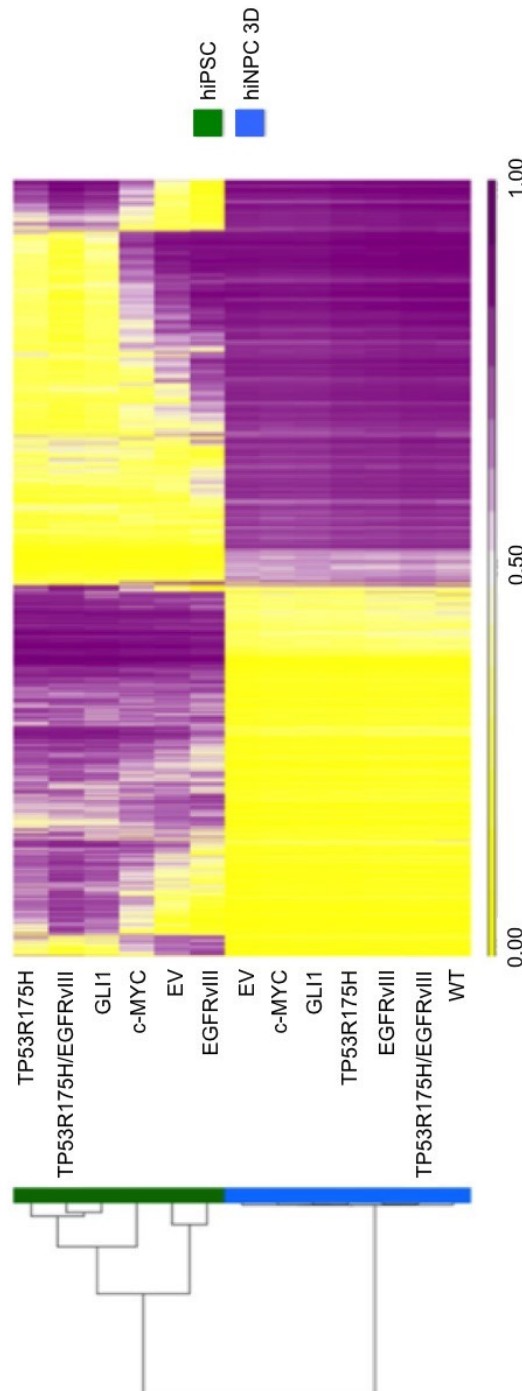


Figure 26 Hierarchical clustering of the hiPSC and 3D hiNPC- oncogene models.

Methylation profiles of the hiPSC- oncogene models (green) and 3D neural induced hiNPC- oncogene models (blue) were compared to each other. The results were visualized in a hierarchical clustering using Partek Genomics Suite.

3.9 Compound screening of the 3D hiNPC-oncogene models

The 3D hiNPC-oncogene models were first tested in a compound screening using the most effective compounds from the small-scale hiPSC-oncogene model compound screening (Table 31). The four most effective compounds were tested as well as the negative (acetaminophen) and positive control (the respective standard of care (SoC)). Similar to the hiPSC-oncogene models vinblastine sulfate reduced the viability most effectively for the 3D hiNPC-oncogene models (Table 31). However, the *EGFRvIII* and the double mutation model were not as sensitive towards the treatment as the other models (Table 31). Panobinostat also reduced the cell viability of the 3D hiNPC-oncogene models more effectively than the other two compounds and the controls (Table 31).

Table 31 Compound screening of 3D hiNPC-oncogene models using the most effective compounds from the hiPSC-oncogene model compound screening.

The four most effective compounds of the hiPSC-oncogene models compound screening were also tested on the 3D-induced hiNPC-oncogene models. Viability was measured using CellTiterGlo®. If no EC₅₀ could be determined the field was marked with an 'X'. All EC₅₀ values are in µM and were calculated using GraphPad Prism 8 (GraphPad Software, CA, USA). Results of cell viability were normalized to DMSO treated hiPSC and the two lowest concentrations (Krebs et al., 2018)

	Panobinostat	Vinblastine sulfate	Lomustine	Duvelisib	Acetaminophen	Staurosporine
hiNPC WT	0.05	0.015	13.96	14.04	X	0.112
hiNPC EV	0.29	0.004	188.8	75.29	X	0.554
hiNPC GLI1	0.45	0.48	2410	53.4	X	0.198
hiNPC c-MYC	0.12	0.019	217.1	48.68	X	0.267
hiNPC TP53R175H	0.02	0.021	191.3	732.9	X	1.657
hiNPC EGFRvIII	1367	7166	1364	1062	X	1.639
hiNPC TP53R175H/EGFRvIII	0.28	3291	270	322.5	X	0.159

Results

3.9.1 Compound screening of the MB hiNPC-oncogene model

The compound screening was conducted using the seven identified compounds for MB and a positive and negative control. As positive control SoC cisplatin was used and acetaminophen was used as a negative control. Results were generated for the migration and cytotoxicity of the hiNPC-oncogene models to determine the benchmark concentration (BMC). The only specific hit for the pSin EV control was observed with cisplatin treatment (Table 32). In comparison, the hiNPC Group 3 model showed only a specific response towards copanlisib but not towards the SoC cisplatin (Table 32). Further, the migration was also reduced when the hiNPC-oncogene models were treated with copanlisib (Table 32). Treatment with the other compounds did not show any specific response or no response at all for migration or cytotoxicity (Table 32).

Table 32 Results of the compound screening for migration and cytotoxicity of MB 3D hiNPC-oncogene models.

The compound screening was performed using nine substances to evaluate their influence on migration and cytotoxicity. For each model the benchmark concentration (BMC) values (in μM) for endpoint BMC_{15} migration and BMC_{10} cytotoxicity were determined. No hits are dark grey, light grey are unspecific hits, petrol are a specific hit and n.r. stands for not reached.

hiNPC model	Drug	Migration	Migration upper limit	Cytotoxicity	Cytotoxicity upper limit
		BMC_{15}	BMC_{15}	BMC_{10}	BMC_{10}
Empty vector control	Acetaminophen (NC)				
	Arsenic trioxide				
	Cisplatin (SoC)			1.8050	4.8012
	Copanlisib	0.00977	0.017502		
	Dasatinib				
	Midostaurin	0.357091	0.618514	2.8979	n.r.
	Regorafenib	5.270442	8.242272		
	Tretinoin				
Vandetanib					
c-Myc	Acetaminophen (NC)				
	Arsenic trioxide				
	Cisplatin (SoC)				
	Copanlisib	0.029397	0.047212	0.3948	0.5376
	Dasatinib	0.03579	0.061645		
	Midostaurin	0.598921	0.812029		
	Regorafenib				
	Tretinoin				
Vandetanib	1.851037	n.r.			

Dark grey: no hit, light grey: unspecific hit, petrol: specific hit. n.r. = not reached

The corresponding concentration-response curves of the specific hits allow direct comparison of the effects of copanlisib and cisplatin on the EV and c-MYC hiNPCs and

Results

illustrate that the SoC, cisplatin, does not decrease the migration of the *c-MYC* hiNPCs in the EV controls (Figure 27). However, it causes cell death of the empty vector controls, whereas the *c-MYC* transduced hiNPCs survive cisplatin treatment. This might indicate poor efficacy of cisplatin in this MB cell model. In contrast to cisplatin, copanlisib treatment has a specific effect on migration and cytotoxicity in *c-MYC* hiNPCs.

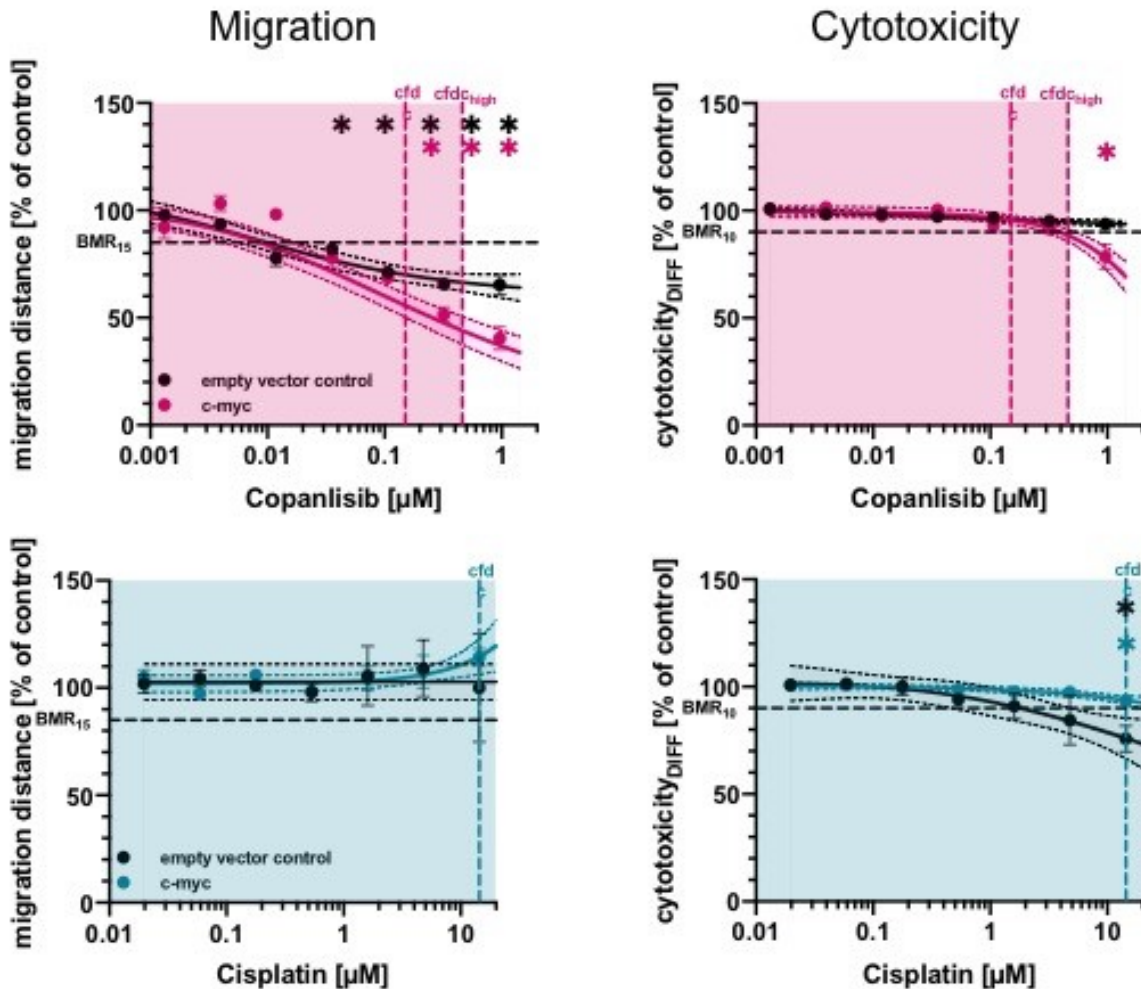


Figure 27 Concentration-response curves of specific hits.

Statistical significance was calculated using the step-down multiple test procedure of, $p \leq 0.05$ is considered significant. In addition to the curve fit, the corresponding confidence bands (shading) are also shown. The colored boxes indicate the tested concentrations that are under the $\text{cfd}_{\text{Chigh}}$ ($3 \times \text{cfd}$) and therefore indicate concentrations that are also reached in patients *in vivo*.

The effects on migration after treatment with both compounds are also seen in light-microscopic images of the migration area (Figure 28).

Results

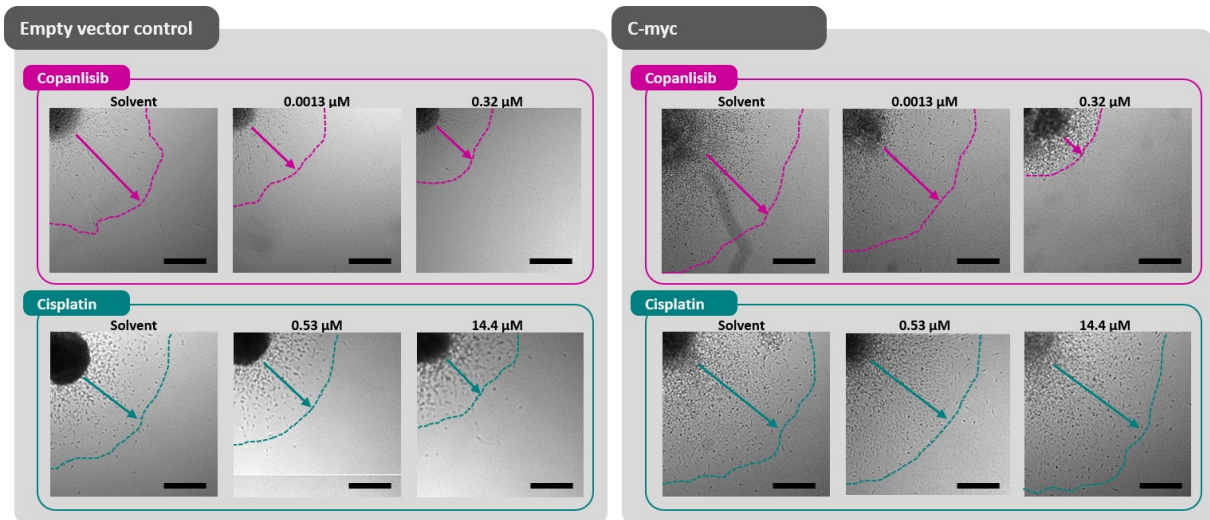


Figure 28 Exemplary migration images of EV and c-MYC hiNPCs treated with copanlisib or cisplatin.

Representative images of solvent controls (left), concentrations around the respective BMC_{15} -value for migration (middle) as well as one high concentration (right) are shown. Scalebar represents 250 μm .

The concentration-response curves of the unspecific hits demonstrate clearly how important it is to take the internal exposure ($cf_{dc} - cf_{dc_{high}}$) into account (Figure 29). While pure examination of the whole concentration range might lead to the impression that dasatanib, midostaurin, regorafenib, and vandetanib treatment also has a favorable effect on migration and to a lesser extend also on the endpoint of cytotoxicity in the analyzed models, taking into account only the concentrations that can be reached *in vivo* by calculating the free drug concentration shows that the significant effects shown here are not within a relevant *in vivo* range.

Results

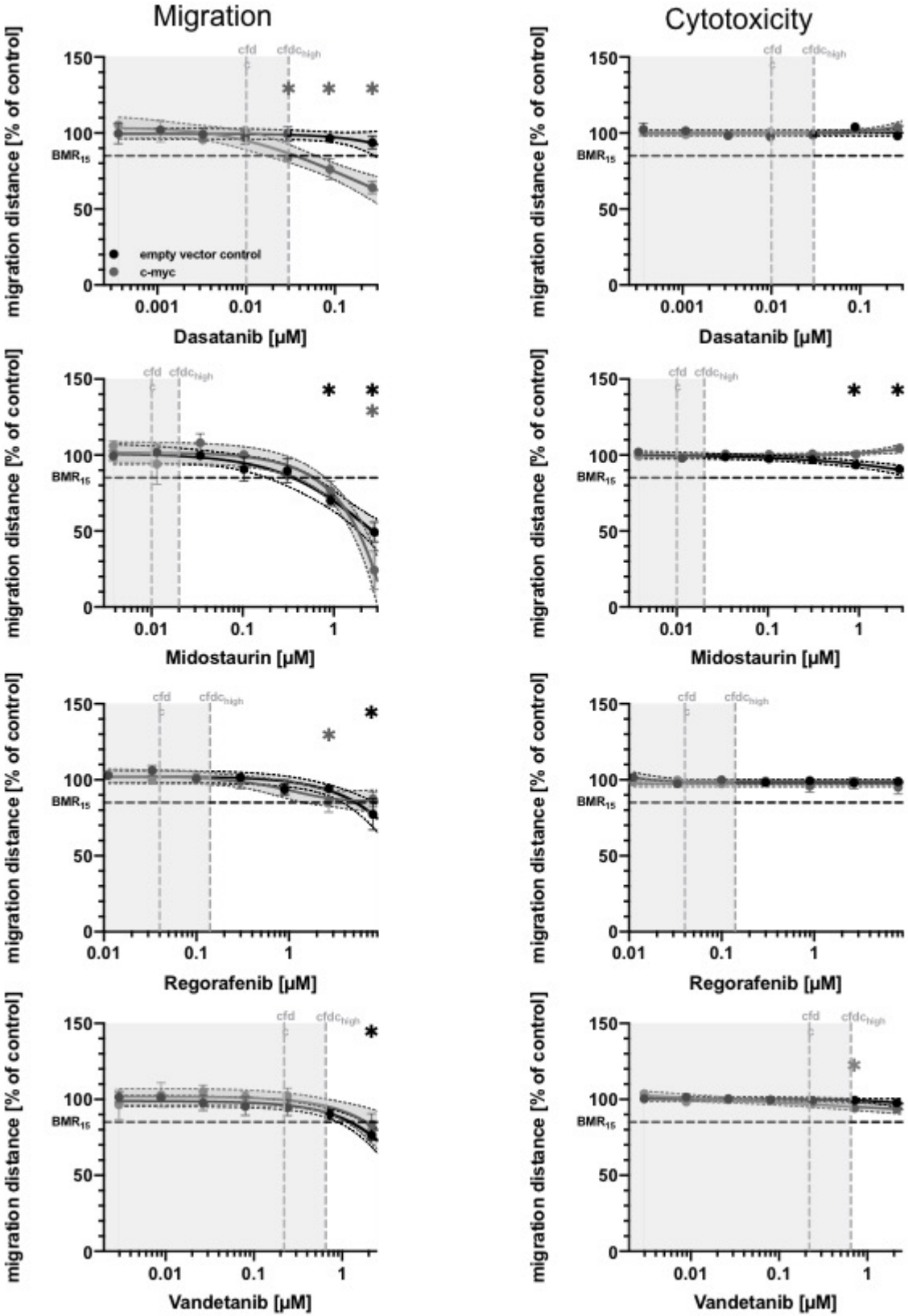


Figure 29 Concentration-response curves of unspecific hits for c-MYC hiNPCs.

Statistical significance was calculated using the step-down multiple test procedure of Dunnett and Tamhane (1991), $p \leq 0.05$ is considered significant. In addition to the curve fit, the corresponding confidence intervals (shading) are also shown. cfd_c = calculated free drug concentration (see Table 1). The colored boxes indicate the tested concentrations that are under the $cfd_{c_{high}}$ ($3 \times cfd_c$) and therefore indicate concentrations that are also reached in patients *in vivo*.

Results

3.9.2 Compound screening of the GBM hiNPC-oncogene model

The nine identified compounds (bosutinib, cabozantinib, copanlisib, dabrafenib, midostaurin, olaparib, regorafenib, trametinib, and vandetanib) for GBM as well as the respective SoC TMZ and the negative control acetaminophen were also tested on the GBM 3D hiNPC-oncogene models to evaluate their influence on the proliferation, migration, and cytotoxicity (Table 33). Similar to the MB hiNPC-oncogene models, it was also observed that the proliferation stopped after some time for all models, therefore it was not possible to evaluate all planned endpoints. Copanlisib had a specific hit for the pSin EV, *TP53R175H*, and *TP53R175H/EGFRvIII* models on migration (Table 33 B). A specific hit for cytotoxicity could be only detected for the double mutant model, when it was treated using copanlisib. All other compounds did not show any specific hit on migration (Table 33 B). The proliferation of the GBM 3D hiNPC-models was also measured when they were treated with the compounds (Table 33). Copanlisib and vandetanib, an inhibitor of vascular epidermal growth factor (*VEGFR*), reduced the proliferation of the pSin EV and *TP53R175H* models (Table 33). Proliferation was also reduced in the *TP53R175H* model when cells were treated with the negative control, acetaminophen, and olaparib (Table 33). However, for the pSin EV and *TP53R175H* models the compounds did not increase the cytotoxicity (Table 33). Proliferation was decreased and at the same cytotoxicity increased in the *TP53R175H/EGFRvIII* model when treated using olaparib (Table 33 A). The only compounds which increased the cytotoxicity were TMZ and vandetanib in the *TP53R175H/EGFRvIII* model (Table 33). Vandetanib decreased the proliferation while no influence was observed after treatment with TMZ (Table 33 A). Similar to the results obtained for migration, the *EGFRvIII* model did not have any specifically reduced proliferation or increased cytotoxicity upon treatment (Table 33).

Results

Table 33 Results of the compound screening for proliferation, migration, and cytotoxicity of GBM 3D hiNPC-oncogene models.

The compound screening was performed using nine substances and two controls to evaluate their influence on migration and cytotoxicity. For each model the benchmark concentration (BMC) values (in μM) for the endpoints proliferation (A) and migration (B) were determined.

A	hiNPC model	Drug	ENDPOINTS PROLIFERATION			
			Proliferation BMC ₅₀	Proliferation upper limit BMC ₅₀	Cytotoxicity PROL BMC ₁₀	Cytotoxicity PROL upper limit BMC ₁₀
EV control	Acetaminophen (NC)					
	Bosutinib					
	Cabozantinib	0.2530	N/A			
	Copanisib	0.0090	0.0323			
	Dabrafenib	1.3989	4.1911			
	Midostaurin	0.4662	N/A			
	Olaparib					
	Regorafenib	0.3306	0.7720			
	Temozolomide (SoC)					
	Trametinib					
	Vandetanib	0.2558	0.8501			
TP53R175H	Acetaminophen (NC)	0.3485	N/A			
	Bosutinib			0.0983	N/A	
	Cabozantinib	1.5809	N/A			
	Copanisib	0.0140	0.0247			
	Dabrafenib					
	Midostaurin	0.0497	0.0941			
	Olaparib	0.3379	N/A			
	Regorafenib	0.1555	0.4633			
	Temozolomide (SoC)					
	Trametinib					
	Vandetanib	0.0878	0.2822			
EGFRvIII	Acetaminophen (NC)					
	Bosutinib					
	Cabozantinib					
	Copanisib					
	Dabrafenib					
	Midostaurin			3.3543	N/A	
	Olaparib					
	Regorafenib	1.4645	5.0928			
	Temozolomide (SoC)					
	Trametinib					
	Vandetanib					
TP53R175H/ EGFRvIII	Acetaminophen (NC)					
	Bosutinib					
	Cabozantinib					
	Copanisib					
	Dabrafenib					
	Midostaurin	0.3822	0.6850	0.2306	1.5254	
	Olaparib	5.4031	13.9294	2.2799	4.5774	
	Regorafenib					
	Temozolomide (SoC)			16.6906	35.8631	
	Trametinib					
	Vandetanib	1.5825	2.7200	0.4100	1.1994	

Dark grey: no hit, light grey: unspecific hit, petrol: specific hit. white = not assessed

Results

B		ENDPOINTS MIGRATION			
hiNPC model	Drug	Migration BMC ₃₀	Migration upper limit BMC ₃₀	Cytotoxicity _{Diff} BMC ₁₀	Cytotoxicity _{Diff} upper limit BMC ₁₀
EV control	Acetaminophen (NC)				
	Bosutinib	0.3531	N/A		
	Cabozantinib				
	Copanlisib	0.1512	N/A		
	Dabrafenib				
	Midostaurin	0.9885	1.4214	2.8979	N/A
	Olaparib				
	Regorafenib	10.8135	N/A		
	Temozolomide (SoC)				
	Trametinib				
	Vandetanib	2.8426	N/A		
TP53R175H	Acetaminophen (NC)				
	Bosutinib	0.4470	N/A		
	Cabozantinib				
	Copanlisib	0.1014	0.1821		
	Dabrafenib				
	Midostaurin	2.1165	2.8797		
	Olaparib				
	Regorafenib				
	Temozolomide (SoC)				
	Trametinib				
	Vandetanib	2.1411	N/A		
EGFRvIII	Acetaminophen (NC)				
	Bosutinib				
	Cabozantinib				
	Copanlisib	0.8954	N/A		
	Dabrafenib				
	Midostaurin	1.4917	2.1033		
	Olaparib				
	Regorafenib				
	Temozolomide (SoC)				
	Trametinib				
	Vandetanib				
TP53R175H/ EGFRvIII	Acetaminophen (NC)				
	Bosutinib				
	Cabozantinib				
	Copanlisib	0.0637	0.1002	0.0558	0.1360
	Dabrafenib				
	Midostaurin	1.4546	1.9056		
	Olaparib				
	Regorafenib				
	Temozolomide (SoC)				
	Trametinib				
	Vandetanib				

Dark grey: no hit, light grey: unspecific hit, petrol: specific hit. white = not assessed

Results

Based on the results of the concentration-response curves, the compounds acetaminophen, copanlisib, olaparib, TMZ, and vandetanib showed a specific hit in the GBM hiNPC-oncogene models.

Acetaminophen was used as a negative control in the compound screening. Surprisingly, a specific hit was detected for the *TP53R175H* model (Figure 30). Due to the lower proliferation rate of the models after some time in culture, it was not possible to generate results for the *EGFRvIII* and *TP53R175H/EGFRvIII* models.

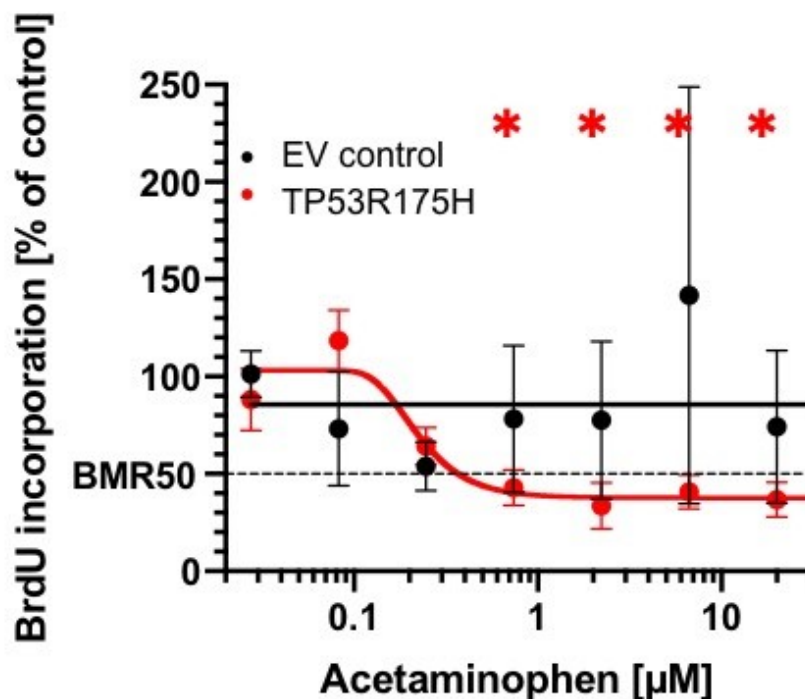


Figure 30 Concentration-response curve for acetaminophen in the GBM 3D hiNPC-oncogene models.

Statistical significance was calculated using the step-down multiple test procedure of, $p \leq 0.05$ is considered significant (Dunnett & Tamhane, 1991).

The SoC TMZ reduced the proliferation only in the cells of model *TP53R175H/EGFRvIII* (Figure 31). However, it was only possible to screen two replicates instead of three due to the lower proliferation rate after some time in cell culture. As the BMC_{50} and the upper limit of the BMC_{50} was reached, the result is defined as a specific hit.

Results

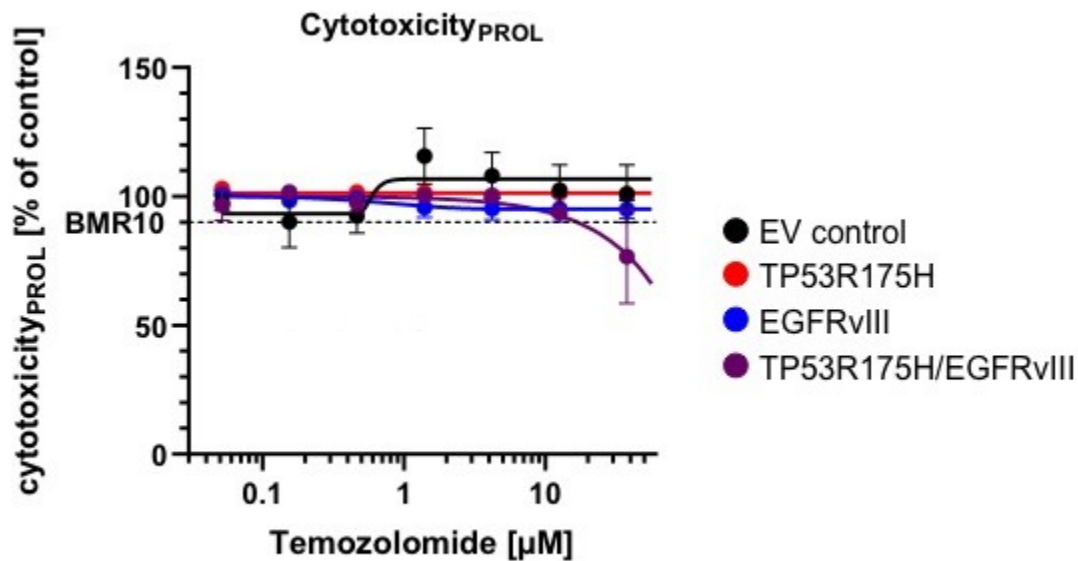


Figure 31 Concentration-response curve for TMZ in the GBM 3D hiNPC-oncogene models.

Statistical significance was calculated using the step-down multiple test procedure of, $p \leq 0.05$ is considered significant (Dunnett & Tamhane, 1991).

Similar to the results of the MB hiNPC-oncogene screening, copanlisib reduced the proliferation in the EV control and the *TP53R175H* models (Figure 32). Comparable results were achieved for the migration for the EV control, *TP53R175H*, and *TP53R175H/EGFRvIII* model. In all models the migration distance was reduced. The cytotoxicity, however, was only reduced in the *TP53R175H/EGFRvIII* model. No specific hits were observed for all tested compounds in the *EGFRvIII* model, no reduction of proliferation or migration was detected.

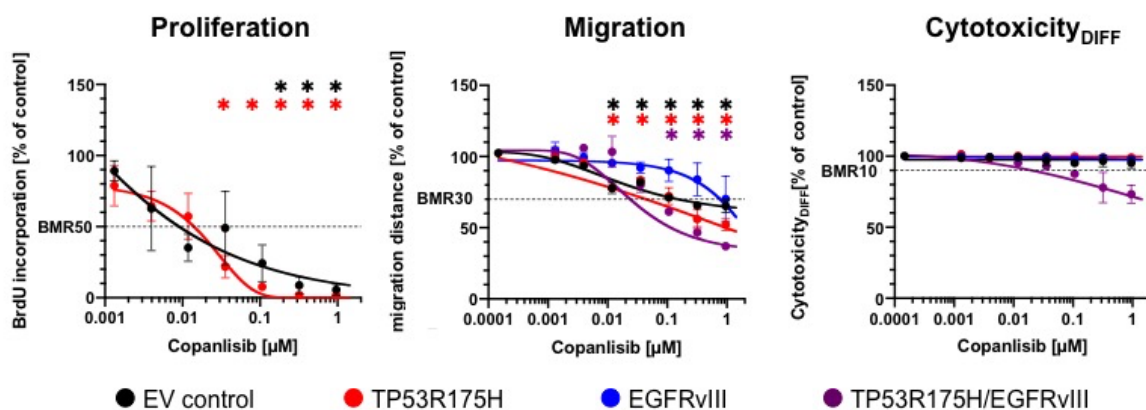


Figure 32 Concentration-response curve for copanlisib in the GBM 3D hiNPC-oncogene models.

Statistical significance was calculated using the step-down multiple test procedure of, $p \leq 0.05$ is considered significant (Dunnett & Tamhane, 1991).

The compound screening using olaparib showed only one specific hit in the *TP53R175H/EGFRvIII* model by reducing cell proliferation (Figure 33). In the EV control a

Results

reduction of proliferation is only observed when higher concentrations of the compound were used.

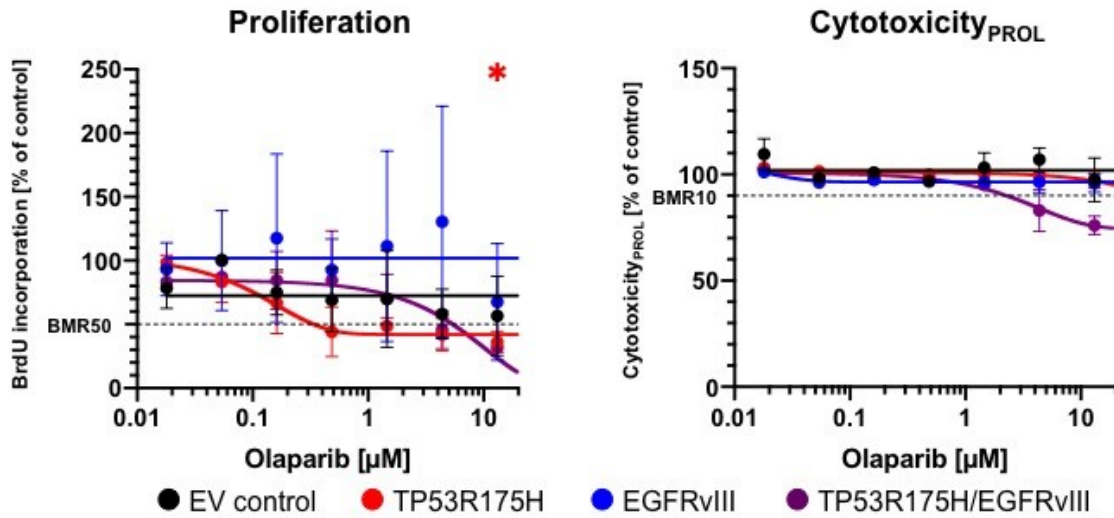


Figure 33 Concentration-response curve for olaparib in the GBM 3D hiNPC-oncogene models.

Statistical significance was calculated using the step-down multiple test procedure of, $p \leq 0.05$ is considered significant (Dunnett & Tamhane, 1991).

Vandetanib had a specific hit in the EV control, *TP53R175H*, and *TP53R175H/EGFRvIII* models and reduced the cell proliferation (Figure 34). Further, the *TP53R175H/EGFRvIII* model showed a higher cytotoxicity during the treatment and was the only model with a specific hit.

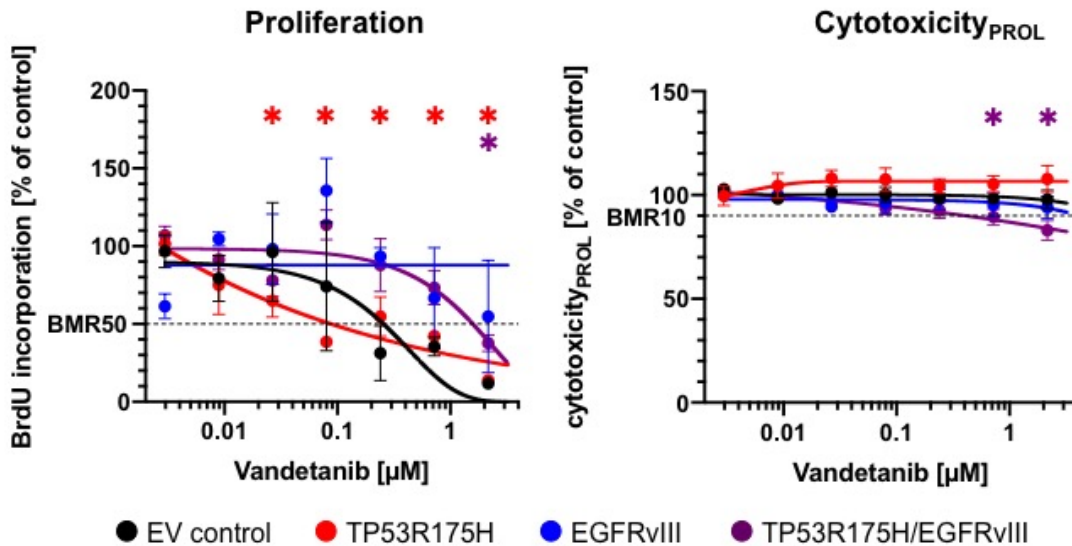


Figure 34 Concentration-response curve for vandetanib in the GBM 3D hiNPC-oncogene models.

Statistical significance was calculated using the step-down multiple test procedure of, $p \leq 0.05$ is considered significant (Dunnett & Tamhane, 1991).

4 Discussion

4.1 Application of *in vitro* test systems

Currently, cancer studies are either performed with established *in vitro* cell lines or primary cell cultures generated from tumor tissue (Boussommier-Calleja, 2020; Katt et al., 2016). However, it was shown that the reproducibility is decreased using established *in vitro* cell models, as the same cell lines develop different physiological behaviors in the laboratories, probably due to genetic drift (Ben-David et al., 2019; Kleensang et al., 2016; Liu et al., 2019). One alternative approach is to generate patient-specific cell lines from tumor tissue. However, this procedure is time-consuming due to the need to establish a proliferating cell culture to utilize the cells in studies and not always successful (Kodack et al., 2017). As an alternative approach, tumor tissue is cultured for a short period *ex vivo* and then utilized for a high-throughput screening (HTS) to identify treatment options. However, over the years, several disadvantages of using tumor tissue from patients have been identified: (i) A selection takes place, as not all cells survive under *in vitro* cell culture conditions (Ben-David et al., 2018; Selich et al., 2016), (ii) tumor heterogeneity may not be represented in the obtained tissue sample (Jacob et al., 2020), and (iii) generated cell lines still evolve and change over time and do not represent the original tumor (Franzen et al., 2021; Neumann et al., 2010). Another approach, which intended to circumvent the mentioned problems, was to produce a stable iPSC culture from a mice GBM tumor (Vatanmakanian et al., 2019). However, this was not feasible as the cancer cells did not reach a pluripotent stage nor obtained GBM marker expression and the reprogramming protocol had to be adapted to obtain a proliferating cell culture (Vatanmakanian et al., 2019). Therefore, this thesis aimed to introduce subgroup-specific genes into hiPSCs to mimic the highly aggressive brain tumors MB and GBM on a stem cell level. Tumor subgroup-specific genes have been introduced into the same genetic background to study their effects. In addition, the application of a pharmacological screening offered the chance to identify differences in sensibility towards the applied drugs. Usage of hiPSCs as a receiver cell line offers several benefits, including many properties of stem cells e.g. pluripotency and self-renewal, and was therefore chosen (Takahashi & Yamanaka, 2006). Human iPSCs can also be differentiated into any desired tissue using differentiation protocols and opens application possibilities to many other disease types especially cancer (Denham & Dottori, 2011). Further, somatic cells of the patient can be used to generate hiPSCs. This has the benefit, that the patient-derived hiPSCs represent exactly the genetic background of the patient including mutations (Onder & Daley, 2012; Zeltner & Studer, 2015). For instance, *in vivo* experiments already proved the

Discussion

feasibility of iPSCs in the treatment or improvement of diseases, e.g. sickle cell anemia in mice (Hanna et al., 2007). Hanna et al. (2007) could prove, that the re-transplanted cells, were healthy and iPSCs can be applied for targeted gene and cell therapy. Taken together, hiPSCs are increasingly used in cancer research and are already used for GBM model creation. Koga et al. (2020) modified and differentiated hiPSCs containing marker genes of the mesenchymal and proneural GBM subtype to study tumor development *in vivo*. The generated cell models were injected into mice to observe the tumor growth and evaluate the tumorigenic capacity of the derived cells. From the derived xenografts, analysis of the transcriptome were conducted and revealed a high similarity to GBM tissue derived from patients (Koga et al., 2020). In addition, using stem cells offers the chance to understand more about the development of tumors, for example during differentiation. In this study, the iPS11 hiPSC line was used, which was generated from human foreskin fibroblasts.

4.2 Subtype-specific hiPSC-oncogene model generation

Human iPSC-oncogene models for MB and GBM were created by the introduction of subtype-specific marker genes. For each subtype one gene was introduced into the hiPSCs by lentiviral transduction. The following genes were cloned into the vector: *CTNNB1 S33Y* (MB-WNT), *GLI1* (MB-SHH), *c-MYC* (MB-Group 3), *PDGFRA* (GBM-proneural), *EGFRvIII* (GBM-classical) and *CD44* (GBM-mesenchymal). Even though all lentiviral vectors were cloned, and integration of the GOI was confirmed by sequencing, it was not possible to generate all MB and GBM hiPSC-models. Only the MB models for SHH and Group 3 as well as the classical subtype for GBM could be produced. In addition to the classical GBM subtype, the models *TP53R175H* and *TP53R175H/EGFRvIII* were also successfully generated. Both models were counted as GBM models during the studies. The *TP53R175H* model was generated as the mesenchymal and proneural GBM subtype commonly have a *TP53* background mutation (Verhaak et al., 2010). The introduced point mutation *TP53R175H* leads to an exchange of arginine for histidine, resulting in a structural change (Cho et al., 1994). This point mutation has a dominant-negative effect and reduces the function of wild-type *TP53* to suppress cell proliferation (Park et al., 1994; Willis et al., 2004). The mutation *TP53R175H* is counted as a hotspot mutation as this allele is commonly mutated in several cancer diseases for example in the pancreas or GBMs (Chiang et al., 2021; Hainaut & Hollstein, 2000; Polireddy et al., 2019). Even though it is uncommon for GBM to have a *TP53* mutation in the classical GBM model, it was decided to generate this model for several reasons (Verhaak et al., 2010). For once, secondary GBM cases have a higher incidence of the co-occurrence of *EGFR* amplification and *TP53* mutations (Ruano et al., 2009; Watanabe et al., 1996). As *TP53* mutations increase the aggressiveness of tumors,

Discussion

it was of interest if differences in behavior and responses towards drug treatment were detectable between the single and double mutations in all three GBM models (Ruano et al., 2009). Further, the generated models can be of interest for other diseases, as e.g. non-small cell lung cancer also often carries *EGFR* and *TP53* mutations (Aggarwal et al., 2018; Canale et al., 2022). The generated hiPSC-oncogene models can be differentiated into multiple tissues due to the differentiation protocols and therefore be used for research of different cancer diseases (Kato et al., 2019). In general, the idea to introduce several mutations into one hiPSC-oncogene model might help to recreate complex tumors and to understand them more with regard to e.g. the heterogeneity of a tumor. However, a proliferating and target gene expressing cell line could not be generated for the models: WNT (MB), mesenchymal (GBM), and proneural (GBM). Even though several attempts were made, both GBM models showed already a higher sensitivity towards the antibiotic used for the selection process and died during the selection or only a few cells survived but did not express the GOI. This might be due to the selection of puromycin-resistant cells or the integration was not successful due to inhibiting processes within the cell (Chen & Townes, 2000; Sutlu et al., 2012). Further, the virus production is not as efficient if larger gene constructs are used (Pirone et al., 2020). To achieve the generation of the hiPSC-models for the more challenging transgenes, a commercial supplier was contacted. However, even in their hands, it was not possible to confirm the expression of the GOI in the models, even though antibiotic selection indicated a successful integration of the plasmid. Therefore, it would be of interest to test the integration of the genes by CRISPR as the integration site of the gene can be specified. At this point it is not possible to state if the integration of the GOI by CRISPR would be more stable and still detectable in the hiNPC-oncogene models.

4.3 Characterization of the hiPSC-oncogene models

Cancer progression and development are caused by deregulation of gene expression or different pathways e.g., SHH, *TP53*, and *MYC* (Fattahi et al., 2018; Sanchez-Vega et al., 2018). Therefore, hiPSC-oncogene models were thoroughly characterized. At first chromosome analysis was performed as genetic modifications and *in vitro* cultivation can cause chromosomal abnormalities (Draper et al., 2004; Laurent et al., 2011; Papathanasiou et al., 2021). The analysis confirmed for all hiPSC-oncogene models a normal male karyotype, which was expected, as the initial hiPSCs were derived from human foreskin fibroblasts (Figure 13; Alstem Inc. CA, USA). In addition, flow cytometry and ICC staining were performed to exclude the influence of lentiviral transduction on the pluripotency of the cells (Figure 12 and Table 27). Expression of the marker proteins OCT3/4, SOX2, and TRA1-60 confirmed the pluripotency (Ben-Porath et al., 2008; Pamies et al., 2017; Schopperle &

Discussion

DeWolf, 2007). Even though the intensity of the expression markers was different for each hiPSC-oncogene model the threshold of 70 % was reached (Sullivan et al., 2018). Thus, the pluripotency of the hiPSC-oncogene models was confirmed (Figure 12 and Table 27). Further, the reproduced models were characterized by the application of OMICS to gain more insight into the regulated pathways and target gene regulation. This was achieved by conducting methylome and transcriptome analyses. Since the genetic background of the hiPSC-oncogene models was the same, it was decided to filter for uniquely regulated genes to identify differentially regulated genes and signaling pathways. This was not applied for the generated models *EGFRvIII*, *TP53R175H*, and *TP53R175H/EGFRvIII* as here in part the same genes were introduced. Hierarchical clustering of the methylome data confirmed the similarity of the hiPSC-oncogene models (Figure 14). Using the methylome data, IPA analyses of canonical pathways and upstream targets were conducted and for the MB models significantly different regulated pathways could be identified (Figure 15, Figure 16, and Figure 17). However, the upstream target analysis for both MB models revealed few significantly regulated genes. Three upstream targets were identified in the *GLI1* model, one of them being *GLI1* itself, confirming that *GLI1* is one of the major regulators in this model. The other upstream targets identified are retinoic acid receptor alpha (*RARA*) and protein kinase C delta (*PRKCD*; Figure 17). *GLI1* and *RARA* are both nuclear transcription factors and regulate brain patterning and neuronal differentiation during embryonic development (Gongal et al., 2011; Ogura et al., 1996; Schneider et al., 2001). *RARA* and *PRKCD* were shown to have an inhibitory effect on *GLI1* (Cai et al., 2009). Volcano plot analysis of the obtained data revealed only one significantly upregulated gene, which was again *GLI1* (Figure 18). These results confirmed and visualized the successful introduction of *GLI1* on the genetic level. To get a better insight into the biological processes changed in the *GLI1* model, the significantly differentially expressed genes were used to perform GO term analysis. As mentioned earlier, *GLI1* is responsible for the patterning of the axis and formation, (neural) development and morphogenesis during embryonic development, and in adults a regulator of homeostasis and stem cell maintenance. *GLI1* regulates all of these events by being one of the major nuclear transcription factors in the SHH pathway, which is a highly conserved pathway (Choudhry et al., 2014). In cancer, a dysregulation of the SHH pathway can initiate, progress, and maintain the disease (Fattahi et al., 2018; Jeng et al., 2020). It was shown, that tumor cells overexpressing the SHH pathway or genes involved in this pathway, have increased cell proliferation and tumor vascularization, and therefore increased tumor growth (Dahmane et al., 1997; di Magliano & Hebrok, 2003; Ingham, 1998). However, the *GLI1* hiPSC-oncogene model did not exert significantly increased viability compared to the other hiPSC-oncogene models (Figure 11). Further, it was shown that CSCs and their pathways can also be affected by dysregulation of *GLI1* or the SHH pathway and

Discussion

can lead to the spreading of the tumor. Taken together, all performed OMIC analyses, including GO terms, revealed that the constructed hiPSC-oncogene model of *GLI1* represents a functional model for the MB SHH subtype.

In contrast to the *GLI1* model, several upstream targets were identified for the Group 3 MB model, which was created by introducing a constant overexpression of *c-MYC*. Under normal circumstances, *c-MYC* is involved in many cellular mechanisms including proliferation, apoptosis, and differentiation. The here identified upstream targets are mostly interaction partners of *c-MYC* for example the nuclear factor kappa B. *NFkB* is a transcriptional regulator which is involved in the development and progression of several diseases e.g. breast cancer, squamous cell carcinoma, or acute myeloid leukemia (Bassères & Baldwin, 2006; Baud & Karin, 2009). It was shown that *NFkB* can regulate the transcription of *c-MYC* through binding to the promoter. Down-regulation of *NFkB* and therefore down-regulation of the target genes can reduce the growth of malignant brain tumors, e.g. MB (Spiller et al., 2011). The GO term analysis identified biological processes, which are in accordance with the function of *c-MYC*, controlling apoptosis and cellular differentiation.

Introducing *EGFRvIII* successfully created the classical GBM subtype. Further, it was decided to include the *in vivo*/in patients rarely found double mutation *TP53R175H/EGFRvIII* (Dittmer et al., 1993; Hollstein et al., 1991; Watanabe et al., 1996; Yoon et al., 2001). *TP53* mutations are commonly observed in various cancer types, as well as it is often a background mutation in GBM patients belonging to the proneural subtype (Verhaak et al., 2010). The three GBM models showed the highest similarity in the hierarchical clustering as well as partly in PCA clustering (Figure 14 and Figure 15). This is expected since all models, except for the *TP53R175H* single mutant, are descendants of each other as first *EGFRvIII* was introduced into the iPS11 cell line before the background mutation *TP53R175H* was introduced. Interestingly, the models *EGFRvIII* and *TP53R175H/EGFRvIII* share a greater similarity in the PCA clustering compared to *TP53R175H*, indicating a higher influence of *EGFRvIII* on the model than *TP53R175H*. In general, for all three GBM models, a diversity of pathways was detected as *EGFR* and *TP53* are involved in many cellular processes. For example, in the models processes seem to be involved in 'systemic lupus erythematosus' (SLE), which is an autoimmune disease that causes inflammation in several tissues. Studies could show that *TP53* mutations can support the development of SLE due to defects in the apoptosis regulation (Miret et al., 2003; Veeranki & Choubey, 2010). Furthermore, it is known that *TP53* does not only function as a tumor suppressor but also as a major regulator of several autoimmune diseases e.g., arthritis and diabetes (Simelyte et al., 2005; Veeranki & Choubey, 2010; Zheng et al., 2005). Another functional pathway identified by IPA enrichment was the 'sirtuin signaling pathway'. Sirtuins are evolutionarily conserved nicotinamide adenine dinucleotide (NAD⁺)-dependent lysine deacylases or ADP-ribosyltransferases. They

Discussion

regulate several cellular processes such as cellular homeostasis, in particular metabolism, inflammation, oxidative stress, and senescence (Warren & MacIver, 2019). However, studies also revealed the function of sirtuin in disease development and progression (Bosch-Presegué & Vaquero, 2011; Chalkiadaki & Guarente, 2015; Kupis et al., 2016). The 'sirtuin signaling pathway' is activated through *SIRT1* which was identified as a regulator of *TP53*-mediated apoptosis pathways (Yi & Luo, 2010). Furthermore, It was also shown that it is, together with *TP53* and the mitochondrial topoisomerase I, important in the response and maintenance of mitochondrial DNA (mtDNA) after doxycycline exposure to preserve myocardial function against genotoxic stress (Li et al., 2019), and could further explain the connection of the GBM cell models to sirtuin related pathways. The clinical relevance has yet to be shown, but it could be of interest for tumor research since sirtuins play an important role in vascular biology of aging and upon *SIRT1* knockout in endothelial cells, the vascular effects after ischemic injury will be destroyed as well as the WNT signaling pathway is altered (Man et al., 2019; Yu et al., 2019). The 'Glucocorticoid Receptor (GR) Signaling' pathway was found to only be involved in the signaling mechanisms of the single mutants *TP53R175H* and *EGFRvIII* but not in the double mutation. The function of glucocorticoids is to maintain glucose homeostasis in response to external factors, and interestingly, it was detected that *SIRT1* is connected to this pathway since it will act as a transcriptional enhancer of the GR transcription (Suzuki et al., 2018). These results suggest that *SIRT1* can influence GR activities, which further contributes to the diverse actions of *SIRT1* on human physiology and pathophysiology. Furthermore, GR has an influence on the epidermal morphogenesis during embryonic development and interacts with *EGFR* (Sanchis et al., 2010). In cancer, especially in solid tumors, the GR pathway is known for its role in angiogenesis and its response to dexamethasone (Shikatani et al., 2012). Unfortunately, in GBM dexamethasone did not change the speed and amount of vascularization in mouse models (Shikatani et al., 2012). Certain GR isoforms, such as the glucocorticoid receptor β (GR β), regulate the malignant phenotypes of e.g. GBM and is also involved in maintenance of stem-like cells in GBM (Hu et al., 2022). This further reflects the successful creation of this model. In general, most of the identified upstream targets are transcription factors and were found in all three models, *TP53R175H*, *EGFRvIII*, and *TP53R175H/EGFRvIII*.

In the IPA analyses, it was not distinguished between gene up- and downregulation, therefore the influence of the gene cannot be interpreted in more detail for the respective model. However, the upstream targets were listed in an ascending order based on the number of target genes, indicating the number of cellular processes the gene is involved in. Each hiPSC-oncogene model shared occurrence of upstream targets but with different number of occurrences and target genes involved. For example *TGFB1* had approximately 40 target genes in the EV model and over 100 in the *EGFRvIII* and *TP53R175H/EGFRvIII*

Discussion

models (Figure 17). Similar results were obtained for *TNF* and *TP53*, which were both not found in the *TP53R175H* model. All three genes, *TGFB1*, *TNF* and *TP53*, are known to be involved in the regulation of cell proliferation, cell survival, growth, and differentiation (Levine, 1997; Massagué, 2012; Roberts & Sporn, 1993; Wang & Lin, 2008; Webster & Vucic, 2020). However, they are also commonly found to be regulators or mutated in cancer diseases of all kinds (Balkwill, 2006; Bieri & Moses, 2006; Guimaraes & Hainaut, 2002; Sethi et al., 2008).

In summary, it was possible to generate hiPSC-oncogene models for MB and GBM subtypes and detect the protein expression of the GOI. Further, GOI specific expression of target genes confirmed the successful generation of the models. The characterization of the hiPSC-oncogene models showed that the cells kept their stem cell characteristics and offer the chance to be used as models for other cancer models than CNS tumors.

4.4 Pharmacological screening of the hiPSC-oncogene models and 3D hiNPC-oncogene models in a small-scale approach

Cell-based pharmacological screening assays are commonly used for drug discovery, and provide a valuable tool for the identification of novel cancer therapeutics, and to personalize patient treatment. In this applied pharmacological screening, nine FDA-approved drugs were tested on the generated hiPSC-models to identify if one model revealed a higher sensitivity towards a drug. In general, all drugs per model were divided into groups based on the reduction of cell viability. In summary, four drugs reduced the cell viability enough to determine the EC_{50} -value. All hiPSC-oncogene models had a different EC_{50} for each drug. Within one 3D hiNPC-oncogene model the EC_{50} varied greatly between the different compounds (Table 28), even though the standard deviation within the three biological replicates was sometimes quite high, it was possible to determine an EC_{50} for four drugs. The generated hiPSC-oncogene models reveal a higher resistance to the drugs than the controls. Similar observations are made with CSCs as they have been shown to survive chemo- and radiotherapy (Clevers, 2011; Dean et al., 2005; Wang et al., 2010). This indicates that the applied drugs might cause side effects in patient treatment as healthy tissues might be affected at lower doses than the tumor cells. As expected, the positive control staurosporine reduced the cell viability in all hiPSC-oncogene models as well as in the control models. Staurosporine is a kinase inhibitor that induces apoptosis in several cell lines (Bertrand et al., 1994; Kabir et al., 2002; Weil et al., 1996). The best working compound was vinblastine which is a cell-cycle-specific drug and prevents the formation of microtubule structures during cell division (Sajó, 1977). Since the discovery of vinblastine, it is tested and used in cancer treatment, including MB (Nobre et al., 2019; Warwick et al., 1960; Whitelaw & Teasdale,

Discussion

1961). Currently, it has FDA approval for the palliative treatment of e.g. breast cancer, Hodgkin lymphoma, and testicular germ cell tumor (<https://www.cancer.gov/about-cancer/treatment/drugs/vinblastinesulfate>). It was found that vinblastine induces the apoptosis of the cells via the TP53 pathway (Tishler & Lamppu, 1996; Tishler et al., 1995). Vinblastine sulfate has already been tested in clinical trials for the treatment of low-grade gliomas with promising results (Bouffet et al., 2012; Lassaletta et al., 2016). Nobre et al. (2019) successfully treated adult MB patients with vinblastine instead of the currently used vincristine, which is another derivate and similar to vinblastine. The study showed that vinblastine reaches similar results as vincristine but side effects as peripheral neuropathy could be prevented (Nobre et al., 2019). The second drug, panobinostat is a histone deacetylase inhibitor and is used to regulate e.g. DNA replication and protein transcription (Choudhary et al., 2009). It was approved in 2015 for the treatment of myeloma in combination with bortezomib and dexamethasone as an increase in survival of the patients was shown (Garnock-Jones, 2015; Laubach et al., 2015). The third best working drug was duvelisib which is a phosphoinositide-3-kinase (PI3K) δ and γ inhibitor. It was approved for the palliative treatment of chronic lymphatic or small lymphocytic lymphoma (Blair, 2018). Several cellular processes, also in tumors, are regulated by PI3K, e.g. cell signaling or proliferation and are therefore regarded as interesting targets for treatment (Brennan et al., 2013; Katso et al., 2001). The fourth drug is lomustine which alkylates DNA and RNA. It has been already applied for a long time in the treatment of GBM as it can pass the BBB (Hochberg et al., 1979; Reni et al., 2000). In combination with bevacizumab, lomustine could prolong the overall survival to 12 months in patients with recurrence GBM tumors (Taal et al., 2014). In this applied pharmacological screening the hiPSC-oncogene models revealed a higher sensitivity towards the other drugs, vinblastine sulfate, panobinostat and duvelisib. However, the application of drugs in *in vitro* systems can only give an idea about the suitability of a drug due to the limitation of the test system. For example, the influence of molecular and immune processes cannot be recreated in this kind of models (Saeidnia et al., 2015). To overcome the difficulties between the benchmark-to-bedside applicability, improvement of the testing system is desired. The development of an improved test system might overcome these struggles by utilizing neurospheres or organoids for CNS-related testing (Fritsche et al., 2011; Lancaster & Huch, 2019; Lancaster et al., 2013; Stockslager et al., 2021; Yu et al., 2018). The most effective compounds of the screening on the hiPSC-oncogene models were also tested on the hiNPC-oncogene models, which were neurally induced following the 3D differentiation protocol. These results confirm that vinblastine sulfate and panobinostat are the most effective compounds as they both reduce the viability in several models. Therefore, the results show a consistency to each other and confirm that

Discussion

the hiPSC-oncogene models and 3D hiNPC-oncogene models show similar responses towards the compounds.

4.5 Neural Differentiation of hiPSC-oncogene models was only successful in 3D

Therefore, it was the idea of this thesis to differentiate the hiPSC-oncogene models into three-dimensional neurospheres to conduct further studies e.g. drug screening and migration assays in a model that is more similar to the *in vivo* tumor situation. As described above, the advantage of hiPSCs is the possibility to differentiate them into almost every cell type of the human body by applying different differentiation protocols. Alone for the neural induction of hiPSCs several differentiation protocols are known (Chambers et al., 2009; Dhara & Stice, 2008; Li et al., 2011). In this project, the commercially available protocol by STEMCELL™ Technologies for the 2D induction was used, as this protocol ensures that every cell is exposed to the same amount of differentiation medium. This protocol initiates the differentiation by inhibiting the TGF- β /BMP-dependent SMAD signaling and takes about three weeks (Chambers et al., 2009). During the applied differentiation protocol in this thesis, the hiPSCs are first transformed into adherent hiNPCs before free-floating spheres are generated. Successful differentiation is only possible as the transcription changes within the cells (Burke et al., 2020; Zimmer et al., 2011). The efficiency of the differentiation depends on the utilized hiPSC line as significant differences were observed in the expression of marker genes (Hu et al., 2010). However, verification of the protein expression of the GOI after the neural differentiation revealed a loss of the protein of interest expressed in the 2D hiNPC-oncogene models. One reason for the loss of the GOI expression could be the transcriptomic changes during neural differentiation (Burke et al., 2020; Zimmer et al., 2011). This might be due to a change of transcription as lentiviral vectors integrate preferentially near active transcription sites (Ciuffi, 2008). As indicated by the methylation profile of the hiPSC-oncogene models and the hiNPCs, the expression profiles are the opposite of each other (Figure 23). It is possible, that the integrated GOIs are located next to genes that are not highly expressed in hiNPCs. This could be one of the reasons why the generated hiPSC-oncogene models lost the expression of the introduced genes after differentiation. However, in the *TP53R175H/EGFRvIII* model only the expression of *EGFR* was detected after the 2D neural induction while *EGFRvIII* expression was not detectable anymore. The neurosphere proliferation medium contains the growth factor epidermal growth factor (EGF) which binds to the corresponding receptor, *EGFR*, and activates its expression (Cohen et al., 1980; Earp et al., 1986). Co-expression of *EGFR* and *EGFRvIII* within one cell is not common (An et al., 2018; Inda et al., 2010). However, in glioma sometimes the heterogeneous expression of

Discussion

EGFR and *EGFRvIII* is found and it was discovered that *EGFRvIII* expression supports the expression of *EGFR* through the kinase activity (An et al., 2018; Inda et al., 2010).

The hierarchical clustering of the hiPSC-oncogene models and the 2D hiNPC-oncogene models reveal differences in the methylation profiles. At first glance, it is obvious that the generated hiNPC-oncogene models are separated into different branches (Figure 23). This is also supported by the methylation profiles depicted in Figure 23. In comparison to the hiPSC-oncogene models, the hiNPC-oncogene models of the EV and *TP53R175H/EGFRvIII* model show a reversed methylation profile compared to the corresponding hiPSC-oncogene models (Figure 23). The other three models are clustered on different branches and share a higher similarity to the hiPSC-oncogene models (Figure 23). It was not possible to generate a proliferating neurosphere culture for these models. As indicated by the methylation profile and the observation of the cell culture, the neural induction was initiated but not completed. For example, the *c-MYC* 2D hiNPC model is located on a separate branch and closer to the successfully generated neurosphere models than to the hiPSC-oncogene models. At the end of the differentiation protocol, the *c-MYC* hiNPC stopped proliferating and could therefore not be used for further experiments. Similar effects were observed for *GLI1* however it was not possible to get enough material for transcriptomic analysis.

The neural differentiation of the hiPSC-oncogene models in 3D was successful and generated a proliferating neurosphere culture for each model. The methylation profiles of the 3D hiNPC-oncogene models reveal a difference in comparison to the methylation profiles of the hiPSC-oncogene models (Figure 26). The methylation profiles of the hiNPC-oncogene models show a reversed methylation profile compared to the corresponding hiPSC-oncogene models (Figure 26). However, most models stopped to proliferate after some time *in vitro*.

Currently, several approaches are performed to establish three-dimensional cultures using patient-derived cells or established cell lines. Neurospheres and organoids offer the opportunity to investigate the interaction and infiltration of different cells and to get a better knowledge about tumor development and gain of their aggressiveness (Drost & Clevers, 2018; Fiorini et al., 2020). An improvement in the model generation is still desirable, especially the *GLI1* model is of interest as it is challenging to establish a proliferating *in vitro* SHH pathway cell line as the SHH activity was reduced in cell cultures in comparison to *in vivo* models (Sasai et al., 2006). Currently, one approach for cultivation of a proliferating SHH-tumor cell line is to cultivate SHH-tumors in flanks of mice and to remove allografts if they reached a size of 400 – 600 μm to conduct studies (Sasai et al., 2006). Therefore, the described approach using hiPSC-oncogene models and differentiate them purely *in vitro* is a could help to overcome this challenge. This might be achieved by testing also different neural transduction protocol for the hiPSCs. Application of the CRISPR system in hiPSCs

Discussion

was already successful and the first GBM models could be produced (Koga et al., 2020; Mandegar et al., 2016). Koga et al. (2020) differentiated the modified iPSCs into NPCs and transplanted them into immunocompromised mice for tumor development. These generated tumors showed an authentic GBM cancer pathobiology and provide a platform to understand tumor development. However, Koga et al. (2020) did not perform a drug screen with the cells.

4.6 Compound screening of 3D hiNPC-oncogene detects promising candidates

The 3D differentiated hiNPC-oncogene models were also tested in a different approach of a pharmacological screening. In this compound screening the effects of the substances were analyzed on migration, proliferation, and cytotoxicity (Table 32 and Table 33). The endpoints of these assays help to make a conclusion about the influence of the compound on the tumor invasiveness/metastasis, proliferation, and survival. Based on available gene expression profiles of tumors from MB and GBM patients, seven (MB) or nine (GBM) compounds, a negative control (acetaminophen), and a positive control (respective SoC) were chosen and tested. For the MB Group 3 model the most promising results were achieved using copanlisib for treatment (Table 32). The *c-MYC* model as well as the EV control showed a specific hit on the migration as a readout for metastasis after copanlisib treatment with a BMC_{15} of 0.029397 μM and 0.00977 μM , respectively (Table 32). Midostaurin, regorafenib, and vandetanib yielded unspecific effects in the EV hiNPCs, the same holds true for dasatinib, midostaurin, and vandetanib in the *c-MYC* hiNPC models, indicating that the BMC_{15} was reached at concentrations that are not within the defined $cfdc_{\text{high}}$ concentration range that can be reached *in vivo* (Table 32).

For the endpoint cytotoxicity cisplatin, the SoC for MB, had only a specific hit in the EV control with a BMC_{10} of 1.8050 μM while copanlisib with a BMC_{10} of 0.3948 μM was the only compound which yielded a specific hit for the *c-MYC* model in this endpoint (Table 32). The corresponding concentration-response curves of the specific hits allow direct comparison of the effects of copanlisib and cisplatin on the EV and *c-MYC* hiNPCs (Figure 27). Based on the results of the concentration-response curves, cisplatin treatment causes cell death in healthy cells while the *c-MYC* cells survive the treatment. This indicates a poor efficacy of cisplatin treatment in the Group 3 MB. In contrast, copanlisib showed a reduction in migration and a higher cytotoxicity in the *c-MYC* cells but not on the EV cells indicating a lower impact on the healthy tissue. Currently, no clinical trials were found using copanlisib, a PI3K inhibitor, for treatment of MB (<https://clinicaltrials.gov>, (Ghasemi et al., 2022)). The PI3K

Discussion

pathway controls cellular processes like cell growth, proliferation, survival, migration, and metabolism (Dimitrova & Arcaro, 2015). All other tested compounds did not show any specific hits on the EV control and *c-MYC* model. The concentration-response curves of the unspecific hits demonstrate clearly how important it is to take the internal exposure ($cf_{dc} - cf_{dc_{high}}$) into account (Figure 29). While pure examination of the whole concentration range might lead to the impression that dasatinib, midostaurin, regorafenib, and vandetanib treatment also has a favorable effect on migration and to a lesser extend also on the endpoint of cytotoxicity in the analyzed models, taking into account only the concentrations that can be reached *in vivo* by calculating the free drug concentration (see material and methods for details) clearly shows that the significant effects shown here are not within a relevant *in vivo* range.

The compound screening of the 3D hiNPC-oncogene models for GBM showed specific hits for acteminophen (NC), copanlisib, olaparib, TMZ (SoC), and vandetanib (Table 33) for the models EV, *TP53R175H*, and *TP53R175H/EGFRvIII*. No specific hits were detected for the *EGFRvIII* model. As tumors with a *EGFRvIII* mutation are resistant towards treatment and often have a poor prognosis (Chistiakov et al., 2017), this result might actually reflect the *in vivo* situation. As the proliferation of the EV control (BMC_{50} of 0.0090 μM) and *TP53R175H* model (BMC_{50} of 0.0140 μM) is reduced to a similar extent when treated with copanlisib, it can be assumed that the healthy tissue is affected in the same way. In can therefore be assumed, that copanlisib treatment in GBM patients is not effective enough. Copanlisib is a PI3K inhibitors. The PI3K pathway is involved in many processes e.g. cell growth, proliferation, and migration (Dimitrova & Arcaro, 2015). As this signaling pathway is very complex, it leads to poor tolerability of the inhibitor in patients. Further, tumors developed alternatives to bypass the PI3K inhibition (Le Rhun et al., 2019). Several clinical studies are/were conducted to identify a potent PI3K inhibitor, among them copanlisib, but it was not tested for treatment of GBMs (Mishra et al., 2021).

Treatment with olaparib reduced the proliferation in *TP53R175H* and *TP53R175H/EGFRvIII*. In the *TP53R175H* models proliferation was already reduced at lower concentrations with a specific hit a BMC_{50} of 0.3379 μM while the double mutant had a specific hit with a BMC_{50} of 5.4031 μM . The EV control did, however, not respond to any concentrations which can be reached in patients. Therefore, olaparib seems to be a promising compound as it does not seem to affect healthy tissue, represented by the EV cells. Olaparib belongs to the group of poly ADP ribose polymerase (PARP) inhibitors and repairs DNA damages like single-strand or double-strand breaks (Bochum et al., 2018). Olaparib is currently tested in five clinical trials for GBM treatment (<https://clinicaltrials.gov>). However, pamiparib is another PARP inhibitor and seems to be more promising for treatment of GBM in combination with TMZ and radiation (Piotrowski et al., 2019).

Discussion

The last tested compound, vandetanib, is a VEGFR and EGFR inhibitor and reduces the angiogenesis and proliferation of tumor cells (Jo et al., 2012; Li et al., 2018). The proliferation was reduced in the EV control and *TP53R175H* with a BMC_{50} of 0.2558 μ M and 0.0878 μ M, respectively (Table 33). Similar to olaprib, the *TP53R175H* model showed the most sensitive response towards the treatment with vandetanib. As the EV control was affected, it can be assumed that proliferation of healthy cells would decrease *in vivo* after vandetanib treatment, therefore it might not be suitable for treatment due to probable side effects. *EGFR* mutations are common in GBM tumors (Pan & Magge, 2020). However, it is challenging to develop an efficient treatment, as *EGFR* mutations commonly found in tumor tissue are located within the extracellular domain of *EGFR* and the compounds need to pass the BBB (Pan & Magge, 2020). In addition, *EGFR* (and also *EGFRvIII*) is located at the top end of a complex signal transduction cascades, which modulates e.g. proliferation, metastasis, and survival of cancer cells leading to many adverse side effects in the clinic and many physiological processes are regulated by *EGFR* (An et al., 2018; Seshacharyulu et al., 2012). Currently, five clinical trials are done with vandetanib but they seem not to be promising due to lack of efficacy (<https://clinicaltrials.gov>, (Kreisl et al., 2012)).

The negative control, acetaminophen, surprisingly had a specific hit on the proliferation of *TP53R175H*. Acetaminophen is a cyclooxygenase inhibitor and involved in the synthesis of prostaglandin (Gerriets et al., 2022). Epidemiological studies also indicate that regular use of non-steroidal anti-inflammatory drugs correlates with a lower incidence of GBM, suggesting that cyclooxygenase-2 and its main brain product, prostaglandin E2 (PGE2), are involved in the development and progression of GBM (S. S. Ayoub, 2021; Qiu et al., 2017). Also, it has already been shown in rat and human GBM cell lines that cyclooxygenase inhibitors, including acetaminophen, lead to decreased proliferation of these cells (Bernardi et al., 2008; Matsuo et al., 2004).

The positive control was TMZ, which is used as the SoC for treatment of GBM. The only model with a higher cytotoxicity after TMZ treatment was *TP53R175H/EGFRvIII*. However, only two repetitions were performed but since the BMC_{50} and the upper limit were reached, the results are interpreted as a specific hit. It is possible that only one model showed a specific hit towards the TMZ treatment due to its mode of action. TMZ is an imidazotetrazine prodrug that is stable at acidic pH but undergoes spontaneous non-enzymatic hydrolysis at neutral or slightly basic pH. Brain tumors such as glioblastoma typically have a more alkaline pH than surrounding healthy tissue, which favors activation of TMZ in tumor tissue (Zhang et al., 2012). The active form of TMZ degrades to the methyl diazonium cation capable of methylating various residues on adenosine and guanine bases, leading to DNA lesions and ultimately apoptosis (Denny et al., 1994; Friedman et al., 2000; Zhang et al., 2012). It is possible that the culture conditions of the hiNPC-oncogene models are not ideal for this

Discussion

mechanism of action. The second explanation could be the fact that it has previously been shown in human GBM tumor lines that different lines respond to different concentrations of TMZ. Moreover, the endpoints were measured after 3 (proliferation) and 2 (migration) days, respectively, while the same study shows that an effect on cell mass as an indicator of proliferation was only observed after 4 to 5 days (Suwala et al., 2018).

This proof-of-concept study demonstrates that the generated hiNPC-oncogene models can be used to identify previously approved drug candidates from databases for clinical testing of brain tumor therapies (Barretina et al., 2012; Yang et al., 2013). A similar approach using cerebellar-derived human neural stem cells to model the Group 3 MB showed similar results (Hanaford et al., 2016). The usage of hiPSCs offers several advantages as described above and guarantees enough starting material (Sayed et al., 2019). In contrast, hiPSCs generated from primary tumor tissue often leads to the loss of the malignant phenotype and are therefore not suitable for drug screening however they help to understand the underlying mechanisms of diseases (Balani et al., 2017; Sidhu et al., 2021). For instance, hiPSCs of chronic myeloid leukemia patients did not have a response towards imatininb treatment while hiPSCs differentiated to hematopoietic progenitor cells and the patients did (Laplane et al., 2015). Even though the generated hiNPC model of Group 3 MB represents only one molecular aspect, a response towards the SoC cisplatin regarding the migration and cytotoxicity was detected. Therefore, the generated hiNPC-oncogene models with the introduced GOI can be utilized for drug screening and might help to create a patient-specific treatment plan.

4.7 Conclusion and outlook

In summary, the idea of this project was the generation of subtype-specific mutations for highly aggressive brain tumors (MB and GBM) in an hiPSC cell culture system, which can be further differentiated into three-dimensional neurospheres, and used for drug testing to identify already FDA-approved drugs for general and personalized treatment of MB and GBM. In this study, it could be shown that it is possible to successfully introduce marker genes of subgroups of MB or GBM to hiPSCs. However, it was not possible for all genes. Therefore, an improvement of the transduction protocol might be beneficial in order to produce all models. Furthermore, during the differentiation following the neural monolayer differentiation protocol (2D) the hiPSC-oncogene models lost the expression of the target gene or it was not possible to generate a proliferating neurospheres culture. Therefore several improvements by adaptations of protocols and methods should be performed that might help to successfully establish personalized hiPSCs tumor models. Changing the neural differentiation protocol from 2D to 3D, helped to maintain the protein expression of the GOI and generate a proliferating neurosphere culture. An additional approach could be the usage of a targeted gene modification system such as e.g. CRISPR/Cas9 as it would minimize the effect of random genome integration. This is of high interest, as it is possible to generate a stable hiPSC bank where the cells have common mutations e.g., oncogenes. For *in vitro* studies these hiPSC-oncogene models can be used to test treatments or to better understand the development of disease as they can be differentiated into the desired tissue. In addition, it would be interesting to investigate why the here-generated models lost the expression of the GOI during 2D neural differentiation. Therefore, a close tracking would be of interest of the 2D hiNPC-oncogene models generated in this thesis to determine the time point when the cells lose the expression of the GOI. The 3D hiNPC-oncogene models were successfully used in a compound screening and proof-of-concept was achieved. Here, with copanlisib a compound was identified which seems to be promising for the treatment of Group 3 MB tumors. It is of interest if other differentiation protocols can be applied to these hiPSC-oncogene models as well to generate other tissues than hiNPCs. Further, additional mutations can be introduced into the hiPSC-oncogene models to establish models which better represent the heterogeneity of the tumors. Therefore, the idea to use hiPSC-oncogene models and differentiate them into the desired tissue are a promising approach to identify and test new treatment approaches.

5 Literature

- Adam, L., Zhong, M., Choi, W., Qi, W., Nicoloso, M., Arora, A., Calin, G., Wang, H., Siefker-Radtke, A., McConkey, D., Bar-Eli, M., & Dinney, C. (2009, Aug 15). miR-200 expression regulates epithelial-to-mesenchymal transition in bladder cancer cells and reverses resistance to epidermal growth factor receptor therapy. *Clin Cancer Res*, *15*(16), 5060-5072. <https://doi.org/10.1158/1078-0432.Ccr-08-2245>
- Aggarwal, C., Davis, C. W., Mick, R., Thompson, J. C., Ahmed, S., Jeffries, S., Bagley, S., Gabriel, P., Evans, T. L., Bauml, J. M., Ciunci, C., Alley, E., Morrissette, J. J. D., Cohen, R. B., Carpenter, E. L., & Langer, C. J. (2018). Influence of TP53 Mutation on Survival in Patients With Advanced EGFR-Mutant Non-Small-Cell Lung Cancer. *JCO Precis Oncol*, *2018*. <https://doi.org/10.1200/po.18.00107>
- Ahmed, M., Chaudhari, K., Babaei-Jadidi, R., Dekker, L. V., & Shams Nateri, A. (2017, Apr). Concise Review: Emerging Drugs Targeting Epithelial Cancer Stem-Like Cells. *Stem Cells*, *35*(4), 839-850. <https://doi.org/10.1002/stem.2579>
- Al-Hajj, M., Wicha, M. S., Benito-Hernandez, A., Morrison, S. J., & Clarke, M. F. (2003). Prospective identification of tumorigenic breast cancer cells. *Proceedings of the National Academy of Sciences of the United States of America*, *100*(7), 3983-3988. <https://doi.org/10.1073/pnas.0530291100>
- Aldoghachi, A. F., Aldoghachi, A. F., Breyne, K., Ling, K. H., & Cheah, P. S. (2022, Apr 6). Recent Advances in the Therapeutic Strategies of Glioblastoma Multiforme. *Neuroscience*. <https://doi.org/10.1016/j.neuroscience.2022.03.030>
- Alther, B., Mylius, V., Weller, M., & Gantenbein, A. R. (2020, 2020/07/01). From first symptoms to diagnosis: Initial clinical presentation of primary brain tumors. *Clinical and Translational Neuroscience*, *4*(2), 2514183X20968368. <https://doi.org/10.1177/2514183X20968368>
- An, Z., Aksoy, O., Zheng, T., Fan, Q. W., & Weiss, W. A. (2018, Mar). Epidermal growth factor receptor and EGFRvIII in glioblastoma: signaling pathways and targeted therapies. *Oncogene*, *37*(12), 1561-1575. <https://doi.org/10.1038/s41388-017-0045-7>
- Ayoub, S. S. (2021, 2021/10/02). Paracetamol (acetaminophen): A familiar drug with an unexplained mechanism of action. *Temperature*, *8*(4), 351-371. <https://doi.org/10.1080/23328940.2021.1886392>
- Ayoub, S. S. (2021). Paracetamol (acetaminophen): A familiar drug with an unexplained mechanism of action. *Temperature (Austin)*, *8*(4), 351-371. <https://doi.org/10.1080/23328940.2021.1886392>
- Bailey, P., & Cushing, H. (1925). Medulloblastoma cerebelli: a common type of midcerebellar glioma of childhood. *Archives of Neurology & Psychiatry*, *14*(2), 192-224.

Literature

- Balani, S., Nguyen, L. V., & Eaves, C. J. (2017, 2017/05/25). Modeling the process of human tumorigenesis. *Nat Commun*, *8*(1), 15422. <https://doi.org/10.1038/ncomms15422>
- Balkwill, F. (2006, 2006/09/01). TNF- α in promotion and progression of cancer. *Cancer and Metastasis Reviews*, *25*(3), 409-416. <https://doi.org/10.1007/s10555-006-9005-3>
- Bao, S., Wu, Q., McLendon, R. E., Hao, Y., Shi, Q., Hjelmeland, A. B., Dewhirst, M. W., Bigner, D. D., & Rich, J. N. (2006, Dec 7). Glioma stem cells promote radioresistance by preferential activation of the DNA damage response. *Nature*, *444*(7120), 756-760. <https://doi.org/10.1038/nature05236>
- Barretina, J., Caponigro, G., Stransky, N., Venkatesan, K., Margolin, A. A., Kim, S., Wilson, C. J., Lehár, J., Kryukov, G. V., Sonkin, D., Reddy, A., Liu, M., Murray, L., Berger, M. F., Monahan, J. E., Morais, P., Meltzer, J., Korejwa, A., Jané-Valbuena, J., Mapa, F. A., Thibault, J., Bric-Furlong, E., Raman, P., Shipway, A., Engels, I. H., Cheng, J., Yu, G. K., Yu, J., Aspesi, P., Jr., de Silva, M., Jagtap, K., Jones, M. D., Wang, L., Hatton, C., Palesscandolo, E., Gupta, S., Mahan, S., Sougnez, C., Onofrio, R. C., Liefeld, T., MacConaill, L., Winckler, W., Reich, M., Li, N., Mesirov, J. P., Gabriel, S. B., Getz, G., Ardlie, K., Chan, V., Myer, V. E., Weber, B. L., Porter, J., Warmuth, M., Finan, P., Harris, J. L., Meyerson, M., Golub, T. R., Morrissey, M. P., Sellers, W. R., Schlegel, R., & Garraway, L. A. (2012, Mar 28). The Cancer Cell Line Encyclopedia enables predictive modelling of anticancer drug sensitivity. *Nature*, *483*(7391), 603-607. <https://doi.org/10.1038/nature11003>
- Bassères, D. S., & Baldwin, A. S. (2006, 2006/10/01). Nuclear factor- κ B and inhibitor of κ B kinase pathways in oncogenic initiation and progression. *Oncogene*, *25*(51), 6817-6830. <https://doi.org/10.1038/sj.onc.1209942>
- Baud, V., & Karin, M. (2009, Jan). Is NF- κ B a good target for cancer therapy? Hopes and pitfalls. *Nat Rev Drug Discov*, *8*(1), 33-40. <https://doi.org/10.1038/nrd2781>
- Behnan, J., Finocchiaro, G., & Hanna, G. (2019, Apr 1). The landscape of the mesenchymal signature in brain tumours. *Brain*, *142*(4), 847-866. <https://doi.org/10.1093/brain/awz044>
- Behnan, J., Stangeland, B., Hosainey, S., Joel, M., Olsen, T., Micci, F., Glover, J., Isakson, P., & Brinckmann, J. (2017). Differential propagation of stroma and cancer stem cells dictates tumorigenesis and multipotency. *Oncogene*, *36*(4), 570-584.
- Beier, D., Proescholdt, M., Reinert, C., Pietsch, T., Jones, D. T. W., Pfister, S. M., Hattingen, E., Seidel, C., Dirven, L., Luerding, R., Reijneveld, J., Warmuth-Metz, M., Bonsanto, M., Bremer, M., Combs, S. E., Rieken, S., Herrlinger, U., Kuntze, H., Mayer-Steinacker, R., Moskopp, D., Schneider, T., Beringer, A., Schlegel, U., Stummer, W., Welker, H., Weyerbrock, A., Paulsen, F., Rutkowski, S., Weller, M., Wick, W., Kortmann, R. D., Bogdahn, U., & Hau, P. (2018, Feb 19). Multicenter pilot study of radiochemotherapy as first-line treatment for adults with medulloblastoma (NOA-07). *Neuro Oncol*, *20*(3), 400-410. <https://doi.org/10.1093/neuonc/nox155>

Literature

- Ben-David, U., Beroukhim, R., & Golub, T. R. (2019, Feb). Genomic evolution of cancer models: perils and opportunities. *Nat Rev Cancer*, *19*(2), 97-109. <https://doi.org/10.1038/s41568-018-0095-3>
- Ben-David, U., Siranosian, B., Ha, G., Tang, H., Oren, Y., Hinohara, K., Strathdee, C. A., Dempster, J., Lyons, N. J., Burns, R., Nag, A., Kugener, G., Cimini, B., Tsvetkov, P., Maruvka, Y. E., O'Rourke, R., Garrity, A., Tubelli, A. A., Bandopadhyay, P., Tsherniak, A., Vazquez, F., Wong, B., Birger, C., Ghandi, M., Thorner, A. R., Bittker, J. A., Meyerson, M., Getz, G., Beroukhim, R., & Golub, T. R. (2018, Aug). Genetic and transcriptional evolution alters cancer cell line drug response. *Nature*, *560*(7718), 325-330. <https://doi.org/10.1038/s41586-018-0409-3>
- Ben-Porath, I., Thomson, M. W., Carey, V. J., Ge, R., Bell, G. W., Regev, A., & Weinberg, R. A. (2008, 2008/05/01). An embryonic stem cell-like gene expression signature in poorly differentiated aggressive human tumors. *Nat Genet*, *40*(5), 499-507. <https://doi.org/10.1038/ng.127>
- Bernardi, A., Frozza, R. L., Jäger, E., Figueiró, F., Bavaresco, L., Salbego, C., Pohlmann, A. R., Guterres, S. S., & Battastini, A. M. (2008, May 31). Selective cytotoxicity of indomethacin and indomethacin ethyl ester-loaded nanocapsules against glioma cell lines: an in vitro study. *Eur J Pharmacol*, *586*(1-3), 24-34. <https://doi.org/10.1016/j.ejphar.2008.02.026>
- Bertrand, R., Solary, E., O'Connor, P., Kohn, K. W., & Pommier, Y. (1994, Apr). Induction of a common pathway of apoptosis by staurosporine. *Exp Cell Res*, *211*(2), 314-321. <https://doi.org/10.1006/excr.1994.1093>
- Bierie, B., & Moses, H. L. (2006, 2006/02/01/). TGF- β and cancer. *Cytokine & Growth Factor Reviews*, *17*(1), 29-40. <https://doi.org/https://doi.org/10.1016/j.cytogfr.2005.09.006>
- Blair, H. A. (2018, 2018/11/01). Duvelisib: First Global Approval. *Drugs*, *78*(17), 1847-1853. <https://doi.org/10.1007/s40265-018-1013-4>
- Bochum, S., Berger, S., & Martens, U. M. (2018). Olaparib. *Recent Results Cancer Res*, *211*, 217-233. https://doi.org/10.1007/978-3-319-91442-8_15
- Bonnet, D., & Dick, J. E. (1997, Jul). Human acute myeloid leukemia is organized as a hierarchy that originates from a primitive hematopoietic cell. *Nat Med*, *3*(7), 730-737. <https://doi.org/10.1038/nm0797-730>
- Bosch-Presegué, L., & Vaquero, A. (2011). The dual role of sirtuins in cancer. *Genes & cancer*, *2*(6), 648-662. <https://doi.org/10.1177/1947601911417862>
- Bouffet, E., Jakacki, R., Goldman, S., Hargrave, D., Hawkins, C., Shroff, M., Hukin, J., Bartels, U., Foreman, N., Kellie, S., Hilden, J., Ettl, M., Wilson, B., Stephens, D., Tabori, U., & Baruchel, S. (2012, 2012/04/20). Phase II Study of Weekly Vinblastine in Recurrent or Refractory Pediatric Low-Grade Glioma. *Journal of Clinical Oncology*, *30*(12), 1358-1363. <https://doi.org/10.1200/JCO.2011.34.5843>

Literature

- Boussommier-Calleja, A. (2020). Chapter 4.1 - In vitro models of cancer. In S. Ladame & J. Y. H. Chang (Eds.), *Bioengineering Innovative Solutions for Cancer* (pp. 273-325). Academic Press. <https://doi.org/https://doi.org/10.1016/B978-0-12-813886-1.00013-9>
- Brabletz, T., Hlubek, F., Spaderna, S., Schmalhofer, O., Hiendlmeyer, E., Jung, A., & Kirchner, T. (2005). Invasion and metastasis in colorectal cancer: epithelial-mesenchymal transition, mesenchymal-epithelial transition, stem cells and beta-catenin. *Cells Tissues Organs*, *179*(1-2), 56-65. <https://doi.org/10.1159/000084509>
- Brandes, A. A., & Franceschi, E. (2014). Shedding Light on Adult Medulloblastoma: Current Management and Opportunities for Advances. *American Society of Clinical Oncology Educational Book*(34), e82-e87. https://doi.org/10.14694/EdBook_AM.2014.34.e82
- Brennan, C. W., Verhaak, R. G. W., McKenna, A., Campos, B., Noushmehr, H., Salama, S. R., Zheng, S., Chakravarty, D., Sanborn, J. Z., Berman, S. H., Beroukhi, R., Bernard, B., Wu, C.-J., Genovese, G., Shmulevich, I., Barnholtz-Sloan, J., Zou, L., Vegesna, R., Shukla, S. A., Ciriello, G., Yung, W. K., Zhang, W., Sougnez, C., Mikkelsen, T., Aldape, K., Bigner, D. D., Van Meir, E. G., Prados, M., Sloan, A., Black, K. L., Eschbacher, J., Finocchiaro, G., Friedman, W., Andrews, D. W., Guha, A., Iacocca, M., O'Neill, B. P., Foltz, G., Myers, J., Weisenberger, D. J., Penny, R., Kucherlapati, R., Perou, C. M., Hayes, D. N., Gibbs, R., Marra, M., Mills, G. B., Lander, E., Spellman, P., Wilson, R., Sander, C., Weinstein, J., Meyerson, M., Gabriel, S., Laird, P. W., Haussler, D., Getz, G., Chin, L., & Network, T. R. (2013). The somatic genomic landscape of glioblastoma. *Cell*, *155*(2), 462-477. <https://doi.org/10.1016/j.cell.2013.09.034>
- Buatois, S., Ueckert, S., Frey, N., Retout, S., & Mentré, F. (2018, Mar 29). Comparison of Model Averaging and Model Selection in Dose Finding Trials Analyzed by Nonlinear Mixed Effect Models. *Aaps j*, *20*(3), 56. <https://doi.org/10.1208/s12248-018-0205-x>
- Burke, E. E., Chenoweth, J. G., Shin, J. H., Collado-Torres, L., Kim, S.-K., Micali, N., Wang, Y., Colantuoni, C., Straub, R. E., Hoepfner, D. J., Chen, H.-Y., Sellers, A., Shibbani, K., Hamersky, G. R., Diaz Bustamante, M., Phan, B. N., Ulrich, W. S., Valencia, C., Jaishankar, A., Price, A. J., Rajpurohit, A., Semick, S. A., Bürli, R. W., Barrow, J. C., Hiler, D. J., Page, S. C., Martinowich, K., Hyde, T. M., Kleinman, J. E., Berman, K. F., Apud, J. A., Cross, A. J., Brandon, N. J., Weinberger, D. R., Maher, B. J., McKay, R. D. G., & Jaffe, A. E. (2020, 2020/01/23). Dissecting transcriptomic signatures of neuronal differentiation and maturation using iPSCs. *Nat Commun*, *11*(1), 462. <https://doi.org/10.1038/s41467-019-14266-z>
- Cai, Q., Li, J., Gao, T., Xie, J., & Evers, B. M. (2009, Jan 23). Protein kinase Cdelta negatively regulates hedgehog signaling by inhibition of Gli1 activity. *J Biol Chem*, *284*(4), 2150-2158. <https://doi.org/10.1074/jbc.M803235200>
- Calabrese, C., Poppleton, H., Kocak, M., Hogg, T. L., Fuller, C., Hamner, B., Oh, E. Y., Gaber, M. W., Finklestein, D., & Allen, M. (2007). A perivascular niche for brain tumor stem cells. *Cancer Cell*, *11*(1), 69-82.
- Canale, M., Andrikou, K., Priano, I., Cravero, P., Pasini, L., Urbini, M., Delmonte, A., Crinò, L., Bronte, G., & Ulivi, P. (2022). The Role of TP53 Mutations in EGFR-Mutated Non-Small-Cell Lung

Literature

- Cancer: Clinical Significance and Implications for Therapy. *Cancers (Basel)*, 14(5), 1143. <https://doi.org/10.3390/cancers14051143>
- Capper, D., Engel, N. W., Stichel, D., Lechner, M., Glöss, S., Schmid, S., Koelsche, C., Schrimpf, D., Niesen, J., Wefers, A. K., Jones, D. T. W., Sill, M., Weigert, O., Ligon, K. L., Olar, A., Koch, A., Forster, M., Moran, S., Tirado, O. M., Sáinz-Jaspeado, M., Mora, J., Esteller, M., Alonso, J., Del Muro, X. G., Paulus, W., Felsberg, J., Reifenberger, G., Glatzel, M., Frank, S., Monoranu, C. M., Lund, V. J., von Deimling, A., Pfister, S., Buslei, R., Ribbat-Idel, J., Perner, S., Gudziol, V., Meinhardt, M., & Schüller, U. (2018, Aug). DNA methylation-based reclassification of olfactory neuroblastoma. *Acta Neuropathol*, 136(2), 255-271. <https://doi.org/10.1007/s00401-018-1854-7>
- Cavalli, F. M. G., Remke, M., Rampasek, L., Peacock, J., Shih, D. J. H., Luu, B., Garzia, L., Torchia, J., Nor, C., Morrissy, A. S., Agnihotri, S., Thompson, Y. Y., Kuzan-Fischer, C. M., Farooq, H., Isaev, K., Daniels, C., Cho, B. K., Kim, S. K., Wang, K. C., Lee, J. Y., Grajkowska, W. A., Perek-Polnik, M., Vasiljevic, A., Faure-Contier, C., Jouvett, A., Giannini, C., Nageswara Rao, A. A., Li, K. K. W., Ng, H. K., Eberhart, C. G., Pollack, I. F., Hamilton, R. L., Gillespie, G. Y., Olson, J. M., Leary, S., Weiss, W. A., Lach, B., Chambless, L. B., Thompson, R. C., Cooper, M. K., Vibhakkar, R., Hauser, P., van Veelen, M. C., Kros, J. M., French, P. J., Ra, Y. S., Kumabe, T., López-Aguilar, E., Zitterbart, K., Sterba, J., Finocchiaro, G., Massimino, M., Van Meir, E. G., Osuka, S., Shofuda, T., Klekner, A., Zollo, M., Leonard, J. R., Rubin, J. B., Jabado, N., Albrecht, S., Mora, J., Van Meter, T. E., Jung, S., Moore, A. S., Hallahan, A. R., Chan, J. A., Tirapelli, D. P. C., Carlotti, C. G., Fouladi, M., Pimentel, J., Faria, C. C., Saad, A. G., Massimi, L., Liao, L. M., Wheeler, H., Nakamura, H., Elbabaa, S. K., Perezpeña-Diazconti, M., Chico Ponce de León, F., Robinson, S., Zapotocky, M., Lassaletta, A., Huang, A., Hawkins, C. E., Tabori, U., Bouffet, E., Bartels, U., Dirks, P. B., Rutka, J. T., Bader, G. D., Reimand, J., Goldenberg, A., Ramaswamy, V., & Taylor, M. D. (2017, Jun 12). Intertumoral Heterogeneity within Medulloblastoma Subgroups. *Cancer Cell*, 31(6), 737-754.e736. <https://doi.org/10.1016/j.ccell.2017.05.005>
- Chalkiadaki, A., & Guarente, L. (2015, 2015/10/01). The multifaceted functions of sirtuins in cancer. *Nature Reviews Cancer*, 15(10), 608-624. <https://doi.org/10.1038/nrc3985>
- Chambers, S. M., Fasano, C. A., Papapetrou, E. P., Tomishima, M., Sadelain, M., & Studer, L. (2009). Highly efficient neural conversion of human ES and iPS cells by dual inhibition of SMAD signaling. *Nature Biotechnology*, 27(3), 275-280.
- Chang, C. H., Housepian, E. M., & Herbert, C., Jr. (1969, Dec). An operative staging system and a megavoltage radiotherapeutic technic for cerebellar medulloblastomas. *Radiology*, 93(6), 1351-1359. <https://doi.org/10.1148/93.6.1351>
- Chang, S. M., Parney, I. F., Huang, W., Anderson, F. A., Jr., Asher, A. L., Bernstein, M., Lillehei, K. O., Brem, H., Berger, M. S., & Laws, E. R. (2005, Feb 2). Patterns of care for adults with newly diagnosed malignant glioma. *Jama*, 293(5), 557-564. <https://doi.org/10.1001/jama.293.5.557>
- Chen, S. F., Chang, Y. C., Nieh, S., Liu, C. L., Yang, C. Y., & Lin, Y. S. (2012). Nonadhesive culture system as a model of rapid sphere formation with cancer stem cell properties. *PLOS ONE*, 7(2), e31864. <https://doi.org/10.1371/journal.pone.0031864>

Literature

- Chen, W. Y., & Townes, T. M. (2000, 2000/01/04). Molecular mechanism for silencing virally transduced genes involves histone deacetylation and chromatin condensation. *Proceedings of the National Academy of Sciences*, *97*(1), 377-382. <https://doi.org/10.1073/pnas.97.1.377>
- Chiang, Y. T., Chien, Y. C., Lin, Y. H., Wu, H. H., Lee, D. F., & Yu, Y. L. (2021, Aug 13). The Function of the Mutant p53-R175H in Cancer. *Cancers (Basel)*, *13*(16). <https://doi.org/10.3390/cancers13164088>
- Chistiakov, D. A., Chekhonin, I. V., & Chekhonin, V. P. (2017, Sep 5). The EGFR variant III mutant as a target for immunotherapy of glioblastoma multiforme. *Eur J Pharmacol*, *810*, 70-82. <https://doi.org/10.1016/j.ejphar.2017.05.064>
- Cho, Y., Gorina, S., Jeffrey, P. D., & Pavletich, N. P. (1994, Jul 15). Crystal structure of a p53 tumor suppressor-DNA complex: understanding tumorigenic mutations. *Science*, *265*(5170), 346-355. <https://doi.org/10.1126/science.8023157>
- Cho, Y.-J., Tsherniak, A., Tamayo, P., Santagata, S., Ligon, A., Greulich, H., Berhoukim, R., Amani, V., Goumnerova, L., & Eberhart, C. G. (2011). Integrative genomic analysis of medulloblastoma identifies a molecular subgroup that drives poor clinical outcome. *Journal of Clinical Oncology*, *29*(11), 1424.
- Choucair, A. K., Levin, V. A., Gutin, P. H., Davis, R. L., Silver, P., Edwards, M. S., & Wilson, C. B. (1986, Nov). Development of multiple lesions during radiation therapy and chemotherapy in patients with gliomas. *J Neurosurg*, *65*(5), 654-658. <https://doi.org/10.3171/jns.1986.65.5.0654>
- Choudhary, C., Kumar, C., Gnäd, F., Nielsen, M. L., Rehman, M., Walther, T. C., Olsen, J. V., & Mann, M. (2009). Lysine acetylation targets protein complexes and co-regulates major cellular functions. *Science*, *325*(5942), 834-840.
- Choudhry, Z., Rikani, A. A., Choudhry, A. M., Tariq, S., Zakaria, F., Asghar, M. W., Sarfraz, M. K., Haider, K., Shafiq, A. A., & Mobassarrah, N. J. (2014, Jan). Sonic hedgehog signalling pathway: a complex network. *Ann Neurosci*, *21*(1), 28-31. <https://doi.org/10.5214/ans.0972.7531.210109>
- Ciuffi, A. (2008, Dec). Mechanisms governing lentivirus integration site selection. *Curr Gene Ther*, *8*(6), 419-429. <https://doi.org/10.2174/156652308786848021>
- Clarke, M. F., Dick, J. E., Dirks, P. B., Eaves, C. J., Jamieson, C. H., Jones, D. L., Visvader, J., Weissman, I. L., & Wahl, G. M. (2006, Oct 1). Cancer stem cells--perspectives on current status and future directions: AACR Workshop on cancer stem cells. *Cancer Res*, *66*(19), 9339-9344. <https://doi.org/10.1158/0008-5472.Can-06-3126>
- Clevers, H. (2011, Mar). The cancer stem cell: premises, promises and challenges. *Nat Med*, *17*(3), 313-319. <https://doi.org/10.1038/nm.2304>

Literature

- Cohen, S., Carpenter, G., & King Jr, L. (1980). Epidermal growth factor-receptor-protein kinase interactions. Co-purification of receptor and epidermal growth factor-enhanced phosphorylation activity. *Journal of Biological Chemistry*, 255(10), 4834-4842.
- Correa, H. (2016, Jun). Li-Fraumeni Syndrome. *J Pediatr Genet*, 5(2), 84-88. <https://doi.org/10.1055/s-0036-1579759>
- Cozzio, A., Passegué, E., Ayton, P. M., Karsunky, H., Cleary, M. L., & Weissman, I. L. (2003, Dec 15). Similar MLL-associated leukemias arising from self-renewing stem cells and short-lived myeloid progenitors. *Genes Dev*, 17(24), 3029-3035. <https://doi.org/10.1101/gad.1143403>
- Cruz Da Silva, E., Mercier, M. C., Etienne-Selloum, N., Dontenwill, M., & Choulier, L. (2021, Apr 9). A Systematic Review of Glioblastoma-Targeted Therapies in Phases II, III, IV Clinical Trials. *Cancers (Basel)*, 13(8). <https://doi.org/10.3390/cancers13081795>
- D'Atri, S., Tentori, L., Lacal, P. M., Graziani, G., Pagani, E., Benincasa, E., Zambruno, G., Bonmassar, E., & Jiricny, J. (1998, Aug). Involvement of the mismatch repair system in temozolomide-induced apoptosis. *Mol Pharmacol*, 54(2), 334-341. <https://doi.org/10.1124/mol.54.2.334>
- Dahmane, N., Lee, J., Robins, P., Heller, P., & Altaba, A. R. i. (1997, 1997/10/01). Activation of the transcription factor Gli1 and the Sonic hedgehog signalling pathway in skin tumours. *Nature*, 389(6653), 876-881. <https://doi.org/10.1038/39918>
- Daneman, R. (2012, Nov). The blood-brain barrier in health and disease. *Ann Neurol*, 72(5), 648-672. <https://doi.org/10.1002/ana.23648>
- Dang, J., Tiwari, S. K., Lichinchi, G., Qin, Y., Patil, V. S., Eroshkin, A. M., & Rana, T. M. (2016). Zika virus depletes neural progenitors in human cerebral organoids through activation of the innate immune receptor TLR3. *Cell Stem Cell*, 19(2), 258-265.
- Dang, L., White, D. W., Gross, S., Bennett, B. D., Bittinger, M. A., Driggers, E. M., Fantin, V. R., Jang, H. G., Jin, S., Keenan, M. C., Marks, K. M., Prins, R. M., Ward, P. S., Yen, K. E., Liao, L. M., Rabinowitz, J. D., Cantley, L. C., Thompson, C. B., Vander Heiden, M. G., & Su, S. M. (2009, 2009/12/01). Cancer-associated IDH1 mutations produce 2-hydroxyglutarate. *Nature*, 462(7274), 739-744. <https://doi.org/10.1038/nature08617>
- Dean, M., Fojo, T., & Bates, S. (2005, Apr). Tumour stem cells and drug resistance. *Nat Rev Cancer*, 5(4), 275-284. <https://doi.org/10.1038/nrc1590>
- Dekker, L. J. M., Verheul, C., Wensveen, N., Leenders, W., Lamfers, M. L. M., Leenstra, S., & Luidert, T. M. (2022, 2022/02/01). Effects of the IDH1 R132H Mutation on the Energy Metabolism: A Comparison between Tissue and Corresponding Primary Glioma Cell Cultures. *ACS Omega*, 7(4), 3568-3578. <https://doi.org/10.1021/acsomega.1c06121>

Literature

- Denham, M., & Dottori, M. (2011). Neural Differentiation of Induced Pluripotent Stem Cells. In G. Manfredi & H. Kawamata (Eds.), *Neurodegeneration: Methods and Protocols* (pp. 99-110). Humana Press. https://doi.org/10.1007/978-1-61779-328-8_7
- Denny, B. J., Wheelhouse, R. T., Stevens, M. F., Tsang, L. L., & Slack, J. A. (1994, Aug 9). NMR and molecular modeling investigation of the mechanism of activation of the antitumor drug temozolomide and its interaction with DNA. *Biochemistry*, *33*(31), 9045-9051. <https://doi.org/10.1021/bi00197a003>
- Dhall, G. (2009, 2009/11/01). Medulloblastoma. *J Child Neurol*, *24*(11), 1418-1430. <https://doi.org/10.1177/0883073809341668>
- Dhara, S. K., & Stice, S. L. (2008, 2008/10/15). Neural differentiation of human embryonic stem cells [<https://doi.org/10.1002/jcb.21891>]. *Journal of Cellular Biochemistry*, *105*(3), 633-640. <https://doi.org/https://doi.org/10.1002/jcb.21891>
- di Magliano, M. P., & Hebrok, M. (2003). Hedgehog signalling in cancer formation and maintenance. *Nature Reviews Cancer*, *3*(12), 903-911.
- Dimitrova, V., & Arcaro, A. (2015). Targeting the PI3K/AKT/mTOR signaling pathway in medulloblastoma. *Curr Mol Med*, *15*(1), 82-93. <https://doi.org/10.2174/1566524015666150114115427>
- Dittmer, D., Pati, S., Zambetti, G., Chu, S., Teresky, A. K., Moore, M., Finlay, C., & Levine, A. J. (1993, May). Gain of function mutations in p53. *Nat Genet*, *4*(1), 42-46. <https://doi.org/10.1038/ng0593-42>
- Draper, J. S., Smith, K., Gokhale, P., Moore, H. D., Maltby, E., Johnson, J., Meisner, L., Zwaka, T. P., Thomson, J. A., & Andrews, P. W. (2004, 2004/01/01). Recurrent gain of chromosomes 17q and 12 in cultured human embryonic stem cells. *Nature Biotechnology*, *22*(1), 53-54. <https://doi.org/10.1038/nbt922>
- Drost, J., & Clevers, H. (2018, 2018/07/01). Organoids in cancer research. *Nature Reviews Cancer*, *18*(7), 407-418. <https://doi.org/10.1038/s41568-018-0007-6>
- DuBridges, R. B., Tang, P., Hsia, H. C., Leong, P. M., Miller, J. H., & Calos, M. P. (1987, Jan). Analysis of mutation in human cells by using an Epstein-Barr virus shuttle system. *Mol Cell Biol*, *7*(1), 379-387. <https://doi.org/10.1128/mcb.7.1.379-387.1987>
- Dunnett, C. W., & Tamhane, A. C. (1991, Jun). Step-down multiple tests for comparing treatments with a control in unbalanced one-way layouts. *Stat Med*, *10*(6), 939-947. <https://doi.org/10.1002/sim.4780100614>
- Dutreix, C., Munarini, F., Lorenzo, S., Roesel, J., & Wang, Y. (2013, Dec). Investigation into CYP3A4-mediated drug-drug interactions on midostaurin in healthy volunteers. *Cancer Chemother Pharmacol*, *72*(6), 1223-1234. <https://doi.org/10.1007/s00280-013-2287-6>

Literature

- Earp, H. S., Austin, K. S., Blaisdell, J., Rubin, R. A., Nelson, K. G., Lee, L. W., & Grisham, J. W. (1986, 1986/04/15/). Epidermal growth factor (EGF) stimulates EGF receptor synthesis. *Journal of Biological Chemistry*, 261(11), 4777-4780. [https://doi.org/https://doi.org/10.1016/S0021-9258\(19\)89171-8](https://doi.org/https://doi.org/10.1016/S0021-9258(19)89171-8)
- Eglen, R. M., & Reisine, T. (2018, 2019/02/01). Human iPS Cell-Derived Patient Tissues and 3D Cell Culture Part 1: Target Identification and Lead Optimization. *SLAS TECHNOLOGY: Translating Life Sciences Innovation*, 24(1), 3-17. <https://doi.org/10.1177/2472630318803277>
- Ekstrand, A. J., Sugawa, N., James, C. D., & Collins, V. P. (1992). Amplified and rearranged epidermal growth factor receptor genes in human glioblastomas reveal deletions of sequences encoding portions of the N-and/or C-terminal tails. *Proceedings of the National Academy of Sciences*, 89(10), 4309-4313.
- Fattahi, S., Pilehchian Langroudi, M., & Akhavan-Niaki, H. (2018, 2018/08/01). Hedgehog signaling pathway: Epigenetic regulation and role in disease and cancer development [<https://doi.org/10.1002/jcp.26506>]. *J Cell Physiol*, 233(8), 5726-5735. <https://doi.org/https://doi.org/10.1002/jcp.26506>
- Fedele, M., Cerchia, L., Pegoraro, S., Sgarra, R., & Manfioletti, G. (2019). Proneural-Mesenchymal Transition: Phenotypic Plasticity to Acquire Multitherapy Resistance in Glioblastoma. *International journal of molecular sciences*, 20(11), 2746. <https://doi.org/10.3390/ijms20112746>
- Fesnak, A. D., June, C. H., & Levine, B. L. (2016). Engineered T cells: the promise and challenges of cancer immunotherapy. *Nat Rev Cancer*, 16(9), 566-581. <https://doi.org/10.1038/nrc.2016.97>
- Fiorini, E., Veghini, L., & Corbo, V. (2020). Modeling Cell Communication in Cancer With Organoids: Making the Complex Simple. *Front Cell Dev Biol*, 8, 166. <https://doi.org/10.3389/fcell.2020.00166>
- Franzen, J., Georgomanolis, T., Selich, A., Kuo, C.-C., Stöger, R., Brant, L., Mulabdić, M. S., Fernandez-Rebollo, E., Grezella, C., Ostrowska, A., Begemann, M., Nikolić, M., Rath, B., Ho, A. D., Rothe, M., Schambach, A., Papantonis, A., & Wagner, W. (2021, 2021/05/19). DNA methylation changes during long-term in vitro cell culture are caused by epigenetic drift. *Communications Biology*, 4(1), 598. <https://doi.org/10.1038/s42003-021-02116-y>
- Friedman, H. S., Kerby, T., & Calvert, H. (2000). Temozolomide and Treatment of Malignant Glioma1. *Clinical Cancer Research*, 6(7), 2585-2597.
- Fritsche, E., Gassmann, K., & Schreiber, T. (2011). Neurospheres as a model for developmental neurotoxicity testing. *Methods Mol Biol*, 758, 99-114. https://doi.org/10.1007/978-1-61779-170-3_7

Literature

- Fukusumi, H., Handa, Y., Shofuda, T., & Kanemura, Y. (2018). Small-scale screening of anticancer drugs acting specifically on neural stem/progenitor cells derived from human-induced pluripotent stem cells using a time-course cytotoxicity test. *PeerJ*, *6*, e4187-e4187. <https://doi.org/10.7717/peerj.4187>
- Furth, J., Kahn, M. C., & Breedis, C. (1937). The transmission of leukemia of mice with a single cell. *The American Journal of Cancer*, *31*(2), 276-282.
- G. B. D. Brain, & Other, C. N. S. C. C. (2019). Global, regional, and national burden of brain and other CNS cancer, 1990-2016: a systematic analysis for the Global Burden of Disease Study 2016. *The Lancet. Neurology*, *18*(4), 376-393. [https://doi.org/10.1016/S1474-4422\(18\)30468-X](https://doi.org/10.1016/S1474-4422(18)30468-X)
- Gajjar, A., Chintagumpala, M., Ashley, D., Kellie, S., Kun, L. E., Merchant, T. E., Woo, S., Wheeler, G., Ahern, V., & Krasin, M. J. (2006). Risk-adapted craniospinal radiotherapy followed by high-dose chemotherapy and stem-cell rescue in children with newly diagnosed medulloblastoma (St Jude Medulloblastoma-96): long-term results from a prospective, multicentre trial. *The Lancet Oncology*, *7*(10), 813-820.
- Galli, R., Binda, E., Orfanelli, U., Cipelletti, B., Gritti, A., De Vitis, S., Fiocco, R., Foroni, C., Dimeco, F., & Vescovi, A. (2004). Isolation and Characterization of Tumorigenic, Stem-like Neural Precursors from Human Glioblastoma. *Cancer Research*, *64*(19), 7011. <https://doi.org/10.1158/0008-5472.CAN-04-1364>
- Garcez, P. P., Loiola, E. C., Madeiro da Costa, R., Higa, L. M., Trindade, P., Delvecchio, R., Nascimento, J. M., Brindeiro, R., Tanuri, A., & Rehen, S. K. (2016). Zika virus impairs growth in human neurospheres and brain organoids. *Science*, *352*(6287), 816-818.
- Garnock-Jones, K. P. (2015, 2015/04/01). Panobinostat: First Global Approval. *Drugs*, *75*(6), 695-704. <https://doi.org/10.1007/s40265-015-0388-8>
- Gaspar, L. E., Fisher, B. J., Macdonald, D. R., LeBer, D. V., Halperin, E. C., Schold, S. C., Jr., & Cairncross, J. G. (1992). Supratentorial malignant glioma: patterns of recurrence and implications for external beam local treatment. *Int J Radiat Oncol Biol Phys*, *24*(1), 55-57. [https://doi.org/10.1016/0360-3016\(92\)91021-e](https://doi.org/10.1016/0360-3016(92)91021-e)
- Gerriets, V., Anderson, J., & Nappe, T. M. (2022). Acetaminophen. In *StatPearls*. StatPearls Publishing
Copyright © 2022, StatPearls Publishing LLC.
- Ghasemi, D. R., Fleischhack, G., Milde, T., & Pajtler, K. W. (2022, Jan 28). The Current Landscape of Targeted Clinical Trials in Non-WNT/Non-SHH Medulloblastoma. *Cancers (Basel)*, *14*(3). <https://doi.org/10.3390/cancers14030679>
- Gibson, P., Tong, Y., Robinson, G., Thompson, M. C., Currie, D. S., Eden, C., Kranenburg, T. A., Hogg, T., Poppleton, H., Martin, J., Finkelstein, D., Pounds, S., Weiss, A., Patay, Z., Scoggins, M., Ogg, R., Pei, Y., Yang, Z. J., Brun, S., Lee, Y., Zindy, F., Lindsey, J. C., Taketo, M. M., Boop, F. A., Sanford, R. A., Gajjar, A., Clifford, S. C., Roussel, M. F., McKinnon, P. J., Gutmann, D. H.,

Literature

- Ellison, D. W., Wechsler-Reya, R., & Gilbertson, R. J. (2010, Dec 23). Subtypes of medulloblastoma have distinct developmental origins. *Nature*, *468*(7327), 1095-1099. <https://doi.org/10.1038/nature09587>
- Gill, B. J., Pisapia, D. J., Malone, H. R., Goldstein, H., Lei, L., Sonabend, A., Yun, J., Samanamud, J., Sims, J. S., Banu, M., Dovas, A., Teich, A. F., Sheth, S. A., MCKhann, G. M., Sisti, M. B., Bruce, J. N., Sims, P. A., & Canoll, P. (2014, Aug 26). MRI-localized biopsies reveal subtype-specific differences in molecular and cellular composition at the margins of glioblastoma. *Proceedings of the National Academy of Sciences of the United States of America*, *111*(34), 12550-12555. <https://doi.org/10.1073/pnas.1405839111>
- Giordana, M. T., Schiffer, P., Lanotte, M., Girardi, P., & Chio, A. (1999, Mar 1). Epidemiology of adult medulloblastoma. *Int J Cancer*, *80*(5), 689-692. [https://doi.org/10.1002/\(sici\)1097-0215\(19990301\)80:5<689::aid-ijc10>3.0.co;2-g](https://doi.org/10.1002/(sici)1097-0215(19990301)80:5<689::aid-ijc10>3.0.co;2-g)
- Glauser, T. A., & Packer, R. J. (1991, Feb). Cognitive deficits in long-term survivors of childhood brain tumors. *Childs Nerv Syst*, *7*(1), 2-12. <https://doi.org/10.1007/bf00263824>
- Glumac, P. M., & LeBeau, A. M. (2018). The role of CD133 in cancer: a concise review. *Clinical and translational medicine*, *7*(1), 18-18. <https://doi.org/10.1186/s40169-018-0198-1>
- Goldstein, A. M., Yuen, J., & Tucker, M. A. (1997, Nov). Second cancers after medulloblastoma: population-based results from the United States and Sweden. *Cancer Causes Control*, *8*(6), 865-871. <https://doi.org/10.1023/a:1018464328836>
- Gongal, P. A., March, L. D., Holly, V. L., Pillay, L. M., Berry-Wynne, K. M., Kagechika, H., & Waskiewicz, A. J. (2011, 2011/07/01/). Hmx4 regulates Sonic hedgehog signaling through control of retinoic acid synthesis during forebrain patterning. *Developmental Biology*, *355*(1), 55-64. <https://doi.org/https://doi.org/10.1016/j.ydbio.2011.04.018>
- Goodenberger, M. L., & Jenkins, R. B. (2012, 2012/12/01/). Genetics of adult glioma. *Cancer Genetics*, *205*(12), 613-621. <https://doi.org/https://doi.org/10.1016/j.cancergen.2012.10.009>
- Gooi, H. C., Thorpe, S. J., Hounsell, E. F., Rumpold, H., Kraft, D., Förster, O., & Feizi, T. (1983). Marker of peripheral blood granulocytes and monocytes of man recognized by two monoclonal antibodies VEP8 and VEP9 involves the trisaccharide 3-fucosyl-N-acetyllactosamine. *European Journal of Immunology*, *13*(4), 306-312.
- Gottardo, N. G., Hansford, J. R., McGlade, J. P., Alvaro, F., Ashley, D. M., Bailey, S., Baker, D. L., Bourdeaut, F., Cho, Y.-J., Clay, M., Clifford, S. C., Cohn, R. J., Cole, C. H., Dallas, P. B., Downie, P., Doz, F., Ellison, D. W., Endersby, R., Fisher, P. G., Hassall, T., Heath, J. A., Hii, H. L., Jones, D. T. W., Junckerstorff, R., Kellie, S., Kool, M., Kotecha, R. S., Lichter, P., Laughton, S. J., Lee, S., McCowage, G., Northcott, P. A., Olson, J. M., Packer, R. J., Pfister, S. M., Pietsch, T., Pizer, B., Pomeroy, S. L., Remke, M., Robinson, G. W., Rutkowski, S., Schoep, T., Shelat, A. A., Stewart, C. F., Sullivan, M., Taylor, M. D., Wainwright, B., Walwyn, T., Weiss, W. A., Williamson, D., & Gajjar, A. (2014, 2014/02/01). Medulloblastoma Down Under 2013: a

Literature

- report from the third annual meeting of the International Medulloblastoma Working Group. *Acta Neuropathol*, 127(2), 189-201. <https://doi.org/10.1007/s00401-013-1213-7>
- Grill, J., Sainte-Rose, C., Jouvét, A., Gentet, J.-C., Lejars, O., Frappaz, D., Doz, F., Rialland, X., Pichon, F., Bertozzi, A.-I., Chastagner, P., Couanet, D., Habrand, J.-L., Raquin, M.-A., Le Deley, M.-C., & Kalifa, C. (2005, 2005/08/01/). Treatment of medulloblastoma with postoperative chemotherapy alone: an SFOP prospective trial in young children. *The Lancet Oncology*, 6(8), 573-580. [https://doi.org/https://doi.org/10.1016/S1470-2045\(05\)70252-7](https://doi.org/https://doi.org/10.1016/S1470-2045(05)70252-7)
- Guimaraes, D. P., & Hainaut, P. (2002, 2002/01/01/). TP53: a key gene in human cancer. *Biochimie*, 84(1), 83-93. [https://doi.org/https://doi.org/10.1016/S0300-9084\(01\)01356-6](https://doi.org/https://doi.org/10.1016/S0300-9084(01)01356-6)
- Hackett, C. H., & Fortier, L. A. (2011, Aug). Embryonic stem cells and iPS cells: sources and characteristics. *Vet Clin North Am Equine Pract*, 27(2), 233-242. <https://doi.org/10.1016/j.cveq.2011.04.003>
- Hainaut, P., & Hollstein, M. (2000). p53 and human cancer: the first ten thousand mutations. *Adv Cancer Res*, 77, 81-137. [https://doi.org/10.1016/s0065-230x\(08\)60785-x](https://doi.org/10.1016/s0065-230x(08)60785-x)
- Han, Q., Liang, H., Cheng, P., Yang, H., & Zhao, P. (2020, 2020-March-18). Gross Total vs. Subtotal Resection on Survival Outcomes in Elderly Patients With High-Grade Glioma: A Systematic Review and Meta-Analysis [Systematic Review]. *Front Oncol*, 10. <https://doi.org/10.3389/fonc.2020.00151>
- Han, S., Liu, Y., Cai, S. J., Qian, M., Ding, J., Larion, M., Gilbert, M. R., & Yang, C. (2020, 2020/05/01). IDH mutation in glioma: molecular mechanisms and potential therapeutic targets. *Br J Cancer*, 122(11), 1580-1589. <https://doi.org/10.1038/s41416-020-0814-x>
- Han, X., Wang, Y., Wei, J., & Han, W. (2019, Nov 29). Multi-antigen-targeted chimeric antigen receptor T cells for cancer therapy. *J Hematol Oncol*, 12(1), 128. <https://doi.org/10.1186/s13045-019-0813-7>
- Hanaford, A. R., Archer, T. C., Price, A., Kahlert, U. D., Maciaczyk, J., Nikkhah, G., Kim, J. W., Ehrenberger, T., Clemons, P. A., Dančík, V., Seashore-Ludlow, B., Viswanathan, V., Stewart, M. L., Rees, M. G., Shamji, A., Schreiber, S., Fraenkel, E., Pomeroy, S. L., Mesirov, J. P., Tamayo, P., Eberhart, C. G., & Raabe, E. H. (2016, Aug 1). DiSCoVERing Innovative Therapies for Rare Tumors: Combining Genetically Accurate Disease Models with In Silico Analysis to Identify Novel Therapeutic Targets. *Clin Cancer Res*, 22(15), 3903-3914. <https://doi.org/10.1158/1078-0432.Ccr-15-3011>
- Hanna, J., Wernig, M., Markoulaki, S., Sun, C. W., Meissner, A., Cassady, J. P., Beard, C., Brambrink, T., Wu, L. C., Townes, T. M., & Jaenisch, R. (2007, Dec 21). Treatment of sickle cell anemia mouse model with iPS cells generated from autologous skin. *Science*, 318(5858), 1920-1923. <https://doi.org/10.1126/science.1152092>
- Hatten, M. E., & Roussel, M. F. (2011). Development and cancer of the cerebellum. *Trends in neurosciences*, 34(3), 134-142.

Literature

- Hegi, M. E., Diserens, A.-C., Gorlia, T., Hamou, M.-F., De Tribolet, N., Weller, M., Kros, J. M., Hainfellner, J. A., Mason, W., & Mariani, L. (2005). MGMT gene silencing and benefit from temozolomide in glioblastoma. *New England Journal of Medicine*, *352*(10), 997-1003.
- Hemmati, H. D., Nakano, I., Lazareff, J. A., Masterman-Smith, M., Geschwind, D. H., Bronner-Fraser, M., & Kornblum, H. I. (2003). Cancerous stem cells can arise from pediatric brain tumors. *Proceedings of the National Academy of Sciences of the United States of America*, *100*(25), 15178-15183. <https://doi.org/10.1073/pnas.2036535100>
- Heo, J. H., Kang, D., Seo, S. J., & Jin, Y. (2022, Feb 28). Engineering the Extracellular Matrix for Organoid Culture. *Int J Stem Cells*, *15*(1), 60-69. <https://doi.org/10.15283/ijsc21190>
- Hochberg, F. H., Linggood, R., Wolfson, L., Baker, W. H., & Kornblith, P. (1979). Quality and Duration of Survival in Glioblastoma Multiforme: Combined Surgical, Radiation, and Lomustine Therapy. *Jama*, *241*(10), 1016-1018. <https://doi.org/10.1001/jama.1979.03290360032023>
- Hofrichter, M., Nimtz, L., Tigges, J., Kabiri, Y., Schröter, F., Royer-Pokora, B., Hildebrandt, B., Schmuck, M., Epanchintsev, A., Theiss, S., Adjaye, J., Egly, J.-M., Krutmann, J., & Fritsche, E. (2017, 2017/12/01/). Comparative performance analysis of human iPSC-derived and primary neural progenitor cells (NPC) grown as neurospheres in vitro. *Stem Cell Research*, *25*, 72-82. <https://doi.org/https://doi.org/10.1016/j.scr.2017.10.013>
- Hollstein, M., Sidransky, D., Vogelstein, B., & Harris, C. C. (1991, Jul 5). p53 mutations in human cancers. *Science*, *253*(5015), 49-53. <https://doi.org/10.1126/science.1905840>
- Hotta, A., Cheung, A. Y. L., Farra, N., Vijayaragavan, K., Séguin, C. A., Draper, J. S., Pasceri, P., Maksakova, I. A., Mager, D. L., Rossant, J., Bhatia, M., & Ellis, J. (2009, 2009/05/01). Isolation of human iPS cells using EOS lentiviral vectors to select for pluripotency. *Nature methods*, *6*(5), 370-376. <https://doi.org/10.1038/nmeth.1325>
- Howe, B., Umrigar, A., & Tsien, F. (2014, Jan 28). Chromosome preparation from cultured cells. *J Vis Exp*(83), e50203. <https://doi.org/10.3791/50203>
- Hu, B.-Y., Weick Jason, P., Yu, J., Ma, L.-X., Zhang, X.-Q., Thomson James, A., & Zhang, S.-C. (2010, 2010/03/02). Neural differentiation of human induced pluripotent stem cells follows developmental principles but with variable potency. *Proceedings of the National Academy of Sciences*, *107*(9), 4335-4340. <https://doi.org/10.1073/pnas.0910012107>
- Hu, Y., Jiang, Y., Zhang, Z., Wang, J., Zhang, B., Gong, L., Ji, L., Pu, Z., Yang, X., Zou, J., & Yin, Y. (2022, Jan). Oncogenic Activity of Glucocorticoid Receptor β Is Controlled by Ubiquitination-Dependent Interaction with USP49 in Glioblastoma Cells. *Mol Cancer Res*, *20*(1), 92-101. <https://doi.org/10.1158/1541-7786.Mcr-20-1068>
- Huang da, W., Sherman, B. T., & Lempicki, R. A. (2009a, Jan). Bioinformatics enrichment tools: paths toward the comprehensive functional analysis of large gene lists. *Nucleic Acids Res*, *37*(1), 1-13. <https://doi.org/10.1093/nar/gkn923>

Literature

- Huang da, W., Sherman, B. T., & Lempicki, R. A. (2009b). Systematic and integrative analysis of large gene lists using DAVID bioinformatics resources. *Nat Protoc*, *4*(1), 44-57. <https://doi.org/10.1038/nprot.2008.211>
- Ichimura, K., Pearson, D. M., Kocialkowski, S., Bäcklund, L. M., Chan, R., Jones, D. T. W., & Collins, V. P. (2009). IDH1 mutations are present in the majority of common adult gliomas but rare in primary glioblastomas. *Neuro-Oncology*, *11*(4), 341-347. <https://doi.org/10.1215/15228517-2009-025>
- Inda, M. M., Bonavia, R., Mukasa, A., Narita, Y., Sah, D. W., Vandenberg, S., Brennan, C., Johns, T. G., Bachoo, R., Hadwiger, P., Tan, P., Depinho, R. A., Cavenee, W., & Furnari, F. (2010, Aug 15). Tumor heterogeneity is an active process maintained by a mutant EGFR-induced cytokine circuit in glioblastoma. *Genes Dev*, *24*(16), 1731-1745. <https://doi.org/10.1101/gad.1890510>
- Ingham, P. W. (1998, 1998/02/01/). The patched gene in development and cancer. *Current opinion in genetics & development*, *8*(1), 88-94. [https://doi.org/https://doi.org/10.1016/S0959-437X\(98\)80067-1](https://doi.org/https://doi.org/10.1016/S0959-437X(98)80067-1)
- Jacob, F., Salinas, R. D., Zhang, D. Y., Nguyen, P. T. T., Schnoll, J. G., Wong, S. Z. H., Thokala, R., Sheikh, S., Saxena, D., Prokop, S., Liu, D.-a., Qian, X., Petrov, D., Lucas, T., Chen, H. I., Dorsey, J. F., Christian, K. M., Binder, Z. A., Nasrallah, M., Brem, S., O'Rourke, D. M., Ming, G.-l., & Song, H. (2020, 2020/01/09/). A Patient-Derived Glioblastoma Organoid Model and Biobank Recapitulates Inter- and Intra-tumoral Heterogeneity. *Cell*, *180*(1), 188-204.e122. <https://doi.org/https://doi.org/10.1016/j.cell.2019.11.036>
- Jamieson, C. H., Ailles, L. E., Dylla, S. J., Muijtjens, M., Jones, C., Zehnder, J. L., Gotlib, J., Li, K., Manz, M. G., Keating, A., Sawyers, C. L., & Weissman, I. L. (2004, Aug 12). Granulocyte-macrophage progenitors as candidate leukemic stem cells in blast-crisis CML. *N Engl J Med*, *351*(7), 657-667. <https://doi.org/10.1056/NEJMoa040258>
- Jeng, K. S., Chang, C. F., & Lin, S. S. (2020, Jan 23). Sonic Hedgehog Signaling in Organogenesis, Tumors, and Tumor Microenvironments. *International journal of molecular sciences*, *21*(3). <https://doi.org/10.3390/ijms21030758>
- Jia, L., Tian, Y., Chen, Y., & Zhang, G. (2018). The silencing of LncRNA-H19 decreases chemoresistance of human glioma cells to temozolomide by suppressing epithelial-mesenchymal transition via the Wnt/ β -Catenin pathway. *Onco Targets Ther*, *11*, 313-321. <https://doi.org/10.2147/ott.S154339>
- Jiang, X., Cao, Y., Li, F., Su, Y., Li, Y., Peng, Y., Cheng, Y., Zhang, C., Wang, W., & Ning, G. (2014, 2014/12/17). Targeting β -catenin signaling for therapeutic intervention in MEN1-deficient pancreatic neuroendocrine tumours. *Nature Communications*, *5*(1), 5809. <https://doi.org/10.1038/ncomms6809>
- Jo, M. Y., Kim, Y. G., Kim, Y., Lee, S. J., Kim, M. H., Joo, K. M., Kim, H. H., & Nam, D. H. (2012, Jul). Combined therapy of temozolomide and ZD6474 (vandetanib) effectively reduces

Literature

- glioblastoma tumor volume through anti-angiogenic and anti-proliferative mechanisms. *Mol Med Rep*, 6(1), 88-92. <https://doi.org/10.3892/mmr.2012.868>
- Johnston, D. L., Keene, D., Strother, D., Taneva, M., Lafay-Cousin, L., Fryer, C., Scheinemann, K., Carret, A.-S., Fleming, A., Afzal, S., Wilson, B., Bowes, L., Zelcer, S., Mpofu, C., Silva, M., Larouche, V., Brossard, J., & Bouffet, E. (2018). Survival Following Tumor Recurrence in Children With Medulloblastoma. *Journal of Pediatric Hematology/Oncology*, 40(3). https://journals.lww.com/jpho-online/Fulltext/2018/04000/Survival_Following_Tumor_Recurrence_in_Children.28.aspx
- Jordan, C. T., Guzman, M. L., & Noble, M. (2006). Cancer stem cells. *New England Journal of Medicine*, 355(12), 1253-1261.
- Juraschka, K., & Taylor, M. D. (2019, 01 Oct. 2019). Medulloblastoma in the age of molecular subgroups: a review. *Journal of Neurosurgery: Pediatrics PED*, 24(4), 353. <https://doi.org/10.3171/2019.5.Peds18381>
- Kabir, J., Lobo, M., & Zachary, I. (2002). Staurosporine induces endothelial cell apoptosis via focal adhesion kinase dephosphorylation and focal adhesion disassembly independent of focal adhesion kinase proteolysis. *The Biochemical journal*, 367(Pt 1), 145-155. <https://doi.org/10.1042/BJ20020665>
- Kahlert, U. D., Maciaczyk, D., Doostkam, S., Orr, B. A., Simons, B., Bogiel, T., Reithmeier, T., Prinz, M., Schubert, J., Niedermann, G., Brabletz, T., Eberhart, C. G., Nikkhah, G., & Maciaczyk, J. (2012, Dec 1). Activation of canonical WNT/beta-catenin signaling enhances in vitro motility of glioblastoma cells by activation of ZEB1 and other activators of epithelial-to-mesenchymal transition. *Cancer Lett*, 325(1), 42-53. <https://doi.org/10.1016/j.canlet.2012.05.024>
- Kahlert, U. D., Nikkhah, G., & Maciaczyk, J. (2013, May 1). Epithelial-to-mesenchymal(-like) transition as a relevant molecular event in malignant gliomas. *Cancer Lett*, 331(2), 131-138. <https://doi.org/10.1016/j.canlet.2012.12.010>
- Kalluri, R., & Weinberg, R. A. (2009, Jun). The basics of epithelial-mesenchymal transition. *J Clin Invest*, 119(6), 1420-1428. <https://doi.org/10.1172/jci39104>
- Karagiannis, P., Takahashi, K., Saito, M., Yoshida, Y., Okita, K., Watanabe, A., Inoue, H., Yamashita, J. K., Todani, M., Nakagawa, M., Osawa, M., Yashiro, Y., Yamanaka, S., & Osafune, K. (2019, Jan 1). Induced Pluripotent Stem Cells and Their Use in Human Models of Disease and Development. *Physiol Rev*, 99(1), 79-114. <https://doi.org/10.1152/physrev.00039.2017>
- Kato, S., Okamura, R., Mareboina, M., Lee, S., Goodman, A., Patel, S. P., Fanta, P. T., Schwab, R. B., Vu, P., Raymond, V. M., Lanman, R. B., Sicklick, J. K., Lippman, S. M., & Kurzrock, R. (2019). Revisiting Epidermal Growth Factor Receptor (EGFR) Amplification as a Target for Anti-EGFR Therapy: Analysis of Cell-Free Circulating Tumor DNA in Patients With Advanced Malignancies. *JCO Precision Oncology*(3), 1-14. <https://doi.org/10.1200/po.18.00180>

Literature

- Katso, R., Okkenhaug, K., Ahmadi, K., White, S., Timms, J., & Waterfield, M. D. (2001, 2001/11/01). Cellular Function of Phosphoinositide 3-Kinases: Implications for Development, Immunity, Homeostasis, and Cancer. *Annual Review of Cell and Developmental Biology*, 17(1), 615-675. <https://doi.org/10.1146/annurev.cellbio.17.1.615>
- Katt, M. E., Placone, A. L., Wong, A. D., Xu, Z. S., & Searson, P. C. (2016). In Vitro Tumor Models: Advantages, Disadvantages, Variables, and Selecting the Right Platform. *Frontiers in bioengineering and biotechnology*, 4, 12-12. <https://doi.org/10.3389/fbioe.2016.00012>
- Kernohan, J. W., Mabon, R. F., & et al. (1949, Feb 2). A simplified classification of the gliomas. *Proc Staff Meet Mayo Clin*, 24(3), 71-75.
- Keßel, H. E., Masjosthusmann, S., Bartmann, K., Blum, J., Dönmez, A., Förster, N., Klose, J., Mosig, A., Pahl, M., Leist, M., Scholze, M., & Fritsche, E. (2022). Biostatistics and its impact on hazard characterization using in vitro developmental neurotoxicity assays. *bioRxiv*, 2022.2010.2018.512648. <https://doi.org/10.1101/2022.10.18.512648>
- Kim, J., Koo, B.-K., & Knoblich, J. A. (2020, 2020/10/01). Human organoids: model systems for human biology and medicine. *Nature Reviews Molecular Cell Biology*, 21(10), 571-584. <https://doi.org/10.1038/s41580-020-0259-3>
- Kim, W. T., & Ryu, C. J. (2017, Jun). Cancer stem cell surface markers on normal stem cells. *BMB Rep*, 50(6), 285-298. <https://doi.org/10.5483/bmbrep.2017.50.6.039>
- Kim, Y., Varn, F. S., Park, S.-H., Yoon, B. W., Park, H. R., Lee, C., Verhaak, R. G. W., & Paek, S. H. (2021, 2021/03/24). Perspective of mesenchymal transformation in glioblastoma. *Acta Neuropathologica Communications*, 9(1), 50. <https://doi.org/10.1186/s40478-021-01151-4>
- Kirson, E. D., Dbalý, V., Tovarys, F., Vymazal, J., Soustiel, J. F., Itzhaki, A., Mordechovich, D., Steinberg-Shapira, S., Gurvich, Z., Schneiderman, R., Wasserman, Y., Salzberg, M., Ryffel, B., Goldsher, D., Dekel, E., & Palti, Y. (2007). Alternating electric fields arrest cell proliferation in animal tumor models and human brain tumors. *Proceedings of the National Academy of Sciences of the United States of America*, 104(24), 10152-10157. <https://doi.org/10.1073/pnas.0702916104>
- Kirson, E. D., Gurvich, Z., Schneiderman, R., Dekel, E., Itzhaki, A., Wasserman, Y., Schatzberger, R., & Palti, Y. (2004, May 1). Disruption of cancer cell replication by alternating electric fields. *Cancer Res*, 64(9), 3288-3295. <https://doi.org/10.1158/0008-5472.can-04-0083>
- Kleensang, A., Vantangoli, M. M., Odwin-DaCosta, S., Andersen, M. E., Boekelheide, K., Bouhifd, M., Fornace, A. J., Li, H.-H., Livi, C. B., Madnick, S., Maertens, A., Rosenberg, M., Yager, J. D., Zhao, L., & Hartung, T. (2016, 2016/07/26). Genetic variability in a frozen batch of MCF-7 cells invisible in routine authentication affecting cell function. *Scientific Reports*, 6(1), 28994. <https://doi.org/10.1038/srep28994>
- Koch, K., Bartmann, K., Hartmann, J., Kapr, J., Klose, J., Kuchovská, E., Pahl, M., Schlüppmann, K., Zühr, E., & Fritsche, E. (2022). Scientific Validation of Human Neurosphere Assays for

Literature

- Developmental Neurotoxicity Evaluation. *Front Toxicol*, 4, 816370.
<https://doi.org/10.3389/ftox.2022.816370>
- Koch, K., Hartmann, R., Schroter, F., Suwala, A. K., Maciaczyk, D., Kruger, A. C., Willbold, D., Kahlert, U. D., & Maciaczyk, J. (2016, Nov 8). Reciprocal regulation of the cholinic phenotype and epithelial-mesenchymal transition in glioblastoma cells. *Oncotarget*, 7(45), 73414-73431.
<https://doi.org/10.18632/oncotarget.12337>
- Kodack, D. P., Farago, A. F., Dastur, A., Held, M. A., Dardaei, L., Friboulet, L., von Flotow, F., Damon, L. J., Lee, D., Parks, M., Dicecca, R., Greenberg, M., Kattermann, K. E., Riley, A. K., Fintelmann, F. J., Rizzo, C., Piotrowska, Z., Shaw, A. T., Gainor, J. F., Sequist, L. V., Niederst, M. J., Engelman, J. A., & Benes, C. H. (2017, Dec 12). Primary Patient-Derived Cancer Cells and Their Potential for Personalized Cancer Patient Care. *Cell Rep*, 21(11), 3298-3309.
<https://doi.org/10.1016/j.celrep.2017.11.051>
- Koga, T., Chaim, I. A., Benitez, J. A., Markmiller, S., Parisian, A. D., Hevner, R. F., Turner, K. M., Hessenauer, F. M., D'Antonio, M., Nguyen, N. D., Saberi, S., Ma, J., Miki, S., Boyer, A. D., Ravits, J., Frazer, K. A., Bafna, V., Chen, C. C., Mischel, P. S., Yeo, G. W., & Furnari, F. B. (2020, Apr 20). Longitudinal assessment of tumor development using cancer avatars derived from genetically engineered pluripotent stem cells. *Nat Commun*, 11(1), 1958.
<https://doi.org/10.1038/s41467-020-15828-2>
- Komiya, Y., & Habas, R. (2008). Wnt signal transduction pathways. *Organogenesis*, 4(2), 68-75.
<https://doi.org/10.4161/org.4.2.5851>
- Kool, M., Korshunov, A., Remke, M., Jones, D. T. W., Schlanstein, M., Northcott, P. A., Cho, Y.-J., Koster, J., Schouten-van Meeteren, A., van Vuurden, D., Clifford, S. C., Pietsch, T., von Bueren, A. O., Rutkowski, S., McCabe, M., Collins, V. P., Bäcklund, M. L., Haberler, C., Bourdeaut, F., Delattre, O., Doz, F., Ellison, D. W., Gilbertson, R. J., Pomeroy, S. L., Taylor, M. D., Lichter, P., & Pfister, S. M. (2012, 2012/04/01). Molecular subgroups of medulloblastoma: an international meta-analysis of transcriptome, genetic aberrations, and clinical data of WNT, SHH, Group 3, and Group 4 medulloblastomas. *Acta Neuropathol*, 123(4), 473-484.
<https://doi.org/10.1007/s00401-012-0958-8>
- Kool, M., Koster, J., Bunt, J., Hasselt, N. E., Lakeman, A., van Sluis, P., Troost, D., Meeteren, N. S., Caron, H. N., Cloos, J., Msić, A., Ylstra, B., Grajkowska, W., Hartmann, W., Pietsch, T., Ellison, D., Clifford, S. C., & Versteeg, R. (2008, Aug 28). Integrated genomics identifies five medulloblastoma subtypes with distinct genetic profiles, pathway signatures and clinicopathological features. *PLOS ONE*, 3(8), e3088.
<https://doi.org/10.1371/journal.pone.0003088>
- Korshunov, A., Remke, M., Werft, W., Benner, A., Ryzhova, M., Witt, H., Sturm, D., Wittmann, A., Schöttler, A., Felsberg, J., Reifenberger, G., Rutkowski, S., Scheurlen, W., Kulozik, A. E., Deimling, A. v., Lichter, P., & Pfister, S. M. (2010). Adult and Pediatric Medulloblastomas Are Genetically Distinct and Require Different Algorithms for Molecular Risk Stratification. *Journal of Clinical Oncology*, 28(18), 3054-3060. <https://doi.org/10.1200/jco.2009.25.7121>

Literature

- Krebs, A., Nyffeler, J., Rahnenführer, J., & Leist, M. (2018). Normalization of data for viability and relative cell function curves. *Altex*, 35(2), 268-271. <https://doi.org/10.14573/1803231>
- Kreisl, T. N., McNeill, K. A., Sul, J., Iwamoto, F. M., Shih, J., & Fine, H. A. (2012, Dec). A phase I/II trial of vandetanib for patients with recurrent malignant glioma. *Neuro Oncol*, 14(12), 1519-1526. <https://doi.org/10.1093/neuonc/nos265>
- Kupis, W., Palyga, J., Tomal, E., & Niewiadomska, E. (2016). The role of sirtuins in cellular homeostasis. *Journal of physiology and biochemistry*, 72(3), 371-380. <https://doi.org/10.1007/s13105-016-0492-6>
- Lancaster, M. A., & Huch, M. (2019, Jul 29). Disease modelling in human organoids. *Dis Model Mech*, 12(7). <https://doi.org/10.1242/dmm.039347>
- Lancaster, M. A., Renner, M., Martin, C.-A., Wenzel, D., Bicknell, L. S., Hurles, M. E., Homfray, T., Penninger, J. M., Jackson, A. P., & Knoblich, J. A. (2013, 2013/09/01). Cerebral organoids model human brain development and microcephaly. *Nature*, 501(7467), 373-379. <https://doi.org/10.1038/nature12517>
- Laplane, L., Beke, A., Vainchenker, W., & Solary, E. (2015, Oct). Concise Review: Induced Pluripotent Stem Cells as New Model Systems in Oncology. *Stem Cells*, 33(10), 2887-2892. <https://doi.org/10.1002/stem.2099>
- Lassaletta, A., Scheinemann, K., Zelcer, S. M., Hukin, J., Wilson, B. A., Jabado, N., Carret, A. S., Lafay-Cousin, L., Larouche, V., Hawkins, C. E., Pond, G. R., Poskitt, K., Keene, D., Johnston, D. L., Eisenstat, D. D., Krishnatry, R., Mistry, M., Arnoldo, A., Ramaswamy, V., Huang, A., Bartels, U., Tabori, U., & Bouffet, E. (2016, Oct 10). Phase II Weekly Vinblastine for Chemotherapy-Naïve Children With Progressive Low-Grade Glioma: A Canadian Pediatric Brain Tumor Consortium Study. *J Clin Oncol*, 34(29), 3537-3543. <https://doi.org/10.1200/jco.2016.68.1585>
- Laubach, J. P., Moreau, P., San-Miguel, J. F., & Richardson, P. G. (2015). Panobinostat for the Treatment of Multiple Myeloma. *Clinical Cancer Research*, 21(21), 4767-4773. <https://doi.org/10.1158/1078-0432.CCR-15-0530>
- Laurent, L. C., Ulitsky, I., Slavin, I., Tran, H., Schork, A., Morey, R., Lynch, C., Harness, J. V., Lee, S., Barrero, M. J., Ku, S., Martynova, M., Semechkin, R., Galat, V., Gottesfeld, J., Belmonte, J. C. I., Murry, C., Keirstead, H. S., Park, H.-S., Schmidt, U., Laslett, A. L., Muller, F.-J., Nievergelt, C. M., Shamir, R., & Loring, J. F. (2011, 2011/01/07/). Dynamic Changes in the Copy Number of Pluripotency and Cell Proliferation Genes in Human ESCs and iPSCs during Reprogramming and Time in Culture. *Cell Stem Cell*, 8(1), 106-118. <https://doi.org/https://doi.org/10.1016/j.stem.2010.12.003>
- Le Rhun, E., Preusser, M., Roth, P., Reardon, D. A., van den Bent, M., Wen, P., Reifenberger, G., & Weller, M. (2019, Nov). Molecular targeted therapy of glioblastoma. *Cancer Treat Rev*, 80, 101896. <https://doi.org/10.1016/j.ctrv.2019.101896>

Literature

- Leary, S. E., & Olson, J. M. (2012, Feb). The molecular classification of medulloblastoma: driving the next generation clinical trials. *Curr Opin Pediatr*, 24(1), 33-39. <https://doi.org/10.1097/MOP.0b013e32834ec106>
- Levine, A. J. (1997). p53, the Cellular Gatekeeper for Growth and Division. *Cell*, 88(3), 323-331. [https://doi.org/10.1016/S0092-8674\(00\)81871-1](https://doi.org/10.1016/S0092-8674(00)81871-1)
- Li, J., Wang, P.-Y., Long, N. A., Zhuang, J., Springer, D. A., Zou, J., Lin, Y., Bleck, C. K. E., Park, J.-H., Kang, J.-G., & Hwang, P. M. (2019). p53 prevents doxorubicin cardiotoxicity independently of its prototypical tumor suppressor activities. *Proceedings of the National Academy of Sciences of the United States of America*, 116(39), 19626-19634. <https://doi.org/10.1073/pnas.1904979116>
- Li, L., Yu, J., Jiao, S., Wang, W., Zhang, F., & Sun, S. (2018). Vandetanib (ZD6474) induces antiangiogenesis through mTOR-HIF-1 alpha-VEGF signaling axis in breast cancer cells. *Onco Targets Ther*, 11, 8543-8553. <https://doi.org/10.2147/ott.S175578>
- Li, W., Sun, W., Zhang, Y., Wei, W., Ambasadhan, R., Xia, P., Talantova, M., Lin, T., Kim, J., Wang, X., Kim, W. R., Lipton, S. A., Zhang, K., & Ding, S. (2011, 2011/05/17). Rapid induction and long-term self-renewal of primitive neural precursors from human embryonic stem cells by small molecule inhibitors. *Proceedings of the National Academy of Sciences*, 108(20), 8299-8304. <https://doi.org/10.1073/pnas.1014041108>
- Libermann, T. A., Nusbaum, H. R., Razon, N., Kris, R., Lax, I., Soreq, H., Whittle, N., Waterfield, M. D., Ullrich, A., & Schlessinger, J. (1985, 1985/01/01). Amplification, enhanced expression and possible rearrangement of EGF receptor gene in primary human brain tumours of glial origin. *Nature*, 313(5998), 144-147. <https://doi.org/10.1038/313144a0>
- Lin, C. Y., Erkek, S., Tong, Y., Yin, L., Federation, A. J., Zapatka, M., Haldipur, P., Kawauchi, D., Risch, T., & Warnatz, H.-J. (2016). Active medulloblastoma enhancers reveal subgroup-specific cellular origins. *Nature*, 530(7588), 57-62.
- Lin, Y. C., Boone, M., Meuris, L., Lemmens, I., Van Roy, N., Soete, A., Reumers, J., Moisse, M., Plaisance, S., Drmanac, R., Chen, J., Speleman, F., Lambrechts, D., Van de Peer, Y., Tavernier, J., & Callewaert, N. (2014, Sep 3). Genome dynamics of the human embryonic kidney 293 lineage in response to cell biology manipulations. *Nat Commun*, 5, 4767. <https://doi.org/10.1038/ncomms5767>
- Liston, D. R., & Davis, M. (2017, Jul 15). Clinically Relevant Concentrations of Anticancer Drugs: A Guide for Nonclinical Studies. *Clin Cancer Res*, 23(14), 3489-3498. <https://doi.org/10.1158/1078-0432.Ccr-16-3083>
- Liu, D. P., Song, H., & Xu, Y. (2010, Feb 18). A common gain of function of p53 cancer mutants in inducing genetic instability. *Oncogene*, 29(7), 949-956. <https://doi.org/10.1038/onc.2009.376>

Literature

- Liu, G., David, B. T., Trawczynski, M., & Fessler, R. G. (2020, Feb). Advances in Pluripotent Stem Cells: History, Mechanisms, Technologies, and Applications. *Stem Cell Rev Rep*, 16(1), 3-32. <https://doi.org/10.1007/s12015-019-09935-x>
- Liu, G., Yuan, X., Zeng, Z., Tunici, P., Ng, H., Abdulkadir, I. R., Lu, L., Irvin, D., Black, K. L., & Yu, J. S. (2006, Dec 2). Analysis of gene expression and chemoresistance of CD133+ cancer stem cells in glioblastoma. *Molecular cancer*, 5, 67. <https://doi.org/10.1186/1476-4598-5-67>
- Liu, Y., Mi, Y., Mueller, T., Kreibich, S., Williams, E. G., Van Drogen, A., Borel, C., Frank, M., Germain, P.-L., Bludau, I., Mehnert, M., Seifert, M., Emmenlauer, M., Sorg, I., Bezrukov, F., Bena, F. S., Zhou, H., Dehio, C., Testa, G., Saez-Rodriguez, J., Antonarakis, S. E., Hardt, W.-D., & Aebersold, R. (2019, 2019/03/01). Multi-omic measurements of heterogeneity in HeLa cells across laboratories. *Nature Biotechnology*, 37(3), 314-322. <https://doi.org/10.1038/s41587-019-0037-y>
- Louis, D. N., Perry, A., Reifenberger, G., von Deimling, A., Figarella-Branger, D., Cavenee, W. K., Ohgaki, H., Wiestler, O. D., Kleihues, P., & Ellison, D. W. (2016, Jun). The 2016 World Health Organization Classification of Tumors of the Central Nervous System: a summary. *Acta Neuropathol*, 131(6), 803-820. <https://doi.org/10.1007/s00401-016-1545-1>
- Louis, D. N., Perry, A., Wesseling, P., Brat, D. J., Cree, I. A., Figarella-Branger, D., Hawkins, C., Ng, H. K., Pfister, S. M., Reifenberger, G., Soffietti, R., von Deimling, A., & Ellison, D. W. (2021). The 2021 WHO Classification of Tumors of the Central Nervous System: a summary. *Neuro-Oncology*, 23(8), 1231-1251. <https://doi.org/10.1093/neuonc/noab106>
- Lowry, N. A., & Temple, S. (2009, Feb 3). Identifying the perpetrator in medulloblastoma: Dorian Gray versus Benjamin Button. *Cancer Cell*, 15(2), 83-85. <https://doi.org/10.1016/j.ccr.2009.01.010>
- Lu, J., Li, D., Zeng, Y., Wang, H., Feng, W., Qi, S., & Yu, L. (2019, Nov-Dec). IDH1 mutation promotes proliferation and migration of glioma cells via EMT induction. *J buon*, 24(6), 2458-2464.
- MacDonald, B. T., Tamai, K., & He, X. (2009, 2009/07/21/). Wnt/ β -Catenin Signaling: Components, Mechanisms, and Diseases. *Developmental Cell*, 17(1), 9-26. <https://doi.org/https://doi.org/10.1016/j.devcel.2009.06.016>
- Mai, P. L., Best, A. F., Peters, J. A., DeCastro, R. M., Khincha, P. P., Loud, J. T., Bremer, R. C., Rosenberg, P. S., & Savage, S. A. (2016). Risks of first and subsequent cancers among TP53 mutation carriers in the National Cancer Institute Li-Fraumeni syndrome cohort. *Cancer*, 122(23), 3673-3681. <https://doi.org/10.1002/cncr.30248>
- Malik, N., & Rao, M. S. (2013). A review of the methods for human iPSC derivation. *Methods in molecular biology (Clifton, N.J.)*, 997, 23-33. https://doi.org/10.1007/978-1-62703-348-0_3
- Man, A. W. C., Li, H., & Xia, N. (2019, 2019-September-12). The Role of Sirtuin1 in Regulating Endothelial Function, Arterial Remodeling and Vascular Aging [Review]. *Frontiers in Physiology*, 10. <https://doi.org/10.3389/fphys.2019.01173>

Literature

- Mandegar, M. A., Huebsch, N., Frolov, E. B., Shin, E., Truong, A., Olvera, M. P., Chan, A. H., Miyaoka, Y., Holmes, K., Spencer, C. I., Judge, L. M., Gordon, D. E., Eskildsen, T. V., Villalta, J. E., Horlbeck, M. A., Gilbert, L. A., Krogan, N. J., Sheikh, S. P., Weissman, J. S., Qi, L. S., So, P. L., & Conklin, B. R. (2016, Apr 7). CRISPR Interference Efficiently Induces Specific and Reversible Gene Silencing in Human iPSCs. *Cell Stem Cell*, *18*(4), 541-553. <https://doi.org/10.1016/j.stem.2016.01.022>
- Martin, A. M., Raabe, E., Eberhart, C., & Cohen, K. J. (2014, Dec). Management of pediatric and adult patients with medulloblastoma. *Curr Treat Options Oncol*, *15*(4), 581-594. <https://doi.org/10.1007/s11864-014-0306-4>
- Massagué, J. (2012, Oct). TGF β signalling in context. *Nat Rev Mol Cell Biol*, *13*(10), 616-630. <https://doi.org/10.1038/nrm3434>
- Massimino, M., Biassoni, V., Gandola, L., Garrè, M. L., Gatta, G., Giangaspero, F., Poggi, G., & Rutkowski, S. (2016, Sep). Childhood medulloblastoma. *Crit Rev Oncol Hematol*, *105*, 35-51. <https://doi.org/10.1016/j.critrevonc.2016.05.012>
- Matsuo, M., Yoshida, N., Zaitzu, M., Ishii, K., & Hamasaki, Y. (2004, Feb). Inhibition of human glioma cell growth by a PHS-2 inhibitor, NS398, and a prostaglandin E receptor subtype EP1-selective antagonist, SC51089. *J Neurooncol*, *66*(3), 285-292. <https://doi.org/10.1023/b:neon.0000014537.15902.73>
- McGowan-Jordan, J., Simons, A., & Schmid, M. (2016). *ISCN : an international system for human cytogenomic nomenclature*. S. Karger AG. <https://doi.org/https://doi.org/10.1159/isbn.978-3-318-06861-0>
- Menyhárt, O., Giangaspero, F., & Győrffy, B. (2019, 2019/03/15). Molecular markers and potential therapeutic targets in non-WNT/non-SHH (group 3 and group 4) medulloblastomas. *Journal of Hematology & Oncology*, *12*(1), 29. <https://doi.org/10.1186/s13045-019-0712-y>
- Merten, O. W., Charrier, S., Laroudie, N., Fauchille, S., Dugué, C., Jenny, C., Audit, M., Zanta-Boussif, M. A., Chautard, H., Radrizzani, M., Vallanti, G., Naldini, L., Noguez-Hellin, P., & Galy, A. (2011, Mar). Large-scale manufacture and characterization of a lentiviral vector produced for clinical ex vivo gene therapy application. *Hum Gene Ther*, *22*(3), 343-356. <https://doi.org/10.1089/hum.2010.060>
- Merten, O. W., Hebben, M., & Bovolenta, C. (2016). Production of lentiviral vectors. *Mol Ther Methods Clin Dev*, *3*, 16017. <https://doi.org/10.1038/mtm.2016.17>
- Micalizzi, D. S., & Ford, H. L. (2009, Oct). Epithelial-mesenchymal transition in development and cancer. *Future Oncol*, *5*(8), 1129-1143. <https://doi.org/10.2217/fon.09.94>
- Miret, C., Molina, R., Filella, X., García-Carrasco, M., Claver, G., Ingelmo, M., Ballesta, A., & Font, J. (2003, Aug-Sep). Relationship of p53 with other oncogenes, cytokines and systemic lupus erythematosus activity. *Tumour Biol*, *24*(4), 185-188. <https://doi.org/10.1159/000074428>

Literature

- Mishra, R., Patel, H., Alanazi, S., Kilroy, M. K., & Garrett, J. T. (2021, Mar 27). PI3K Inhibitors in Cancer: Clinical Implications and Adverse Effects. *International journal of molecular sciences*, 22(7). <https://doi.org/10.3390/ijms22073464>
- Molina, J. R., Hayashi, Y., Stephens, C., & Georgescu, M. M. (2010, Jun). Invasive glioblastoma cells acquire stemness and increased Akt activation. *Neoplasia*, 12(6), 453-463. <https://doi.org/10.1593/neo.10126>
- Morin, P. J., Sparks, A. B., Korinek, V., Barker, N., Clevers, H., Vogelstein, B., & Kinzler, K. W. (1997, Mar 21). Activation of beta-catenin-Tcf signaling in colon cancer by mutations in beta-catenin or APC. *Science*, 275(5307), 1787-1790. <https://doi.org/10.1126/science.275.5307.1787>
- Mosmann, T. (1983, Dec 16). Rapid colorimetric assay for cellular growth and survival: application to proliferation and cytotoxicity assays. *J Immunol Methods*, 65(1-2), 55-63. [https://doi.org/10.1016/0022-1759\(83\)90303-4](https://doi.org/10.1016/0022-1759(83)90303-4)
- Nduom, E. K., Yang, C., Merrill, M. J., Zhuang, Z., & Lonser, R. R. (2013, Aug). Characterization of the blood-brain barrier of metastatic and primary malignant neoplasms. *J Neurosurg*, 119(2), 427-433. <https://doi.org/10.3171/2013.3.Jns122226>
- Network, C. G. A. R. (2008). Comprehensive genomic characterization defines human glioblastoma genes and core pathways. *Nature*, 455(7216), 1061.
- Neumann, E., Riepl, B., Knedla, A., Lefèvre, S., Tarner, I. H., Grifka, J., Steinmeyer, J., Schölmerich, J., Gay, S., & Müller-Ladner, U. (2010, 2010/05/12). Cell culture and passaging alters gene expression pattern and proliferation rate in rheumatoid arthritis synovial fibroblasts. *Arthritis Research & Therapy*, 12(3), R83. <https://doi.org/10.1186/ar3010>
- Nickel, A. C., Picard, D., Qin, N., Wolter, M., Kaulich, K., Hewera, M., Pauck, D., Marquardt, V., Torga, G., Muhammad, S., Zhang, W., Schnell, O., Steiger, H. J., Hänggi, D., Fritsche, E., Her, N. G., Nam, D. H., Carro, M. S., Remke, M., Reifenberger, G., & Kahlert, U. D. (2021, 2021/12/01/). Longitudinal stability of molecular alterations and drug response profiles in tumor spheroid cell lines enables reproducible analyses. *Biomedicine & Pharmacotherapy*, 144, 112278. <https://doi.org/https://doi.org/10.1016/j.biopha.2021.112278>
- Nikfarjam, L., & Farzaneh, P. (2012, Winter). Prevention and detection of Mycoplasma contamination in cell culture. *Cell J*, 13(4), 203-212.
- Nimtz, L., Hartmann, J., Tigges, J., Masjosthusmann, S., Schmuck, M., Keßel, E., Theiss, S., Köhrer, K., Petzsch, P., Adjaye, J., Wigmann, C., Wiczorek, D., Hildebrandt, B., Bendt, F., Hübenthal, U., Brockerhoff, G., & Fritsche, E. (2020, 2020/05/01/). Characterization and application of electrically active neuronal networks established from human induced pluripotent stem cell-derived neural progenitor cells for neurotoxicity evaluation. *Stem Cell Res*, 45, 101761. <https://doi.org/https://doi.org/10.1016/j.scr.2020.101761>

Literature

- Nobre, L., Pauck, D., Golbourn, B., Maue, M., Bouffet, E., Remke, M., & Ramaswamy, V. (2019, Jun). Effective and safe tumor inhibition using vinblastine in medulloblastoma. *Pediatr Blood Cancer*, 66(6), e27694. <https://doi.org/10.1002/psc.27694>
- Nobusawa, S., Watanabe, T., Kleihues, P., & Ohgaki, H. (2009, Oct 1). IDH1 mutations as molecular signature and predictive factor of secondary glioblastomas. *Clin Cancer Res*, 15(19), 6002-6007. <https://doi.org/10.1158/1078-0432.Ccr-09-0715>
- Northcott, P. A., Buchhalter, I., Morrissy, A. S., Hovestadt, V., Weischenfeldt, J., Ehrenberger, T., Gröbner, S., Segura-Wang, M., Zichner, T., & Rudneva, V. A. (2017). The whole-genome landscape of medulloblastoma subtypes. *Nature*, 547(7663), 311-317.
- Northcott, P. A., Hielscher, T., Dubuc, A., Mack, S., Shih, D., Remke, M., Al-Halabi, H., Albrecht, S., Jabado, N., Eberhart, C. G., Grajkowska, W., Weiss, W. A., Clifford, S. C., Bouffet, E., Rutka, J. T., Korshunov, A., Pfister, S., & Taylor, M. D. (2011, Aug). Pediatric and adult sonic hedgehog medulloblastomas are clinically and molecularly distinct. *Acta Neuropathol*, 122(2), 231-240. <https://doi.org/10.1007/s00401-011-0846-7>
- Northcott, P. A., Jones, D. T., Kool, M., Robinson, G. W., Gilbertson, R. J., Cho, Y. J., Pomeroy, S. L., Korshunov, A., Lichter, P., Taylor, M. D., & Pfister, S. M. (2012, Dec). Medulloblastomics: the end of the beginning. *Nat Rev Cancer*, 12(12), 818-834. <https://doi.org/10.1038/nrc3410>
- Northcott, P. A., Korshunov, A., Witt, H., Hielscher, T., Eberhart, C. G., Mack, S., Bouffet, E., Clifford, S. C., Hawkins, C. E., French, P., Rutka, J. T., Pfister, S., & Taylor, M. D. (2011, Apr 10). Medulloblastoma comprises four distinct molecular variants. *J Clin Oncol*, 29(11), 1408-1414. <https://doi.org/10.1200/jco.2009.27.4324>
- Northcott, P. A., Shih, D. J., Peacock, J., Garzia, L., Sorana Morrissy, A., Zichner, T., Stütz, A. M., Korshunov, A., Reimand, J., & Schumacher, S. E. (2012). Subgroup-specific structural variation across 1,000 medulloblastoma genomes. *Nature*, 488(7409), 49-56.
- Oberheim Bush, N. A., & Chang, S. (2016, 2016/12/01). Treatment Strategies for Low-Grade Glioma in Adults. *Journal of Oncology Practice*, 12(12), 1235-1241. <https://doi.org/10.1200/JOP.2016.018622>
- Ogura, T., Alvarez, I. S., Vogel, A., Rodríguez, C., Evans, R. M., & Izpisua Belmonte, J. C. (1996, Feb). Evidence that Shh cooperates with a retinoic acid inducible co-factor to establish ZPA-like activity. *Development*, 122(2), 537-542. <https://doi.org/10.1242/dev.122.2.537>
- Ohgaki, H., & Kleihues, P. (2013, Feb 15). The definition of primary and secondary glioblastoma. *Clin Cancer Res*, 19(4), 764-772. <https://doi.org/10.1158/1078-0432.Ccr-12-3002>
- Okita, K., Ichisaka, T., & Yamanaka, S. (2007, Jul 19). Generation of germline-competent induced pluripotent stem cells. *Nature*, 448(7151), 313-317. <https://doi.org/10.1038/nature05934>

Literature

- Okita, K., Nakagawa, M., Hyenjong, H., Ichisaka, T., & Yamanaka, S. (2008, Nov 7). Generation of mouse induced pluripotent stem cells without viral vectors. *Science*, 322(5903), 949-953. <https://doi.org/10.1126/science.1164270>
- Onder, T. T., & Daley, G. Q. (2012). New lessons learned from disease modeling with induced pluripotent stem cells. *Current opinion in genetics & development*, 22(5), 500-508.
- Ostrom, Q. T., Gittleman, H., Liao, P., Rouse, C., Chen, Y., Dowling, J., Wolinsky, Y., Kruchko, C., & Barnholtz-Sloan, J. (2014). CBTRUS statistical report: primary brain and central nervous system tumors diagnosed in the United States in 2007-2011. *Neuro-Oncology*, 16 Suppl 4(Suppl 4), iv1-iv63. <https://doi.org/10.1093/neuonc/nou223>
- Packer, R. J., Sutton, L. N., Atkins, T. E., Radcliffe, J., Bunin, G. R., D'Angio, G., Siegel, K. R., & Schut, L. (1989, 01 Jan. 1989). A prospective study of cognitive function in children receiving whole-brain radiotherapy and chemotherapy: 2-year results. *Journal of Neurosurgery*, 70(5), 707-713. <https://doi.org/10.3171/jns.1989.70.5.0707>
- Pamies, D., Bal-Price, A., Simeonov, A., Tagle, D., Allen, D., Gerhold, D., Yin, D., Pistollato, F., Inutsuka, T., Sullivan, K., Stacey, G., Salem, H., Leist, M., Daneshian, M., Vemuri, M. C., McFarland, R., Coecke, S., Fitzpatrick, S. C., Lakshmipathy, U., Mack, A., Wang, W. B., Yamazaki, D., Sekino, Y., Kanda, Y., Smirnova, L., & Hartung, T. (2017). Good Cell Culture Practice for stem cells and stem-cell-derived models. *Altex*, 34(1), 95-132. <https://doi.org/10.14573/altex.1607121>
- Pan, E., Pellarin, M., Holmes, E., Smirnov, I., Misra, A., Eberhart, C. G., Burger, P. C., Biegel, J. A., & Feuerstein, B. G. (2005). Isochromosome 17q Is a Negative Prognostic Factor in Poor-Risk Childhood Medulloblastoma Patients. *Clinical Cancer Research*, 11(13), 4733-4740. <https://doi.org/10.1158/1078-0432.Ccr-04-0465>
- Pan, P. C., & Magge, R. S. (2020, Nov 11). Mechanisms of EGFR Resistance in Glioblastoma. *International journal of molecular sciences*, 21(22). <https://doi.org/10.3390/ijms21228471>
- Papapetrou, E. P. (2016). Patient-derived induced pluripotent stem cells in cancer research and precision oncology. *Nat Med*, 22(12), 1392-1401. <https://doi.org/10.1038/nm.4238>
- Papathanasiou, S., Markoulaki, S., Blaine, L. J., Leibowitz, M. L., Zhang, C.-Z., Jaenisch, R., & Pellman, D. (2021, 2021/10/06). Whole chromosome loss and genomic instability in mouse embryos after CRISPR-Cas9 genome editing. *Nat Commun*, 12(1), 5855. <https://doi.org/10.1038/s41467-021-26097-y>
- Park, D. J., Nakamura, H., Chumakov, A. M., Said, J. W., Miller, C. W., Chen, D. L., & Koeffler, H. P. (1994, Jul). Transactivational and DNA binding abilities of endogenous p53 in p53 mutant cell lines. *Oncogene*, 9(7), 1899-1906.
- Parsons, D. W., Li, M., Zhang, X., Jones, S., Leary, R. J., Lin, J. C.-H., Boca, S. M., Carter, H., Samayoa, J., Bettegowda, C., Gallia, G. L., Jallo, G. I., Binder, Z. A., Nikolsky, Y., Hartigan, J., Smith, D. R., Gerhard, D. S., Fults, D. W., VandenBerg, S., Berger, M. S., Marie, S. K. N., Shinjo, S. M. O., Clara, C., Phillips, P. C., Minturn, J. E., Biegel, J. A., Judkins, A. R., Resnick, A. C., Storm, P. B.,

Literature

- Curran, T., He, Y., Rasheed, B. A., Friedman, H. S., Keir, S. T., McLendon, R., Northcott, P. A., Taylor, M. D., Burger, P. C., Riggins, G. J., Karchin, R., Parmigiani, G., Bigner, D. D., Yan, H., Papadopoulos, N., Vogelstein, B., Kinzler, K. W., & Velculescu, V. E. (2011). The Genetic Landscape of the Childhood Cancer Medulloblastoma. *Science*, *331*(6016), 435-439. <https://doi.org/doi:10.1126/science.1198056>
- Phillips, H. S., Kharbanda, S., Chen, R., Forrest, W. F., Soriano, R. H., Wu, T. D., Misra, A., Nigro, J. M., Colman, H., Soroceanu, L., Williams, P. M., Modrusan, Z., Feuerstein, B. G., & Aldape, K. (2006, Mar). Molecular subclasses of high-grade glioma predict prognosis, delineate a pattern of disease progression, and resemble stages in neurogenesis. *Cancer Cell*, *9*(3), 157-173. <https://doi.org/10.1016/j.ccr.2006.02.019>
- Piotrowski, A. F., Puduvalli, V. K., Wen, P. Y., Campian, J. L., Colman, H., Pearlman, M. L., Butowski, N. A., Battiste, J., Glass, J. R., Cloughesy, T. F., Schiff, D., van den Bent, M. J., Walbert, T., Ahluwalia, M. S., Badruddoja, M. a., Kalra, A., Aregawi, D. G., Weller, M., Ramakrishnan, V., Zhang, K., Wood, K., Mellinghoff, I. K., & Shih, K. (2019). ACTR-39. PAMIPARIB IN COMBINATION WITH RADIATION THERAPY (RT) AND/OR TEMOZOLOMIDE (TMZ) IN PATIENTS WITH NEWLY DIAGNOSED OR RECURRENT/REFRACTORY (R/R) GLIOBLASTOMA (GBM); PHASE 1B/2 STUDY UPDATE. *Neuro-Oncology*.
- Pirona, A. C., Oktriani, R., Boettcher, M., & Hoheisel, J. D. (2020). Process for an efficient lentiviral cell transduction. *Biology Methods and Protocols*, *5*(1), bpaa005. <https://doi.org/10.1093/biomethods/bpaa005>
- Polireddy, K., Singh, K., Pruski, M., Jones, N. C., Manisundaram, N. V., Ponnella, P., Ouellette, M., Van Buren, G., Younes, M., Bynon, J. S., Dar, W. A., & Bailey, J. M. (2019, Jul 1). Mutant p53(R175H) promotes cancer initiation in the pancreas by stabilizing HSP70. *Cancer Lett*, *453*, 122-130. <https://doi.org/10.1016/j.canlet.2019.03.047>
- Porterfield, V. (2020, Feb/Mar). Neural Progenitor Cell Derivation Methodologies for Drug Discovery Applications. *Assay Drug Dev Technol*, *18*(2), 89-95. <https://doi.org/10.1089/adt.2019.921>
- Portet, S. (2020). A primer on model selection using the Akaike Information Criterion. *Infect Dis Model*, *5*, 111-128. <https://doi.org/10.1016/j.idm.2019.12.010>
- Price, S. J., & Gillard, J. H. (2011, Dec). Imaging biomarkers of brain tumour margin and tumour invasion. *Br J Radiol*, *84 Spec No 2*(Spec Iss 2), S159-167. <https://doi.org/10.1259/bjr/26838774>
- Prince, M. E., & Ailles, L. E. (2008, Jun 10). Cancer stem cells in head and neck squamous cell cancer. *J Clin Oncol*, *26*(17), 2871-2875. <https://doi.org/10.1200/jco.2007.15.1613>
- Qiu, J., Shi, Z., & Jiang, J. (2017, Jan). Cyclooxygenase-2 in glioblastoma multiforme. *Drug Discov Today*, *22*(1), 148-156. <https://doi.org/10.1016/j.drudis.2016.09.017>
- Quinlan, A., & Rizzolo, D. (2017). Understanding medulloblastoma. *Journal of the American Academy of PAs*, *30*(10).

Literature

https://journals.lww.com/jaapa/Fulltext/2017/10000/Understanding_medulloblastoma.7.aspx

R Development Core Team. (2010). *R: A language and environment for statistical computing* In R Foundation for Statistical Computing.

Ramaswamy, V., Remke, M., Bouffet, E., Faria, C. C., Perreault, S., Cho, Y. J., Shih, D. J., Luu, B., Dubuc, A. M., Northcott, P. A., Schüller, U., Gururangan, S., McLendon, R., Bigner, D., Fouladi, M., Ligon, K. L., Pomeroy, S. L., Dunn, S., Triscott, J., Jabado, N., Fontebasso, A., Jones, D. T., Kool, M., Karajannis, M. A., Gardner, S. L., Zagzag, D., Nunes, S., Pimentel, J., Mora, J., Lipp, E., Walter, A. W., Ryzhova, M., Zheludkova, O., Kumirova, E., Alshami, J., Croul, S. E., Rutka, J. T., Hawkins, C., Tabori, U., Codispori, K. E., Packer, R. J., Pfister, S. M., Korshunov, A., & Taylor, M. D. (2013, Nov). Recurrence patterns across medulloblastoma subgroups: an integrated clinical and molecular analysis. *Lancet Oncol*, *14*(12), 1200-1207. [https://doi.org/10.1016/s1470-2045\(13\)70449-2](https://doi.org/10.1016/s1470-2045(13)70449-2)

Ramaswamy, V., & Taylor, M. D. (2017, 2017/07/20). Medulloblastoma: From Myth to Molecular. *Journal of Clinical Oncology*, *35*(21), 2355-2363. <https://doi.org/10.1200/JCO.2017.72.7842>

Rao, C. S., & Karunakara, K. (2021, 2021/05/01). A comprehensive review on brain tumor segmentation and classification of MRI images. *Multimedia Tools and Applications*, *80*(12), 17611-17643. <https://doi.org/10.1007/s11042-020-10443-1>

Rapoport, S. I. (2001, Oct). Advances in osmotic opening of the blood-brain barrier to enhance CNS chemotherapy. *Expert Opin Investig Drugs*, *10*(10), 1809-1818. <https://doi.org/10.1517/13543784.10.10.1809>

Ray, S., Chaturvedi, N. K., Bhakat, K. K., Rizzino, A., & Mahapatra, S. (2021, Dec 28). Subgroup-Specific Diagnostic, Prognostic, and Predictive Markers Influencing Pediatric Medulloblastoma Treatment. *Diagnostics (Basel)*, *12*(1). <https://doi.org/10.3390/diagnostics12010061>

Raza, S. M., Lang, F. F., Aggarwal, B. B., Fuller, G. N., Wildrick, D. M., & Sawaya, R. (2002). Necrosis and Glioblastoma: A Friend or a Foe? A Review and a Hypothesis. *Neurosurgery*, *51*(1), 2-13. <https://doi.org/10.1097/00006123-200207000-00002>

Read, T. A., Fogarty, M. P., Markant, S. L., McLendon, R. E., Wei, Z., Ellison, D. W., Febbo, P. G., & Wechsler-Reya, R. J. (2009, Feb 3). Identification of CD15 as a marker for tumor-propagating cells in a mouse model of medulloblastoma. *Cancer Cell*, *15*(2), 135-147. <https://doi.org/10.1016/j.ccr.2008.12.016>

Reni, M., Ferreri, A. J. M., Landoni, C., & Villa, E. (2000). Salvage Therapy With Temozolomide in an Immunocompetent Patient With Primary Brain Lymphoma. *JNCI: Journal of the National Cancer Institute*, *92*(7), 575-576. <https://doi.org/10.1093/jnci/92.7.575>

Reya, T., Morrison, S. J., Clarke, M. F., & Weissman, I. L. (2001, Nov 1). Stem cells, cancer, and cancer stem cells. *Nature*, *414*(6859), 105-111. <https://doi.org/10.1038/35102167>

Literature

- Reynolds, B. A., Tetzlaff, W., & Weiss, S. (1992, Nov). A multipotent EGF-responsive striatal embryonic progenitor cell produces neurons and astrocytes. *J Neurosci*, *12*(11), 4565-4574. <https://doi.org/10.1523/jneurosci.12-11-04565.1992>
- Reynolds, B. A., & Weiss, S. (1992, Mar 27). Generation of neurons and astrocytes from isolated cells of the adult mammalian central nervous system. *Science*, *255*(5052), 1707-1710. <https://doi.org/10.1126/science.1553558>
- Rieber, J., Remke, M., Hartmann, C., Korshunov, A., Burkhardt, B., Sturm, D., Mechtersheimer, G., Wittmann, A., Greil, J., Blattmann, C., Witt, O., Behnisch, W., Halatsch, M. E., Orakcioglu, B., von Deimling, A., Lichter, P., Kulozik, A., & Pfister, S. (2009, Jul). Novel oncogene amplifications in tumors from a family with Li-Fraumeni syndrome. *Genes Chromosomes Cancer*, *48*(7), 558-568. <https://doi.org/10.1002/gcc.20665>
- Risau, W., & Wolburg, H. (1990, May). Development of the blood-brain barrier. *Trends Neurosci*, *13*(5), 174-178. [https://doi.org/10.1016/0166-2236\(90\)90043-a](https://doi.org/10.1016/0166-2236(90)90043-a)
- Ritz, C., Baty, F., Streibig, J. C., & Gerhard, D. (2015). Dose-Response Analysis Using R. *PLOS ONE*, *10*(12), e0146021. <https://doi.org/10.1371/journal.pone.0146021>
- Roberts, A. B., & Sporn, M. B. (1993). Physiological actions and clinical applications of transforming growth factor- β (TGF- β). *Growth factors*, *8*(1), 1-9.
- Romer, J., & Curran, T. (2005). Targeting Medulloblastoma: Small-Molecule Inhibitors of the Sonic Hedgehog Pathway as Potential Cancer Therapeutics. *Cancer Research*, *65*(12), 4975-4978. <https://doi.org/10.1158/0008-5472.CAN-05-0481>
- Roos, W. P., Batista, L. F. Z., Naumann, S. C., Wick, W., Weller, M., Menck, C. F. M., & Kaina, B. (2007, 2007/01/01). Apoptosis in malignant glioma cells triggered by the temozolomide-induced DNA lesion O6-methylguanine. *Oncogene*, *26*(2), 186-197. <https://doi.org/10.1038/sj.onc.1209785>
- Rossi, A., Caracciolo, V., Russo, G., Reiss, K., & Giordano, A. (2008). Medulloblastoma: from molecular pathology to therapy. *Clin Cancer Res*, *14*(4), 971-976. <https://doi.org/10.1158/1078-0432.CCR-07-2072>
- Rowe, R. G., & Daley, G. Q. (2019, 2019/07/01). Induced pluripotent stem cells in disease modelling and drug discovery. *Nature Reviews Genetics*, *20*(7), 377-388. <https://doi.org/10.1038/s41576-019-0100-z>
- Ruano, Y., Ribalta, T., de Lope, Á. R., Campos-Martín, Y., Fiaño, C., Pérez-Magán, E., Hernández-Moneo, J.-L., Mollejo, M., & Meléndez, B. (2009). Worse Outcome in Primary Glioblastoma Multiforme With Concurrent Epidermal Growth Factor Receptor and p53 Alteration. *American Journal of Clinical Pathology*, *131*(2), 257-263. <https://doi.org/10.1309/ajcp64ybdvctirwv>

Literature

- Rubinfeld, B., Souza, B., Albert, I., Müller, O., Chamberlain, S. H., Masiarz, F. R., Munemitsu, S., & Polakis, P. (1993, Dec 10). Association of the APC gene product with beta-catenin. *Science*, 262(5140), 1731-1734. <https://doi.org/10.1126/science.8259518>
- Rutkowski, S., Bode, U., Deinlein, F., Ottensmeier, H., Warmuth-Metz, M., Soerensen, N., Graf, N., Emser, A., Pietsch, T., & Wolff, J. E. (2005). Treatment of early childhood medulloblastoma by postoperative chemotherapy alone. *New England Journal of Medicine*, 352(10), 978-986.
- Rutkowski, S., von Hoff, K., Emser, A., Zwiener, I., Pietsch, T., Figarella-Branger, D., Giangaspero, F., Ellison, D. W., Garre, M. L., Biassoni, V., Grundy, R. G., Finlay, J. L., Dhall, G., Raquin, M. A., & Grill, J. (2010, Nov 20). Survival and prognostic factors of early childhood medulloblastoma: an international meta-analysis. *J Clin Oncol*, 28(33), 4961-4968. <https://doi.org/10.1200/jco.2010.30.2299>
- Saeidnia, S., Manayi, A., & Abdollahi, M. (2015). From in vitro Experiments to in vivo and Clinical Studies; Pros and Cons. *Current Drug Discovery Technologies*, 12(4), 218-224. <https://doi.org/http://dx.doi.org/10.2174/1570163813666160114093140>
- Sajó, I. (1977). Vinblastine inhibition of microtubule assembly in vitro. *Acta Biochim Biophys Acad Sci Hung*, 12(3), 259-261.
- Sanchez-Vega, F., Mina, M., Armenia, J., Chatila, W. K., Luna, A., La, K. C., Dimitriadoy, S., Liu, D. L., Kantheti, H. S., Saghafeina, S., Chakravarty, D., Daian, F., Gao, Q., Bailey, M. H., Liang, W. W., Foltz, S. M., Shmulevich, I., Ding, L., Heins, Z., Ochoa, A., Gross, B., Gao, J., Zhang, H., Kundra, R., Kandoth, C., Bahceci, I., Dervishi, L., Dogrusoz, U., Zhou, W., Shen, H., Laird, P. W., Way, G. P., Greene, C. S., Liang, H., Xiao, Y., Wang, C., Iavarone, A., Berger, A. H., Bivona, T. G., Lazar, A. J., Hammer, G. D., Giordano, T., Kwong, L. N., McArthur, G., Huang, C., Tward, A. D., Frederick, M. J., McCormick, F., Meyerson, M., Van Allen, E. M., Cherniack, A. D., Ciriello, G., Sander, C., & Schultz, N. (2018, Apr 5). Oncogenic Signaling Pathways in The Cancer Genome Atlas. *Cell*, 173(2), 321-337.e310. <https://doi.org/10.1016/j.cell.2018.03.035>
- Sanchis, A., Bayo, P., Sevilla, L. M., & Pérez, P. (2010). Glucocorticoid receptor antagonizes EGFR function to regulate eyelid development. *Int J Dev Biol*, 54(10), 1473-1480. <https://doi.org/10.1387/ijdb.103071as>
- Sanders, S., & Debinski, W. (2020, Apr 16). Challenges to Successful Implementation of the Immune Checkpoint Inhibitors for Treatment of Glioblastoma. *International journal of molecular sciences*, 21(8). <https://doi.org/10.3390/ijms21082759>
- Sasai, K., Romer, J. T., Lee, Y., Finkelstein, D., Fuller, C., McKinnon, P. J., & Curran, T. (2006). Shh Pathway Activity Is Down-Regulated in Cultured Medulloblastoma Cells: Implications for Preclinical Studies. *Cancer Research*, 66(8), 4215-4222. <https://doi.org/10.1158/0008-5472.CAN-05-4505>

Literature

- Sayed, N., Ameen, M., & Wu, J. C. (2019, Apr 15). Personalized medicine in cardio-oncology: the role of induced pluripotent stem cell. *Cardiovasc Res*, *115*(5), 949-959. <https://doi.org/10.1093/cvr/cvz024>
- Scheer, M., Leisz, S., Sorge, E., Storozhuk, O., Prell, J., Ho, I., & Harder, A. (2022). Neurofibromatosis Type 1 Gene Alterations Define Specific Features of a Subset of Glioblastomas. *International journal of molecular sciences*, *23*(1). <https://doi.org/10.3390/ijms23010352>
- Schiff, D., Brown, P. D., & Giannini, C. (2007). Outcome in adult low-grade glioma. *Neurology*, *69*(13), 1366. <https://doi.org/10.1212/01.wnl.0000277271.47601.a1>
- Schneider, C. A., Rasband, W. S., & Eliceiri, K. W. (2012). NIH Image to ImageJ: 25 years of image analysis. *Nature methods*, *9*(7), 671-675. <https://doi.org/10.1038/nmeth.2089>
- Schneider, R. A., Hu, D., Rubenstein, J. L. R., Maden, M., & Helms, J. A. (2001). Local retinoid signaling coordinates forebrain and facial morphogenesis by maintaining FGF8 and SHH. *Development*, *128*(14), 2755-2767. <https://doi.org/10.1242/dev.128.14.2755>
- Schopperle, W. M., & DeWolf, W. C. (2007, Mar). The TRA-1-60 and TRA-1-81 human pluripotent stem cell markers are expressed on podocalyxin in embryonal carcinoma. *Stem Cells*, *25*(3), 723-730. <https://doi.org/10.1634/stemcells.2005-0597>
- Schüller, U., Heine, V. M., Mao, J., Kho, A. T., Dillon, A. K., Han, Y. G., Huillard, E., Sun, T., Ligon, A. H., Qian, Y., Ma, Q., Alvarez-Buylla, A., McMahon, A. P., Rowitch, D. H., & Ligon, K. L. (2008, Aug 12). Acquisition of granule neuron precursor identity is a critical determinant of progenitor cell competence to form Shh-induced medulloblastoma. *Cancer Cell*, *14*(2), 123-134. <https://doi.org/10.1016/j.ccr.2008.07.005>
- Selich, A., Daudert, J., Hass, R., Philipp, F., von Kaisenberg, C., Paul, G., Cornils, K., Fehse, B., Rittinghausen, S., Schambach, A., & Rothe, M. (2016). Massive Clonal Selection and Transiently Contributing Clones During Expansion of Mesenchymal Stem Cell Cultures Revealed by Lentiviral RGB-Barcode Technology. *Stem Cells Translational Medicine*, *5*(5), 591-601. <https://doi.org/10.5966/sctm.2015-0176>
- Seshacharyulu, P., Ponnusamy, M. P., Haridas, D., Jain, M., Ganti, A. K., & Batra, S. K. (2012). Targeting the EGFR signaling pathway in cancer therapy. *Expert opinion on therapeutic targets*, *16*(1), 15-31.
- Sethi, G., Sung, B., & Aggarwal, B. B. (2008). TNF: a master switch for inflammation to cancer. *Frontiers in Bioscience-Landmark*, *13*(13), 5094-5107.
- Shah, N., Lin, B., Sibenaller, Z., Ryken, T., Lee, H., Yoon, J.-G., Rostad, S., & Foltz, G. (2011). Comprehensive Analysis of MGMT Promoter Methylation: Correlation with MGMT Expression and Clinical Response in GBM. *PLOS ONE*, *6*(1), e16146. <https://doi.org/10.1371/journal.pone.0016146>

Literature

- Shergalis, A., Bankhead, A., 3rd, Luesakul, U., Muangsin, N., & Neamati, N. (2018, Jul). Current Challenges and Opportunities in Treating Glioblastoma. *Pharmacol Rev*, *70*(3), 412-445. <https://doi.org/10.1124/pr.117.014944>
- Shikatani, E. A., Trifonova, A., Mandel, E. R., Liu, S. T. K., Roudier, E., Krylova, A., Szigiato, A., Beaudry, J., Riddell, M. C., & Haas, T. L. (2012). Inhibition of Proliferation, Migration and Proteolysis Contribute to Corticosterone-Mediated Inhibition of Angiogenesis. *PLOS ONE*, *7*(10), e46625. <https://doi.org/10.1371/journal.pone.0046625>
- Shukla, G., Alexander, G. S., Bakas, S., Nikam, R., Talekar, K., Palmer, J. D., & Shi, W. (2017). Advanced magnetic resonance imaging in glioblastoma: a review. *Chinese Clinical Oncology*, *6*(4), 7. <https://cco.amegroups.com/article/view/15820>
- Si, D., Yin, F., Peng, J., & Zhang, G. (2020). High Expression of CD44 Predicts a Poor Prognosis in Glioblastomas. *Cancer Manag Res*, *12*, 769-775. <https://doi.org/10.2147/cmar.S233423>
- Sidaway, P. (2017, 2017/10/01). Glioblastoma subtypes revisited. *Nature Reviews Clinical Oncology*, *14*(10), 587-587. <https://doi.org/10.1038/nrclinonc.2017.122>
- Sidhu, I., Barwe, S. P., Pillai, R. K., & Gopalakrishnapillai, A. (2021, Oct 9). Harnessing the Power of Induced Pluripotent Stem Cells and Gene Editing Technology: Therapeutic Implications in Hematological Malignancies. *Cells*, *10*(10). <https://doi.org/10.3390/cells10102698>
- Siegel, T., Rubinstein, R., Bokstein, F., Schwartz, A., Lossos, A., Shalom, E., Chisin, R., & Gomori, J. M. (2000, Apr). In vivo assessment of the window of barrier opening after osmotic blood-brain barrier disruption in humans. *J Neurosurg*, *92*(4), 599-605. <https://doi.org/10.3171/jns.2000.92.4.0599>
- Sigal, A., & Rotter, V. (2000). Oncogenic Mutations of the p53 Tumor Suppressor: The Demons of the Guardian of the Genome. *Cancer Research*, *60*(24), 6788-6793. <https://cancerres.aacrjournals.org/content/canres/60/24/6788.full.pdf>
- Simelyte, E., Rosengren, S., Boyle, D. L., Corr, M., Green, D. R., & Firestein, G. S. (2005, Jun). Regulation of arthritis by p53: critical role of adaptive immunity. *Arthritis Rheum*, *52*(6), 1876-1884. <https://doi.org/10.1002/art.21099>
- Simpson, F., Kerr, M. C., & Wicking, C. (2009, May-Jun). Trafficking, development and hedgehog. *Mech Dev*, *126*(5-6), 279-288. <https://doi.org/10.1016/j.mod.2009.01.007>
- Singh, S. K., Clarke, I. D., Terasaki, M., Bonn, V. E., Hawkins, C., Squire, J., & Dirks, P. B. (2003). Identification of a Cancer Stem Cell in Human Brain Tumors. *Cancer Research*, *63*(18), 5821. <http://cancerres.aacrjournals.org/content/63/18/5821.abstract>
- Singh, S. K., Hawkins, C., Clarke, I. D., Squire, J. A., Bayani, J., Hide, T., Henkelman, R. M., Cusimano, M. D., & Dirks, P. B. (2004, 2004/11/01). Identification of human brain tumour initiating cells. *Nature*, *432*(7015), 396-401. <https://doi.org/10.1038/nature03128>

Literature

- Somers, A., Jean, J. C., Sommer, C. A., Omari, A., Ford, C. C., Mills, J. A., Ying, L., Sommer, A. G., Jean, J. M., Smith, B. W., Lafyatis, R., Demierre, M. F., Weiss, D. J., French, D. L., Gadue, P., Murphy, G. J., Mostoslavsky, G., & Kotton, D. N. (2010, Oct). Generation of transgene-free lung disease-specific human induced pluripotent stem cells using a single excisable lentiviral stem cell cassette. *Stem Cells*, *28*(10), 1728-1740. <https://doi.org/10.1002/stem.495>
- SongTao, Q., Lei, Y., Si, G., YanQing, D., HuiXia, H., XueLin, Z., LanXiao, W., & Fei, Y. (2012, Feb). IDH mutations predict longer survival and response to temozolomide in secondary glioblastoma. *Cancer Sci*, *103*(2), 269-273. <https://doi.org/10.1111/j.1349-7006.2011.02134.x>
- Sonoda, Y., Saito, R., Kanamori, M., Kumabe, T., Uenohara, H., & Tominaga, T. (2014). The association of subventricular zone involvement at recurrence with survival after repeat surgery in patients with recurrent glioblastoma. *Neurologia medico-chirurgica*, *54*(4), 302-309. <https://doi.org/10.2176/nmc.oa.2013-0226>
- Spiller, S. E., Logsdon, N. J., Deckard, L. A., & Sontheimer, H. (2011). Inhibition of nuclear factor kappa-B signaling reduces growth in medulloblastoma in vivo. *BMC Cancer*, *11*, 136-136. <https://doi.org/10.1186/1471-2407-11-136>
- Stadtfeld, M., Nagaya, M., Utikal, J., Weir, G., & Hochedlinger, K. (2008). Induced pluripotent stem cells generated without viral integration. *Science*, *322*(5903), 945-949. <https://doi.org/10.1126/science.1162494>
- Stockslager, M. A., Malinowski, S., Touat, M., Yoon, J. C., Geduldig, J., Mirza, M., Kim, A. S., Wen, P. Y., Chow, K.-H., Ligon, K. L., & Manalis, S. R. (2021, 2021/10/05/). Functional drug susceptibility testing using single-cell mass predicts treatment outcome in patient-derived cancer neurosphere models. *Cell Reports*, *37*(1), 109788. <https://doi.org/https://doi.org/10.1016/j.celrep.2021.109788>
- Stuebaker, A. W., Kreofsky, C. R., Pierson, C. R., Russell, S. J., Galanis, E., & Raffel, C. (2010). Treatment of medulloblastoma with a modified measles virus. *Neuro-Oncology*, *12*(10), 1034-1042. <https://doi.org/10.1093/neuonc/noq057>
- Stupp, R., Hegi, M. E., Mason, W. P., van den Bent, M. J., Taphoorn, M. J., Janzer, R. C., Ludwin, S. K., Allgeier, A., Fisher, B., Belanger, K., Hau, P., Brandes, A. A., Gijtenbeek, J., Marosi, C., Vecht, C. J., Mokhtari, K., Wesseling, P., Villa, S., Eisenhauer, E., Gorlia, T., Weller, M., Lacombe, D., Cairncross, J. G., & Mirimanoff, R. O. (2009, May). Effects of radiotherapy with concomitant and adjuvant temozolomide versus radiotherapy alone on survival in glioblastoma in a randomised phase III study: 5-year analysis of the EORTC-NCIC trial. *Lancet Oncol*, *10*(5), 459-466. [https://doi.org/10.1016/s1470-2045\(09\)70025-7](https://doi.org/10.1016/s1470-2045(09)70025-7)
- Stupp, R., Mason, W. P., van den Bent, M. J., Weller, M., Fisher, B., Taphoorn, M. J., Belanger, K., Brandes, A. A., Marosi, C., Bogdahn, U., Curschmann, J., Janzer, R. C., Ludwin, S. K., Gorlia, T., Allgeier, A., Lacombe, D., Cairncross, J. G., Eisenhauer, E., & Mirimanoff, R. O. (2005, Mar 10). Radiotherapy plus concomitant and adjuvant temozolomide for glioblastoma. *N Engl J Med*, *352*(10), 987-996. <https://doi.org/10.1056/NEJMoa043330>

Literature

- Stupp, R., Taillibert, S., Kanner, A. A., Kesari, S., Steinberg, D. M., Toms, S. A., Taylor, L. P., Lieberman, F., Silvani, A., Fink, K. L., Barnett, G. H., Zhu, J. J., Henson, J. W., Engelhard, H. H., Chen, T. C., Tran, D. D., Sroubek, J., Tran, N. D., Hottinger, A. F., Landolfi, J., Desai, R., Caroli, M., Kew, Y., Honnorat, J., Idbaih, A., Kirson, E. D., Weinberg, U., Palti, Y., Hegi, M. E., & Ram, Z. (2015, Dec 15). Maintenance Therapy With Tumor-Treating Fields Plus Temozolomide vs Temozolomide Alone for Glioblastoma: A Randomized Clinical Trial. *Jama*, *314*(23), 2535-2543. <https://doi.org/10.1001/jama.2015.16669>
- Sturm, D., Witt, H., Hovestadt, V., Khuong-Quang, D. A., Jones, D. T., Konermann, C., Pfaff, E., Tönjes, M., Sill, M., Bender, S., Kool, M., Zapatka, M., Becker, N., Zucknick, M., Hielscher, T., Liu, X. Y., Fontebasso, A. M., Ryzhova, M., Albrecht, S., Jacob, K., Wolter, M., Ebinger, M., Schuhmann, M. U., van Meter, T., Frühwald, M. C., Hauch, H., Pekrun, A., Radlwimmer, B., Niehues, T., von Komorowski, G., Dürken, M., Kulozik, A. E., Madden, J., Donson, A., Foreman, N. K., Drissi, R., Fouladi, M., Scheurlen, W., von Deimling, A., Monoranu, C., Roggendorf, W., Herold-Mende, C., Unterberg, A., Kramm, C. M., Felsberg, J., Hartmann, C., Wiestler, B., Wick, W., Milde, T., Witt, O., Lindroth, A. M., Schwartzentruber, J., Faury, D., Fleming, A., Zakrzewska, M., Liberski, P. P., Zakrzewski, K., Hauser, P., Garami, M., Klekner, A., Bogner, L., Morrissy, S., Cavalli, F., Taylor, M. D., van Sluis, P., Koster, J., Versteeg, R., Volckmann, R., Mikkelsen, T., Aldape, K., Reifenberger, G., Collins, V. P., Majewski, J., Korshunov, A., Lichter, P., Plass, C., Jabado, N., & Pfister, S. M. (2012, Oct 16). Hotspot mutations in H3F3A and IDH1 define distinct epigenetic and biological subgroups of glioblastoma. *Cancer Cell*, *22*(4), 425-437. <https://doi.org/10.1016/j.ccr.2012.08.024>
- Su, L. K., Vogelstein, B., & Kinzler, K. W. (1993, Dec 10). Association of the APC tumor suppressor protein with catenins. *Science*, *262*(5140), 1734-1737. <https://doi.org/10.1126/science.8259519>
- Sugawa, N., Ekstrand, A. J., James, C. D., & Collins, V. P. (1990). Identical splicing of aberrant epidermal growth factor receptor transcripts from amplified rearranged genes in human glioblastomas. *Proceedings of the National Academy of Sciences*, *87*(21), 8602-8606.
- Sui, H., Zhu, L., Deng, W., & Li, Q. (2014). Epithelial-mesenchymal transition and drug resistance: role, molecular mechanisms, and therapeutic strategies. *Oncol Res Treat*, *37*(10), 584-589. <https://doi.org/10.1159/000367802>
- Sullivan, S., Stacey, G. N., Akazawa, C., Aoyama, N., Baptista, R., Bedford, P., Bennaceur Griscelli, A., Chandra, A., Elwood, N., Girard, M., Kawamata, S., Hanatani, T., Latsis, T., Lin, S., Ludwig, T. E., Malygina, T., Mack, A., Mountford, J. C., Noggle, S., Pereira, L. V., Price, J., Sheldon, M., Srivastava, A., Stachelscheid, H., Velayudhan, S. R., Ward, N. J., Turner, M. L., Barry, J., & Song, J. (2018, Oct). Quality control guidelines for clinical-grade human induced pluripotent stem cell lines. *Regen Med*, *13*(7), 859-866. <https://doi.org/10.2217/rme-2018-0095>
- Sung, H., Ferlay, J., Siegel, R. L., Laversanne, M., Soerjomataram, I., Jemal, A., & Bray, F. (2021, May). Global Cancer Statistics 2020: GLOBOCAN Estimates of Incidence and Mortality Worldwide for 36 Cancers in 185 Countries. *CA Cancer J Clin*, *71*(3), 209-249. <https://doi.org/10.3322/caac.21660>

Literature

- Susanto, E., Marin Navarro, A., Zhou, L., Sundström, A., van Bree, N., Stantic, M., Moslem, M., Taylor, J., Rietdijk, J., Zubillaga, V., Hübner, J.-M., Weishaupt, H., Wolfsberger, J., Alafuzoff, I., Nordgren, A., Magnaldo, T., Siesjö, P., Johnsen John, I., Kool, M., Tammimies, K., Darabi, A., Swartling Fredrik, J., Falk, A., & Wilhelm, M. (2020, 2020/08/18). Modeling SHH-driven medulloblastoma with patient iPS cell-derived neural stem cells. *Proceedings of the National Academy of Sciences*, *117*(33), 20127-20138. <https://doi.org/10.1073/pnas.1920521117>
- Sutlu, T., Nyström, S., Gilljam, M., Stellan, B., Applequist, S. E., & Alici, E. (2012, 2012/10/01). Inhibition of Intracellular Antiviral Defense Mechanisms Augments Lentiviral Transduction of Human Natural Killer Cells: Implications for Gene Therapy. *Human Gene Therapy*, *23*(10), 1090-1100. <https://doi.org/10.1089/hum.2012.080>
- Suwala, A. K., Koch, K., Rios, D. H., Aretz, P., Uhlmann, C., Ogorek, I., Felsberg, J., Reifenberger, G., Köhrer, K., Deenen, R., Steiger, H. J., Kahlert, U. D., & Maciaczyk, J. (2018, Apr 27). Inhibition of Wnt/beta-catenin signaling downregulates expression of aldehyde dehydrogenase isoform 3A1 (ALDH3A1) to reduce resistance against temozolomide in glioblastoma in vitro. *Oncotarget*, *9*(32), 22703-22716. <https://doi.org/10.18632/oncotarget.25210>
- Suzuki, S., Iben, J. R., Coon, S. L., & Kino, T. (2018, Feb 5). SIRT1 is a transcriptional enhancer of the glucocorticoid receptor acting independently to its deacetylase activity. *Mol Cell Endocrinol*, *461*, 178-187. <https://doi.org/10.1016/j.mce.2017.09.012>
- Taal, W., Oosterkamp, H. M., Walenkamp, A. M., Dubbink, H. J., Beerepoot, L. V., Hanse, M. C., Buter, J., Honkoop, A. H., Boerman, D., de Vos, F. Y., Dinjens, W. N., Enting, R. H., Taphoorn, M. J., van den Berkmortel, F. W., Jansen, R. L., Brandsma, D., Bromberg, J. E., van Heuvel, I., Vernhout, R. M., van der Holt, B., & van den Bent, M. J. (2014, Aug). Single-agent bevacizumab or lomustine versus a combination of bevacizumab plus lomustine in patients with recurrent glioblastoma (BELOB trial): a randomised controlled phase 2 trial. *Lancet Oncol*, *15*(9), 943-953. [https://doi.org/10.1016/s1470-2045\(14\)70314-6](https://doi.org/10.1016/s1470-2045(14)70314-6)
- Takahashi, K., Tanabe, K., Ohnuki, M., Narita, M., Ichisaka, T., Tomoda, K., & Yamanaka, S. (2007, Nov 30). Induction of pluripotent stem cells from adult human fibroblasts by defined factors. *Cell*, *131*(5), 861-872. <https://doi.org/10.1016/j.cell.2007.11.019>
- Takahashi, K., & Yamanaka, S. (2006, Aug 25). Induction of pluripotent stem cells from mouse embryonic and adult fibroblast cultures by defined factors. *Cell*, *126*(4), 663-676. <https://doi.org/10.1016/j.cell.2006.07.024>
- Takebe, N., Harris, P. J., Warren, R. Q., & Ivy, S. P. (2011, 2011/02/01). Targeting cancer stem cells by inhibiting Wnt, Notch, and Hedgehog pathways. *Nature Reviews Clinical Oncology*, *8*(2), 97-106. <https://doi.org/10.1038/nrclinonc.2010.196>
- Taylor, M. D., Liu, L., Raffel, C., Hui, C. C., Mainprize, T. G., Zhang, X., Agatep, R., Chiappa, S., Gao, L., Lowrance, A., Hao, A., Goldstein, A. M., Stavrou, T., Scherer, S. W., Dura, W. T., Wainwright, B., Squire, J. A., Rutka, J. T., & Hogg, D. (2002, Jul). Mutations in SUFU predispose to medulloblastoma. *Nat Genet*, *31*(3), 306-310. <https://doi.org/10.1038/ng916>

Literature

- Taylor, M. D., Northcott, P. A., Korshunov, A., Remke, M., Cho, Y. J., Clifford, S. C., Eberhart, C. G., Parsons, D. W., Rutkowski, S., Gajjar, A., Ellison, D. W., Lichter, P., Gilbertson, R. J., Pomeroy, S. L., Kool, M., & Pfister, S. M. (2012, Apr). Molecular subgroups of medulloblastoma: the current consensus. *Acta Neuropathol*, *123*(4), 465-472. <https://doi.org/10.1007/s00401-011-0922-z>
- Taylor, R. E., Bailey, C. C., Robinson, K., Weston, C. L., Ellison, D., Ironside, J., Lucraft, H., Gilbertson, R., Tait, D. M., & Walker, D. A. (2003). Results of a randomized study of preradiation chemotherapy versus radiotherapy alone for nonmetastatic medulloblastoma: The International Society of Paediatric Oncology/United Kingdom Children's Cancer Study Group PNET-3 Study. *Journal of Clinical Oncology*, *21*(8), 1581-1591.
- Thiery, J. P. (2002, Jun). Epithelial-mesenchymal transitions in tumour progression. *Nat Rev Cancer*, *2*(6), 442-454. <https://doi.org/10.1038/nrc822>
- Thompson, E. M., Ashley, D., & Landi, D. (2020, Apr). Current medulloblastoma subgroup specific clinical trials. *Transl Pediatr*, *9*(2), 157-162. <https://doi.org/10.21037/tp.2020.03.03>
- Thompson, M. C., Fuller, C., Hogg, T. L., Dalton, J., Finkelstein, D., Lau, C. C., Chintagumpala, M., Adesina, A., Ashley, D. M., Kellie, S. J., Taylor, M. D., Curran, T., Gajjar, A., & Gilbertson, R. J. (2006, Apr 20). Genomics identifies medulloblastoma subgroups that are enriched for specific genetic alterations. *J Clin Oncol*, *24*(12), 1924-1931. <https://doi.org/10.1200/jco.2005.04.4974>
- Tigges, J., Bielec, K., Brockerhoff, G., Hildebrandt, B., Hübenthal, U., Kapr, J., Koch, K., Teichweyde, N., Wieczorek, D., Rossi, A., & Fritsche, E. (2021). Academic application of Good Cell Culture Practice for induced pluripotent stem cells. *Altex*, *38*(4), 595-614. <https://doi.org/10.14573/altex.2101221>
- Tishler, R. B., & Lamppu, D. M. (1996, Jul). The interaction of taxol and vinblastine with radiation induction of p53 and p21 WAF1/CIP1. *Br J Cancer Suppl*, *27*, S82-85.
- Tishler, R. B., Lamppu, D. M., Park, S., & Price, B. D. (1995). Microtubule-active Drugs Taxol, Vinblastine, and Nocodazole Increase the Levels of Transcriptionally Active p53. *Cancer Research*, *55*(24), 6021. <http://cancerres.aacrjournals.org/content/55/24/6021.abstract>
- Tiwary, S., Morales, J. E., Kwiatkowski, S. C., Lang, F. F., Rao, G., & McCarty, J. H. (2018, 2018/05/29). Metastatic Brain Tumors Disrupt the Blood-Brain Barrier and Alter Lipid Metabolism by Inhibiting Expression of the Endothelial Cell Fatty Acid Transporter Mfsd2a. *Scientific Reports*, *8*(1), 8267. <https://doi.org/10.1038/s41598-018-26636-6>
- Trimboli, A. J., Fukino, K., de Bruin, A., Wei, G., Shen, L., Tanner, S. M., Creasap, N., Rosol, T. J., Robinson, M. L., Eng, C., Ostrowski, M. C., & Leone, G. (2008, Feb 1). Direct evidence for epithelial-mesenchymal transitions in breast cancer. *Cancer Res*, *68*(3), 937-945. <https://doi.org/10.1158/0008-5472.Can-07-2148>

Literature

- Uchida, N., Buck, D. W., He, D., Reitsma, M. J., Masek, M., Phan, T. V., Tsukamoto, A. S., Gage, F. H., & Weissman, I. L. (2000, Dec 19). Direct isolation of human central nervous system stem cells. *Proceedings of the National Academy of Sciences of the United States of America*, *97*(26), 14720-14725. <https://doi.org/10.1073/pnas.97.26.14720>
- Uemura, T., Takamatsu, K., Ikeda, M., Okada, M., Kazuki, K., Ikada, Y., & Nakamura, H. (2012, Mar 2). Transplantation of induced pluripotent stem cell-derived neurospheres for peripheral nerve repair. *Biochem Biophys Res Commun*, *419*(1), 130-135. <https://doi.org/10.1016/j.bbrc.2012.01.154>
- Uhlmann, C., Kuhn, L. M., Tigges, J., Fritsche, E., & Kahlert, U. D. (2020, Mar). Efficient Modulation of TP53 Expression in Human Induced Pluripotent Stem Cells. *Curr Protoc Stem Cell Biol*, *52*(1), e102. <https://doi.org/10.1002/cpsc.102>
- Valent, P., Bonnet, D., De Maria, R., Lapidot, T., Copland, M., Melo, J. V., Chomienne, C., Ishikawa, F., Schuringa, J. J., Stassi, G., Huntly, B., Herrmann, H., Soulier, J., Roesch, A., Schuurhuis, G. J., Wöhrer, S., Arock, M., Zuber, J., Cerny-Reiterer, S., Johnsen, H. E., Andreeff, M., & Eaves, C. (2012, 2012/11/01). Cancer stem cell definitions and terminology: the devil is in the details. *Nature Reviews Cancer*, *12*(11), 767-775. <https://doi.org/10.1038/nrc3368>
- van der Sanden, B., Dhobb, M., Berger, F., & Wion, D. (2010, Nov 1). Optimizing stem cell culture. *J Cell Biochem*, *111*(4), 801-807. <https://doi.org/10.1002/jcb.22847>
- Vatanmakanian, M., Yousefi, H., Mashouri, L., Aref, A. R., Khamisipour, G., Bitaraf, A., & Alizadeh, S. (2019, Oct). Generation of Induced Pluripotent Cancer Cells from Glioblastoma Multiform Cell Lines. *Cell Reprogram*, *21*(5), 238-248. <https://doi.org/10.1089/cell.2019.0046>
- Veeranki, S., & Choubey, D. (2010). Systemic lupus erythematosus and increased risk to develop B cell malignancies: role of the p200-family proteins. *Immunology letters*, *133*(1), 1-5. <https://doi.org/10.1016/j.imlet.2010.06.008>
- Verger, A., & Langen, K. J. (2017). PET Imaging in Glioblastoma: Use in Clinical Practice. In S. De Vleeschouwer (Ed.), *Glioblastoma*. Codon Publications
- Copyright: The Authors. <https://doi.org/10.15586/codon.glioblastoma.2017.ch9>
- Verhaak, R. G., Hoadley, K. A., Purdom, E., Wang, V., Qi, Y., Wilkerson, M. D., Miller, C. R., Ding, L., Golub, T., Mesirov, J. P., Alexe, G., Lawrence, M., O'Kelly, M., Tamayo, P., Weir, B. A., Gabriel, S., Winckler, W., Gupta, S., Jakkula, L., Feiler, H. S., Hodgson, J. G., James, C. D., Sarkaria, J. N., Brennan, C., Kahn, A., Spellman, P. T., Wilson, R. K., Speed, T. P., Gray, J. W., Meyerson, M., Getz, G., Perou, C. M., & Hayes, D. N. (2010, Jan 19). Integrated genomic analysis identifies clinically relevant subtypes of glioblastoma characterized by abnormalities in PDGFRA, IDH1, EGFR, and NF1. *Cancer Cell*, *17*(1), 98-110. <https://doi.org/10.1016/j.ccr.2009.12.020>
- Visvader, J. E., & Lindeman, G. J. (2008, Oct). Cancer stem cells in solid tumours: accumulating evidence and unresolved questions. *Nat Rev Cancer*, *8*(10), 755-768. <https://doi.org/10.1038/nrc2499>

Literature

- Vladoiu, M. C., El-Hamamy, I., Donovan, L. K., Farooq, H., Holgado, B. L., Sundaravadanam, Y., Ramaswamy, V., Hendrikse, L. D., Kumar, S., Mack, S. C., Lee, J. J. Y., Fong, V., Juraschka, K., Przelicki, D., Michealraj, A., Skowron, P., Luu, B., Suzuki, H., Morrissy, A. S., Cavalli, F. M. G., Garzia, L., Daniels, C., Wu, X., Qazi, M. A., Singh, S. K., Chan, J. A., Marra, M. A., Malkin, D., Dirks, P., Heisler, L., Pugh, T., Ng, K., Notta, F., Thompson, E. M., Kleinman, C. L., Joyner, A. L., Jabado, N., Stein, L., & Taylor, M. D. (2019, Aug). Childhood cerebellar tumours mirror conserved fetal transcriptional programs. *Nature*, *572*(7767), 67-73. <https://doi.org/10.1038/s41586-019-1158-7>
- Wang, J., Wakeman, T. P., Lathia, J. D., Hjelmeland, A. B., Wang, X. F., White, R. R., Rich, J. N., & Sullenger, B. A. (2010, Jan). Notch promotes radioresistance of glioma stem cells. *Stem Cells*, *28*(1), 17-28. <https://doi.org/10.1002/stem.261>
- Wang, X., & Lin, Y. (2008, Nov). Tumor necrosis factor and cancer, buddies or foes? *Acta Pharmacol Sin*, *29*(11), 1275-1288. <https://doi.org/10.1111/j.1745-7254.2008.00889.x>
- Ward, E., DeSantis, C., Robbins, A., Kohler, B., & Jemal, A. (2014, Mar-Apr). Childhood and adolescent cancer statistics, 2014. *CA Cancer J Clin*, *64*(2), 83-103. <https://doi.org/10.3322/caac.21219>
- Warren, J. L., & MacIver, N. J. (2019, 2019-July-11). Regulation of Adaptive Immune Cells by Sirtuins [Review]. *Frontiers in Endocrinology*, *10*. <https://doi.org/10.3389/fendo.2019.00466>
- Warwick, O. H., Darte, J. M., Brown, T. C., Beer, C. T., Cutts, J. H., & Noble, R. L. (1960, Aug). Some biological effects of Vincaloblastine, an alkaloid in *Vinca rosea* Linn in patients with malignant disease. *Cancer Res*, *20*, 1032-1040.
- Waszak, S. M., Northcott, P. A., Buchhalter, I., Robinson, G. W., Sutter, C., Groebner, S., Grund, K. B., Brugières, L., Jones, D. T. W., Pajtler, K. W., Morrissy, A. S., Kool, M., Sturm, D., Chavez, L., Ernst, A., Brabetz, S., Hain, M., Zichner, T., Segura-Wang, M., Weischenfeldt, J., Rausch, T., Mardin, B. R., Zhou, X., Baciu, C., Lawerenz, C., Chan, J. A., Varlet, P., Guerrini-Rousseau, L., Fults, D. W., Grajkowska, W., Hauser, P., Jabado, N., Ra, Y. S., Zitterbart, K., Shringarpure, S. S., De La Vega, F. M., Bustamante, C. D., Ng, H. K., Perry, A., MacDonald, T. J., Hernáiz Driever, P., Bendel, A. E., Bowers, D. C., McCowage, G., Chintagumpala, M. M., Cohn, R., Hassall, T., Fleischhack, G., Eggen, T., Wesenberg, F., Feychting, M., Lannering, B., Schüz, J., Johansen, C., Andersen, T. V., Röösl, M., Kuehni, C. E., Grotzer, M., Kjaerheim, K., Monoranu, C. M., Archer, T. C., Duke, E., Pomeroy, S. L., Shelagh, R., Frank, S., Sumerauer, D., Scheurlen, W., Ryzhova, M. V., Milde, T., Kratz, C. P., Samuel, D., Zhang, J., Solomon, D. A., Marra, M., Eils, R., Bartram, C. R., von Hoff, K., Rutkowski, S., Ramaswamy, V., Gilbertson, R. J., Korshunov, A., Taylor, M. D., Lichter, P., Malkin, D., Gajjar, A., Korbel, J. O., & Pfister, S. M. (2018, Jun). Spectrum and prevalence of genetic predisposition in medulloblastoma: a retrospective genetic study and prospective validation in a clinical trial cohort. *Lancet Oncol*, *19*(6), 785-798. [https://doi.org/10.1016/s1470-2045\(18\)30242-0](https://doi.org/10.1016/s1470-2045(18)30242-0)
- Watanabe, K., Tachibana, O., Sata, K., Yonekawa, Y., Kleihues, P., & Ohgaki, H. (1996, Jul). Overexpression of the EGF receptor and p53 mutations are mutually exclusive in the evolution of primary and secondary glioblastomas. *Brain Pathol*, *6*(3), 217-223; discussion 223-214. <https://doi.org/10.1111/j.1750-3639.1996.tb00848.x>

Literature

- Webster, J. D., & Vucic, D. (2020). The Balance of TNF Mediated Pathways Regulates Inflammatory Cell Death Signaling in Healthy and Diseased Tissues. *Front Cell Dev Biol*, *8*, 365. <https://doi.org/10.3389/fcell.2020.00365>
- Weil, M., Jacobson, M. D., Coles, H. S., Davies, T. J., Gardner, R. L., Raff, K. D., & Raff, M. C. (1996, Jun). Constitutive expression of the machinery for programmed cell death. *J Cell Biol*, *133*(5), 1053-1059. <https://doi.org/10.1083/jcb.133.5.1053>
- Weller, M., Cloughesy, T., Perry, J. R., & Wick, W. (2013, Jan). Standards of care for treatment of recurrent glioblastoma--are we there yet? *Neuro Oncol*, *15*(1), 4-27. <https://doi.org/10.1093/neuonc/nos273>
- Wert, G. d., & Mummery, C. (2003). Human embryonic stem cells: research, ethics and policy. *Human reproduction*, *18*(4), 672-682.
- Whitelaw, D. M., & Teasdale, J. M. (1961, Sep 2). Vincalokoblastine in the treatment of malignant disease. *Can Med Assoc J*, *85*(10), 584-591.
- WHO Classification of Tumours Editorial Board. (2021). *World Health Organization Classification of Tumours of the Central Nervous System* (5th ed., Vol. 6). International Agency for Research on Cancer.
- Willis, A., Jung, E. J., Wakefield, T., & Chen, X. (2004, 2004/03/01). Mutant p53 exerts a dominant negative effect by preventing wild-type p53 from binding to the promoter of its target genes. *Oncogene*, *23*(13), 2330-2338. <https://doi.org/10.1038/sj.onc.1207396>
- Wilne, S. H., Ferris, R. C., Nathwani, A., & Kennedy, C. R. (2006). The presenting features of brain tumours: a review of 200 cases. *Archives of Disease in Childhood*, *91*(6), 502. <https://doi.org/10.1136/adc.2005.090266>
- Wilson, T. A., Karajannis, M. A., & Harter, D. H. (2014). Glioblastoma multiforme: State of the art and future therapeutics. *Surg Neurol Int*, *5*, 64. <https://doi.org/10.4103/2152-7806.132138>
- Wirsching, H. G., Galanis, E., & Weller, M. (2016). Glioblastoma. *Handb Clin Neurol*, *134*, 381-397. <https://doi.org/10.1016/b978-0-12-802997-8.00023-2>
- Wishart, D. S., Knox, C., Guo, A. C., Shrivastava, S., Hassanali, M., Stothard, P., Chang, Z., & Woolsey, J. (2006). DrugBank: a comprehensive resource for in silico drug discovery and exploration. *Nucleic Acids Res*, *34*(suppl_1), D668-D672. <https://doi.org/10.1093/nar/gkj067>
- Wong, A. J., Bigner, S. H., Bigner, D. D., Kinzler, K. W., Hamilton, S. R., & Vogelstein, B. (1987). Increased expression of the epidermal growth factor receptor gene in malignant gliomas is invariably associated with gene amplification. *Proceedings of the National Academy of Sciences*, *84*(19), 6899-6903.

Literature

- Xiao, H., Bid, H. K., Jou, D., Wu, X., Yu, W., Li, C., Houghton, P. J., & Lin, J. (2015). A Novel Small Molecular STAT3 Inhibitor, LY5, Inhibits Cell Viability, Cell Migration, and Angiogenesis in Medulloblastoma Cells *. *Journal of Biological Chemistry*, 290(6), 3418-3429. <https://doi.org/10.1074/jbc.M114.616748>
- Yan, H., Parsons, D. W., Jin, G., McLendon, R., Rasheed, B. A., Yuan, W., Kos, I., Batinic-Haberle, I., Jones, S., & Riggins, G. J. (2009). IDH1 and IDH2 mutations in gliomas. *New England Journal of Medicine*, 360(8), 765-773.
- Yan, X. Z., van den Beucken, J. J., Both, S. K., Yang, P. S., Jansen, J. A., & Yang, F. (2014, Aug). Biomaterial strategies for stem cell maintenance during in vitro expansion. *Tissue Eng Part B Rev*, 20(4), 340-354. <https://doi.org/10.1089/ten.TEB.2013.0349>
- Yang, W., Soares, J., Greninger, P., Edelman, E. J., Lightfoot, H., Forbes, S., Bindal, N., Beare, D., Smith, J. A., Thompson, I. R., Ramaswamy, S., Futreal, P. A., Haber, D. A., Stratton, M. R., Benes, C., McDermott, U., & Garnett, M. J. (2013, Jan). Genomics of Drug Sensitivity in Cancer (GDSC): a resource for therapeutic biomarker discovery in cancer cells. *Nucleic Acids Res*, 41(Database issue), D955-961. <https://doi.org/10.1093/nar/gks1111>
- Yang, Z. J., Ellis, T., Markant, S. L., Read, T. A., Kessler, J. D., Bourbonoulas, M., Schüller, U., Machold, R., Fishell, G., Rowitch, D. H., Wainwright, B. J., & Wechsler-Reya, R. J. (2008, Aug 12). Medulloblastoma can be initiated by deletion of Patched in lineage-restricted progenitors or stem cells. *Cancer Cell*, 14(2), 135-145. <https://doi.org/10.1016/j.ccr.2008.07.003>
- Yao, M., Li, S., Wu, X., Diao, S., Zhang, G., He, H., Bian, L., & Lu, Y. (2018, 2018/08/01). Cellular origin of glioblastoma and its implication in precision therapy. *Cellular & Molecular Immunology*, 15(8), 737-739. <https://doi.org/10.1038/cmi.2017.159>
- Yee, J. (2010). Turning somatic cells into pluripotent stem cells. *Nature Education*, 3(9), 25.
- Yi, J., & Luo, J. (2010). SIRT1 and p53, effect on cancer, senescence and beyond. *Biochimica et biophysica acta*, 1804(8), 1684-1689. <https://doi.org/10.1016/j.bbapap.2010.05.002>
- Yoon, K. S., Lee, M. C., Kang, S. S., Kim, J. H., Jung, S., Kim, Y. J., Lee, J. H., Ahn, K. Y., Lee, J. S., & Cheon, J. Y. (2001, Aug). p53 mutation and epidermal growth factor receptor overexpression in glioblastoma. *J Korean Med Sci*, 16(4), 481-488. <https://doi.org/10.3346/jkms.2001.16.4.481>
- Yu, F., Yuan, Y., Li, D., Kou, Y., Jiang, B., & Zhang, P. (2019, Jan). The effect of lentivirus-mediated SIRT1 gene knockdown in the ATDC5 cell line via inhibition of the Wnt signaling pathway. *Cell Signal*, 53, 80-89. <https://doi.org/10.1016/j.cellsig.2018.09.016>
- Yu, J., Vodyanik, M. A., Smuga-Otto, K., Antosiewicz-Bourget, J., Frane, J. L., Tian, S., Nie, J., Jonsdottir, G. A., Ruotti, V., Stewart, R., Slukvin, I., & Thomson, J. A. (2007, Dec 21). Induced pluripotent stem cell lines derived from human somatic cells. *Science*, 318(5858), 1917-1920. <https://doi.org/10.1126/science.1151526>

Literature

- Yu, K. K.-H., Taylor, J. T., Pathmanaban, O. N., Youshani, A. S., Beyit, D., Dutko-Gwozdz, J., Benson, R., Griffiths, G., Peers, I., Cueppens, P., Telfer, B. A., Williams, K. J., McBain, C., Kamaly-Asl, I. D., & Bigger, B. W. (2018). High content screening of patient-derived cell lines highlights the potential of non-standard chemotherapeutic agents for the treatment of glioblastoma. *PLOS ONE*, *13*(3), e0193694. <https://doi.org/10.1371/journal.pone.0193694>
- Yuan, B., Wang, G., Tang, X., Tong, A., & Zhou, L. (2022, Mar 28). Immunotherapy of glioblastoma: recent advances and future prospects. *Hum Vaccin Immunother*, *1*-16. <https://doi.org/10.1080/21645515.2022.2055417>
- Yuan, X., Curtin, J., Xiong, Y., Liu, G., Waschmann-Hogiu, S., Farkas, D. L., Black, K. L., & Yu, J. S. (2004, Dec 16). Isolation of cancer stem cells from adult glioblastoma multiforme. *Oncogene*, *23*(58), 9392-9400. <https://doi.org/10.1038/sj.onc.1208311>
- Zahumenska, R., Nosal, V., Smolar, M., Okajcekova, T., Skovierova, H., Strnadel, J., & Halasova, E. (2020, Nov 24). Induced Pluripotency: A Powerful Tool for In Vitro Modeling. *International journal of molecular sciences*, *21*(23). <https://doi.org/10.3390/ijms21238910>
- Zeltner, N., & Studer, L. (2015). Pluripotent stem cell-based disease modeling: current hurdles and future promise. *Current opinion in cell biology*, *37*, 102-110.
- Zeltzer, P. M., Boyett, J. M., Finlay, J. L., Albright, A. L., Rorke, L. B., Milstein, J. M., Allen, J. C., Stevens, K. R., Stanley, P., Li, H., Wisoff, J. H., Geyer, J. R., McGuire-Cullen, P., Stehbens, J. A., Shurin, S. B., & Packer, R. J. (1999, Mar). Metastasis stage, adjuvant treatment, and residual tumor are prognostic factors for medulloblastoma in children: conclusions from the Children's Cancer Group 921 randomized phase III study. *J Clin Oncol*, *17*(3), 832-845. <https://doi.org/10.1200/jco.1999.17.3.832>
- Zhang, C., Liu, J., Zhong, J. F., & Zhang, X. (2017, 2017/06/24). Engineering CAR-T cells. *Biomarker Research*, *5*(1), 22. <https://doi.org/10.1186/s40364-017-0102-y>
- Zhang, J., Stevens, M. F., & Bradshaw, T. D. (2012, Jan). Temozolomide: mechanisms of action, repair and resistance. *Curr Mol Pharmacol*, *5*(1), 102-114. <https://doi.org/10.2174/1874467211205010102>
- Zhang, Y., Dube, C., Gibert, M., Jr., Cruickshanks, N., Wang, B., Coughlan, M., Yang, Y., Setiady, I., Deveau, C., Saoud, K., Grello, C., Oxford, M., Yuan, F., & Abounader, R. (2018, Sep 1). The p53 Pathway in Glioblastoma. *Cancers (Basel)*, *10*(9). <https://doi.org/10.3390/cancers10090297>
- Zhao, J. (2016). Cancer stem cells and chemoresistance: The smartest survives the raid. *Pharmacol Ther*, *160*, 145-158.
- Zheng, S.-J., Lamhamedi-Cherradi, S.-E., Wang, P., Xu, L., & Chen, Y. H. (2005). Tumor Suppressor p53 Inhibits Autoimmune Inflammation and Macrophage Function. *Diabetes*, *54*(5), 1423-1428. <https://doi.org/10.2337/diabetes.54.5.1423>

Literature

- Zhou, T., Benda, C., Duzinger, S., Huang, Y., Li, X., Li, Y., Guo, X., Cao, G., Chen, S., Hao, L., Chan, Y. C., Ng, K. M., Ho, J. C., Wieser, M., Wu, J., Redl, H., Tse, H. F., Grillari, J., Grillari-Voglauer, R., Pei, D., & Esteban, M. A. (2011, Jul). Generation of induced pluripotent stem cells from urine. *J Am Soc Nephrol*, *22*(7), 1221-1228. <https://doi.org/10.1681/asn.2011010106>
- Zhou, Y.-y., & Zeng, F. (2013, 2013/10/01/). Integration-free Methods for Generating Induced Pluripotent Stem Cells. *Genomics, Proteomics & Bioinformatics*, *11*(5), 284-287. <https://doi.org/https://doi.org/10.1016/j.gpb.2013.09.008>
- Zhukova, N., Ramaswamy, V., Remke, M., Pfaff, E., Shih, D. J., Martin, D. C., Castelo-Branco, P., Baskin, B., Ray, P. N., Bouffet, E., von Bueren, A. O., Jones, D. T., Northcott, P. A., Kool, M., Sturm, D., Pugh, T. J., Pomeroy, S. L., Cho, Y. J., Pietsch, T., Gessi, M., Rutkowski, S., Bogнар, L., Klekner, A., Cho, B. K., Kim, S. K., Wang, K. C., Eberhart, C. G., Fevre-Montange, M., Fouladi, M., French, P. J., Kros, M., Grajkowska, W. A., Gupta, N., Weiss, W. A., Hauser, P., Jabado, N., Jouvett, A., Jung, S., Kumabe, T., Lach, B., Leonard, J. R., Rubin, J. B., Liau, L. M., Massimi, L., Pollack, I. F., Shin Ra, Y., Van Meir, E. G., Zitterbart, K., Schuller, U., Hill, R. M., Lindsey, J. C., Schwalbe, E. C., Bailey, S., Ellison, D. W., Hawkins, C., Malkin, D., Clifford, S. C., Korshunov, A., Pfister, S., Taylor, M. D., & Tabori, U. (2013, Aug 10). Subgroup-specific prognostic implications of TP53 mutation in medulloblastoma. *J Clin Oncol*, *31*(23), 2927-2935. <https://doi.org/10.1200/jco.2012.48.5052>
- Zimmer, B., Kuegler, P. B., Baudis, B., Genewsky, A., Tanavde, V., Koh, W., Tan, B., Waldmann, T., Kadereit, S., & Leist, M. (2011). Coordinated waves of gene expression during neuronal differentiation of embryonic stem cells as basis for novel approaches to developmental neurotoxicity testing. *Cell Death Differ*, *18*(3), 383-395. <https://doi.org/10.1038/cdd.2010.109>
- Zlokovic, B. V. (2008, Jan 24). The blood-brain barrier in health and chronic neurodegenerative disorders. *Neuron*, *57*(2), 178-201. <https://doi.org/10.1016/j.neuron.2008.01.003>
- Zulch, K. J. (1979). Histological typing of tumours of the central nervous system. *International histological classification of tumours No 21.*, 19-24.

6 Abbreviations

°C	Degrees celsius
APC	adenomatous polyposis coli
BBB	Blood brain barrier
bFGF	basic fibroblast growth factor
BMC	benchmark concentration
BMCU	upper limit of benchmark concentration
BMFZ	biological-medical research center
BMP	bone morphogenetic protein
bp	Base pairs
BSA	Bovine serum albumin
c-MYC	Myelocytomatosis oncogene
CAR	chimeric antigen receptor
CAS	chemical abstract service registry number
Cas9	CRISPR associated protein 9
CD44	CD44 molecule
CDKN2A	cyclin-dependent kinase inhibitor 2A
cDNA	Copy DNA
CNS	central nervous system
COX-2	cyclooxygenase-2
CRISPR	clustered regularly interspaced palindromic repeats
CSCs	cancer stem cells
CT	Computer tomography
CTG	Cell Titer Glo®
CTNNB1	β-catenin
dH2O	deionized H2O
DMEM	Dulbecco's Modified Eagle Medium
DMSO	Dimethylsulfoxid
DNA	desoxyribonucleic acid
dNTPs	desoxynucleosidtriphosphate
DPBS -/-	Dulbescco's phosphate-buffered saline without calcium and magnesium
E. coli	<i>Escherichia coli</i>
EC50	Effective concentration 50
EDTA	Ethylendiaminetetraacetic acid
EGF	Epidermal growth factor
EGFP	enhanced green fluorescent protein
EGFR	Epidermal growth factor receptor

Abbreviations

EGFRvIII	epidermal growth factor receptor variant III
EMT	epithelial-to-mesenchymal transition
ESCs	embryonic stem cells
EV	Empty vector
FBS	Fetal bovine serum
FDA	U.S. Food and Drug Administration
FGF	Fibroblast growth factor
FWD	Forward
GBM	Glioblastoma
GLI1	Glioma-associated oncogene homolog 1
GLI2	Glioma-associated oncogene 2
GO	Gene ontology
GOI	Gene of interest
GR	Glucocorticoid Receptor
GR β	glucocorticoid receptor β
h	hours
HA	Hyaluronic acid
HCl	Hydrochloric acid
hEGF	human epidermal growth factor
HEPES	4-(2-hydroxyethyl)-1-piperazineethanesulfonic acid
hiNPCs	Human induced neural progenitor cells
hiPSC	Human induced pluripotent stem cells
HTS	high-throughput screening
ICC	immunocytochemistry
IDH1	isocitrat dehydrogenase 1
IDH2	isocitrat dehydrogenase 2
IPA	Ingenuity Pathway Analysis
kb	kilobase
kDa	kilodalton
l	liter
M-MLV	Moloney murine leukemia virus
mA	milliampere
MB	Medulloblastoma
MCS	multiple cloning site
MERTK	MER proto-oncogene tyrosine kinase
MG	Matrigel®
MGMT	O-6-methylguanine-DNA methyltransferase
min	Minutes(s)
ml	Milliliter

Abbreviations

mm	Millimeter
mM	Millimolar
MRI	magnetic resonance imaging
mRNA	messenger RNA
mtDNA	mitochondrial DNA
MTT	Thiazolyl Blue Trazolium Bromide
MYC	myelocytomatosis oncogene
MYCN	myelocytomatosis oncogene N
NaCl	Sodium chloride
NAD	nicotinamide adenine dinucleotide
NANOG	Nanog homeobox
NDM	Neural differentiation medium
NESTIN	neuroepithelial stem cell protein
NF1	neurofibromin 1
<i>NFκB</i>	nuclear factor kappa B
NIM	Neural induction medium
nM	nanomolar
nm	nanometer(s)
NPCs	neural progenitor cells
NPM	Neural proliferation medium
NS	neurospheres
OCT3/4	octamer-binding transcription factor 3/4
OCT4	octamer-binding transcription factor 4
p-value	Probability value
P/S	Penicillin/Streptomycin
PARP	Poly ADP ribose polymerase
PBS -/-	Phosphate buffer saline without Magnesium and chloride
PCA	Principal component analysis
PCR	polymerase chain reaction
PDGFRA	platelet-derived growth factor receptor alpha
PDL	Poly-D-lysin
PEG	Polyethylene glycol
PET	positron emission tomography
PFA	Paraformaldehyde
PGE2	prostaglandin E2
PLO	Poly-L-ornithine
Poly-HEMA	Poly-2-hydroxyethyl methacrylate
PRDM6	putative histone-lysine N-methyltransferase
PRKCD	protein kinase C delta

Abbreviations

PTCH1	Patched1
PTEN	phosphatase and tensin homolog
qPCR	Quantitative real-time PCR
RARA	retinoic acid receptor alpha
RE	restriction enzymes
RNA	ribonucleic acid
Rock inhibitor	Rho-associated coiled coil forming protein/threonine kinase inhibitor Y-27632 2HCl
rpm	Rotations per minute
RV	Reverse
s	seconds
S.O.C.	super optimal broth with catabolite repression
SDS	Sodium dodecyl sulfate
SLE	systemic lupus erythematosus
SMADi	SMAD inhibition
SMO	smoothend
SoC	Standard of care
SOX2	SRY-box transcription factor 2
SUFU	suppressor of fused homolog
TAE	Tris-acetate-EDTA
<i>TGF-β1</i>	tumor growth factor- β 1
TMZ	Temozolomide
TP53	tumor protein 53
TRA-1-60	Tumor rejection antigen 1-60
TRA-1-81	Tumor rejection antigen 1-81
Tris	Tris(hydroxymethyl)aminomethane
TTFields	tumor-treating fields
Tween®-20	Polyoxyethylene (20) sorbitan monolaurate
V	Volt
VEGFR	vascular epidermal growth factor
WHO	World Health Organization
WNT	wingless-related integration site
WT	Wild type
μ l	microlitre
μ M	Micromolar

7 List of Figures

Figure 1 WHO classification of brain tumor.....	7
Figure 2 Overview of medulloblastoma subtypes.....	10
Figure 3 Simplified model about the origin of cancer stem cells.....	18
Figure 4 Overview over the usage of hiPSC.....	20
Figure 5 Vector map of the modified pSin vector.....	41
Figure 6 Neural induction of hiPSC in 2D and 3D.....	70
Figure 7 Decision tree of data evaluation for hiNPC compound screening.....	78
Figure 8 Gel electrophoresis of the amplification of the GOI.....	81
Figure 9 Protein expression of introduced target genes in the successfully generated hiPSC- oncogene models.....	82
Figure 10 Mycoplasma gel picture of the successfully generated hiPSC-oncogene models.....	83
Figure 11 Viability of hiPSC-oncogene models.....	84
Figure 12 Immunocytochemical staining of the hiPSC-oncogene models.....	86
Figure 13 Karyograms of all hiPSC-oncogene models.....	87
Figure 14 Hierarchical clustering of hiPSC-oncogene models.....	88
Figure 15 PCA of hiPSC-oncogene models.....	89
Figure 16 Significantly regulated canonical signaling pathways of hiPSC-oncogene models.	90
Figure 17 Significantly regulated upstream targets of all hiPSC-oncogene models. Uniquely regulated genes were identified by comparing all hiPSC-oncogene models with each other.....	91
Figure 18 Volcano plot for all hiPSC-oncogene models.....	93
Figure 19 GO terms of all hiPSC-oncogene models.....	95
Figure 20 Concentration-response curves to determine the EC ₅₀ for all hiPSC-oncogene models.....	97
Figure 21 ICC staining of 2D hiNPC-oncogene models.....	102
Figure 22 Protein expression of EGFR in 2D hiNPC-oncogene models.....	103
Figure 23 Hierarchical clustering of the hiPSC-oncogene and 2D iNPC-oncogene models.	105
Figure 24 PCA clustering of 2D iNPC-oncogene models.....	106
Figure 25 mRNA Expression of the GOI in 3D hiNPC-oncogene models.....	108
Figure 26 Hierarchical clustering of the hiPSC and 3D hiNPC-oncogene models.....	109
Figure 27 Concentration-response curves of specific hits.....	112

List of figures

Figure 28 Exemplary migration images of EV and c-MYC hiNPCs treated with copanlisib or cisplatin.	113
Figure 29 Concentration-response curves of unspecific hits for c-MYC hiNPCs.	114
Figure 30 Concentration-response curve for acetaminophen in the GBM 3D hiNPC-oncogene models.	118
Figure 31 Concentration-response curve for TMZ in the GBM 3D hiNPC-oncogene models.	119
Figure 32 Concentration-response curve for copanlisib in the GBM 3D hiNPC-oncogene models.	119
Figure 33 Concentration-response curve for olaparib in the GBM 3D hiNPC-oncogene models.	120
Figure 34 Concentration-response curve for vandetanib in the GBM 3D hiNPC-oncogene models.	120

8 List of Tables

Table 1 Overview of the glioblastoma subgroups.	15
Table 2 Medulloblastoma (MB) and glioblastoma (GBM) subgroup-specific genes of interest.	37
Table 3 Phusion polymerase PCR reaction mix.	38
Table 4 Phusion polymerase PCR conditions.	38
Table 5 Primers for gene amplification.	39
Table 6 Digestion of insert with the gene of interest.	40
Table 7 Digestion of the modified pSin receiver vector.	40
Table 8 Overview of all sequences of the respective genes of interest (5' – 3').	42
Table 9 Ligation reaction mix with <i>CD44</i> and <i>c-MYC</i> and vector using T4 DNA ligase.	49
Table 10 Reaction set up for the Cold Fusion™.	50
Table 11 Primer sequence for lab-derived mycoplasma PCR.	57
Table 12 Reaction set-up for mycoplasma PCR master mix.	57
Table 13 PCR conditions for lab-derived mycoplasma PCR.	57
Table 14 PCR conditions for commercially mycoplasma PCR.	58
Table 15 Primary antibodies used for Western blot and detection of the proteins.	60
Table 16 Secondary antibodies used for Western blot and protein detection.	61
Table 17 Overview of the flow cytometry staining.	63
Table 18 Antibodies used for immunocytochemical staining.	66
Table 19 Drugs used for the pharmacological screening in hiPSCs.	67
Table 20 Reverse transcription of RNA into cDNA reaction mix.	71
Table 21 Thermocycler conditions for cDNA synthesis.	72
Table 22 Thermo cycler protocol for qPCR.	72
Table 23 Primer used for qPCR.	73
Table 24 Antibodies used for detection of neural progenitor markers by flow cytometry.	73
Table 25 Overview of the staining and used antibodies for each sample.	75
Table 26 Identified compounds for the compound-screening in hiNPCs.	77
Table 27 FACS expression of the stem cell marker in the generated hiPSC-oncogene models.	85
Table 28 Effective concentration (EC) ₅₀ of the drugs were determined for all hiPSC- oncogene models.	99
Table 29 Quality of the 2D neural induction.	100

List of tables

Table 30 Expression of the stem cell marker and NPC marker in 3D neural induced hiNPC- oncogene models.	107
Table 31 Compound screening of 3D hiNPC-oncogene models using the most effective compounds from the hiPSC-oncogene model compound screening.....	110
Table 32 Results of the compound screening for migration and cytotoxicity of MB 3D hiNPC- oncogene models.	111
Table 33 Results of the compound screening for proliferation, migration, and cytotoxicity of GBM 3D hiNPC-oncogene models.	116

9 Publications

Efficient modulation of TP53 Expression in human induced pluripotent stem cells

Constanze Uhlmann*, Lisa-Maria Kuhn, Julia Tigges, Ellen Fritsche, Ulf Dietrich Kahlert

*Constanze Krambrich's maiden name was Constanze Uhlmann.

Journal:	Current Protocols in stem cell biology
Impact Factor:	2.69
Contribution to the publication:	80 % Planning, evaluation, and performance of all experiments, writing of the manuscript draft
Type of authorship:	First-authorship
Status of the publication:	Published 28 th December 2019
DOI:	10.1002/cpsc.102

Efficient Modulation of TP53 Expression in Human Induced Pluripotent Stem Cells

Constanze Uhlmann,¹ Lisa-Maria Kuhn,² Julia Tigges,³ Ellen Fritsche,³ and Ulf Dietrich Kahlert^{1,4,5}

¹Department of Neurosurgery, University Hospital Düsseldorf, Düsseldorf, Germany

²Department of Pediatric Oncology, Hematology and Clinical Immunology, Medical Faculty, Center of Child and Adolescent Health, Heinrich-Heine University, Düsseldorf, Germany

³IUF–Leibniz Research Institute for Environmental Medicine, Düsseldorf, Germany

⁴German Cancer Consortium (DKTK), partner site Essen, Düsseldorf, Germany

⁵Corresponding author: Ulf.Kahlert@med.uni-duesseldorf.de

TP53 point mutations are found in 50% of all cancers and seem to play an important role in cancer pathogenesis. Thus, human induced pluripotent stem cells (hiPSCs) overexpressing mutant TP53 are a valuable tool for the generation of in vitro models of cancer stem cells or for in vivo xenograft models. Here, we describe a protocol for the alteration of gene expression in hiPSCs via overexpression of a mutant form of the *TP53* (R249S) gene using lentiviral transduction. A high amount of TP53 protein is detected 1 week after transduction and antibiotic selection. Differentiation of transduced hiPSCs gives insight into better understanding cancer formation in different tissues and may be a useful tool for genetic or pharmacologic screening assays. © 2019 The Authors.

Basic Protocol 1: Production and concentration of third-generation lentivirus

Support Protocol 1: Cloning of gene of interest into modulation vector

Support Protocol 2: Preparation of DMEM GlutaMAXTM with 10% fetal bovine serum and 1% penicillin-streptomycin

Basic Protocol 2: Transduction of human induced pluripotent stem cells and selection of positively transfected cells

Support Protocol 3: Preparation of Matrigel[®]-coated plates

Support Protocol 4: Preparation of mTeSRTM 1 medium

Keywords: hiPSC | lentiviral transduction | molecular alteration | TP53

How to cite this article:

Uhlmann, C., Kuhn, L.-M., Tigges, J., Fritsche, E., & Kahlert, U. D. (2020). Efficient modulation of TP53 expression in human induced pluripotent stem cells. *Current Protocols in Stem Cell Biology*, 52, e102. doi: 10.1002/cpsc.102

INTRODUCTION

Due to their infinite availability, human induced pluripotent stem cells (hiPSCs) offer the opportunity to perform unlimited numbers of in vitro experiments. Further, hiPSC differentiation into a desired tissue allows studying physiologic processes in human-relevant cell systems. By introducing disease-specific mutations, these cells allow for studying genetic origins of disease in a tissue-specific manner with those cells. Most tumors have TP53 mutations. Among the six hot-spot mutations of *TP53*, TP53 R249S (exchange of

**CURRENT
PROTOCOLS**
A Wiley Brand

Current Protocols in Stem Cell Biology e102, Volume 52
Published in Wiley Online Library (wileyonlinelibrary.com).
doi: 10.1002/cpsc.102

© 2019 The Authors. This is an open access article under the terms of the Creative Commons Attribution License, which permits use, distribution and reproduction in any medium, provided the original work is properly cited.

Uhlmann et al.

1 of 15

arginine for serine) is a point mutation, which causes a structural change of the protein and thereby enhances cell proliferation (Bullock & Fersht, 2001; Friedler et al., 2004; Kollareddy et al., 2015). Genetic manipulation of cells by lentiviral transduction introduces mutations in a stable and efficient manner (Naldini et al., 1996). Here, we apply this procedure to hiPSCs using a vector containing mutated TP53 (Rapti et al., 2015; Zare et al., 2016).

In this article, we report two basic protocols that have been enlisted that describe the process of hiPSC lentiviral transduction to generate genetically modified stable cell lines. In summary, Basic Protocol 1 describes the production of third-generation lentivirus with HEK 293T cells, and Basic Protocol 2 describes the generation of TP53 R249S transduced cells with the use of a lentiviral vector.

NOTE: hiPSCs are grown in standard laboratory conditions, in a humidified incubator (37°C, 5% CO₂).

NOTE: Virus production and transduction of hiPSCs requires a biosafety level 2 (BSL2) laminar flow cabinet.

NOTE: All solutions and equipment must be sterile if they come in contact with cells.

**BASIC
PROTOCOL 1**

PRODUCTION AND CONCENTRATION OF THIRD-GENERATION LENTIVIRUS

This protocol is used for the production of concentrated third-generation lentivirus. Concentrated lentivirus is produced to transduce cells (e.g., hiPSCs). All work in our laboratory is performed in BSL2 facility. However, the level of biosafety containment should be in accordance with institutional and governmental guidelines. A proper risk assessment must be done prior to beginning the work. The equipment and laminar flow hood used must be sterilized in accordance with your local rules on risk assessment when working with lentivirus.

Materials

HEK 293T cells
 Dulbecco's modified Eagle medium (DMEM) GlutaMAX™ containing 10% (v/v) fetal bovine serum (FBS) and 1% (v/v) penicillin-streptomycin (see Support Protocol 2)
 DMEM (e.g., Thermo Fisher Scientific, cat. no. 41965039)
 Plasmid DNA
 Third-generation lentivirus plasmids:
 pMDLg/pRRE (Addgene #12251; see Fig. 1)
 pRSV-REV (Addgene #12253; see Fig. 2)
 pMD2.G (Addgene #12259; see Fig. 3)
 FuGENE® HD Transfection Reagent (e.g., Promega, cat. no. 231A)
 Dulbecco's phosphate-buffered saline (DPBS) without calcium or magnesium (e.g., Thermo Fisher Scientific, cat. no. 14190094)
 DMEM GlutaMAX™ containing 10% (v/v) FBS (e.g., Sigma-Aldrich, cat. no. F7524)
 50% (v/v) polyethylene glycol (PEG) in distilled, deionized water
 1.5 M NaCl, prepared in distilled, deionized water

 10-cm plastic dishes (e.g., Greiner Bio-One, cat. no. 664160)
 Cell culture incubator (37°C, 5% CO₂)
 0.5- and 1.5-ml microcentrifuge tube
 15-ml conical tube

Uhlmann et al.

2 of 15

Current Protocols in Stem Cell Biology

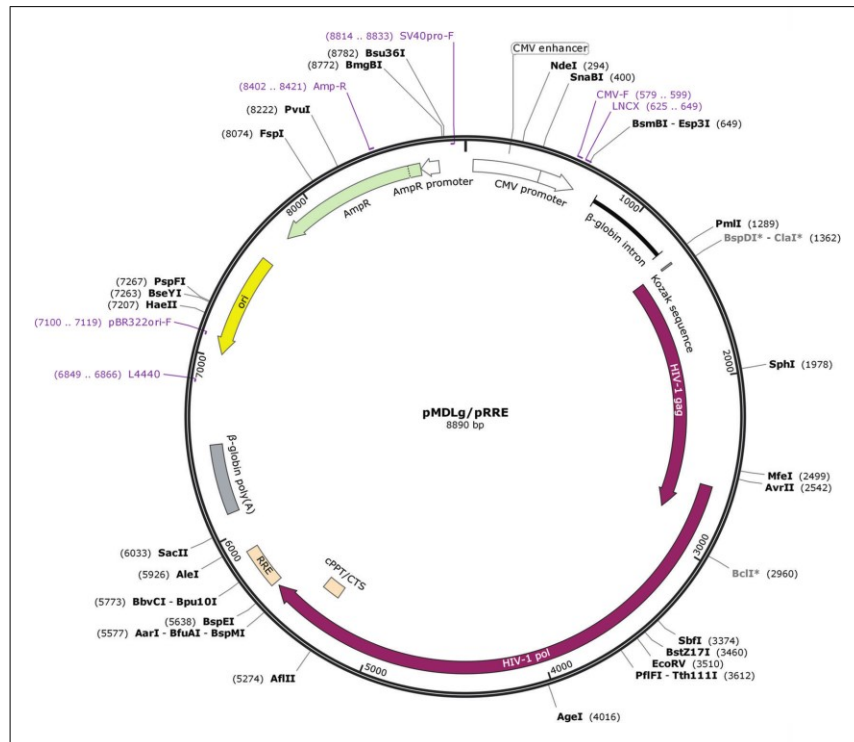


Figure 1 Vector map of the third-generation lentiviral packaging plasmid pMDLg/pRRE (Addgene #12251).

- 10-ml syringe
- 0.45- μ m syringe filter (e.g., VWR, cat. no. 514-0063)
- Vortex mixer
- Refrigerated centrifuge (e.g., Hettich® Rotina 38R with fixed-angle rotor, cat. no.1792)

Preparation

1. Plate HEK 293T cells in a 10-cm dish with 10 ml DMEM GlutaMAX™ containing 10% FBS and 1% penicillin-streptomycin.

HEK 293T cells used in this protocol were kindly provided by Dr. Astrid Weyerbrock, Department of Neurosurgery, University Hospital Freiburg, Freiburg, Germany.

Day 0

2. Allow cells to reach 80% to 90% confluency. Prepare infection solution in a 1.5-ml microcentrifuge tube in the following order:

- 800 μ l DMEM
- 8 μ g plasmid DNA
- 4 μ g pMDLg/pRRE
- 2 μ g pRSV-REV
- 2 μ g pMD2.G
- 60 μ l FuGENE® HD.

Uhlmann et al.

3 of 15

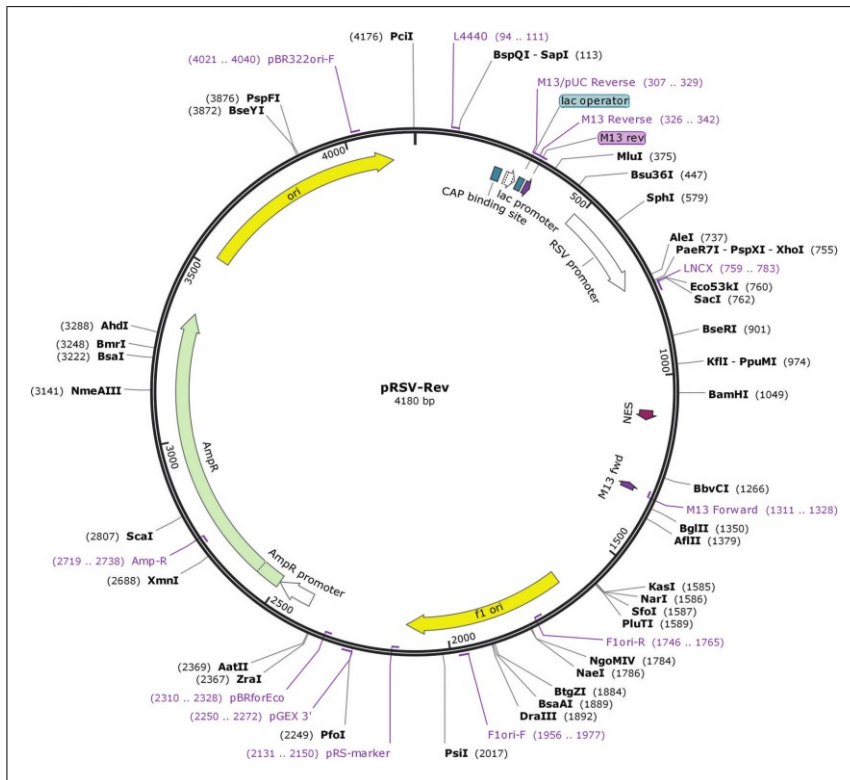


Figure 2 Vector map of the third-generation lentiviral packaging plasmid pRSV-Rev (Addgene #12253).

3. Pipet solution up and down, and incubate for at least 10 min at room temperature.
4. Meanwhile, wash HEK 293T cells with DPBS.
5. Add 10 ml DMEM GlutaMAXTM containing 10% FBS without antibiotics to each dish.
6. After incubation, add infection solution dropwise to each dish. Move dish gently to distribute solution, and incubate at 37°C with 5% CO₂.

Day 1

7. Remove supernatant and add 10 ml DMEM GlutaMAXTM containing 10% FBS and 1% penicillin-streptomycin.

Days 2, 3, and 4

8. To a 15-ml conical tube, add 1 ml of 50% PEG. Separately, connect syringe with a 0.45-µm filter. Pull the plunger out of the syringe out, and store it sterile in its packaging.
9. Fill syringe with supernatant, and filter supernatant into the 15-ml conical tube containing PEG by pushing the plunger.
10. Throw away syringe and filter.

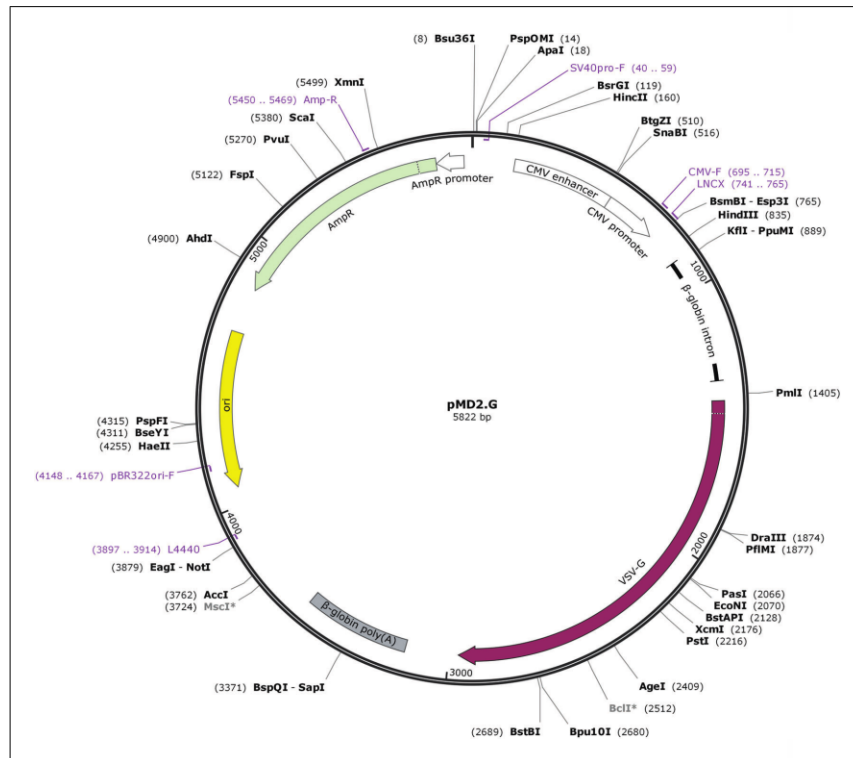


Figure 3 Vector map of the VSV-G envelope-expressing plasmid (Addegne #12259).

11. Add 10 ml DMEM GlutaMAX™ containing 10% FBS and 1% penicillin-streptomycin to dish.
12. Add 1.2 ml of 1.5 M NaCl to each conical tube.
13. Mix solution containing supernatant, PEG, and NaCl well by vortexing or shaking, and store at 4°C until further use on day 5.

Day 5

14. Precool centrifuge to 4°C.
15. Centrifuge conical tubes (from step 13) 30 min at 7000 × g, 4°C.
16. Check if a pellet is visible.

At times, it might be difficult to see the pellet due to the contrast. The pellet from day 3 might be smaller than from the days before.

17. After centrifugation, place tubes on ice.
18. Remove supernatant under sterile conditions, being careful not to disturb the pellet. Aspirate remaining supernatant gently with a pipette tip.
19. Resuspend pellets from all three tubes (days 2, 3, and 4) to a final volume of 400 µl DPBS (1:75 dilution of original sample volume).

Uhlmann et al.

5 of 15

**SUPPORT
PROTOCOL 1**

20. Prepare 40- μ l aliquots in 1.5-ml or 0.5-ml microcentrifuge tubes.

In order to maintain efficiency, avoid continuously freezing and thawing the virus by preparing ready-to-use aliquots.

21. Store aliquots at -80°C or use immediately.

CLONING OF GENE OF INTEREST INTO MODULATION VECTOR

This protocol describes the cloning procedure for inserting the TP53 R249S point mutation into a vector by a restriction enzyme-based process, leading to overexpression of the TP53 variant. The plasmid backbone is based on pSin-Ef2-Nanong-Pur (Addgene #16578; Fig. 4) and was modified with an EGFP tag at the N-terminal end, multiple cloning site, and removal of the Nanog gene sequence.

The free software SnapGene Viewer (GSL Biotech; available at <https://www.snapgene.com/>) was used to prepare the virtual cloning file and to design the oligomers. After cloning and purification of the plasmid from *E. coli*, the plasmid can be used for virus production.

Materials

Template for gene sequence: pLenti6/V5-p53_R249S (Addgene #22935)

Phusion high-fidelity DNA polymerase and buffer (e.g., New England Biolabs, cat. no. M0530L)

10 mM dNTP mix

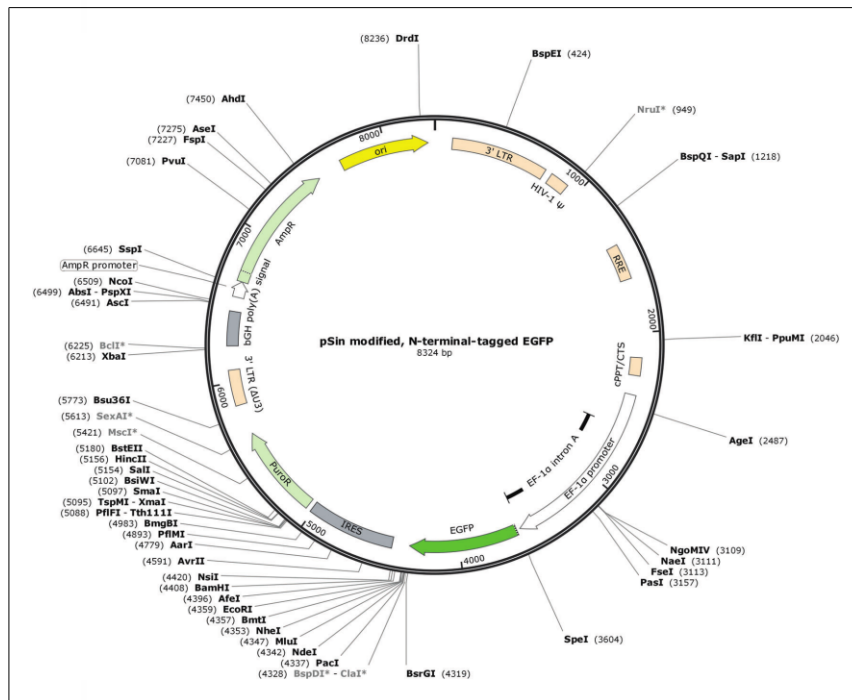


Figure 4 Vector map of the modified pSin vector containing N-terminal-tagged EGFP and based on the original pSin-EF2-Nanong-Pur vector (Addgene #16578). The vector is used for cloning the gene of interest.

10 μ M TP53 forward oligomer: 5'-CCTTAATTAAAATGGAGGAGCCGCAGTC
A-3'

10 μ M TP53 reverse oligomer: 5'-GGAATTCATATGTCAGTCTGAGTCAGG
CCCTT-3'

DNA containing gene of interest (GOI)

Agarose

1 \times Tris-acetate-EDTA (TAE) buffer

SYBR[®] Safe DNA gel stain (e.g., Thermo Fisher Scientific, cat. no. S33102)

6 \times DNA gel loading dye (e.g., Thermo Fisher Scientific, cat. no. R0611)

1-kb DNA ladder (e.g., Thermo Fisher Scientific, cat. no. SM1331)

E.Z.N.A.[®] Cycle Pure Kit, V-spin (e.g., Omega Bio-Tek, cat. no. D6492)

10 \times CutSmart[®] Buffer (e.g., New England Biolabs, cat. no. B7204S)

NdeI restriction enzyme (e.g., New England Biolabs, cat. no. R0111)

PacI restriction enzyme (e.g., New England Biolabs, cat. no. R0547)

pSin-EF2 modulation vector (based on vector pSin-EF2-Nanog-Pur; Addgene
#16578; see Fig. 4)

E.Z.N.A.[®] Gel Extraction Kit, V-spin (e.g., Omega Bio-Tek, cat. no. D2500)

10 \times T4 DNA ligase and buffer (e.g., New England Biolabs, cat. no. M0202)

TOP10 chemically competent cells (e.g., New England Biolabs, cat. no. C3019)

LB medium with and without 100 μ g/ml ampicillin

10-cm LB agar plates with 100 μ g/ml ampicillin (e.g., Applichem, cat. no. A0839)

Glycerol

E.Z.N.A.[®] Plasmid Mini Kit I, V-spin (e.g., Omega Bio-Tek, cat. no. D6943)

NucleoBond[®] Xtra Midi/Maxi (e.g., Machery-Nagel, cat. no. 740410)

Computer running SnapGene Viewer (available at <https://www.snapgene.com/>)

PCR reaction tubes

Thermal cycler

Spectrophotometer capable of measuring DNA concentration

1.5-ml microcentrifuge tube

16°C and 37°C incubators, with shaking capabilities

UV transilluminator

Scalpel

42°C heating block

Laboratory shaker

Parafilm[®] M (e.g., Bemis Company, cat. no. PM996)

15-ml conical tubes

Cyrovials

Preparation

Design plasmid and DNA oligomers

1. Choose a restriction site located at the multiple cloning site that cuts the vector only once. These enzymes should not cut your GOI. Use a DNA documentation program such as SnapGene Viewer to plan the cloning. To maintain the reading frame, bases might have to be added between the restriction site and the GOI. It is possible to use any base, but take care that no stop codon is generated.

We recommend adenosine or thymidine to have a lower melting temperature.

2. Check which restriction enzymes cut your vector only once and not your GOI. If you have chosen two enzymes, check the efficiency of both enzymes in the restriction buffer, and if possible, use the same buffer for both enzymes.

You can use the following website for help: <https://nebcloner.neb.com/#/redigest>.

Uhlmann et al.

7 of 15

- Design oligomers for cloning, which include the restriction site, additional bases, and around 20 to 30 bases of your GOI. Use the table from New England Biolabs, and add bases according to the restriction enzyme (https://www.neb.com/-/media/nebus/files/chart-image/cleavage_oligonucleotides_old.pdf?la=en).

PCR amplify gene of interest

- As a template for the GOI, use either a plasmid or cDNA.

In our case, we used the pLenti6/V5-p53-R249S plasmid (Addgene #22935).

- In PCR reaction tubes, set up a PCR as follows (50 μ l total PCR volume):

32.5 μ l water
 10 μ l of 5 \times Phusion buffer
 1 μ l of 10 mM dNTP mix
 2.5 μ l of 10 μ M TP53 forward oligomer
 2.5 μ l of 10 μ M TP53 reverse oligomer
 2 μ l DNA
 0.5 μ l Phusion polymerase.

In the case of cDNA, plasmid DNA, and genomic DNA, dilute to 50 to 100 ng.

Use a high-fidelity polymerase with proofreading function to get a high accuracy of your GOI. This is especially important if you have a gene with a point mutation.

- Run PCR using a thermal cycler and the following conditions:

1 cycle	30 s	98°C	(initial denaturation)
29 cycles	10 s	98°C	(denaturation)
	30 s	variable	(annealing)
	30 s per kb	72°C	(extension)
1 cycle	10 min	72°C	(final extension)
Final step	indefinitely	4°C	(hold).

Use 60°C for the annealing temperature for the first time. If 60°C does not work, try a temperature gradient to detect the optimal annealing temperature.

- Prepare a 1% (w/v) agarose gel with 1 \times TAE and SYBR[®] Safe (1:10,000 dilution) to assess PCR amplification. Run 5 μ l sample mixed with 6 \times DNA gel loading dye. Use a 1-kb DNA ladder to identify the size of your GOI. Run gel at 130 V for 15 min.
- Purify PCR products with a positive result using the E.Z.N.A.[®] Cycle Pure Kit following the manufacturer's instructions.
- Elute sample in 25 μ l water. To achieve a higher concentration, prewarm water to 50°C. Measure concentration with a spectrophotometer.

The concentration of the sample should vary between 10 and 50 ng/ μ l.

- Freeze sample at -20°C , or proceed with digestion.

Digest PCR product and vector

- Prepare each digestion in a 1.5-ml microcentrifuge tube as follows (30 μ l total volume):

24 μ l purified PCR product
 3 μ l of 10 \times CutSmart[®] Buffer
 1 μ l restriction enzyme NdeI
 1 μ l restriction enzyme PacI
 1 μ l water.

Transform

27. Let TOP10 chemically competent cells thaw on ice for 10 min. Use one vial of competent cells per ligation reaction.
28. Add 10 µl ligation mixture to chemically competent cells in a 1.5-ml microcentrifuge tube. Mix gently by tapping tube.
29. Incubate on ice for 10 min.
30. Place reaction tube in a 42°C heating block for 1 min (heat shock).
31. Stop reaction by placing cells on ice for 2 min (cold shock).
32. Add 300 µl LB medium without antibiotics.
33. Shake at 37°C for 40 min at 800 rpm.
34. Spread 150 µl cells on 10-cm LB agar plates containing ampicillin.
35. Incubate plate overnight at 37°C. Do not incubate longer than 16 hr.

The ligation control should technically have no clones. The ligation control is done to determine the experimental background. If colonies grow on the control plate, it might be undigested or contain religated vector. There should be no or a significantly lower number of colonies on the ligation control plate compared with the ligation plate of your GOI.

36. Wrap plate with Parafilm® M, and store at 4°C until further use.

Analyze plasmid

37. Pick 3 to 5 clones from each plate, and individually add to 15-ml conical tubes containing 5 ml LB medium with ampicillin.

For each tube pick a separate colony (e.g., with a sterile pipet tip).

38. Incubate culture overnight at 37°C with shaking at 250 rpm. Do not incubate longer than 16 hr.
39. Prepare a glycerol stock of the cultures in a cryovial by adding 500 µl culture to 500 µl glycerol. Store at –80°C for further use.
40. Perform a mini-prep with the remaining culture using the E.Z.N.A.® Plasmid Mini Kit I following manufacturer's instructions.
41. Perform a digest of plasmid to control integration of the insert. As a control, digest 200 to 300 ng plasmid as described above. Stop digestion after 2 hr.
42. Check digestion on agarose gel to see whether two bands of the correct size are visible. Discard any plasmids that do not contain inserts or have fragments of the wrong size.
43. Prepare sample for sequencing according to requirements.

Check how many micrograms of vector DNA are required by the chosen sequencing company and if the primer should be added or sent separately. Inform yourself how long the sequenced area is or if different lengths can be booked. For sequencing, you can use the forward or reverse primer from the PCR amplification. If you have a point mutation in your GOI, make sure the sequenced area covers the mutation. If the forward or reverse primer does not cover the point mutation, you can design your own sequencing primer. Choose a site around 20 to 30 bp before or after your point mutation because sequencing is poor at the beginning. The primer should have a length of ~20 bp.

44. Compare sequencing results with your own vector, which contains the GOI. If it matches, proceed with the next step.
45. Prepare a midi- or maxi-prep from the positive plasmid to obtain enough material for virus production.
We recommend using a NucleoBond® Xtra Midi/Maxi Kit for plasmid purification and following manufacturer's instructions.
46. Measure concentration.
47. Freeze plasmid at -20°C until further use.

PREPARATION OF DMEM GlutaMAX™ WITH 10% FETAL BOVINE SERUM AND 1% PENICILLIN-STREPTOMYCIN

This protocol describes the preparation of DMEM GlutaMAX™ containing a final concentration of 10% (v/v) FBS and 1% (v/v) penicillin-streptomycin for culturing HEK 293T cells.

Materials

FBS
DMEM GlutaMAX™
Penicillin-streptomycin
0.45- μm bottle-cap filter

1. Under sterile conditions, filter 50 ml FBS with a 0.45- μm bottle-cap filter. Add 445 ml DMEM GlutaMAX™.
2. Mix medium by swirling flask.
3. Remove 10 ml per 10-cm dish to be used later for virus preparation, and store at 4°C .
4. Add to the remaining medium the appropriate amount of penicillin-streptomycin. Store medium at 4°C .

TRANSDUCTION OF HUMAN INDUCED PLURIPOTENT STEM CELLS AND SELECTION OF POSITIVELY TRANSFECTED CELLS

This protocol can be used for transduction of hiPSCs with highly concentrated third-generation lentivirus. All work should be performed in accordance with the appropriate biosafety containment level, which is determined by institutional and governmental guidelines. The equipment and laminar flow hood used must be sterilized in accordance with local rules and risk assessment with regard to use of lentivirus.

Materials

hiPSC (e.g., IMR90-04; WiCell Research Institute)
mTeSR™1 culture medium with and without puromycin (see Support Protocol 4)
0.5 mM EDTA in DPBS
Highly concentrated lentivirus (see Basic Protocol 1)

Matrigel®-coated 12-well plate (see Support Protocol 3)
Cell culture incubator

1. Culture hiPSCs in a Matrigel®-coated 12-well plate using mTeSR™1 culture medium.

For a detailed description of culturing hiPSCs, see Chen (2012).

**SUPPORT
PROTOCOL 2**

**BASIC
PROTOCOL 2**

Uhlmann et al.

11 of 15

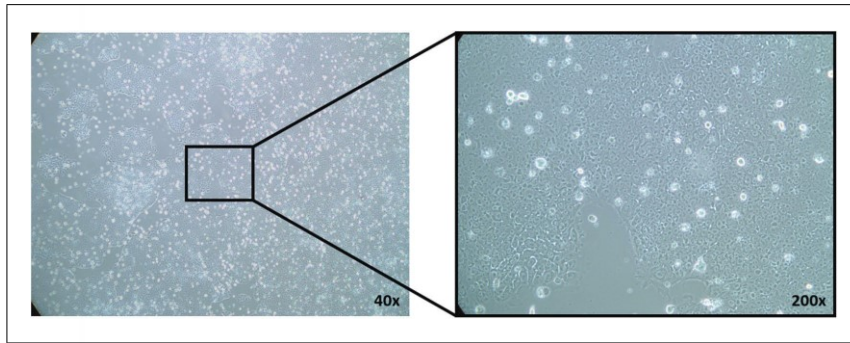


Figure 5 IMR90-04 cells on the day of transduction. Cells should show a similar confluency of 60% to 80%.

2. Split hiPSCs with 0.5 mM EDTA.
3. When cells reach 60% to 80% confluency (Fig. 5), change medium (1 ml per well), and add 1 vial (40 μ l) concentrated virus to each well.
4. The next day, remove 500 μ l supernatant, and add 500 μ l fresh medium.
5. After 48 hr, remove all medium, and add 1 ml fresh medium.
6. Perform antibiotic selection after 72 hr using culture medium containing 1 μ g/ml puromycin.
The concentration of the antibiotic should be determined beforehand by performing a killing curve for each cell line. After 2 days of selection, it is possible to see if cells survive. Cells that do not survive selection will detach.
7. Split cells at least once in a plate containing medium with puromycin to achieve a more efficient selection.
You can use a 6-well plate to expand the cells. On the next day, you can check if cells have attached and survived the splitting.
8. After 1 week stop antibiotic selection, and culture cells without antibiotics.
9. Expand cell culture, and use for assays.

**SUPPORT
PROTOCOL 3**

PREPARATION OF MATRIGEL[®]-COATED PLATES

This protocol explains in short how to prepare Matrigel[®]-coated 6- or 12-well plates.

Materials

- Matrigel[®], hESC-qualified matrix (e.g., Corning, cat. no. 354277)
- KnockOut DMEM (e.g., Invitrogen, cat. no. 10829018)
- 15-ml conical tubes
- 12-well plate (e.g., Greiner Bio-One, cat. no. 657160)
- 6-well plate (e.g., Greiner Bio-One, cat. no. 665180)
- Parafilm[®] M (e.g., Bemis Company, cat. no. PM996)

1. Thaw Matrigel[®] and precool pipet tips to 4°C overnight.
2. For an even distribution, gently swirl Matrigel[®], and keep on ice at all times.

Uhlmann et al.

12 of 15

3. Dilute 10 ml Matrigel[®] with 10 ml KnockOut DMEM. Gently pipet up and down with a precooled pipet. Prepare 0.5-ml aliquots in 15-ml conical tubes, and store at -20°C until further use.
4. To coat a plate, retrieve an aliquot from the freezer. Under sterile conditions, add an additional 1 ml KnockOut DMEM to tube, and allow to thaw.
5. Mix tube well by inverting.
6. Add 13.5 ml KnockOut DMEM, and gently mix by pipetting up and down. Prevent air bubbles and ensure everything is mixed.
7. Add 0.5 ml Matrigel[®]-containing solution to each well of a 12-well plate or 1 ml for a 6-well plate.
8. Swirl plate for an even distribution, and ensure the entire surface is covered. Seal plate with Parafilm[®] M, and incubate at room temperature for 1 hr.

Plates can be stored at 4°C for up to 2 weeks.

Under sterile conditions, Matrigel[®] solution is removed before use, and an appropriate volume of mTeSRTM1 medium is added for cell culture. For 12-well and 6-well plates, 1 ml and 2 ml of mTeSRTM1 medium is used for each well, respectively.

9. If stored at 4°C , remove plate from refrigerator 5 min before use, and equilibrate at room temperature.

PREPARATION OF mTeSRTM1 MEDIUM

This protocol describes the preparation of mTeSRTM1 medium for culturing hiPSCs.

Materials

mTeSRTM1 basal medium and 5 \times supplement (e.g., StemCell Technologies, cat. no. 85850)
 10,000 U/ml penicillin-streptomycin (e.g., Pan Biotech, cat. no. P06-07100)
 50-ml conical tubes

1. Thaw mTeSRTM1 5 \times supplement at room temperature or at 4°C overnight.
2. On a sterile work bench, add 100 ml mTeSRTM1 5 \times supplement to 400 ml mTeSRTM1 basal medium.
3. Add 5 ml of 10,000 U/ml penicillin-streptomycin.
4. Mix well by shaking, and prepare 40-ml aliquots in 50-ml conical tubes. Store at -20°C .
5. Thaw frozen aliquots at room temperature or at 4°C overnight. Store at 4°C after thawing.

COMMENTARY

Background Information

Human cell cultures are being used to study diseases in various contexts. Frequently, patient-derived cell systems, such as cancer cell lines, are the only biological matrix used in biomedical research. Recent evidence demonstrated the limitations of cancer cell lines as a tool to use in the field of pharmacology (Ben-David et al., 2018). The low rate

of success to reproduce findings of drug response when using cancer cell lines has been previously highlighted (Begley & Ellis, 2012; Haibe-Kains et al., 2013; Prinz, Schlange, & Asadullah, 2011). Recently, alternative donor-derived cancer modeling technologies, based on the introduction of defined molecular alterations in non-neoplastic cells, have emerged (Hegde, Karanikas, & Evers, 2016;

**SUPPORT
 PROTOCOL 4**

Uhlmann et al.

13 of 15

Sancho-Martinez et al., 2016). Those synthetic cancer systems, as an alternative to classic cancer cell lines, may be of use in basic and translational cancer research. Here we present a detailed description of the initial steps for generation of synthetic cancer systems using hiPSCs. The use of hiPSCs is ethically accepted, and cancer models arising from a single cell of origin may be useful for fundamental basic science, as well as for translational and screening applications.

Critical Parameters and Troubleshooting

There are several critical parameters during the generation of TP53 R249S–mutated hiPSCs. Use of a highly standardized, quality-controlled hiPSC culture is of importance. The culture should be regularly checked for the expression of hiPSC markers (e.g., OCT3/4, SSEA4, Nanog, and Sox2), a normal karyotype (Steichen, Hannoun, Luce, Hauet, & Dubart-Kupperschmitt, 2019), and typical stem cell morphology with high nuclei to cytoplasm ratio and prominent nucleoli (Fig. 5; for details see Wakui et al. 2017). Successful generation of transduced hiPSCs depends further on the efficiency of the third-generation lentivirus and the ratio between cells and virus. Reducing the number of cells by reducing medium or increasing the quantity of virus by using more than one vial per experiment could improve the efficiency of the final outcome. At times, the high viral titer can be toxic to the cells; therefore, a reduction of the viral burden by dilution should be tested first (Abbaslipour et al., 2019). After transduction, select hiPSCs to obtain a homogenous culture. For antibiotic selection, a killing curve should be done to determine the optimal antibiotic dosage. Splitting/passaging cells into antibiotic-containing medium should be done on the second or third day of selection. Some promoters can be silenced over time or show no activity in stem cells (Chung et al., 2002; Xia, Zhang, Zieth, & Zhang, 2007). If cell transduction does not work, it would be best to try different promoters (e.g., EF1 α ; Zhang et al., 2017). At first, we used a cytomegalovirus promoter; however, after cloning the genes into an EF1 α promoter-driven vector, we could transduce the hiPSCs.

Understanding Results

With the help of this protocol, it is possible to transduce hiPSCs with TP53 R249S. After 1 week of antibiotic selection, the cells can be

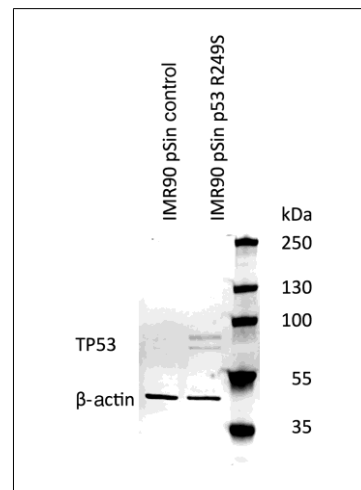


Figure 6 Western blot depicting TP53 overexpression. A total of 40 μ g protein was loaded on the gel. The primary antibodies used were anti-p53 (Abcam, cat. no. ab28) and β -actin (13E5) (Cell Signaling Technology, cat. no. 4970). The TP53 band for pSin TP53 R249S runs at \sim 80 kDa due to the fusion of EGFP and TP53 R249S.

expanded, and overexpression of TP53 can be detected (Fig. 6). These protocols have been replicated in another stem cell line (data not shown).

Time Considerations

Preparation of the lentivirus and transduction of hiPSCs takes about 2.5 weeks. Lentivirus production takes \sim 1 week if the vector and HEK 293T cells are ready to use. After 1 week the virus is concentrated and can be used for transduction of hiPSCs. Transduction of hiPSCs requires 10 days. The virus is incubated with the hiPSCs for 3 days, and subsequently antibiotic selection begins and continues for the next 7 days. After selection, depending on the cell material, it can take up to 1 week to obtain enough cell material for the first experiments to validate expression of the molecular alteration.

Acknowledgments

This research has been funded by the Federal Ministry of Education and Research of Germany in the framework of VIP+ (BMBF, 03VP03791/92).

The authors thank Prof. Dr. Jay Gopalakrishnan and Anand Ramani (Heinrich-Heine

University, Düsseldorf, Germany) for providing the modified pSin-EF2 modulation vector and cloning equipment; Anand Ramani, Gabriele Brockerhoff, and Ulrike Hübenthal for their technical support; and Ann-Christin Nickel for her help with the manuscript.

Literature Cited

- Abbaslipour, M., Khosravi, M. A., Zeinali, S., Khanahmad, H., Karimipour, M., & Azadmanesh, K. (2019). Improvement of K562 cell line transduction by FBS mediated attachment to the cell culture plate. *BioMed Research International*, 2019, 9540702. doi: 10.1155/2019/9540702.
- Begley, C. G., & Ellis, L. M. (2012). Drug development: Raise standards for preclinical cancer research. *Nature*, 483(7391), 531–533. doi: 10.1038/483531a.
- Ben-David, U., Siranosian, B., Ha, G., Tang, H., Oren, Y., Hinohara, K., ... Golub, T. R. (2018). Genetic and transcriptional evolution alters cancer cell line drug response. *Nature*, 560(7718), 325–330. doi: 10.1038/s41586-018-0409-3.
- Bullock, A. N., & Fersht, A. R. (2001). Rescuing the function of mutant p53. *Nature Reviews Cancer*, 1(1), 68–76. doi: 10.1038/35094077.
- Chen, G. (2012). Splitting hESC/hiPSC lines with EDTA in feeder free conditions. In L. Girard (Ed.), *StemBook [Internet]*. Cambridge, MA: Harvard Stem Cell Institute. doi: 10.3824/stembook.1.88.1.
- Chung, S., Andersson, T., Sonntag, K. C., Bjorklund, L., Isacson, O., & Kim, K. S. (2002). Analysis of different promoter systems for efficient transgene expression in mouse embryonic stem cell lines. *Stem Cells*, 20(2), 139–145. doi: 10.1634/stemcells.20-2-139.
- Friedler, A., DeDecker, B. S., Freund, S. M., Blair, C., Rudiger, S., & Fersht, A. R. (2004). Structural distortion of p53 by the mutation R249S and its rescue by a designed peptide: Implications for “mutant conformation”. *Journal of Molecular Biology*, 336(1), 187–196. doi: 10.1016/j.jmb.2003.12.005.
- Haibe-Kains, B., El-Hachem, N., Birkbak, N. J., Jin, A. C., Beck, A. H., Aerts, H. J., & Quackenbush, J. (2013). Inconsistency in large pharmacogenomic studies. *Nature*, 504(7480), 389–393. doi: 10.1038/nature12831.
- Hegde, P. S., Karanikas, V., & Evers, S. (2016). The where, the when, and the how of immune monitoring for cancer immunotherapies in the era of checkpoint inhibition. *Clinical Cancer Research*, 22(8), 1865–1874. doi: 10.1158/1078-0432.CCR-15-1507.
- Hollstein, M., Sidransky, D., Vogelstein, B., & Harris, C. C. (1991). p53 mutations in human cancers. *Science*, 253(5015), 49–53. doi: 10.1126/science.1905840.
- Kollareddy, M., Dimitrova, E., Vallabhaneni, K. C., Chan, A., Le, T., Chauhan, K. M., ... Martinez, L. A. (2015). Regulation of nucleotide metabolism by mutant p53 contributes to its gain-of-function activities. *Nature Communications*, 6, 7389–7389. doi: 10.1038/ncomms8389.
- Naldini, L., Blomer, U., Galloway, P., Ory, D., Mulligan, R., Gage, F. H., ... Trono, D. (1996). In vivo gene delivery and stable transduction of nondividing cells by a lentiviral vector. *Science*, 272(5259), 263–267. doi: 10.1126/science.272.5259.263.
- Prinz, F., Schlange, T., & Asadullah, K. (2011). Believe it or not: How much can we rely on published data on potential drug targets? *Nature Reviews Drug Discovery*, 10(9), 712. doi: 10.1038/nrd3439-c1.
- Rapti, K., Stillitano, F., Karakikes, I., Nonnenmacher, M., Weber, T., Hulot, J. S., & Hajar, R. J. (2015). Effectiveness of gene delivery systems for pluripotent and differentiated cells. *Molecular Therapy. Methods & Clinical Development*, 2, 14067. doi: 10.1038/mtm.2014.67.
- Sancho-Martinez, I., Nivet, E., Xia, Y., Hishida, T., Aguirre, A., Ocampo, A., ... Izpisua Belmonte, J. C. (2016). Establishment of human iPSC-based models for the study and targeting of glioma initiating cells. *Nature Communications*, 7, 10743. doi: 10.1038/ncomms10743.
- Steichen, C., Hannoun, Z., Luce, E., Hauet, T., & Dubart-Kupferschmitt, A. (2019). Genomic integrity of human induced pluripotent stem cells: Reprogramming, differentiation and applications. *World Journal of Stem Cells*, 11(10), 729–747. doi: 10.4252/wjsc.v11.i10.729.
- Wakui, T., Matsumoto, T., Matsubara, K., Kawasaki, T., Yamaguchi, H., & Akutsu, H. (2017). Method for evaluation of human induced pluripotent stem cell quality using image analysis based on the biological morphology of cells. *Journal of Medical Imaging*, 4(4), 044003. doi: 10.1117/1.Jmi.4.4.044003.
- Xia, X., Zhang, Y., Zieth, C. R., & Zhang, S.-C. (2007). Transgenes delivered by lentiviral vector are suppressed in human embryonic stem cells in a promoter-dependent manner. *Stem Cells and Development*, 16(1), 167–176. doi: 10.1089/scd.2006.0057.
- Zare, M., Soleimani, M., Mohammadian, M., Akbarzadeh, A., Havasi, P., & Zarghami, N. (2016). Efficient biotechnological approach for lentiviral transduction of induced pluripotent stem cells. *Artificial Cells, Nanomedicine, and Biotechnology*, 44(2), 743–748. doi: 10.3109/21691401.2014.982804.
- Zhang, M., Niibe, K., Kondo, T., Kamano, Y., Saeki, M., & Egusa, H. (2017). Gene delivery and expression systems in induced pluripotent stem cells. In K. Sasaki, O. Suzuki, N. Takahashi (Eds.), *Interface oral health science 2016*. Singapore: Springer.

Uhlmann et al.

15 of 15

Publications

Progenitor cells derived from gene-engineered human induced pluripotent stem cells as synthetic cancer cell alternatives for in vitro pharmacology

Constanze Uhlmann*, Ann-Christin Nickel, Daniel Picard, Andrea Rossi, Guanzhang Li, Barbara Hildebrandth, Grabiele Brockerhoff, Farina Bendt, Ulrike Hübenthal, Michael Hewera, Hans-Jakob Steiger, Dagmar Wieczorek, Aristoteles Perrakis, Wei Zhang, Marc Remke, Katharina Koch, Julia Tigges, Roland S. Croner, Ellen Fritsche, Ulf D. Kahlert

*Constanze Krambrich's maiden name was Constanze Uhlmann.

Journal:	Biotechnology Journal
Impact Factor:	3.91
Contribution to the publication:	50 %
	Planning, evaluation, and performance of part of the experiments, writing of part of the material and methods
Type of authorship:	First-authorship
Status of the publication:	Published 8 th March 2022
DOI:	10.1002/biot.202100693

RESEARCH ARTICLE

Progenitor cells derived from gene-engineered human induced pluripotent stem cells as synthetic cancer cell alternatives for in vitro pharmacology

Constanze Uhlmann¹ | Ann-Christin Nickel¹ | Daniel Picard^{2,3,4} | Andrea Rossi⁵ | Guanzhang Li⁶ | Barbara Hildebrandt⁷ | Gabriele Brockerhoff⁵ | Farina Bendt⁵ | Ulrike Hübenthal⁵ | Michael Hewera¹  | Hans-Jakob Steiger¹ | Dagmar Wieczorek⁷ | Aristoteles Perrakis⁸ | Wei Zhang⁶ | Marc Remke^{2,3,4} | Katharina Koch⁵ | Julia Tigges⁵ | Roland S. Croner⁸ | Ellen Fritsche^{5,9} | Ulf D. Kahlert⁸

¹Department for Neurosurgery, Medical Faculty and University Medical Center Düsseldorf, Heinrich-Heine-University, Düsseldorf, Germany

²Division of Pediatric Neuro-Oncogenomics, German Cancer Research Center (DKFZ), Heidelberg, German Consortium for Translational Cancer Research (DKTK), partner site Essen/Düsseldorf, Düsseldorf, Germany

³Department of Pediatric Oncology, Hematology, and Clinical Immunology, Medical Faculty, University Hospital Düsseldorf, Düsseldorf, Germany

⁴Department of Neuropathology, Medical Faculty, Heinrich-Heine-University, Düsseldorf, Germany

⁵Leibniz Research Institute for Environmental Medicine, Düsseldorf, Germany

⁶Beijing Neurosurgical Institute, Capital Medical University, Beijing, P. R. China

⁷Institute of Human Genetics, Medical Faculty and University Hospital Düsseldorf, Heinrich-Heine-University Düsseldorf, Germany

⁸Molecular and Experimental Surgery, University Clinic for General, Visceral and Vascular Surgery, University Medical Center Magdeburg and Faculty of Medicine, Otto-von-Guericke-University Magdeburg, Magdeburg, Germany

⁹Medical Faculty, Heinrich-Heine University, Düsseldorf, Germany

Correspondence

Ulf Dietrich Kahlert, Molecular and Experimental Surgery, University Clinic for General, Visceral and Vascular Surgery, University Medical Center Magdeburg and Faculty of Medicine, Otto-von-Guericke-University Magdeburg Leipzig Strasse 44, 39120 Magdeburg. Email: ulf.kahlert@med.ovgu.de

Abstract

Limitations in genetic stability and recapitulating accurate physiological disease properties challenge the utility of patient-derived (PD) cancer models for reproducible and translational research. A portfolio of isogenic human induced pluripotent stem cells (hiPSCs) with different pan-cancer relevant oncoprotein signatures followed by differentiation into lineage-committed progenitor cells was genetically engineered. Characterization on molecular and biological level validated successful stable genetic alterations in pluripotency state as well as upon differentiation to prove the functionality of our approach. Meanwhile proposing core molecular networks possibly involved

Abbreviations: EC50, effective concentration 50 percent viability; EGFR^{III}, epidermal growth factor receptor variant III; EV, empty vector; FACS, fluorescence activated cell sorting; Gli1, glioma-associated oncogene 1; GO, gene ontology; HDAC, histone deacetylase; hiPSC, human induced pluripotent stem cells; IPA, Ingenuity pathway analysis; MTT, thiazolyl blue tetrazolium bromide; NPC, neural progenitor cells; PBS, phosphate buffer saline; PD, patient-derived; TP53, tumor protein 53; WT, wildtype

This is an open access article under the terms of the Creative Commons Attribution-NonCommercial License, which permits use, distribution and reproduction in any medium, provided the original work is properly cited and is not used for commercial purposes.

© 2022 The Authors. *Biotechnology Journal* published by Wiley-VCH GmbH

in early dysregulation of stem cell homeostasis, the application of our cell systems in comparative substance testing indicates the potential for cancer research such as identification of augmented therapy resistance of stem cells in response to activation of distinct oncogenic signatures.

KEYWORDS

cancer stem cells, c-MYC, EGFR, GLI1, in vitro pharmacology, induced pluripotent stem cells, progenitor cells, TP53

1 | INTRODUCTION

In vitro tumor models present the basic fundament of early-stage cancer research. Processing of tumor tissue, derived from surgical resection, to establish chronic in vitro models presents the traditional attempt in human cancer disease-modeling.¹ Historically, this approach has been proven to be successful, as a large portion of our current oncology blockbusters are based on discoveries made in such patient-derived (PD) model systems.² With the emergence of evidence that dysregulated stem cells are responsible for cardinal aspects of initiation and progression of malignant tumors,³ stem cell technologies impact the creation of recent PD cancer models with the establishment of spheroid, organoid, or assembloid culture protocols to generate cellular more complex – and therefore more physiologically relevant – test systems.⁴ However, the recent advancements in molecular technology revealed that genetic instability of cancer cell lines occurs which seems to be a driver of heterogeneity of results.^{5–7} Moreover, the molecular and cellular heterogeneity of the malignant tumors not only reasons why thereof-derived cell models, originating from a spatially isolated piece of the resection specimen, are incapable of sufficiently recapitulating tumor properties,⁸ but also makes it virtually impossible to isolate and present a functional model for the cell of origin for the entire tumor. Those fundamental disease modeling aspects have been proposed to be contributing factors to the so-called “reproducibility crisis in cancer research,” which is suggested to be a cardinal factor for the ethical and economical dilemma of low frequency of successful translation of preclinical cancer research findings into clinical use.^{9–11}

With the technological advancements in cell biology and cell engineering, the recent years documented the emergence of alternative tumor modeling procedures avoiding the use of patient material.¹² As such, hiPSCs derived from healthy donors present an unlimited resource of cells to serve as receiver matrixes for genetic elements encoding for cancer-relevant transformations. Such healthy donor-derived tumor models – herein referred to as hiPSC-oncogene models – manifest themselves as a sustainable alternative disease modeling strategy in the current cancer research community^{13–18} complementing the portfolio of lab tools alongside the use of PD systems. It is speculated that iPSC models of cancer, derived through synthetic approaches or reprogramming of tumor cells, may be beneficial to

homogeneously depict a cell of origin of cancers.^{12,19} Moreover, we have recently shown that hiPSC-oncogene models present a functional in vitro platform suitable for long-term storage while ensuring longitudinal reproducibility for in vitro substance testing.²⁰

This work presents the generation, characterization, and application of isogenic hiPSCs with overexpression of different pan-cancer relevant oncogenes including tumor protein 53 (TP53) R175H, glioma-associated oncogene 1 (GLI1), c-MYC, and epidermal growth factor receptor variant III (EGFRvIII) and their subsequent differentiation in tissue-specific progenitor cells. Given that malignant brain tumors present a disease class with clinical unmet needs, we chose to differentiate the hiPSC-oncogene models into the neural lineage (referred to as neural progenitor cells/ NPCs) as our example for application. The identification of biomarker-related differences in resistance to chemotherapies indicates the potential of our functional systems for early-stage drug development or the personalized medicine market.

2 | EXPERIMENTAL SECTION

2.1 | Cell culture

The hiPSC line iPSC11 was obtained from Alstem Inc. (CA, USA) and provided with accompanied cell line characterization (early 2019). Cells were cultured as previously published.²¹ Details are described in the supplementary material. Single-cell splitting was performed for propagation and setup of functional assays and is described in detail in the supplementary materials. Cellular viability was measured using the thiazolyl blue tetrazolium bromide (MTT; Sigma-Aldrich #M2128, MO, USA) assay as previously described.²² Neural differentiation was conducted via 3D differentiation protocol as described elsewhere.²³ The generated free-floating 3D-spheres were cultured in poly-(2-hydroxyethyl methacrylate) (polyHEMA) coated dishes with neural proliferation medium (DMEM and Ham's F12 in a 2:1 (v:v) ratio; 2% B27; 1% Penicillin/Streptomycin Gibco, Invitrogen) containing 20 ng per ml FGF and 20 ng per ml EGF (Peprotec, Germany). Proliferating NPCs at a diameter of 300–500 μm were cut once a week into 200 \times 200 μm^2 using a tissue chopper to expand the culture as described before.²³

2.2 | Cloning

Each vector with our genes of interest (GOI; GLI1, c-MYC, TP53R175H, and EGFRvIII) was cloned as previously described.¹⁸ A detailed protocol can be found in the supplementary material.

2.3 | Lentivirus production

Generation of lentiviral particles was done with a 3rd generation lentiviral packaging system as described previously¹⁸ and in the supplementary material.

2.4 | Transduction of hiPSCs

Lentiviral transduction of hiPSCs was performed as previously published²² and in the supplementary material.

2.5 | Western blot

Proteins were extracted from cells with a cold protein lysis buffer and a proteinase inhibitor mixture (Roche Applied Science #11697498001, Basel, Switzerland). Protein concentration was determined with the DC Protein Assay Kit (Bio-Rad Laboratories Inc., CA, USA). Protein lysates were separated on a precast gradient SDS-PAGE gel (Bio-Rad Laboratories Inc., #4561083, CA, USA) and transferred on a nitrocellulose membrane. Proteins were blocked using 5% milk (TP53R175H) or 5% bovine serum albumin (GLI1, EGFRvIII, c-MYC) in TBS-T. Primary antibodies were incubated in blocking solution on a vertical shaker at 4°C overnight. Primary antibodies were GLI1 (Cell Signaling Technologies #2643S, 1:1,000, MA, USA), c-MYC (Invitrogen #13-2500, 1:1,000, CA, USA), TP53 (Cell Signaling Technologies #2524S, 1:1,000, MA, USA), EGFR (Cell Signaling Technologies #4267S, 1:1,000, MA, USA), and the housekeeping gene GAPDH (ProteinTech Group Inc., #60004-1, 1:5,000, IL, USA). The next day, secondary anti-mouse and anti-rabbit antibodies conjugated with a fluorophore (LI-COR Biosciences #926-68072; #926-32211, NE, USA) or peroxidase (Jackson ImmunoResearch Laboratories Inc. #115-035-144; #115-035-003, PA, USA) were diluted 1:10,000 in the blocking reagent and incubated for 1 h at room temperature (RT). PageRuler Prestained Protein Ladder (ThermoFisher #26616) was used to verify band sizes. Proteins of transgenes run 29 kDa higher due to the EGFP-tag expression encoded the used pSin backbone. Signal was detected for fluorescence with the LI-COR Odyssey CLX Imager (LI-COR Biosciences, NE, USA) or film-based system for peroxidase-coupled antibodies to detect the chemiluminescent signal with SuperSignal West Pico (Thermo Fisher Scientific, MA, USA). The film-based system was used to detect the protein expression of c-MYC, all other proteins were detected via the fluorescence signal.

2.6 | DNA methylation analysis

DNA was extracted according to the manufacturers' instructions (DNA Blood Tissue Kit, Qiagen, Germany). Samples were diluted to a concentration of 25 ng μl^{-1} and sent in for analysis to the German Cancer Research Center (DKFZ, Heidelberg, Germany). DNA was bisulfite converted and applied to the Infinium MethylationEPIC Array (Illumina Inc., CA, USA). Molecular subgrouping, copy number profiling, and beta-methylation were performed as described before.²⁵ Principle component analysis (PCA) was conducted using Partek Genomics Suite (Partek Incorporated, MO, USA) using the covariance option, where genes with a higher variance have more influence on the clustering.

Ingenuity pathway analysis (IPA; Qiagen, Germany) was conducted using genes with probes that were unique to each sample and had differential expression (<0.3582 unmethylated and ≥ 0.3582 methylated) except for the TP53R175H/EGFRvIII where genes present in the single stable lines could also be in the double stable line.²⁵ IPA was run with default settings except for the knowledge base where high-confidence predictions were added. The significance cut-off for IPA was set to p -value < 0.05 for identification of canonical pathways and upstream regulators. Additionally, for upstream regulators, biological drugs, all chemical and miRNA entries, were filtered out. UPputative upstream targets were filtered to include at least three target genes to be considered for further analysis. According to instructions of application specialists of the next generation molecular cancer diagnostic platform (www.molecularneuropathology.org), one biological replicate/condition was submitted for DNA-methylation assessment. The relevant was uploaded in NCBI GEO with timestamped metadata description and could be made available upon request.

2.7 | Gene expression analysis

Total RNA of three biological replicates was extracted using the RNA Spin Column Extraction Kit (Macherey-Nagel, Germany) and transferred to the Biological-Medical Research Center (BMFZ) of the Heinrich-Heine-University Düsseldorf, Germany. RNA was prepared according to the manufacturer's instructions using the VAHTS Stranded mRNA-Seq Library Prep Kit for IlluminaV2 (Vazyme, China). A 300 ng of total RNA was used for the preparation and library amplification. For sequencing, the HiSeq 3000 platform (Illumina Inc., CA, USA) was used. Each sample was sequenced with 2×151 base pairs (bp) paired-end read and with at least 50 million reads. Results were analyzed using *R software*. All samples were analyzed compared to the empty vector (EV) control using the unpaired student's *t*-test. Additionally, the fold change was calculated with the ratio of the average gene expression. Significantly increased genes were described with a p -value < 0.05 in *t*-test and fold change values > 2 . Decreased genes had a p -value of < 0.05 and fold changes < 0.05 . The results of the differentially expressed genes were displayed in volcano plots drawn in *R*. The significantly increased or decreased genes obtained from the volcano plot analysis were analyzed using the online tool DAVID

Bioinformatics Resources 6.8.^{26,27} *Homo sapiens* was selected as background. The obtained gene ontology (GO) terms were sorted in ascending order of *p*-value. The relevant was uploaded in NCBI GEO with timestamped metadata description and can be made available upon request.

2.8 | Flow cytometry analysis

Stem cell marker expression on the cell was evaluated using the BD Stemflow Human Pluripotent Stem Cell Transcription Factor Analysis Kit (Becton, Dickinson and Company #560589, CA, USA). The detailed protocol could be found in the supplementary material. For NPCs, spheres were chopped to 0.1 mm and singularized using Accutase. In brief, 5×10^5 cells were stained each using the following antibodies: PerCP-Cy 5.5 Mouse anti-Oct3/4 (BD, 51-9006267), PE Mouse anti-Human Pax-6 (BD, 561552), Alexa Fluor 647 Mouse Anti-Nestin (560341), PerCP-Cy 5.5 Mouse IgG1, K Isotype Control (BD, 51-9006267), PE Mouse IgG2a, k Isotype Control (BD, 558595), and Alexa Fluor 647 Mouse IgG1 K Isotype Control (BD, 557732). Assessment of cell viability included live staining of the cells using the fixable viability stain (Fvs) 510 (#564406; BD, USA). Briefly: Cells were stained with Fvs 510 for 15 min at room temperature. Then, cells were washed using BD Staining buffer (#554656). After washing, cells were fixed in BD Cytotfix fixation buffer (#554655) for 20 min at room temperature. Then, cells were permeabilized using cold BD Phosflow Perm Buffer III (#558050) for 30 min on ice, before staining for Oct3/4-PerCP, Pax6-PE, and Nestin-Alexa 647 and respective isotype controls for 30 min at room temperature in BD Stain buffer. Cells were washed and resuspended in staining buffer and analyzed using a BD FACSCantoTM II system using BD FACS Diva Software Version 6.1.3.

2.9 | Immunocytochemistry

Immunocytochemical (ICC) staining of hiPSCs was performed using the stem cell markers Alexa Fluor 555 OCT3/4 (BD Bioscience #560306, CA, USA) and Alexa Fluor 647 TRA-1-60 (BD Bioscience #560122, CA, USA) in a dilution of 1:50. Each hiPSCs model, reaching 80%–90% confluence in a 6 well plate, was split in a 1:10 ratio²¹ in 96 wells of a 96-well plate. Cells were cultivated with daily medium change and fixed with 4% paraformaldehyde (PFA) at 37°C for 30 min when distinguished colonies were still visible (\approx 40%–50% confluency). Fixed cells were stored in DPBS –/– at 4°C in the dark until the staining was started. At first, cells were washed three times using 100 μ l per well phosphate buffer saline (PBS) and permeabilized using 0.1% Triton X-100 diluted in PBS. After blocking with 10% goat-serum (Merck #G9023, Germany) in PBS, conjugated antibodies against OCT3/4 and TRA-1-60 and 1% Hoechst33258 (100 μ l per well; Sigma Aldrich, Germany) were incubated overnight at 4°C. The next morning, antibodies were discarded and cells were washed three times with 100 μ l PBS per well. Marker expression was detected in the Cellomics ArrayScan VTI (Thermo Scientific, MA, USA) with the Photometrics X1 camera

(Thermo Scientific, MA, USA). Pictures were merged and brightness was adapted in ImageJ.

2.10 | Cytogenetic analysis of generated hiPSC-oncogene models

Karyotype analysis of wildtype (WT) and generated hiPSC-oncogene models was performed at the Institute of Human Genetics at the University Hospital Düsseldorf, Germany as described in Tigges et al.²¹

2.11 | In vitro pharmacology

Prominent FDA-approved drugs used in cancer therapy were selected (Table S2) to validate the utility of the hiPSC-oncogene models and thereof derived NPCs to have utility in functional assays. Most drugs function as inhibitors to prevent signal transduction or cell proliferation. As a positive control, staurosporine was used and paracetamol, a well-known pain medication, was used as a negative control. All drugs were applied in serial dilution yielding the following concentrations: 20 μ M, 2 μ M, 200 nM, 20 nM, 2 nM, 200 pM, and 2 pM. Cell viability of technical triplicates in three biological replicates was assessed, similar as conducted before.²⁴

For hiPSC: Viability was measured after 48 h of incubation time using MTT as described above. Normalization of results was done in reference to DMSO-treated hiPSCs and the two lowest concentrations.²⁸ Drugs were analyzed for their efficiency based on the effective concentration 50 (EC50) using the GraphPad Prism 8 software (GraphPad Software, CA, USA). The upper threshold was set to the value of 100 for subsequent curve-fitting calculations. The evaluation of the in vitro drug response experiments resulted in the stratification of the substances according to their average efficacy over all models, namely good, medium, and low efficacy (Table S2).

For NPCs: Spheres were dissociated using TrypLE Express (Gibco, Thermo Fischer, Germany). Briefly, the spheres were washed once with PBS and dissociated using 500 μ l TrypLE for up to 3 minutes. Cells were washed with a 5 ml neural proliferation medium and quantified using Trypan blue exclusion assay. To perform the drug screen, 5000 cells per well were seeded in 30 μ l of the aforementioned medium into 384 well plates and treated with drugs based on the results in the hiPSC-screen (analysis was focussed on the substances that showed altered effectivity when introducing oncogene overexpression). Substance effects on cell viability were assessed after 72 h drug exposure using luminescence-based CellTiterGlo (Promega, Germany) as previously described.²⁹

2.12 | RT-qPCR

The analysis of gene expression was conducted using an SYBR green-based method on BioRad instrumentation. Details on the method, comprising RNA extraction, cDNA synthesis, and PCR were described in

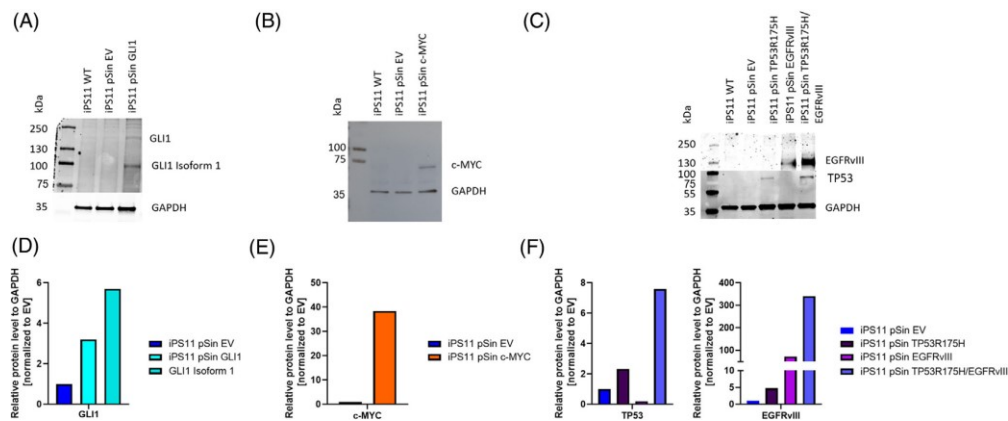


FIGURE 1 Verification of lentiviral transduction via Western blot. Protein lysates were analyzed for expression of GLI1 (A+D), c-MYC (B+E), as well as TP53 and EGFRvIII (C+F). Expression was validated in comparison to the protein expression of GAPDH for GLI1 (D), c-MYC (E), and TP53R175H/EGFRvIII (F). Representative pictures of the Western blots are shown which were also used for the quantification. WT, wild type; EV, empty vector; GLI1, glioma-associated oncogene 1; TP53, tumor protein 53; EGFRvIII, epidermal growth factor receptor variant III

more detail before.²² Primers used can be found in Table S3. The fold change in gene expression was calculated using the delta-delta method ($-\Delta\Delta Ct$) and statistical analysis was performed using GraphPad Prism 8 software and Microsoft Excel. As a statistical test, one-way ANOVA was performed.

3 | RESULTS

3.1 | Generation of hiPSC lines with stable oncogene overexpression

Vectors for the 3rd generation lentiviral packaging system were cloned and Sanger sequencing verified successful integration of the GOI. Positive sequenced vectors were used for the lentivirus production and transduction of hiPSCs. Successful integration was verified by protein expression of the target genes via western blot which confirmed overexpression of GLI1, c-MYC, TP53, and EGFRvIII (Figure 1A–C).

Expression of the respective oncoproteins was quantified in comparison to the housekeeping protein GAPDH and normalized to the expression in the empty vector (EV) control. Quantification revealed a three- and five-fold increase for the expression of GLI1 and the GLI1 isoform 1 (respectively, Figure 1A and D). Overexpression of c-MYC (Figure 1B) was 38-fold compared to iPS11 EV (Figure 1E). The created single mutation lines TP53R175H and EGFRvIII as well as the double mutation line of TP53R175H/EGFRvIII displayed overexpression of both, TP53 and EGFRvIII (Figure 1C and F). For the single mutation, the increase of TP53 was two-fold, while expression of TP53 in the double mutation was nearly 7.5-times as high as in the TP53R175H model alone (Figure 1F). Expression of EGFRvIII in the single mutation is about 20-fold increase, in the double mutation we reached up to 350-

fold increase, (Figure 1F). Viability assessment over 4 days in culture with all models compared to WT and EV control revealed no significant changes in viability (Figure S1). Figure 1 shows representative western blots of our assessments.

3.2 | Expression of stem cell markers by hiPSC-oncogene models

To exclude an effect of the introduced oncogenes on hiPSCs pluripotency, respective stem cell marker expression was analyzed using FACS analysis and ICC staining. For FACS analysis we used the common stem cell markers NANOG, SOX2, and OCT3/4, all of which are transcription factors that are expressed in hiPSCs and have been termed the “core” pluripotency factors in human embryonic stem cells.³⁰ This combination of markers has been widely used to characterize iPSCs.³¹

All cell lines expressed the analyzed markers over the threshold of 70%,^{29,30} in detail: iPS11 c-MYC and iPS11 TP53R175H/EGFRvIII had the lowest expression of NANOG/SOX2 with 78.16% and 75.78%, respectively (Table 1). For the gate of SOX2/OCT3/4, the lowest expression was detected in the double mutation with TP53R175H/EGFRvIII with 84.22%. All other models reached an expression of over 92% (Table 1).

Further, stem cell marker expression of TRA-1-60 and OCT3/4 was analyzed by ICC staining. For all analyzed hiPSC lines, WT, and generated models, we detected an expression of both stem cell markers, although in the EV and EGFRvIII models the staining was less intense (Figure 2). Overall, based on the FACS and ICC staining results, oncogene overexpression does not seem to influence the stemness characteristics of the generated hiPSC-oncogene models. In addition, we confirmed a normal male karyotype of all models using classical G-banding,

TABLE 1 Stem cell marker expression of hiPSC- oncogene models

model	NANOG/SOX2	SOX2/OCT3/4
iPS11-EV	94.45	93.84
iPS11-c-MYC	78.16	92.06
iPS11-GLI1	90.98	94.38
iPS11-TP53R175H	91.37	94.97
iPS11-EGFRvIII	86.39	92.36
iPS11-TP53R175H/EGFRvIII	75.78	84.22

All models were stained against NANOG, SOX2, and OCT3/4. Gates were set for NANOG/SOX2 and SOX2/OCT3/4. Expression of markers was measured via flow cytometry and indicates the pluripotency of the hiPSC models. All values are listed in % of viable cells. Exemplary dot blots of the data acquisition are presented in Supplementary files.

thereby confirming the chromosomal integrity of the models (Figure S2). FACS dot blots of example rounds of staining of hiPSC- oncogene models are provided in Figure S8.

3.3 | DNA-methylation analysis of hiPSC models

To further characterize the generated hiPSC- oncogene models, we conducted methylome analyses. The methylome profiles of all models were filtered to identify uniquely methylated (<0.3582) and unmethylated (≥ 0.3582) areas. In the hierarchical clustering, each of the hiPSC- oncogene models revealed a unique methylation profile (Figure 3A). The controls, WT and EV, had a different methylation profile than the generated hiPSC- oncogene models (Figure 3A). Models with the

expression of TP53R175H and EGFRvIII were clustered together as well and displayed the highest difference toward the control models (Figure 3A).

In accordance with the hierarchical cluster, small variations were identified between the TP53R175H, EGFRvIII, and TP53R175H/EGFRvIII models in the PCA (Figure 3B). This analysis was conducted to identify epigenetic variations between the hiPSC- oncogene models. The EV control had the highest epigenetic variation and clustered the furthest away from all other models (Figure 3B). In addition, we performed the Qiagen IPA to identify upstream targets of the respective hiPSC- oncogene models and canonical pathways using the genes with uniquely (un)methylated probes. For the TP53R175H, EGFRvIII, and TP53R175H/EGFRvIII models we did not apply the filter of uniquely regulated genes as genes of the single stable lines could also be expressed in the double stable line. Upstream targets were analyzed for each hiPSC- oncogene model and genes which interact with our introduced oncogenes were detected (Figure 3C). Details of strongest dysregulated signaling pathways and associated upstream gene targets, as well as overrepresented gene ontologies upon individual oncogene activation, can be found in Figures S3–S5.

3.4 | Transcriptome analysis of hiPSC models

Compared to EV control, all hiPSC- oncogene models had ≈ 30 – 40 genes that are either up- or downregulated except for the EGFRvIII model, in which we identified around 60–80 differentially regulated genes (Figure 4A). For each of the GLI1, c-MYC, and EGFRvIII models we detected one highly significantly up-regulated gene, which was the

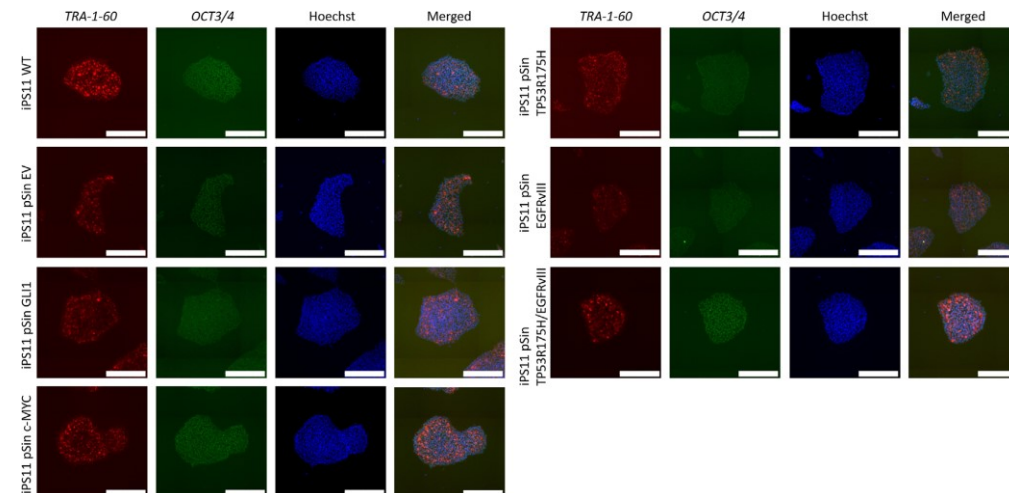


FIGURE 2 Immunocytochemical staining of hiPSC- oncogene models. Generated hiPSC models were stained with stem cell markers to verify their stemness properties using antibodies against TRA-1-60 (red) and OCT3/4 (green), nuclei were counterstained with Hoechst 33258 (blue). Six technical replicates were stained for each model. One representative hiPSC colony is displayed for each model. The scale bar is 250 μ m. Pictures were evaluated with ImageJ

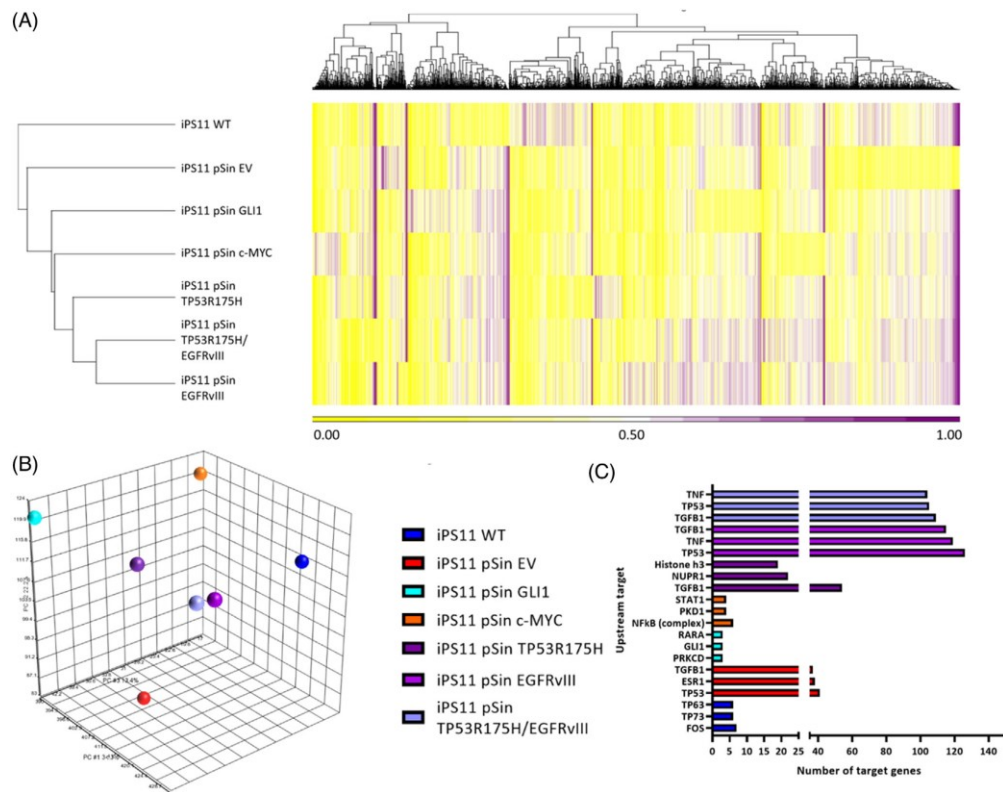


FIGURE 3 Hierarchical and PCA clustering and identification of upstream targets. Methylation profiles of the samples were compared to each other for uniquely regulated genes and visualized in a hierarchical cluster using Partek Genomics Suite (Partek Incorporated, MO, USA; (A)). Uniquely regulated genes were identified by comparison of the generated models to the iPS11 EV line. TP53R175H, EGFRvIII, and TP53R175H/EGFRvIII were analyzed together. Further, principal component analysis (PCA) was performed and the generated hiPSC-oncogene models were clustered using Partek Genomics Suite (Partek Incorporated, MO, USA; (B)). Methylation and PCA clustering were analyzed using the ingenuity pathway analysis (IPA; Qiagen, Germany) to identify upstream targets (C). TP53R175H, EGFRvIII, and TP53R175H/EGFRvIII were analyzed together as the genes were introduced in a single- and double-mutation cell line. For each model, we display the three upstream targets based on the number of target genes. The significance cut-off value for IPA was set at $p < 0.05$. One biological replicate was analyzed for each model

introduced oncogene of the respective model, indicating a successful gene integration and regulation (as defined by negative $\log p$ -value > 4 as compared to EV control model; Figure 4A). The double construct TP53R175H/EGFRvIII was the only model which had one gene (complement C7) highly significantly down-regulated (as defined by negative $\log p$ -value > 4 as compared to EV control model). We further evaluated the significantly regulated genes using GO enrichment analysis (Figure 4B). Transcriptomic changes in our hiPSC-oncogene models feature expression changes that have been described before in association with the introduced oncogenes. We did not detect any significantly enriched GO terms in the WT cells compared to the EV control.

3.5 | Lineage differentiation

A central verification for the suitability of our disease modeling attempt is the ability of hiPSC oncogene models to differentiate into lineage-committed progenitors, as oncogenes acquire their tumorigenic potential in the context of tissues and somatic cells. Table 2 shows the reduction of pluripotency marker and induction of NPC markers upon application of differentiation protocol verifying the maintenance of differentiation potential of our engineered models. FACS dot blots of example rounds of staining NPCs are provided in Figure S8.

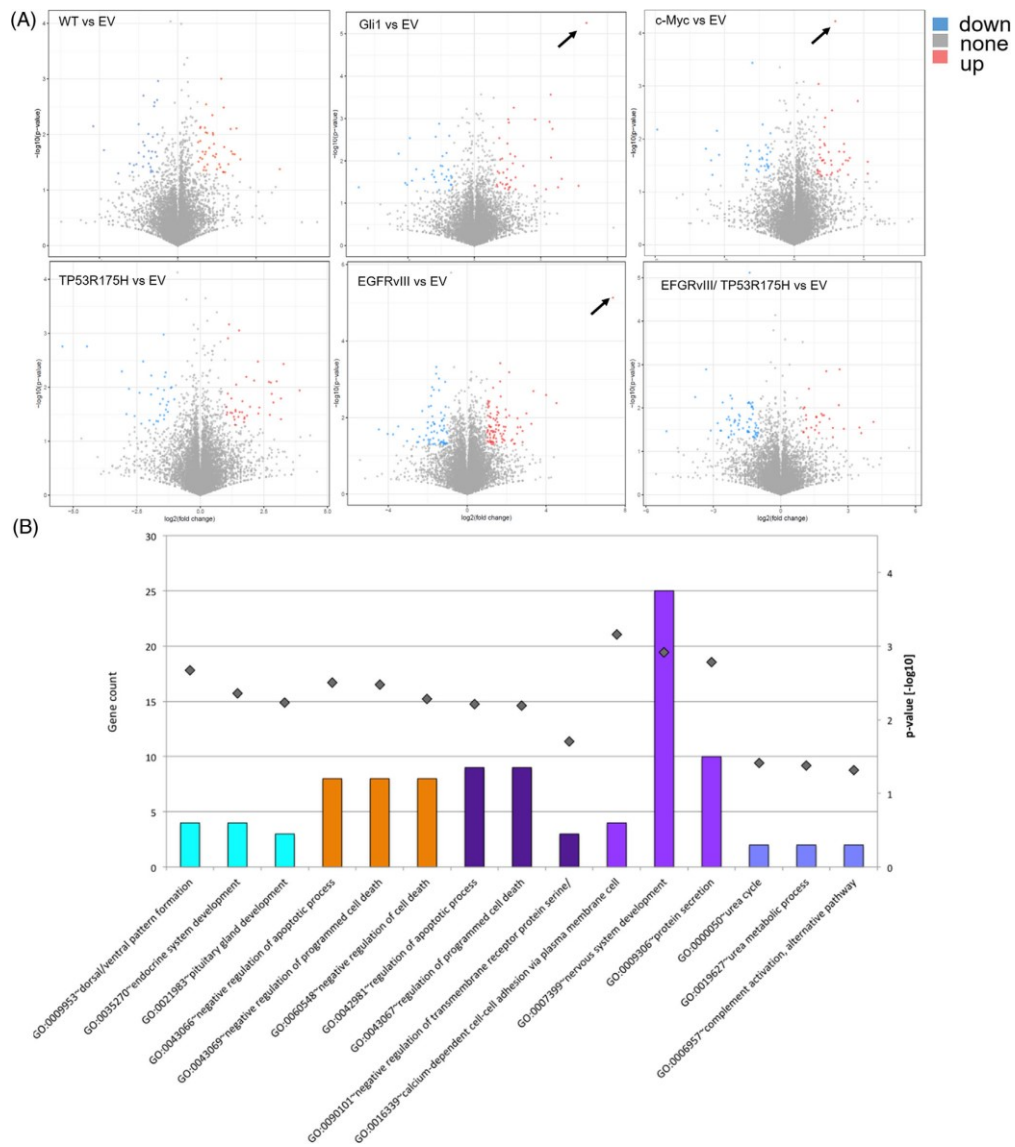


FIGURE 4 Volcano plot and enrichment analysis for transcriptome analysis in hiPSC-oncogene models. A volcano plot was done for all models and results of individual models were compared to the empty vector (EV) control (A). Based on the RNA transcriptome sequencing, we analyzed the significance (unpaired student's t-test, p -value < 0.05) and fold change. Genes are either significantly increased (fold change > 2, red), decreased (fold change < 0.5, blue) or not regulated (< 2 and > 0.5, gray). The y-axis indicates the significance of the gene regulation. A volcano plot was created with R. Arrows are used to mark the respective highest specific upregulated genes. Gene ontology (GO) terms were analyzed for the significantly regulated genes from the volcano plot. GO terms were analyzed by using the online tool DAVID Bioinformatics Resources 6.8 (B). Results were sorted in ascending order and the first three significant GO terms for each hiPSC-oncogene model are displayed. No significant GO term could be identified for the WT in comparison to the empty vector control (EV). The gene count is visualized using the columns and the p -values using dots

TABLE 2 Expression of stem cell marker OCT3/4 and neural progenitor markers PAX6 and Nestin on lineage-committed progenitor cells (NPCs) derived from oncogene overexpressing hiPSCs

model	PAX6	OCT3/4	Nestin
iNSP-EV	50.8	7.9	78.4
NPC-c-Myc	68.8	7.6	89.2
NPC-Gli1	26.5	74.2	97.4
NPC-TP53R175H	62	58.2	94.5
NPC-EGFRvIII	50.5	15.3	91.8
NPC-EGFRvIII/TP53R175H	47.3	33.8	88.1

Expression of markers was measured via flow cytometry and indicates the lineage commitment of the models. All values are listed in % of viable cells. Exemplary dot blots of the data acquisition are presented in Supplementary files.

3.6 | Molecular characterization of progenitor cells

To validate the lineage commitment we chose the current state-of-the-art DNA-methylation-based molecular cancer diagnostics used in clinical pathology.²⁵ Figure 5 shows a clear separation of hiPSC models (due to their monolayer growth designated as 2D) compared to their lineage differentiated counterparts (due to their spheroidal growth designated as 3D). Hierarchical clustering (Figure 5A) and principal com-

ponent analysis (PCA, Figure 5B). Figure 5C shows the continuous overexpression of the relevant oncogenes in the progenitors derived from the respective hiPCS model. This data validates the functionality of the basic concept of our method and indicates its versatility as a cell platform to generate modularly altered and tissue-specific cell systems derived from a highly homogenous population of cells of origin.

3.7 | Biomarker overexpression causes specific and comparable alterations in drug resistance in pluripotent and differentiated cells

Analyses of the resulting concentration-response curves reveal that WT and EV controls in the hiPSC models exert similar responses toward the drug treatments (Table 3, Figure S6). The highest efficacy on reducing cell viability was vinblastine sulfate (EC50 values between 0.0001 and 0.0008 μ M) followed by panobinostat (EC50 values between 0.02 and 0.14 μ M; Table 3; Figure S6). While a similar pattern of stress resistance to the kinase inhibitor panobinostat in EV/WT models was detected, we found an about 5-fold higher resistance in the GLI1 and a 7-fold higher resistance in the TP53R175H/EGFRvIII model. Likewise, resistance to the prominent, cell cycle progression targeting cancer drug vinblastine sulfate was increased in the GLI1-

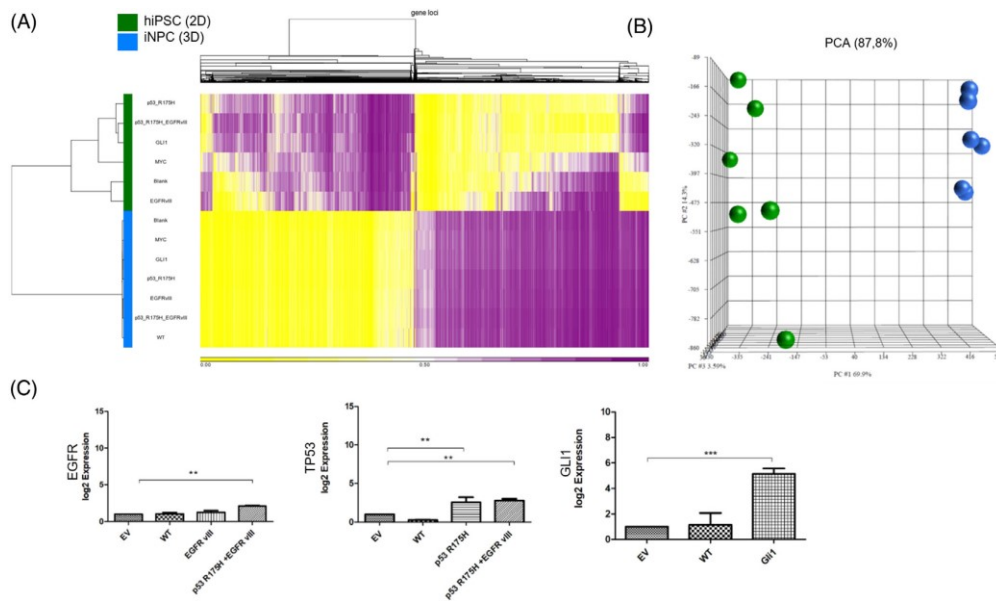


FIGURE 5 Molecular characterization of lineage differentiated progenitors. (A+ B) DNA methylation patterns of hiPSC models (grown in 2D) are compared to differentiated counterparts differentiated (neural progenitors, grown as 3D spheres). Hierarchical clustering (A) and PCA (B) of the DNA-methylome of the cells. (C) RT-qPCR-based validation of overexpression of oncogenes EGFR, p53, and Gli1 in the 3D differentiation-derived neural progenitors

TABLE 3 In vitro pharmacology response in hiPSC-oncogene models

Substance	iPS11-WT	iPS11- EV	iPS11-GLI1	iPS11-cMYC	iPS11-TP53R 175H	iPS11-EGFRvIII	iPS11- EGFRvIII/ TP53R175H
Panobinostat	0.0228	0.0222	0.1085	0.0531	0.0207	0.0290	0.1401
Vinblastine sulfate	0.0003	0.0001	0.0072	0.0006	0.0001	0.0008	0.0005
Apatinib mesylate	X	X	X	X	X	X	X
Lomustine	10.16	16.76	X	19.54	17.33	14.25	X
Duvelisib	7.9080	5.8080	16.21	13.03	6.1720	5.3680	6.2790
Cariprazine	X	X	X	X	X	X	X
Calcium folinate	X	X	X	X	X	X	X
Rivastigmine	X	X	X	X	X	X	X
Almotriptan malate	X	X	X	X	X	X	X
Paracetamol	X	X	X	X	X	X	X
Staurosporine	0.3972	0.1621	0.3872	1.4940	0.1951	0.2240	0.3585

All results were analyzed and effective concentrations (EC) 50 of all drugs were calculated using GraphPad Prism 8 (GraphPad Software, CA, USA). Cell viability results were normalized to DMSO treated hiPSCs and the two lowest concentrations²⁸. EC50 values are listed in μM and "X" indicates that an EC50 was not reached. WT, wild type; EV, empty vector; GLI1, glioma-associated oncogene 1; TP53, tumor protein 53; EGFRvIII, epidermal growth factor receptor variant III.

TABLE 4 In vitro pharmacology response in NPC models

Substance	NPC WT	NPC -EV	NPC -GLI1	NPC -c-MYC	NPC - TP53R175H	NPC -EGFRvIII	NPC- EGFRvIII/ TP53R175H
Panobinostat	0.05164	0.2940	0.4568	0.1237	0.01986	1.367	0.2856
Vinblastine sulfate	0.01518	0.003848	0.4806	0.01955	0.02161	7.166	3.291
Lomustine	13.96	188.8	2410	217.10	191.30	1364	270
Duvelisib	14.04	75.29	53.4	48.68	732.90	1062	322.50
Paracetamol	X	X	X	X	X	X	X
Staurosporine	0.1118	0.5545	0.1986	0.2675	1.657	1.639	0.1599

Effective concentrations (EC) 50 of all selected substances based on the indicative drug testing results in the hiPSCs-oncogene models. Drug treatment effects on cell viability were calculated using GraphPad Prism 8 (GraphPad Software, CA, USA). Cell viability results were normalized to DMSO treated NPCs and the two lowest concentrations.²⁶ EC50 values are listed in μM and "X" indicates that an EC50 was not reached. WT, wild type; EV, empty vector; GLI1, glioma-associated oncogene 1; TP53, tumor protein 53; EGFRvIII, epidermal growth factor receptor variant III.

(over 100-fold) and the EGFRvIII models (about 10-fold). Sigmoidal concentration-response curves for each hiPSC model can be found in the supplementary files (Figure S6). Importantly, a similar drug resistance pattern was observed in the differentiated NPCs (Table 4, Figure S7). Out of the experimental treatment arms, only panobinostat and vinblastine sulfate showed solid efficacy on the cells suitable for intermodel comparisons of drug resistance. Compared to EV/blank control, vinblastine resistance in Gli1 models increased about 10-fold and about 1000-fold in EGFRvIII models. Induction of Gli1 increased the resistance to panobinostat about 3-times and roughly 10-times in the EGFRvIII model. Of note, the addition of TP53R175H decreased the resistance to this drug. Taken together, this data is a proof of concept that such single cell of origin-derived, hiPSC-based cancer in vitro analogs are a suitable addition for validating biomarker-associated alterations in drug resistance identified when relying on PD cancer models only.

4 | DISCUSSION

PD in vitro systems represent the gold standard of functional human tumor models. Despite technical advances in culture technologies, research results relying on PD tumor models may be limited in their reproducibility and pathophysiological relevance, especially when relying on established cell lines and in the context of drug development.^{5,10} Together with the emergence of stem cell and genetic engineering technologies as dedicated future key innovation markets, those may be reasons why healthy donor-derived, synthetically generated in vitro cancer alternatives using stem cells penetrate the research sector as a valuable contribution to science projects.^{12,15,32} In this project, aiming toward the development of a platform technology for substance testing, we generated a collection of hiPSC-oncogene models and thereof derived lineage-committed progenitors (neural progenitor cells/ NPCs) and utilized them in identifying biomarker-associated drug resistances.

effect of the chosen oncoproteins in the context of human stemness. Although our platform technology has several technical limitations, given its theoretic potential to be amendable in any lineage differentiation, we believe it has significant value for cancer precision medicine applications, such as the development of targeted therapies of validation of the off-target potential of drugs on noncancer stem cells. Our platform provides off-the-shelf readiness, easing possible dissemination.

ACKNOWLEDGEMENT

The authors thank T Klein, Department of Genetics, and J Gopalakrishnan, Institute of Human Genetics (all Heinrich-Heine University Düsseldorf, Germany), and J. Klose (IUF Düsseldorf, Germany) for their support in this project and stimulating scientific discussions.

Open access funding enabled and organized by Projekt DEAL.

CONFLICTS OF INTEREST

The authors declare no conflict of interest.

DATA AVAILABILITY STATEMENT

Upon request, the generated hiPSC-oncogene model systems together with their respective sequencing data will be available to the academic field under MTA regulations. OMICS data is stored in the NCBI GEO database as indicated in the respective method sections.

ORCID

Michael Hewera  <https://orcid.org/0000-0002-4918-2875>

REFERENCES

- Stringer, B. W., Day, B. W., D'souza, R. C. J., Jamieson, P. R., Ensbey, K. S., Bruce, Z. C., Lim, Y. C., Goasdoué, K., Offenhäuser, C., Akgül, S., Allan, S., Robertson, T., Lucas, P., Tolleson, G., Campbell, S., Winter, C., Do, H., Dobrovic, A., Inglis, P.-L., ... Boyd, A. W. (2019). A reference collection of patient-derived cell line and xenograft models of proneural, classical and mesenchymal glioblastoma. *Science Reports*, 9, 4902.
- Chabner, B. A. (2016). NCI-60 cell line screening: A radical departure in its time. *JNCI: Journal of the National Cancer Institute*, 108, djv388.
- Atashzar, M. R., Baharlou, R., Karami, J., Abdollahi, H., Rezaei, R., Pourramezan, F., & Zoljalali Moghaddam, S. H. (2020). Cancer stem cells: A review from origin to therapeutic implications. *Journal of Cellular Physiology*, 235, 790–803.
- Pyo, D. H., Hong, H. K., Lee, W. Y., & Cho, Y. B. (2020). Patient-derived cancer modeling for precision medicine in colorectal cancer: Beyond the cancer cell line. *Cancer Biology & Therapy*, 21, 495–502.
- Ben-David, U., Siranosian, B., Ha, G., Tang, H., Oren, Y., Hinohara, K., Strathdee, C. A., Dempster, J., Lyons, N. J., Burns, R., Nag, A., Kugener, G., Cimini, B., Tsvetkov, P., Maruvka, Y. E., O'Rourke, R., Garrity, A., Tubelli, A. A., Bandopadhyay, P., ... Golub, T. R. (2018). Genetic and transcriptional evolution alters cancer cell line drug response. *Nature*, 560, 325–330.
- Ben-David, U., Ha, G., Tseng, Y.-Y., Greenwald, N. F., Oh, C., Shih, J., McFarland, J. M., Wong, B., Boehm, J. S., Beroukhim, R., & Golub, T. R. (2017). Patient-derived xenografts undergo mouse-specific tumor evolution. *Nature Genetics*, 49, 1567–1575.
- Ben-David, U., Beroukhim, R., & Golub, T. R. (2019). Genomic evolution of cancer models: Perils and opportunities. *Nature Reviews Cancer*, 19, 97–109.
- Yu, K., Chen, B., Aran, D., Charalef, J., Yau, C., Wolf, D. M., Van 'T Veer, L. J., Butte, A. J., Goldstein, T., & Sirotta, M. (2019). Comprehensive transcriptomic analysis of cell lines as models of primary tumors across 22 tumor types. *Nature Communication*, 10, 3574.
- Freedman, L. P., Cockburn, I. M., & Simcoe, T. S. (2015). The economics of reproducibility in preclinical research. *Plos Biology*, 13, e1002165.
- Haibe-Kains, B., El-Hachem, N., Birkbak, N. J., Jin, A. C., Beck, A. H., Aerts, H. J. W. L., & Quackenbush, J. (2013). Inconsistency in large pharmacogenomic studies. *Nature*, 504, 389–393.
- Mak, I. W., Evaniew, N., & Ghert, M. (2014). Lost in translation: Animal models and clinical trials in cancer treatment. *American Journal of Translational Research*, 6, 114–118.
- Mehrjardi, N. Z., Hänggi, D., & Kahlert, U. D. (2020). Current biomarker-associated procedures of cancer modeling—a reference in the context of IDH1 mutant glioma. *Cell Death & Disease*, 11, 998.
- Hanaford, A. R., Archer, T. C., Price, A., Kahlert, U. D., Maciaczyk, J., Nikkha, G., Kim, J. W., Ehrenberger, T., Clemons, P. A., Dančík, V., Seashore-Ludlow, B., Viswanathan, V., Stewart, M. L., Rees, M. G., Shamji, A., Schreiber, S., Fraenkel, E., Pomeroy, S. L., Mesirov, J. P., ... Raabe, E. H. (2016). DiSCoVERing innovative therapies for rare tumors: Combining genetically accurate disease models with in silico analysis to identify novel therapeutic targets. *Clinical Cancer Research*, 22, 3903–3914.
- Pamies, D., Zurich, M.-G., & Hartung, T. (2020). Organotypic models to study human glioblastoma: Studying the beast in its ecosystem. *iScience*, 23, 101633.
- Sancho-Martinez, I., Nivet, E., Xia, Y., Hishida, T., Aguirre, A., Ocampo, A., Ma, L., Morey, R., Krause, M. N., Zembrzycki, A., Ansgore, O., Vazquez-Ferrer, E., Dubova, I., Reddy, P., Lam, D., Hishida, Y., Wu, M.-Z., Esteban, C. R., O'leary, D., ... Izpisua Belmonte, J. C. (2016). Establishment of human iPSC-based models for the study and targeting of glioma initiating cells. *Nature Communication*, 7, 10743.
- Smith, R. C., & Tabar, V. (2019). Constructing and deconstructing cancers using human pluripotent stem cells and organoids. *Cell Stem Cell*, 24, 12–24.
- Zhang, M., Vandana, J. J., Lacko, L., & Chen, S. (2020). Modeling cancer progression using human pluripotent stem cell-derived cells and organoids. *Stem Cell Research*, 49, 102063.
- Uhlmann, C., Kuhn, L.-M., Tigges, J., Fritsche, E., & Kahlert, U. D. (2020). Efficient modulation of TP53 expression in human induced pluripotent stem cells. *Current Protocols in Stem Cell Biology*, 52, e102.
- Kim, J., Hoffman, J. P., Alpaugh, R. K., Rhim, A. D., Reichert, M., Stanger, B. Z., Furth, E. E., Sepulveda, A. R., Yuan, C.-X., Won, K.-J., Donahue, G., Sands, J., Gumbs, A. A., & Zaret, K. S. (2013). An iPSC line from human pancreatic ductal adenocarcinoma undergoes early to invasive stages of pancreatic cancer progression. *Cell Reports*, 3, 2088–2099.
- Khan, D., Nickel, A.-C., Jeising, S., Uhlmann, C., Muhammad, S., Hänggi, D., Fischer, I., & Kahlert, U. D. (2021). Testing the stability of drug resistance on cryopreserved, gene-engineered human induced pluripotent stem cells. *Pharmaceuticals (Basel)*, 14, 919.
- Tigges, J., Bielec, K., Brockerhoff, G., Hildebrandt, B., Hübenthal, U., Kapr, J., Koch, K., Teichweyde, N., Wiczorek, D., Rossi, A., & Fritsche, E. (2021). Academic application of Good Cell Culture Practice for induced pluripotent stem cells. *AlTEX*, 38, 595–614.
- Kahlert, U. D., Maciaczyk, D., Doostkam, S., Orr, B. A., Simons, B., Bogiel, T., Reithmeier, T., Prinz, M., Schubert, J., Niedermann, G., Brabletz, T., Eberhart, C. G., Nikkha, G., & Maciaczyk, J. (2012). Activation of canonical WNT/ β -catenin signaling enhances in vitro motility of glioblastoma cells by activation of ZEB1 and other activators of epithelial-to-mesenchymal transition. *Cancer Letters*, 325, 42–53.
- Nimt, L., Hofrichter, M., Kabiri, Y., Egly, J., Theiss, S., Adjaye, J., & Fritsche E. (2016). Pluripotent stem cell-derived neurospheres as an alternative in vitro method to study neurotoxic effects on multielectrode arrays. MEA Meeting 2016 | 10th International Meeting on Substrate-Integrated Electrode Arrays.

24. Koch, K., Hartmann, R., Tsiampali, J., Uhlmann, C., Nickel, A.-C., He, X., Kamp, M. A., Sabel, M., Barker, R. A., Steiger, H.-J., Hänggi, D., Willbold, D., Maciaczyk, J., & Kahlert, U. D. (2020). A comparative pharmacometabolic study of glutaminase inhibitors in glioma stem-like cells confirms biological effectiveness but reveals differences in target-specificity. *Cell Death Discovery*, 6, 20.
25. Capper, D., Jones, D. T. W., Sill, M., Hovestadt, V., Schrimpf, D., Sturm, D., Koelsche, C., Sahm, F., Chavez, L., Reuss, D. E., Kratz, A., Wefers, A. K., Huang, K., Pajtler, K. W., Schweizer, L., Stichel, D., Olar, A., Engel, N. W., Lindenberg, K., ... Pfister, S. M. (2018). DNA methylation-based classification of central nervous system tumours. *Nature*, 555, 469–474.
26. Huang da, W., Sherman, B. T., & Lempicki, R. A. (2009). Systematic and integrative analysis of large gene lists using DAVID bioinformatics resources. *Nature Protocols*, 4, 44–57.
27. Huang da, W., Sherman, B. T., & Lempicki, R. A. (2009). Bioinformatics enrichment tools: Paths toward the comprehensive functional analysis of large gene lists. *Nucleic Acids Research*, 37, 1–13.
28. Krebs, A., Nyffeler, J., Rahnenführer, J., & Leist, M. (2018). Normalization of data for viability and relative cell function curves. *Altex*, 35, 268–271.
29. Nickel, A. C., Picard, D., Qin, N., Wolter, M., Kaulich, K., Hewera, M., Pauck, D., Marquardt, V., Torga, G., Muhammad, S., Zhang, W., Schnell, O., Steiger, H.-J., Hänggi, D., Fritsche, E., Her, N.-G., Nam, D.-H., Carro, M. S., Remke, M., ... Kahlert, U. D. (2021). Longitudinal stability of molecular alterations and drug response profiles in tumor spheroid cell lines enables reproducible analyses. *Biomedicine & Pharmacotherapy*, 144, 112278.
30. Boyer, L. A., Lee, T. I., Cole, M. F., Johnstone, S. E., Levine, S. S., Zucker, J. P., Guenther, M. G., Kumar, R. M., Murray, H. L., Jenner, R. G., Gifford, D. K., Melton, D. A., Jaenisch, R., & Young, R. A. (2005). Core transcriptional regulatory circuitry in human embryonic stem cells. *Cell*, 122, 947–956.
31. Pamies, D., Bal-Price, A., Simeonov, A., Tagle, D., Allen, D., Gerhold, D., Yin, D., Pistollato, F., Inutsuka, T., Sullivan, K., Stacey, G., Salem, H., Leist, M., Daneshian, M., Vemuri, M. C., McFarland, R., Coecke, S., Fitzpatrick, S. C., Lakshminpathy, U., ... Hartung, T. (2017). Good cell culture practice for stem cells and stem-cell-derived models. *Altex*, 34, 95–132.
32. Koga, T., Chaim, I. A., Benitez, J. A., Markmiller, S., Parisian, A. D., Hevner, R. F., Turner, K. M., Hessenauer, F. M., D'antonio, M., Nguyen, N.-P. D., Saberi, S., Ma, J., Miki, S., Boyer, A. D., Ravits, J., Frazer, K. A., Bafna, V., Chen, C. C., Mischel, P. S., ... Furnari, F. B. (2020). Longitudinal assessment of tumor development using cancer avatars derived from genetically engineered pluripotent stem cells. *Nature Communication*, 11, 550.
33. Kandath, C., McLellan, M. D., Vandin, F., Ye, K., Niu, B., Lu, C., Xie, M., Zhang, Q., McMichael, J. F., Wyczalkowski, M. A., Leiserson, M. D. M., Miller, C. A., Welch, J. S., Walter, M. J., Wendl, M. C., Ley, T. J., Wilson, R. K., Raphael, B. J., & Ding, L. (2013). Mutational landscape and significance across 12 major cancer types. *Nature*, 502, 333–339.
34. Massagué, J. (2008). TGFbeta in cancer. *Cell*, 134, 215–230.
35. Tishler, R. B., Lamppu, D. M., Park, S., & Price, B. D. (1995). Microtubule-active drugs taxol, vinblastine, and nocodazole increase the levels of transcriptionally active p53. *Cancer Research*, 55, 6021–6025.
36. Cheng, Y.-W., Liao, L.-D., Yang, Q., Chen, Y., Nie, P.-J., Zhang, X.-J., Xie, J.-J., Shan, B.-E., Zhao, L.-M., Xu, L.-Y., & Li, E.-M. (2018). The histone deacetylase inhibitor panobinostat exerts anticancer effects on esophageal squamous cell carcinoma cells by inducing cell cycle arrest. *Cell Biochemistry and Function*, 36, 398–407.
37. Greve, G., Schiffmann, I., Pfeifer, D., Pantic, M., Schüller, J., & Lübbert, M. (2015). The pan-HDAC inhibitor panobinostat acts as a sensitizer for erlotinib activity in EGFR-mutated and -wildtype non-small cell lung cancer cells. *BMC Cancer*, 15, 947.
38. Sonnemann, J., Marx, C., Becker, S., Wittig, S., Palani, C. D., Krämer, O. H., & Beck, J. F. (2014). p53-dependent and p53-independent anticancer effects of different histone deacetylase inhibitors. *British Journal of Cancer*, 110, 656–667.
39. Falkenberg, K. J., Newbold, A., Gould, C. M., Luu, J., Trapani, J. A., Matthews, G. M., Simpson, K. J., & Johnstone, R. W. (2016). A genome scale RNAi screen identifies GLI1 as a novel gene regulating vorinostat sensitivity. *Cell Death and Differentiation*, 23, 1209–1218.
40. Staunstrup, N. H., Moldt, B., Mátés, L., Villesen, P., Jakobsen, M., Ivics, Z., Izsvák, Z., & Mikkelsen, J. G. (2009). Hybrid lentivirus-transposon vectors with a random integration profile in human cells. *Molecular Therapy*, 17, 1205–1214.
41. Woods, N.-B., Muessig, A., Schmidt, M., Flygare, J., Olsson, K., Salmon, P., Trono, D., von Kalle, C., & Karlsson, S. (2003). Lentiviral vector transduction of NOD/SCID repopulating cells results in multiple vector integrations per transduced cell: Risk of insertional mutagenesis. *Blood*, 101, 1284–1289.

SUPPORTING INFORMATION

Additional supporting information may be found in the online version of the article at the publisher's website.

How to cite this article: Uhlmann, C., Nickel, A.-C., Picard, D., Rossi, A., Li, G., Hildebrandt, B., Brockerhoff, G., Bendt, F., Hübenthal, U., Hewera, M., Steiger, H.-J., Wiczorek, D., Perrakis, A., Zhang, W., Remke, M., Koch, K., Tigges, J., Croner, R. S., Fritsche, E., & Kahlert, U. D. (2022). Progenitor cells derived from gene-engineered human induced pluripotent stem cells as synthetic cancer cell alternatives for in vitro pharmacology. *Biotechnology Journal*, 17, e2100693. <https://doi.org/10.1002/biot.202100693>

Publications

A genetically modified hiPSC-based in vitro model to identify novel drug candidates for type 3 medulloblastoma treatment

Julia Tigges, **Constanze Uhlmann***, Katharina Koch, Arif Dönmez, Ann-Christin Nickel, Farina Bendt, Ulrike Hübenthal, Gabriele Brockerhoff, Daniel Picard, Andrea Rossi, Ulf Dietrich Kahlert, Ellen Fritsche

*Constanze Krambrich's maiden name was Constanze Uhlmann.

Journal:	Cancers
Impact Factor:	6.575 (2021)
Contribution to the publication:	20 %
Type of authorship:	Co-authorship; generation of hiPSC-oncogene models
Status of the publication:	Revision



1 Article

2 A genetically modified hiPSC-based *in vitro* model to identify 3 novel drug candidates for type 3 medulloblastoma treatment

4 Julia Tigges¹, Constanze Uhlmann², Katharina Koch¹, Arif Dönmez¹, Ann-Christin Nickel², Farina Bendt¹, Ulrike
5 Hübenthal¹, Gabriele Brockerhoff¹, Daniel Picard^{3,4,5}, Andrea Rossi¹, Ulf Dietrich Kahlert⁶, Ellen Fritsche^{1,7,*}

6
7
8
9
10
11
12
13
14
15
16
17
18
19
20
21
22

¹ IUF - Leibniz Research Institute for Environmental Medicine, Duesseldorf, Germany, JT: Julia.Tigges@UF-Duesseldorf.de, KK: Katharina.Koch@UF-Duesseldorf.de, AD: Arif.Doenmez@UF-Duesseldorf.de, FB: Farina.Bendt@UF-Duesseldorf.de, UH: Ulrike.Huebenthal@UF-Duesseldorf.de, GB: Gabriele.Brockerhoff@UF-Duesseldorf.de, AR: Andrea.Rosse@UF-Duesseldorf.de, EF: Ellen.Fritsche@UF-Duesseldorf.de
² Department of Neurosurgery, University Hospital Düsseldorf, Düsseldorf, Germany, CU: Constanze.Uhlmann@hu.de, ACN: ann-christin.nickel@hu.de
³ Division of Pediatric Neuro-Oncogenomics, German Cancer Research Center (DKFZ), Heidelberg, German Consortium for Translational Cancer Research (DKTK), partner site Essen/Düsseldorf, Düsseldorf, Germany
⁴ Department of Pediatric Oncology, Hematology, and Clinical Immunology, Medical Faculty, University Hospital Düsseldorf, Düsseldorf, Germany, Daniel.Picard@med.uni-duesseldorf.de
⁵ Department of Neuropathology, Medical Faculty, Heinrich-Heine-University, Düsseldorf, Germany
⁶ Molecular and Experimental Surgery, University Clinic for General-, Visceral-, Vascular- and Trans-Plantation Surgery, Medical Faculty and University Hospital Magdeburg, Otto-von Guericke University, Magdeburg, Germany, ulf.kahlert@med.ovgu.de
⁷ Medical Faculty, Heinrich-Heine-University, Duesseldorf, Germany
* Correspondence: Ellen.Fritsche@UF-Duesseldorf.de

Citation: Tigges, J.; Uhlmann, C.; Koch, K.; Dönmez, A.; Nickel, A.-C.; Bendt, F.; Hübenthal, U.; Brockerhoff, G.; Picard, D.; Rossi A.; Kahlert U.D.; Fritsche, E. A genetically modified hiPSC-based *in vitro* model to identify novel drug candidates for type 3 medulloblastoma treatment. *Cancers* **2022**, *14*, x. <https://doi.org/10.3390/xxxxx>

Academic Editor: Firstname Lastname

Received: date

Accepted: date

Published: date

Publisher's Note: MDPI stays neutral with regard to jurisdictional claims in published maps and institutional affiliations.



Copyright: © 2022 by the authors. Submitted for possible open access publication under the terms and conditions of the Creative Commons Attribution (CC BY) license (<https://creativecommons.org/licenses/by/4.0/>).

Simple Summary: Medulloblastoma is one of the most common brain tumors in children and is very difficult to treat. One type of this tumor in particular, called medulloblastoma type 3, leads to the death of most of the affected children. So-called tumor stem cells are being discussed as the cause of this tumor. In our work, we have now attempted to recreate this type of cells in the culture dish, thereby having the opportunity to identify potential drugs that could be of benefit to affected patients.

Abstract: With an incidence of 6 in 1 million children under 15 years of age, medulloblastoma (MB) is the second most common malignant brain tumor in children. This type of cancer is characterized by high inter-tumoral heterogeneity responsible for the limited effects of standardized therapeutic procedures. Amongst the different subtypes of MB, the type 3 subgroup, characterized by a mutation in the c-myc gene, has the lowest survival rate and in comparison to the other subgroups these patients have a higher metastasis rate. As tumor stem cells are discussed to contribute to MB formation we here present an approach to use genetically modified human induced pluripotent stem cells (hiPSC) as an *in vitro* model for MB-subtype specific drug screening. Therefore, we used an algorithm to associate gene activity and drug sensitivity in published gene expression profiles of clinical cohorts of other tumor types. The identified drug candidates were screened for their effects on tumor cell migration and cytotoxicity in a lentivirally generated hiPSC-based MB *in vitro* model and the respective empty vector control. Cisplatin as the standard of care for MB, as well as acetaminophen as a non-efficient therapeutic were included in the study. Using this procedure, we identified copanlisib, an α - and δ -isoform-specific phosphoinositide 3-kinase (PI3K) inhibitor, to reduce migration and cell survival stronger in the MB-tumor models than in the control cells. Furthermore, cisplatin treatment had a significant effect on tumor cell survival, however, the controls were more affected than the *in vitro* tumor models, indicating a possible favorable effect of copanlisib treatment for group 3 MB patients. In conclusion, this study provides a proof-of-concept that genetically modified, hiPSC-based, tumor subgroup-specific *in vitro* models might be useful to identify novel, previously approved drug candidates from existing databases for clinical testing of novel brain tumor therapies.

50
51
52

Keywords: medulloblastoma; patient-specific hiPSC; copanlisib, MYC, *in vitro* model, drug screening

53

54

1. Introduction

55

56

57

58

59

60

61

62

63

64

With an incidence of 6 per one million [1] medulloblastoma (MB; WHO grade IV) is the second most malignant tumor of the central nervous system (CNS) in children [2]. As defined by the World Health Organization (WHO), MB is classified on the basis of a combination of molecular and histopathological features and is divided into four molecular subgroups: WNT-activated, SHH-activated, and the non-WNT/non-SHH groups 3 and 4 [2,3]. Group 3 MB is an embryonal tumor of the cerebellum which occurs predominantly in infants and young children [3,4] and accounts for approximately 40% of MB cases in childhood [2]. Up to 45% of these patients already have metastasis at the time of diagnosis which yields in a 5-year survival rate of under 60%, representing the worst survival outcome of the four subgroups [3,5,6].

65

66

67

68

69

70

71

72

73

74

75

The genetic background of group 3 MB is poorly understood [7–10], yet high levels of the MYC proto-oncogene are present in 17% of these tumors and are considered a hallmark mutation of group 3 MBs [5,11]. C-myc amplification is highly associated with poor outcome in patients [11–13], which is partly due to poor response to conventional treatment like craniospinal radiation and high-dose chemotherapy [4,14]. Furthermore, it has been reported that about 25% of MB patients, especially young children, suffer from severe long-term treatment side effects including hearing loss, short stature, stroke, cerebrovascular disease, endocrine disorders, and neurocognitive deficits [15–18] that have a significant impact on their quality of life [19]. Therefore, the identification of improved therapeutic strategies which are on the one hand more effective than the current standard of care, and on the other hand are less toxic are urgently needed.

76

77

78

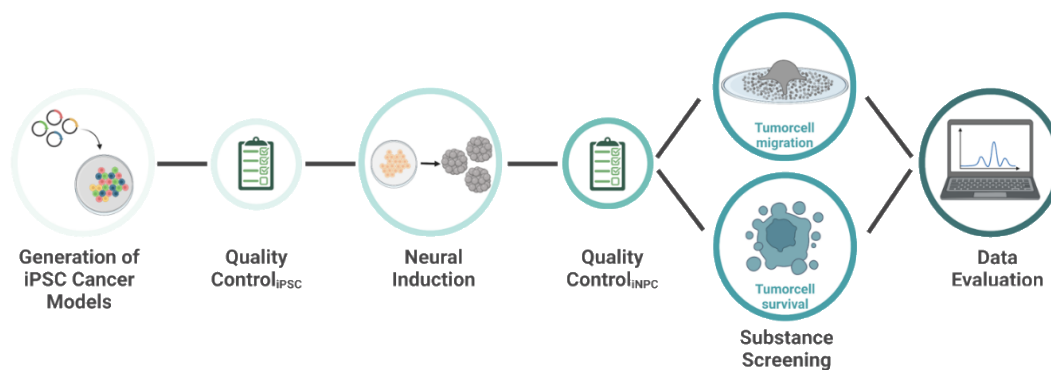
79

80

81

82

The identification of molecular MB subgroups combined with state-of-the-art biotechnology opens up new opportunities for personalized therapeutic approaches. In this proof-of-concept study, we used a genetically modified hiPSC tumor model for group 3 MB, c-myc-hiPSC, which were then neurally induced to c-myc-hiNPCs and cultured as three-dimensional aggregates to screen different already FDA-approved drugs for their effect on hiNPC migration as a readout for invasiveness/metastasis, and tumor cell survival (Fig. 1).



83

84

85

86

87

Figure 1. Experimental Setup. hiPSC tumor models for medulloblastoma type 3 and the respective empty vector control were generated using lentiviral transduction. hiPSC tumor models were quality controlled using flow cytometry and afterwards neurally induced to hiNPCs. These models were again quality controlled and then used for a drug screening to analyze the effects of different drugs on cell migration and cell survival. Finally, the data was evaluated bioinformatically. Figure created with BioRender.com.

88

89
90
91
92
93
94
95
96
97
98
99
100
101
102
103
104
105
106
107
108
109
110
111
112
113
114
115
116
117
118
119
120
121
122
123
124
125
126
127
128

2. Materials and Methods

2.1. Selection of drugs

Drug prediction was based on gene expression profiles of clinical cohorts (freely available through data portals such as (<https://hgserver1.amc.nl/cgi-bin/r2/main.cgi>)). Significant genes were determined using student T-test ($p < 0.05$ and fold change ± 2), uploaded to PanDrugs (<https://www.pandrugs.org>) and queried for potential drugs. The identified drugs were ranked according to the G- and D-scores, whereby the G-score measures the biological relevance of the gene in the tumoral process (range 0 - 1) and the D-score measures the suitability of the drug according to the genomic profile (-1 - 1), negative values corresponding to resistance and positive values corresponding to sensitivity. The so identified drugs were then sorted according to their effectiveness and further inclusion criteria were defined. These included the mode of action of the drug in question, the ability to cross the blood-brain barrier, and applicability in the laboratory (e.g. radioactive drugs were excluded). The top 7 drug candidates selected in this way (see Table 1) were then investigated in the hiPSC-based cell models for their effect with regard to hiNPC migration and cytotoxicity. In addition, we tested cisplatin, the respective standard of care, and acetaminophen, a substance that should have no effect on the hiPSC-based model and served as a negative control.

To ensure that we used concentrations that could be achieved *in vivo* in patients, we searched the literature for the C_{max} concentrations and protein binding for each compound ([20–22]; Daily Med (<https://dailymed.nlm.nih.gov/dailymed/>)). We then determined the calculated free drug concentration (cfdc) by taking the published protein binding into account and defined that the observed effect in our *in vitro* models must be in the range of $cfdc_{high}$ ($cfdc \times 3$) to be considered a specific effect (see also Fig. 3) and ensured that the tested concentration range included the C_{max} for the respective substance.

Table 1. Background information on substances used for drug screening.

Substance	CAS#	C_{max} [μ M]	Protein Binding [%]	cfdc [μ M]	$cfdc_{high}$ [μ M]	Concentra- tions tested [μ M]
Acetaminophen [21] (NK)	103-90-2	120.00	20.00	96.00	288.00	0.0274 – 20
Arsenic trioxide [20]	1327-53-3	0.91	75.00	0.69	2.08	0.0012 – 0.91
Cisplatin [20] (SoC)	15663-27-1	14.40	0.00	14.40	43.20	0.0198 – 14.4
Copanlisib*	1032568-63-0	0.96	84.20	0.15	0.46	0.0001 – 0.96
Dasatinib [20]	302962-49-8	0.26	96.00	0.01	0.03	0.0004 – 0.264
Midostaurin [22]	120685-11-2	2.78	99.80	0.01	0.02	0.0038 – 2.776
Regorafenib [20]	755037-03-7	8.08	99.50	0.04	0.12	0.0111 – 8.08
Tretinoin [20]	302-79-4	1.15	95.00	0.06	0.17	0.0016 – 1.15
Vandetanib [20]	443913-73-3	2.16	90.00	0.22	0.65	0.003 – 2.16

cfdc = calculated free drug concentration; $cfdc_{high}$ = $cfdc \times 3$; SoC = Standard of Care; NC = negative control; *Information taken from: Daily Med (<https://dailymed.nlm.nih.gov/dailymed/>).

All drugs, except for arsenic trioxid, which was purchased from Merck (Darmstadt, Germany), were ordered from MedChemExpress (USA).

2.2. hiPSC culture

hiPSCs were cultured as previously described in detail [23].

2.3. Generation of *c-myc* hiNPCs and respective empty vector controls

2.3.1. Lentivirus generation

HEK293T cells for lentivirus production were plated on a 10 cm dish and cultured in DMEM GlutaMax (ThermoFisher #31966-021) with 10% FBS and 1% Pen/Strep (P/S) to

129 reach a confluency of ~70% after 24 hours. Cells were transfected using the lentiviral
130 packaging plasmids and the vector containing the GOI as previously described [24]; the
131 plasmid pSin-EF2-Nanog-Pur (addgene, #16578) was modified using the c-Myc sequence
132 from the pCDH-Flag-c-Myc plasmid (addgene, #102626). In a 1.5 ml reaction tube the
133 transfection mixture was prepared. At first, 800 µl of DMEM were mixed with 8 µg of
134 the vector containing the GOI and the lentiviral packaging plasmids (4 µg of VSVG, 2 µg
135 REV and 2 µg g'p). 60 µl of the transfection reagent FuGENE® HD (Promega, WI, USA)
136 were added and the reaction was incubated for at least 10 min at RT. During the incuba-
137 tion time, spent medium was removed from the HEK293T cells and washed once using
138 DPBS⁻ and 10 ml of fresh medium DMEM/FBS was added. Afterwards, the transfection
139 mixture was added dropwise to the medium and plates were moved in an eight-shaped
140 manner to ensure an even distribution. Cells were incubated at 37°C and 5% CO₂ until
141 the next day. After 24 h, spent medium was replaced by fresh medium containing 1%
142 P/S and after additional 48 h, 72 h und 96 h supernatant was collected and filtered using
143 a 0.45 µm filter (VWR, #514-0063) in a 15 ml conical tube. Filtrate was mixed with 50 %
144 polyethylenglycol (PEG) and 1.5 M NaCl and stored at 4°C. One day after the last collec-
145 tion, supernatants were centrifuged at 7000 g for 30 min at 4°C. Supernatant was re-
146 moved and the pellets were resuspended and pooled in 400 µL DPBS⁻. Aliquots with a
147 volume of 40 µL were prepared and stored at -80°C until further use.

148

149

2.3.2. Lentiviral transduction of hiPSC

150

151

152

153

154

155

156

157

158

159

2.4. Neural induction and basic hiNPC cell culture

160

161

162

163

164

165

166

167

168

169

170

171

172

173

174

175

176

177

178

179

180

181

182

2.5. Flow cytometry

FACS analysis of hiPSCs for the stem cell markers OCT3/4, NESTIN, SOX2, and SSEA4 were performed as previously described in detail using the BDTM Human Pluripotent Stem Cell Transcription Factor Analysis Kit (Becton, Dickinson and Company, NJ, USA; [23]).

hiNPCs were stained for OCT3/4, NESTIN, and the proliferation marker Ki-67 (Table 2).

183

184

Table 2. Immunocytochemistry antibodies.

Antibody/dye	Company
PerCP-Cy 5.5 Mouse anti-Oct3/4	Becton, Dickinson and Company #51-9006267
Alexa Fluor 647 Mouse Anti-Nestin	Becton, Dickinson and Company #560341
Alexa Fluor 488 Mouse anti-Ki-67	Becton, Dickinson and Company #558616
PerCP-Cy 5.5 Mouse IgG1, K Isotype Control	Becton, Dickinson and Company #51-9006267
Alexa Fluor 647 Mouse IgG1 K Isotype Control	Becton, Dickinson and Company #557732
Alexa Fluor 488 Mouse IgG1 K Isotype Control	Becton, Dickinson and Company # 557782
Fixable viability stain 510	Becton, Dickinson and Company #564406

185

186

187

188

189

190

191

192

193

194

195

196

197

198

199

200

201

202

203

204

205

206

207

208

209

210

211

212

213

214

215

216

217

218

hiNPC spheres of two plates were collected in a reaction tube and centrifuged at 300 g for 5 min before washing once with pre-warmed PBS^{-/-}. The cell pellet was resuspended using 600 µl Accutase and incubated three times for 5 min at 37°C and then centrifuged at 300 g. Every 5 min pellets were resuspended by pipetting 10 times up and down. After the last incubation step, cells were centrifuged for 5 min at 300 g and washed once using PBS^{-/-}. Cells were resuspended in 1 ml PBS^{-/-} and counted using a Neubauer counting chamber. For each staining condition at least 5×10⁵ cells were used. On the first day, samples 1,5,6 and 7 and sample 2,3 and 4 (Table 3) were processed in one reaction tube. Cells were centrifuged and washed once in PBS^{-/-} before they were resuspended in 500 µl PBS^{-/-}. Fixable viability stain 510 was added to the tube containing the samples 2,3 and 4 and directly vortexed. The samples were incubated for 15 min at RT in the dark and afterwards centrifuged at 300 g for 5 min and washed twice using the BD staining buffer. For fixation cells were incubated in BD Cytotfix Fixation Buffer for 20 min at RT in the dark and washed twice using 300 µl and centrifuged at 500 g for 5 min. After the last washing step cells were vortexed for dissociation and 100 µl of ice cold BD Phosflow Perm Buffer III per sample were added, vortexed and incubated on ice for 30 min. After this step, cells were frozen at -80°C and either processed on the next day or stored up to 6 months. Thawed samples were then distributed evenly to get the 8 samples. Cells were washed twice using 200 µl BD Stain Buffer and centrifuged at 500 g for 5 min and resuspended in 100 µl BD Stain Buffer. Samples were stained using the antibodies against OCT3/4, NESTIN and Ki-67 as well as the respective isotype controls for 30 min at RT in the dark and washed twice using 1 ml of BD Stain Buffer, centrifuged for 5 min at 500 g and resuspended in 300 µl BD Stain Buffer. Resuspended cells were measured immediately using a BD Canto™ flow cytometer.

219
220

221

Table 3. Overview of the staining and used antibodies for each sample.

Sample	Viability dye	Antibody
1	-	-
2	+	-
3	+	Oct3/4-PerCP-Cy5.5
		Nestin-Alexa 647
		V450 Mouse anti-Ki 67
4	+	Isotype control PerCP-Cy5.5
		Isotype control AF 647
		Isotype control V450
5	-	Oct3/4-PerCP-Cy5.5
6	-	Nestin-Alexa 647
7	-	V450 Mouse anti-Ki 67

222

223

224

225

226

227

228

229

230

231

232

233

234

235

236

237

238

239

240

241

242

243

244

2.6. Immunocytochemistry

hiNPCs were stained for the neuronal markers β (III)Tubulin and NESTIN. Briefly, proliferating hiNPCs grown as neurospheres were chopped to 200 μ m two days prior to plating. One sphere of 300 μ m was plated in one well of a 0.1 mg/mL poly-D-lysine-hydrobromide (PDL)-0.01mg/mL laminin-coated 96-well plate in 100 μ l neural differentiation medium (NDM) containing DMEM (Life Technologies, USA), Hams F12 (Life Technologies, USA; 3:19 supplemented with 1x B27 (Invitrogen GmbH, Germany)) and 1x N2 supplement (Invitrogen, Germany). For each staining condition six technical replicates were plated. hiNPCs were kept under differentiating conditions for 24 hours and then fixed using 4% paraformaldehyde (PFA) in DPBS⁻ at 37°C for 30 min. Afterwards PFA was discarded and cells were washed 3 times using DPBS⁻. For immunocytochemical staining hiNPCs were permeabilized using 0.1% Triton X-100 diluted in PBS for 20 min at RT. Cells were washed and blocked in 10% goat-serum (Merck, Germany) and incubated overnight with the primary antibodies for β (III)Tubulin and NESTIN (Table 2). Next day, spheres were washed three times using PBS and incubated with the secondary antibody (Table 2). At the same time, nuclei were stained using 1% Hoechst 34580 (#H21486, ThermoFisher Scientific). Secondary antibody and Hoechst were incubated for 1h at 37°C. Cells were washed three times using 100 μ l PBS. Fluorescence was detected using the Cellomics Arraycan CTI (Thermo Fisher Scientific, MA, USA) and pictures were taken using the PhotometricsTM X1 camera (Thermo Fisher Scientific, MA, USA). Pictures were merged and adapted for their brightness in ImageJ [28].

245

Table 4. Antibodies used for immunocytochemical staining of hiNPCs.

Antibody	Dilution	Company
BD TM Anti-Nestin Alexa Fluor [®] 647 #560341	1:200	Becton, Dickinson and Company (Franklin Lakes, NJ, USA)
Anti- β -Tubulin III antibody produced in rabbit; #T2200	1:250	Merck (Darmstadt, Germany)
Goat anti-Rabbit IgG(H+L) Cross-Absorbed Secondary Antibody, Alexa Fluor TM 546; A11010	1:500	ThermoFisher Scientific (Waltham, Massachusetts, USA)

246

247

2.7. hiNPC Migration

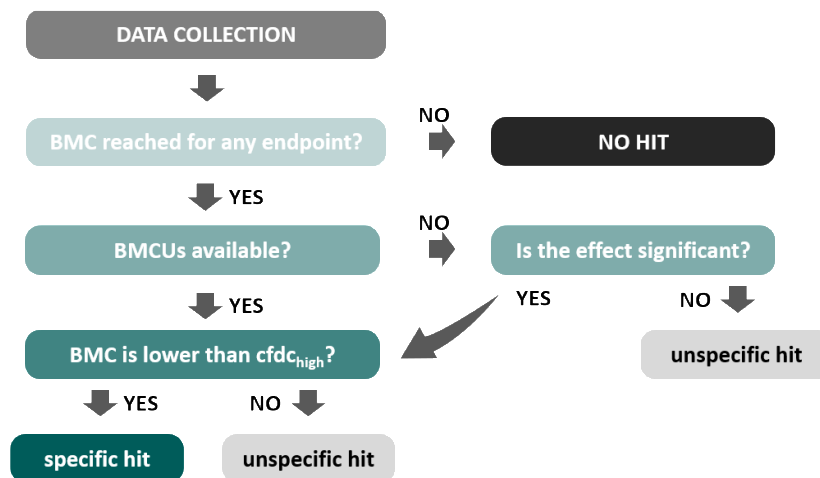
248 Analysis of hiNPC migration was performed as described before [27] with minor
249 changes. Briefly, upon plating of hiNPC neurospheres on PDL-laminin matrices, hiNPCs
250 radially migrate out of the sphere core, forming a circular migration area. The migration
251 distance of cells was assessed manually after 48 hours using bright-field microscopic
252 images taken with the Cellomics ArrayScan using a 50-fold magnification, by measuring
253 the radial distance of the furthest migrated cells to the sphere core as number of pixels
254 following conversion into μm using Fiji Image J software [28].

255 256 2.8. Cytotoxicity Assay

257 Cytotoxicity was assessed in parallel to the migration analysis to discriminate spe-
258 cific compound effects from unspecific effects originating from reduced cell viability as
259 previously described [27]. Briefly, after 48 hours of chemical exposure, cytotoxicity was
260 determined by measuring the release of lactate dehydrogenase (LDH) from cells with
261 damaged membranes (CytoTox-ONE Homogeneous Membrane Integrity Assay;
262 #G7891, Promega, United States). As lysis control for the LDH assay, neurospheres were
263 incubated for 45 min with 0.2% Triton X-100. Fluorescence was measured with a Tecan
264 infinite M200 Pro reader (ex: 540 nm; em: 590 nm). The relative fluorescence unit (RFU)
265 values of the replicates were averaged and medium without cells was used to correct for
266 background fluorescence.

267 268 2.9. Data evaluation and statistics

269 The effects of the analyzed substances on cytotoxicity and migration as a measure
270 of tumor cell invasiveness/metastasis were investigated using endpoints from the neu-
271 rosphere assay [27]. To bioinformatically evaluate and subsequently classify the data as
272 shown in Figure 2, we applied a custom-generated and R-based evaluation pipeline [29].
273 The compound-treated samples were normalized to the respective solvent controls and
274 the curves were subsequently re-normalized [according to 30]. The R package drc [31]
275 served as the basis for the curve fits. To find the fit model that best describes the given
276 data, we used linear, sigmoidal, monotonic, and non-monotonic curve fit models and
277 used the Akaike information criterion of each model as an indicator of the best fit [32,33].
278 We then analyzed the data according to the decision diagram shown in Figure 2. Briefly,
279 we first determined if the BMC for a given endpoint was reached. If yes, the upper limit
280 (BMCU) was available and lower than the calculated $\text{cfdc}_{\text{Chigh}}$ we defined it as a specific
281 hit (Fig. 2). If the BMCU was reached but the BMC was higher than the $\text{cfdc}_{\text{Chigh}}$, the hit
282 was defined as unspecific. If the BMCU was not reached, and the effect was not signifi-
283 cant, it was defined as an unspecific hit. Finally, if the respective BMC_{15} for migration or
284 BMC_{10} for cytotoxicity was not reached, the compound was classified as no hit.
285



286
287
288
289
290
291
292
293
294

Figure 2: Decision tree of data evaluation.

We evaluated the data using the benchmark method. This is used in toxicology as a statistical-mathematical analysis of concentration-response data. A benchmark concentration (BMC) for each endpoint is estimated, which leads to an effect with a certain probability. The BMC is thus linked to a BM-response (BMR) fixed in advance (based on the dispersion of the solvent controls), e.g. a 15% reduction in migration distance (Table 5).

Table 5. BMC finding.

hiNPC Model	Migration [% sc]	Cytotoxicity [% sc]
Empty vector control	13.40	3.77
C-myc	13.19	2.86
Mean	13.30	3.31
	BM R₁₅	BM R₁₀

sc = solvent control; BMR = bench mark response.

296
297
298
299
300
301
302
303
304
305

For all experiments, at least three independent biological replicates with at least three technical replicates each were performed. Experiments were defined as independent if they were generated with hiNPCs from a different passage number. Results are presented as mean ± SEM. For calculating concentration-response curves, a sigmoidal curve fit was applied using GraphPadPrism software. Statistical significance was calculated using the step-down multiple test procedure of Dunnett and Tamhane [34], $p \leq 0.05$ was considered significant.

3. Results

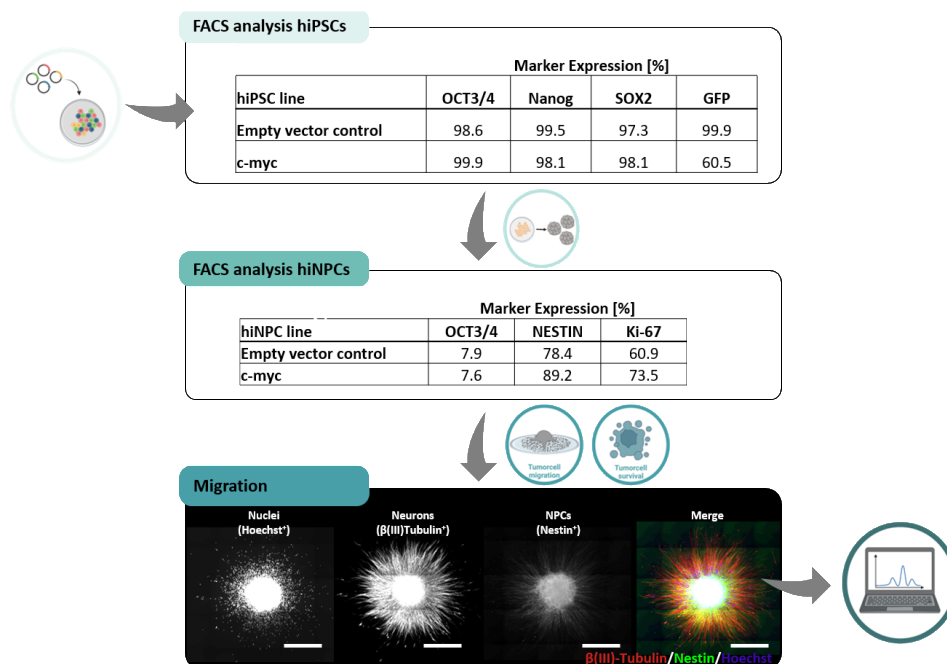
3.1. Quality control and characterization of cell models used

For quality control, flow cytometric analyses (FACS) were performed in both generated hiPSC lines, c-myc and empty vector (EV), and analyzed for expression of the classical stem cell markers OCT3/4, NANOG, and SOX2 (Fig. 3). As the EV cells (pSin) expressed GFP, we also examined this marker to ensure that the cells contained the desired insert and confirm vector integration. The expression of the stem cell markers in both lines was well above the limit of 70% defined by us and others [23], and GFP expression in the c-myc model was also only slightly below this threshold at 60.5% (Fig. 3).

306
307
308
309
310
311
312
313
314

315
316
317
318
319
320
321
322
323
324

Subsequently, the two hiPSC tumor cell lines were neurally induced and, as a control, the markers OCT3/4 (stem cells), NESTIN (NPC marker), and Ki-67 (proliferation marker) were analyzed by flow cytometry. As expected, the expression of OCT3/4 after neural induction was very low at just under 8% in both hiNPC models, and the NPC marker NESTIN was expressed at 78.4%, and 89.2%, respectively. To verify that the lentivirally generated hiNPCs also displayed normal migration and differentiation behavior, we further plated the cells on an PDL-laminin matrix and differentiated them for 24 hours, after which β (III)Tubulin⁺ and NESTIN⁺ cells migrated out of the sphere core (Fig. 2). These results thus confirmed that the models were suitable for further investigation.



325
326
327
328
329
330
331
332
333
334
335
336
337
338
339
340
341
342
343
344

Figure 3. Quality control and characterization of the models. Results of FACS analysis of hiPSC tumor models (upper panel), FACS analysis of neurally induced hiNPC models (middle panel), and a representative immunocytochemical staining of 24 hours migrated EV hiNPCs (lower panel) are shown. Scale bar represents 500 μ m. Figure created with BioRender.com.

3.2. Drug Screening

For drug screening both hiNPC models were plated on a PDL-laminin matrix and exposed to the selected drugs (arsenic trioxide, cisplatin, copanlisib, dasatinib, midostaurin, acetaminophen, regorafenib, tretinoin, and vantenanib) for 48 hours under differentiating conditions before the migration distance and cytotoxicity were analyzed. Data evaluation revealed that only copanlisib had a specific effect on the migration of the EV control and c-myc hiNPCs with a BMC₁₅ of 0.00977 μ M and 0.029397 μ M, respectively (Table 6). Midostaurin, regorafenib, and vandetanib yielded unspecific effects in the EV hiNPCs, the same holds true for dasatinib, midostaurin, and vandetanib in the c-myc hiNPC models, indicating that the BMC₁₅ was reached at concentrations that are not within the defined cfd_{high} concentration range that can be reached *in vivo* (Table 6). For the endpoint of cytotoxicity only the standard of care, cisplatin, displayed a specific hit with a BMC₁₀ of 1.8050 μ M in the EV hiNPCs, while midostaurin was an unspecific hit in these models. Copanlisib with a BMC₁₀ of 0.3948 μ M was the sole specific hit in the c-myc hiNPCs for the endpoint of cytotoxicity (Table 6).

345
346
347
348
349
350
351
352

353
354

Table 6. Results of the substance screening in both hiNPC models. BMC₁₅ for migration and BMC₁₀ for cytotoxicity are listed.

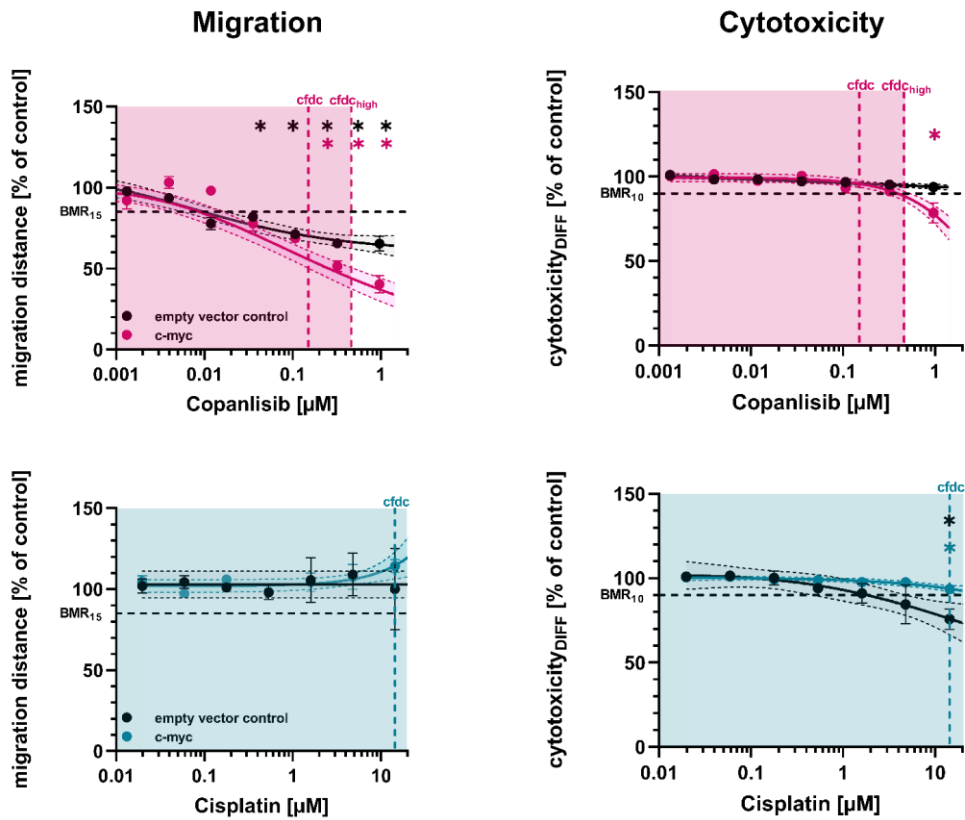
hiNPC model	Drug	Migration	Migration	Cytotoxicity	Cytotoxicity
		BMC ₁₅	upper limit BMC ₁₅	BMC ₁₀	upper limit BMC ₁₀
Empty vector control	Acetaminophen (NK)				
	Arsenic trioxide				
	Cisplatin (SoC)			1.8050	4.8012
	Copanlisib	0.00977	0.017502		
	Dasatinib				
	Midostaurin	0.357091	0.618514	2.8979	n.r.
	Regorafenib	5.270442	8.242272		
	Tretinoin				
	Vandetanib				
C-myc	Acetaminophen (NK)				
	Arsenic trioxide				
	Cisplatin (SoC)				
	Copanlisib	0.029397	0.047212	0.3948	0.5376
	Dasatinib	0.03579	0.061645		
	Midostaurin	0.598921	0.812029		
	Regorafenib				
	Tretinoin				
	Vandetanib	1.851037	n.r.		

355

356
357
358
359
360
361
362
363
364
365
366
367
368

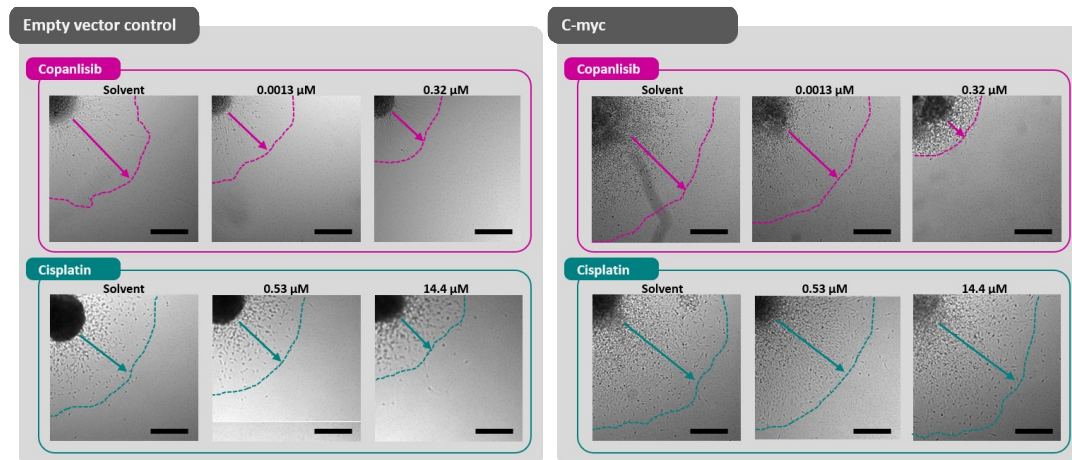
Dark grey: no hit, light grey: unspecific hit, petrol: specific hit. n.r. = not reached

The corresponding concentration-response curves of the specific hits (Fig. 4) allow direct comparison of the effects of copanlisib and cisplatin on the EV and c-myc hiNPCs and illustrate that the standard of care, cisplatin, does not decrease the migration of the c-myc hiNPCs in the EV controls. However, it causes cell death of the empty vector controls, whereas the c-myc transduced hiNPCs survive cisplatin treatment. This might indicate poor efficacy of cisplatin in this MB cell model. In contrast to cisplatin, copanlisib treatment has a specific effect on migration and cytotoxicity in c-myc hiNPCs. Accordingly, copanlisib could potentially suppress tumor invasion/metastasis in patients while leading to tumor cell death, mainly with less impact on the surrounding healthy cells. Therefore, treatment with copanlisib might indeed have an added value for the therapy of group 3 MB patients.



369 **Figure 4.** Concentration-response curves of specific hits. Statistical significance was calculated using the step-down multiple test
 370 procedure of Dunnett and Tamhane [34], $p \leq 0.05$ is considered significant. In addition to the curve fit, the corresponding confi-
 371 dence bands (shading) are also shown. Cfcdc = calculated free drug concentration (see Table 1). The colored boxes indicate the tested
 372 concentrations that are under the $cfcdc_{high}$ ($3 \times cfcdc$) and therefore indicate concentrations that are also reached in patients *in vivo*.
 373
 374

375 The effects on migration after treatment with both compounds are also clearly seen
 376 in light-microscopic images of the migration area (Fig. 5).
 377



378
 379 **Figure 5.** Exemplary migration images of EV and c-myc hiNPCs treated with copanlisib or cisplatin. Representative images of solvent controls (left), concentrations around the respective $BM C_{15}$ -value for migration (middle) as well as one high concentration (right) are shown. Scalebar represents 250 μm .
 381
 382

383

384

385

386

387

388

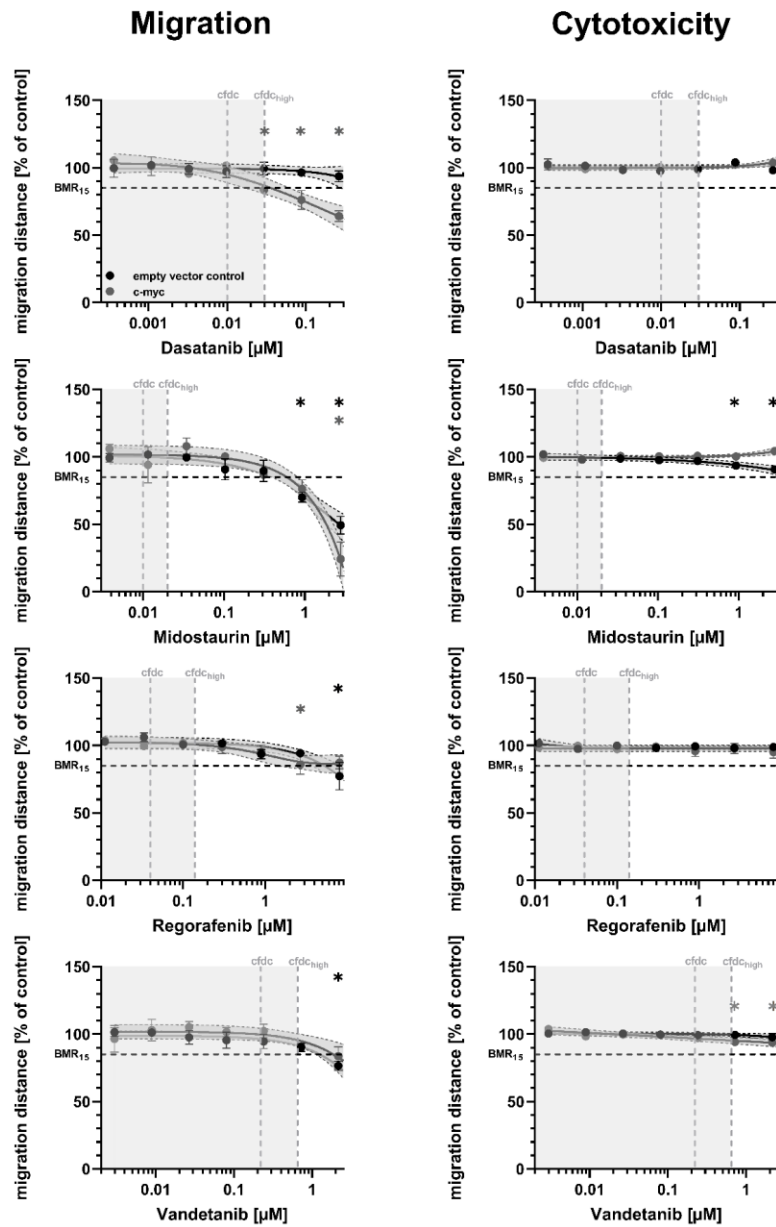
389

390

391

392

Finally, the concentration-response curves of the unspecific hits (Fig. 6) demonstrate clearly how important it is to take the internal exposure ($cf_{dc} - cf_{dc_{high}}$) into account. While pure examination of the whole concentration range might lead to the impression that dasatanib, midostaurin, regorafenib, and vandetanib treatment also has a favorable effect on migration and to a lesser extend also on the endpoint of cytotoxicity in the analyzed models, taking into account only the concentrations that can be reached *in vivo* by calculating the free drug concentration (see material and methods for details) clearly shows that the significant effects shown here are not within a relevant *in vivo* range.



393
 394 **Figure 6.** Concentration-response curves of unspecific hits. Statistical significance was calculated using the step-down multiple test
 395 procedure of Dunnett and Tamhane [34], $p \leq 0.05$ is considered significant. In addition to the curve fit, the corresponding confi-
 396 dence intervals (shading) are also shown. cf_{dc} = calculated free drug concentration (see Table 1). The colored boxes indicate the
 397 tested concentrations that are under the $cf_{dc_{high}}$ ($3 \times cf_{dc}$) and therefore indicate concentrations that are also reached in patients *in*
 398 *vitro*.
 399

400

4. Discussion

401

402

403

404

405

406

407

408

409

410

411

412

413

414

415

416

417

With this proof-of-concept study we demonstrate that genetically modified, hiPSC-based, tumor subgroup-specific *in vitro* models can be used to identify novel, previously approved drug candidates from existing databases [35,36] for clinical testing of brain tumor therapies. This is in line with a previous report that used a similar approach on the base of cerebellar-derived human neural stem cells to model group 3 MB [37]. Using hiPSCs as the initial cell type to introduce tumor-specific mutations lacks ethical concerns while guaranteeing sufficient starting material independent of cell lines or animal models [38]. This is a great advantage over primary human tumor cell lines, as clinical samples are difficult to access [39]. However, while patient-derived hiPSC samples greatly increased our understanding of the underlying mechanism of diseases [40], using hiPSC from primary cancer cells or tissues for drug screening does not seem to be a promising approach as it often leads to the loss of the malignant phenotype of the original cell [41]. Human iPSCs generated from CML patients are a striking example. While the patients responded to the drug Imatinib, a tyrosine kinase inhibitor, their hiPSC were resistant to the drug. However, differentiating the hiPSC into hematopoietic progenitor cells, which more closely resembled the original tumor, restored their sensitivity [42].

418

419

420

421

422

423

424

425

426

For this reason, we generated hiNPC from the synthetic hiPSC cancer model, i.e. c-myc⁺ non-WNT/non-SHH group 3 MB model as this is the most-aggressive MB subgroup with the worst survival outcome [3,5,6]. Furthermore, with 5- to 10-fold fewer mutations compared to other solid tumors, MB represents an ideal tumor for such a proof-of-concept study [43]. Although the exact pathogenesis of these tumors remains elusive, different studies name Nestin⁺ NPCs as likely candidates for the MB cellular origin [44–49]. We cultured the Nestin⁺ hiNPC as three dimensional (3D) neurospheres, which are thought to mimic the tumor microenvironment better than 2D cultures, thereby improving clinical translation [39].

427

428

429

430

431

432

433

434

435

436

437

438

439

440

441

We are well aware that our model only recapitulates one molecular aspect of group 3 MB, c-myc amplification, and lacks other genetic modifications described in this kind of tumors, e.g. MYCN or OTX2 amplification and single nucleotide variants in *SMARCA4*, *KBTBD4*, *CTDNEP1*, and *KMT2D*, as well as cytogenetic events like gain of chromosomes 1q, 7, and 18 or loss of chromosomes 8, 10q, 11, and 17q [19]. Nevertheless, we were able to recapitulate the phenotype of decreased response to the standard-of-care chemotherapeutic agent, cisplatin, regarding the endpoints migration and cytotoxicity. We argue that this work serves as a proof-of-concept towards a more personalized medicine. As generating patient-specific hiPSC-lines often takes too long to be of use for a personalized drug screening, we here propose the concept of establishing a panel of different synthetic hiNPC-tumor models, e.g. one for every different brain tumor subtype. Once the molecular profile of the patient's tumor is determined, these models can be utilized for personalized drug screening. This approach saves time and money, and might be advantageous in deciding which treatment regime is best for the patient-specific tumor.

442

443

444

445

446

447

448

449

Using this approach, we identified copanlisib as a possible treatment for group 3 MBs. Our literature search revealed that there are as yet no clinical trials of copanlisib for the treatment of patients with medulloblastoma (<https://clinicaltrials.gov>; [50]). Copanlisib is already used under the brand name Aliqopa for the treatment of relapsed follicular lymphoma (<https://go.drugbank.com>) and is an α - and δ -isoform-specific phosphoinositide 3-kinase (PI3K) inhibitor. The PI3K/AKT/mTOR (PAM) signaling pathway controls important cellular responses, such as cell growth and proliferation, survival, migration, and metabolism [51]. This intracellular signaling pathway is frequently affected by ge-

450 netic and epigenetic alterations in malignant brain tumors, including medulloblastoma.
451 There are already approaches in clinical trials to investigate the safety and efficacy of
452 agents that affect the PAM pathway in malignant brain tumors. However, this approach
453 is proving difficult in the development of new therapeutic approaches due to the com-
454 plexity of the PAM pathway [51]. Thus, copanlisib is our first candidate that seems to
455 confirm the hypothesis that tumor subset-specific cell models based on hiPSC could be
456 used to identify new therapeutic options.

457 5. Conclusions

458 Taken together, our proof-of-concept study suggests that tumor subgroup-specific,
459 synthetic brain tumor models might be valuable tools for finding alternative treatment
460 strategies for these devastating diseases. Clearly, more studies modelling additional tu-
461 mor subgroups will strengthen the confidence in this strategy. Possibly, this concept
462 might also be transferred to other tumor types, especially tumors with stem cells en-
463 rolled in their pathogeneses.

464 Author Contributions:

465 Conceptualization, E.F.; J.T.; U.D.K.; methodology, F.B.; U.H., G.B., C.U.; A.R.; software, A.D.;
466 D.P.; A.C.N.; validation, J.T.; A.D.; formal analysis, J.T.; A.D.; K.K.; investigation, J.T.; C.U.; re-
467 sources, E.F.; U.D.K.; writing—original draft preparation, J.T.; writing—review and editing, E.F.;
468 K.K.; visualization, J.T.; K.K.; supervision, E.F.; K.K.; project administration, J.T.; E.F.; funding ac-
469 quisition, E.F.; U.D.K.. All authors have read and agreed to the published version of the manu-
470 script.

471 **Funding:** This research was funded by the German Federal Ministry of Education and Research
472 (BMBF) validation of innovation potential fund plus (VIP+), grant number 03VP03791/92.

473 **Data Availability Statement:** Upon request, the generated hiPSC-oncogene model systems to-
474 gether with their respective sequencing data will be available to the academic field under MTA
475 regulations.

476 **Acknowledgments:** UDK thanks HJ Steiger, Lumino, CH for long-lasting support.

477 **Conflicts of Interest:** EF, AD, and KK are shareholders of DNTOX GmbH, the other authors de-
478clare no conflict of interest.

479 References

- 480 1. Partap, S.; Curran, E.K.; Propp, J.M.; Le, G.M.; Sainani, K.L.; Fisher, P.G. Medulloblastoma Incidence Has Not
481 Changed over Time: A CBTRUS Study. *J. Pediatr. Hematol. Oncol.* **2009**, *31*, 970–971,
482 doi:10.1097/MPH.0b013e3181bbc502.
- 483 2. WHO Classification of Tumours Editorial Board *Central Nervous System Tumours*; 5th ed.; 2021; Vol. 6;.
- 484 3. Taylor, M.D.; Northcott, P.A.; Korshunov, A.; Remke, M.; Cho, Y.J.; Clifford, S.C.; Eberhart, C.G.; Parsons,
485 D.W.; Rutkowski, S.; Gajjar, A.; et al. Molecular Subgroups of Medulloblastoma: The Current Consensus. *Acta*
486 *Neuropathol.* **2012**, *123*, 465–472, doi:10.1007/s00401-011-0922-z.
- 487 4. Northcott, P.A.; Robinson, G.W.; Kratz, C.P.; Mabbott, D.J.; Pomeroy, S.L.; Clifford, S.C.; Rutkowski, S.; Ellison,
488 D.W.; Malkin, D.; Taylor, M.D.; et al. Medulloblastoma. *Nat. Rev. Dis. Prim.* **2019**, *5*.
- 489 5. Northcott, P.A.; Buchhalter, I.; Morrissy, A.S.; Hovestadt, V.; Weischenfeldt, J.; Ehrenberger, T.; Gröbner, S.;
490 Segura-Wang, M.; Zichner, T.; Rudneva, V.A.; et al. The Whole-Genome Landscape of Medulloblastoma
491 Subtypes. *Nature* **2017**, *547*, 311–317, doi:10.1038/nature22973.
- 492 6. Northcott, P.A.; Korshunov, A.; Witt, H.; Hielscher, T.; Eberhart, C.G.; Mack, S.; Bouffet, E.; Clifford, S.C.;
493 Hawkins, C.E.; French, P.; et al. Medulloblastoma Comprises Four Distinct Molecular Variants. *J. Clin. Oncol.*
494 **2011**, *29*, 1408–1414, doi:10.1200/JCO.2009.27.4324.
- 495 7. Northcott, P.A.; Korshunov, A.; Pfister, S.M.; Taylor, M.D. The Clinical Implications of Medulloblastoma

- 496 Subgroups. *Nat. Rev. Neurol.* 2012, 8, 340–351.
- 497 8. Northcott, P.A.; Jones, D.T.W.; Kool, M.; Robinson, G.W.; Gilbertson, R.J.; Cho, Y.J.; Pomeroy, S.L.; Korshunov,
498 A.; Lichter, P.; Taylor, M.D.; et al. Medulloblastomics: The End of the Beginning. *Nat. Rev. Cancer* 2012, 12, 818–
499 834.
- 500 9. Gajjar, A.J.; Robinson, G.W. Medulloblastoma - Translating Discoveries from the Bench to the Bedside. *Nat. Rev.*
501 *Clin. Oncol.* 2014, 11, 714–722.
- 502 10. Khatua, S. Evolving Molecular Era of Childhood Medulloblastoma: Time to Revisit Therapy. *Futur. Oncol.* 2016,
503 12, 107–117.
- 504 11. Ellison, D.W.; Kocak, M.; Dalton, J.; Megahed, H.; Lusher, M.E.; Ryan, S.L.; Zhao, W.; Nicholson, S.L.; Taylor,
505 R.E.; Bailey, S.; et al. Definition of Disease-Risk Stratification Groups in Childhood Medulloblastoma Using
506 Combined Clinical, Pathologic, and Molecular Variables. *J. Clin. Oncol.* 2011, 29, 1400–1407,
507 doi:10.1200/JCO.2010.30.2810.
- 508 12. Scheurlen, W.G.; Schwabe, G.C.; Joos, S.; Mollenhauer, J.; Sörensen, N.; Köhl, J. Molecular Analysis of
509 Childhood Primitive Neuroectodermal Tumors Defines Markers Associated with Poor Outcome. *J. Clin. Oncol.*
510 1998, 16, 2478–2485, doi:10.1200/JCO.1998.16.7.2478.
- 511 13. Eberhart, C.G.; Kratz, J.; Wang, Y.; Summers, K.; Stearns, D.; Cohen, K.; Dang, C. V.; Burger, P.C.
512 Histopathological and Molecular Prognostic Markers in Medulloblastoma: C-Myc, N-Myc, TrkC, and
513 Anaplasia. *J. Neuropathol. Exp. Neurol.* 2004, 63, 441–449, doi:10.1093/jnen/63.5.441.
- 514 14. von Bueren, A.O.; Oehler, C.; Shalaby, T.; von Hoff, K.; Pruschy, M.; Seifert, B.; Gerber, N.U.; Warmuth-Metz,
515 M.; Stearns, D.; Eberhart, C.G.; et al. C-MYC Expression Sensitizes Medulloblastoma Cells to Radio- and
516 Chemotherapy and Has No Impact on Response in Medulloblastoma Patients. *BMC Cancer* 2011, 11,
517 doi:10.1186/1471-2407-11-74.
- 518 15. Wang, J.; Garancher, A.; Ramaswamy, V.; Wechsler-Reya, R.J. Medulloblastoma: From Molecular Subgroups to
519 Molecular Targeted Therapies. *Annu. Rev. Neurosci.* 2018, 41, 207–232.
- 520 16. Liu, X.; Ding, C.; Tan, W.; Zhang, A. Medulloblastoma: Molecular Understanding, Treatment Evolution, and
521 New Developments. *Pharmacol. Ther.* 2020, 210.
- 522 17. Ribi, K.; Relly, C.; Landolt, M.A.; Alber, F.D.; Boltshauser, E.; Grotzer, M.A. Outcome of Medulloblastoma in
523 Children: Long-Term Complications and Quality of Life. *Neuropediatrics* 2005, 36, 357–365,
524 doi:10.1055/s-2005-872880.
- 525 18. Jakacki, R.I.; Burger, P.C.; Zhou, T.; Holmes, E.J.; Kocak, M.; Onar, A.; Goldwein, J.; Mehta, M.; Packer, R.J.;
526 Tarbell, N.; et al. Outcome of Children with Metastatic Medulloblastoma Treated with Carboplatin during
527 Craniospinal Radiotherapy: A Children’s Oncology Group Phase I/II Study. *J. Clin. Oncol.* 2012, 30, 2648–2653,
528 doi:10.1200/JCO.2011.40.2792.
- 529 19. Juraschka, K.; Taylor, M.D. Medulloblastoma in the Age of Molecular Subgroups: A Review: JNSPG 75th
530 Anniversary Invited Review Article. *J. Neurosurg. Pediatr.* 2019, 24, 353–363.
- 531 20. Liston, D.R.; Davis, M. Clinically Relevant Concentrations of Anticancer Drugs: A Guide for Nonclinical
532 Studies. *Clin. Cancer Res.* 2017, 23, 3489–3498.
- 533 21. Ayoub, S.S. Paracetamol (Acetaminophen): A Familiar Drug with an Unexplained Mechanism of Action.
534 *Temperature* 2021, 8, 351–371.
- 535 22. Dutreix, C.; Munarini, F.; Lorenzo, S.; Roesel, J.; Wang, Y. Investigation into CYP3A4-Mediated Drug-Drug
536 Interactions on Midostaurin in Healthy Volunteers. *Cancer Chemother. Pharmacol.* 2013, 72, 1223–1234,
537 doi:10.1007/s00280-013-2287-6.

- 538 23. Tigges, J.; Bielec, K.; Brockerhoff, G.; Hildebrandt, B.; Hübenthal, U.; Kapr, J.; Koch, K.; Teichweyde, N.;
539 Wiczorek, D.; Rossi, A.; et al. Academic Application of Good Cell Culture Practice for Induced Pluripotent
540 Stem Cells. *ALTEX* **2021**, *38*, 595–614, doi:10.14573/altex.2101221.
- 541 24. Uhlmann, C.; Kuhn, L.M.; Tigges, J.; Fritsche, E.; Kahlert, U.D. Efficient Modulation of TP53 Expression in
542 Human Induced Pluripotent Stem Cells. *Curr. Protoc. Stem Cell Biol.* **2020**, *52*, doi:10.1002/cpsc.102.
- 543 25. Nimtz, L.; Hartmann, J.; Tigges, J.; Masjosthusmann, S.; Schmuck, M.; Keßel, E.; Theiss, S.; Köhrer, K.; Petzsch,
544 P.; Adjaye, J.; et al. Characterization and Application of Electrically Active Neuronal Networks Established
545 from Human Induced Pluripotent Stem Cell-Derived Neural Progenitor Cells for Neurotoxicity Evaluation.
546 *Stem Cell Res.* **2020**, *45*, doi:10.1016/j.scr.2020.101761.
- 547 26. Hofrichter, M.; Nimtz, L.; Tigges, J.; Kabiri, Y.; Schröter, F.; Royer-Pokora, B.; Hildebrandt, B.; Schmuck, M.;
548 Epanchintsev, A.; Theiss, S.; et al. Comparative Performance Analysis of Human iPSC-Derived and Primary
549 Neural Progenitor Cells (NPC) Grown as Neurospheres in Vitro. *Stem Cell Res.* **2017**, *25*, 72–82,
550 doi:10.1016/j.scr.2017.10.013.
- 551 27. Koch, K.; Bartmann, K.; Hartmann, J.; Kapr, J.; Klose, J.; Kuchovská, E.; Pahl, M.; Schlüppmann, K.; Zühr, E.;
552 Fritsche, E. Scientific Validation of Human Neurosphere Assays for Developmental Neurotoxicity Evaluation.
553 *Front. Toxicol.* **2022**, *4*, doi:10.3389/ftox.2022.816370.
- 554 28. Schneider, C.A.; Rasband, W.S.; Eliceiri, K.W. NIH Image to ImageJ: 25 Years of Image Analysis. *Nat. Methods*
555 **2012**, *9*, 671–675.
- 556 29. Keßel, E.H.; Masjosthusmann, S.; Bartmann, K.; Blum, J.; Förster, N.; Klose, J.; Mosig, A.; Pahl, M.; Leist, M.;
557 Fritsche, E. Biostatistics and Its Impact on Hazard Characterization Using in Vitro Developmental
558 Neurotoxicity Assays. *bioRxiv* **2022**, 2022.10.18.512648, doi:10.1101/2022.10.18.512648.
- 559 30. Krebs, A.; Nyffeler, J.; Karreman, C.; Schmidt, B.Z.; Kappenberg, F.; Mellert, J.; Pallocca, G.; Pastor, M.;
560 Rahnenführer, J.; Leist, M. Determination of Benchmark Concentrations and Their Statistical Uncertainty for
561 Cytotoxicity Test Data and Functional in Vitro Assays. *ALTEX* **2020**, *37*, 155–163, doi:10.14573/altex.1912021.
- 562 31. Ritz, C.; Baty, F.; Streibig, J.C.; Gerhard, D. Dose-Response Analysis Using R. *PLoS One* **2015**, *10*,
563 doi:10.1371/journal.pone.0146021.
- 564 32. Buatois, S.; Ueckert, S.; Frey, N.; Retout, S.; Mentré, F. Comparison of Model Averaging and Model Selection in
565 Dose Finding Trials Analyzed by Nonlinear Mixed Effect Models. *AAPS J.* **2018**, *20*,
566 doi:10.1208/s12248-018-0205-x.
- 567 33. Portet, S. A Primer on Model Selection Using the Akaike Information Criterion. *Infect. Dis. Model.* **2020**, *5*, 111–
568 128, doi:10.1016/j.idm.2019.12.010.
- 569 34. Dunnett, C.W.; Tamhane, A.C. Step-down Multiple Tests for Comparing Treatments with a Control in
570 Unbalanced One-way Layouts. *Stat. Med.* **1991**, *10*, 939–947, doi:10.1002/sim.4780100614.
- 571 35. Yang, W.; Soares, J.; Greninger, P.; Edelman, E.J.; Lightfoot, H.; Forbes, S.; Bindal, N.; Beare, D.; Smith, J.A.;
572 Thompson, I.R.; et al. Genomics of Drug Sensitivity in Cancer (GDSC): A Resource for Therapeutic Biomarker
573 Discovery in Cancer Cells. *Nucleic Acids Res.* **2013**, *41*, doi:10.1093/nar/gks1111.
- 574 36. Barretina, J.; Caponigro, G.; Stransky, N.; Venkatesan, K.; Margolin, A.A.; Kim, S.; Wilson, C.J.; Lehár, J.;
575 Kryukov, G. V.; Sonkin, D.; et al. The Cancer Cell Line Encyclopedia Enables Predictive Modelling of
576 Anticancer Drug Sensitivity. *Nature* **2012**, *483*, 603–607, doi:10.1038/nature11003.
- 577 37. Hanaford, A.R.; Archer, T.C.; Price, A.; Kahlert, U.D.; Maciaczyk, J.; Nikkhah, G.; Kim, J.W.; Ehrenberger, T.;
578 Clemons, P.A.; Dančik, V.; et al. DiSCoVERing Innovative Therapies for Rare Tumors: Combining Genetically
579 Accurate Disease Models with in Silico Analysis to Identify Novel Therapeutic Targets. *Clin. Cancer Res.* **2016**,

- 580 22, 3903–3914, doi:10.1158/1078-0432.CCR-15-3011.
- 581 38. Sayed, N.; Ameen, M.; Wu, J.C. Personalized Medicine in Cardio-Oncology: The Role of Induced Pluripotent
582 Stem Cell. *Cardiovasc. Res.* 2019, *115*, 949–959.
- 583 39. Niu, N.; Wang, L. In Vitro Human Cell Line Models to Predict Clinical Response to Anticancer Drugs.
584 *Pharmacogenomics* 2015, *16*, 273–285.
- 585 40. Sidhu, I.; Barwe, S.P.; Pillai, R.K.; Gopalakrishnapillai, A. Harnessing the Power of Induced Pluripotent Stem
586 Cells and Gene Editing Technology: Therapeutic Implications in Hematological Malignancies. *Cells* 2021, *10*.
- 587 41. Balani, S.; Nguyen, L. V.; Eaves, C.J. Modeling the Process of Human Tumorigenesis. *Nat. Commun.* 2017, *8*.
- 588 42. Laplane, L.; Beke, A.; Vainchenker, W.; Solary, E. Concise Review: Induced Pluripotent Stem Cells as New
589 Model Systems in Oncology. *Stem Cells* 2015, *33*, 2887–2892, doi:10.1002/stem.2099.
- 590 43. Parsons, D.W.; Li, M.; Zhang, X.; Jones, S.; Leary, R.J.; Lin, J.C.H.; Boca, S.M.; Carter, H.; Samayoa, J.;
591 Bettegowda, C.; et al. The Genetic Landscape of the Childhood Cancer Medulloblastoma. *Science (80-.)*. 2011,
592 *331*, 435–439, doi:10.1126/science.1198056.
- 593 44. Vladoiu, M.C.; El-Hamamy, I.; Donovan, L.K.; Farooq, H.; Holgado, B.L.; Sundaravadanam, Y.; Ramaswamy,
594 V.; Hendrikse, L.D.; Kumar, S.; Mack, S.C.; et al. Childhood Cerebellar Tumours Mirror Conserved Fetal
595 Transcriptional Programs. *Nature* 2019, *572*, 67–73, doi:10.1038/s41586-019-1158-7.
- 596 45. Kawachi, D.; Ogg, R.J.; Liu, L.; Shih, D.J.H.; Finkelstein, D.; Murphy, B.L.; Rehg, J.E.; Korshunov, A.;
597 Calabrese, C.; Zindy, F.; et al. Novel MYC-Driven Medulloblastoma Models from Multiple Embryonic
598 Cerebellar Cells. *Oncogene* 2017, *36*, 5231–5242, doi:10.1038/onc.2017.110.
- 599 46. Tao, R.; Murad, N.; Xu, Z.; Zhang, P.; Okonechnikov, K.; Kool, M.; Rivero-Hinojosa, S.; Lazarski, C.; Zheng, P.;
600 Liu, Y.; et al. MYC Drives Group 3 Medulloblastoma through Transformation of Sox2⁺ Astrocyte Progenitor
601 Cells. *Cancer Res.* 2019, *79*, 1967–1980, doi:10.1158/0008-5472.CAN-18-1787.
- 602 47. Pei, Y.; Moore, C.E.; Wang, J.; Tewari, A.K.; Eroshkin, A.; Cho, Y.J.; Witt, H.; Korshunov, A.; Read, T.A.; Sun,
603 J.L.; et al. An Animal Model of MYC-Driven Medulloblastoma. *Cancer Cell* 2012, *21*, 155–167,
604 doi:10.1016/j.ccr.2011.12.021.
- 605 48. Huang, G.H.; Xu, Q.F.; Cui, Y.H.; Li, N.; Bian, X.W.; Lv, S.Q. Medulloblastoma Stem Cells: Promising Targets
606 in Medulloblastoma Therapy. *Cancer Sci.* 2016, *107*, 583–589.
- 607 49. Louis, D.N.; Perry, A.; Reifenberger, G.; von Deimling, A.; Figarella-Branger, D.; Cavenee, W.K.; Ohgaki, H.;
608 Wiestler, O.D.; Kleihues, P.; Ellison, D.W. The 2016 World Health Organization Classification of Tumors of the
609 Central Nervous System: A Summary. *Acta Neuropathol.* 2016, *131*, 803–820.
- 610 50. Ghasemi, D.R.; Fleischhack, G.; Milde, T.; Pajtler, K.W. The Current Landscape of Targeted Clinical Trials in
611 Non-WNT/Non-SHH Medulloblastoma. *Cancers (Basel)*. 2022, *14*.
- 612 51. Dimitrova, V.; Arcaro, A. Targeting the PI3K/AKT/MTOR Signaling Pathway in Medulloblastoma. *Curr. Mol.*
613 *Med.* 2015, *15*, 82–93, doi:10.2174/1566524015666150114115427.

614

10 Danksagung

Ich möchte mich bei Frau Prof. Dr. Ellen Fritsche für die umfassende Betreuung und Unterstützung während der gesamten Promotion bedanken. Vielen Dank für die Übernahme der Betreuung in dem Kooperationsprojekt, dadurch war es mir erst möglich das interessante Thema zu bearbeiten.

Bei Herrn Prof. Dr. Thomas Klein möchte ich mich für die fakultätsübergreifende Betreuung und Übernahme der Mentorenschaft, durch die meine Dissertation möglich war, sowie den Austausch während meiner Promotion bedanken.

Des Weiteren möchte ich mich bei PD Dr. Ulf Kahlert bedanken, der in Kooperation mit Ellen Fritsche das Projekt geplant hat. Er hat mich in der Projektplanung und Durchführung stetig an der Neurochirurgischen Klinik in Düsseldorf unterstützt.

Zudem möchte ich mich herzlich bei Julia Tigges bedanken, durch deren Input hätte ich es nicht soweit geschafft, vielen Dank für dein offenes Ohr, deine Ratschläge und vor allem deine Hilfe!!! Insbesondere deine Betreuung in der letzten Phase der Arbeit war für mich sehr hilfreich!

Ich möchte mich bei allen Mitarbeitern der Neurochirurgie Düsseldorf bedanken, insbesondere jedoch bei meinen Laborpartnern: Ann-Christin Nickel, Julia Tsiampali, Suad Yusuf, Philippe Aretz, Michael Hewera und allen anderen! Dank euch gingen manche Inkubationszeiten, lange Arbeitstage und Wochenendeinsätze wie im Flug vorbei und wir hatten immer eine Menge Spaß! Vielen Dank auch für eure Unterstützung bei den vielen Projekten im Labor!

Ebenso möchte ich mich bei allen Mitarbeitern der AG Fritsche bedanken. Danke an Gaby, Ulrike und Farina, ihr habt mir viele Methoden beigebracht und auch viel Arbeit in meine Projekte investiert und mich immer unterstützt wo es ging.

Ebenso möchte ich bei Daniel bedanken, der mir mit den Auswertungen geholfen hat und sich immer die Zeit genommen hat, die Daten auszuwerten und mir alles zu erklären. Vielen Dank!

Vielen Dank auch an Prof. Dr. Jay Gopalakrishnan und an Dr. Andrea Rossi und deren Mitarbeiter, durch deren Unterstützung ich wichtige Fortschritte im Projekt erreichen konnte.

Ich danke meiner Familie, Freunden und Arbeitskollegen für eure Unterstützung während der gesamten Promotion.

Danksagung

Mein besonderer Dank geht an Ceddy, der mich während meiner gesamten Promotion kontinuierlich unterstützt hat und auch immer wieder motiviert hat. Vielen Dank für deine Unterstützung auch wenn es in manchen Phasen der Promotion sehr anstrengend mit mir war 😊!